PERFORMANCE CHARACTERISTICS OF HYBRID COOLING TOWERS

by

Pieter Cornelis Oosthuizen

Thesis presented in partial fulfilment of the requirements for the degree Master of Engineering
at the University of Stellenbosch

Thesis Supervisor: Prof. D.G. Kröger

Department of Mechanical Engineering
University of Stellenbosch
September 1995

DECLARATION

I, the undersigned, hereby declare that the work contained in this thesis is my own work and has not previously in its entirety or in part been submitted at any university for a degree.

01/12/95

Date

ABSTRACT

Different wet/dry and dry/wet cooling tower configurations are investigated and the advantages and disadvantages of separate and combined (hybrid) configurations are discussed. Some existing hybrid towers are also discussed.

The different plume prediction models that are found in the literature are investigated and the psychrometrics behind the formation of visible plumes are discussed. Psychrometric models are given for a few different plume abatement tower geometries.

A theoretical model is developed with which the thermal performance of hybrid towers can be predicted. This theoretical model makes use of adapted wet and dry cooling tower theories. A computer program was developed to determine the thermal performance of a parallel path air flow and series path water flow rectangular hybrid tower. A sample calculation of the hybrid tower solution, in which the converged values are used, is given.

A wet cooling tower fill for use in the hybrid tower was tested, from which correlations for the transfer characteristics and the pressure drop coefficients were generated. Sample calculations to show how the transfer characteristics and the pressure loss coefficients were obtained from the experimental data are given. The Chebyshev method of numerical integration, that was used to determine the transfer characteristics, is discussed. A method for determining a more appropriate and accurate pressure loss coefficient is derived.

Experiments were done on cylindrical and rectangular model cooling tower sectors to determine the size of the inlet circulation areas. Correlations with which the size of the ineffective fill area in wet cooling towers can be predicted were obtained from the experimental data.

Keywords: Hybrid cooling towers, Plume abatement, Fill performance prediction, Ineffective fill area

SAMEVATTING

Verskeie nat/droeë en droeë/nat koeltoring konfigurasies is bespreek en die voor en nadele van afsonderlike en gekombineerde (hibriede) torings is beskou. 'n Studie is gemaak van bestaande hibriede torings.

Modelle om die vorming van sigbare pluime te voorspel is ondersoek, en die psigrometrie agter die vorming van sigbare pluime word bespreek vir 'n paar hibriede koeltoring geometrieë.

'n Teoretiese model is ontwikkel om die termiese vermoeë van 'n hibriede koeltoring te voorspel, asook die vermoeë van die toring om pluimvorming te voorkom. In die ontwikkeling van hierdie model is van bestaande nat en droeë koeltoring teorieë gebruik gemaak. 'n Rekenaar program is ontwikkel om 'n parallele lugvloei, serie watervloei, reghoekige hibriede toring se verkoelingsvermoeë te bepaal, en 'n monsterberekening van die program se finale iterasie tydens so 'n oplosproses is gegee.

'n Nat koeltoring pakking vir gebruik in die hibriede toring is getoets, en korrelasies vir die bepaling van die pakking se oordrags (warmte en massa) karakteristiek en drukverlies koeffisient tydens verskillende bedryfstoestande is opgestel. 'n Monsterberekening is gedoen om te wys hoe die pakkingsdata verwerk is om die verskillende oordrags karakteristieke en drukverlies koeffisiente te bepaal. Die Chebyshev numeriese integrasie metode om die oordrag (warmte en massa) deur so 'n pakking te bepaal is ondersoek. 'n Metode om 'n drukverlies-koeffisient te bepaal waarmee die drukverlies deur die pakking meer akkuraat voorspel kan word is ontwikkel.

Toetse is gedoen om die grootte van die lug sirkulasiearea deur die bundels van ronde en reghoekige model koeltoringseksies te bepaal. Vanaf hierdie resultate is korrelasies opgestel wat gebruik kan word om die grootte van die oneffektiewe pakkingsareas in koeltorings te voorspel.

Sleutelwoorde: Hibriede koeltorings, Pluimvorming, Pakkings karrakteristieke, Oneffektiewe pakkingsareas

ACKNOWLEDGEMENTS

The author would like to thank the following persons and institutions for their assistance and/or contributions during the course of this study:

- My thesis supervisor Prof. D.G. Kröger for his guidance and support.

- The Foundation for Research and Development and the University of Stellenbosch for their financial support.

- My family and friends for their support.

TABLE OF CONTENTS

NOMENCLATURE

Symbols

a	Surface area per unit volume; Constant	m^2/m^3 or [-]
A	Area	m^2
b	Constant	[-]
C	Heat capacity	J/Ks or kg/s
C_r	Heat capacity ratio	[-]
C_D	Drag coefficient	[-]
c_p	Specific heat	J/kgK
D	Diffusivity of water vapour in air	m^2/s
d	Diameter	m
e_f	Surface effectiveness	[-]
f_D	D' Arcy friction factor	[-]
F	Force	N
h	Heat transfer coefficient	W/m^{2}K
h_d	Transfer coefficient for enthalpy transfer in wet section	kg/m^{2}s
g	Gravitational acceleration	m/s^2
G	Mass flux	kg/m^{2}s
H	Height	m
i	Enthalpy	J/kg
k	Thermal conductivity	W/mK
K	Pressure loss coefficient	[-]
L	Length	m
m	Mass flow rate	kg/s
n	Rotational speed; Number	rpm or [-]
NTU	Number of transfer units	[-]
p	Pressure	N/m^2
P	Pitch; Power	m or W

Q	Heat transfer rate	W
Ry	Characteristic flow parameter	m^{-1}
r	Radius	m
s	Tip clearance	m
t	Thickness	m
T	Temperature	K or °C
U	Overall heat transfer coefficient	W/m^{2}K
v	Velocity	m/s
V	Volume flow rate	m^3/s
W	Width	m
w	Humidity ratio of air	kg vapour/kg dry air
z	Height above reference level	m

Greek Symbols

α	Angle; Energy correction factor	degrees
δ	Berman's correction factor	J/kg
ε	Effectiveness	[-]
Ω	Air/vapour density correction factor	[-]
η	Efficiency	[-]
μ	Dynamic viscosity	kg/sm
ξ	Temperature lapse rate for saturated air	K/m
π	Pi	[-]
ρ	Density	kg/m^3
σ	Surface tension	N/m
ϕ	Constant	[-]

Subscripts

a	Dry air; Air side
av	Air/vapour mixture where property is calculated per kilogram mixture
atm	Atmospheric

c	Contraction
ct	Cooling tower inlet
d	Droplet; Dry
D	Drag
de	Drift eliminators
dif	Diffuser
e	Exit; Effective; Evaporative
f	Fin
fi	Fill
fs	Fill supports
fr	Frontal; Fin root
ft	Fin tip
fan	Fan
fdis	Fan discharge
fsuc	Fan suction
h	Related to heat transfer
he	Heat exchanger
i	Inlet; Based on the inside
il	Inlet louvers
ir	Inlet rounding
l	Leakage: Longitudinal
m	Mean
ma	Air/vapour mixture where property is calculated per kilogram dry air
me	Mixing elements
max	Maximum
min	Minimum
mfan	Model fan
n	Nozzle
na	Noise attenuator elements
o	Outlet; Based on the outside

p	Related to pressure change; Per pass
s	Saturated; Tower wall
sp	Spray zone
$sfan$	Specified fan
t	Transversal; Tip; Tube, Total
v	Vapour
w	Water; Wet
wb	Wet bulb
wd	Water distribution system
r	Root
ref	Referred value
rz	Rain zone
ts	Tower supports
z	Height z

Superscripts

*	Based on the static pressure drop where momentum effects are excluded

Dimensionless groups

Nu	Nusselt number	$\frac{hd}{k}$
Pr	Prandtl number	$\frac{\mu c_p}{k}$
Re	Reynolds number,	$\frac{\rho v d}{\mu}$

CHAPTER

ONE

INTRODUCTION

From spraying ponds to hybrid towers - Evolution of the cooling tower

It is known from the second law of thermodynamics that energy cannot be destroyed, and that all spontaneous processes are to some extent irreversible. During these irreversible processes there is a degradation of energy, of which heat is the lowest attainable form. Heat is actually a very useful form of energy, but its usefulness declines as its temperature decreases. Below a certain temperature, that differs for various industries, heat turns from a resource into a waste product, and this waste heat has to be disposed of in some or other way. The atmosphere and the hydrosphere have up to now been the most convenient media for removing waste heat. After absorbing the heat these media radiate it back to space, from where it originally came as radiation energy from the sun. Cooling towers are mostly used to transfer the waste heat back to the atmosphere, and once-through cooling methods are used to transfer the waste heat to the hydrosphere. Figure 1.1 gives a schematic layout of the different cooling systems that can be considered in the power generating industry.

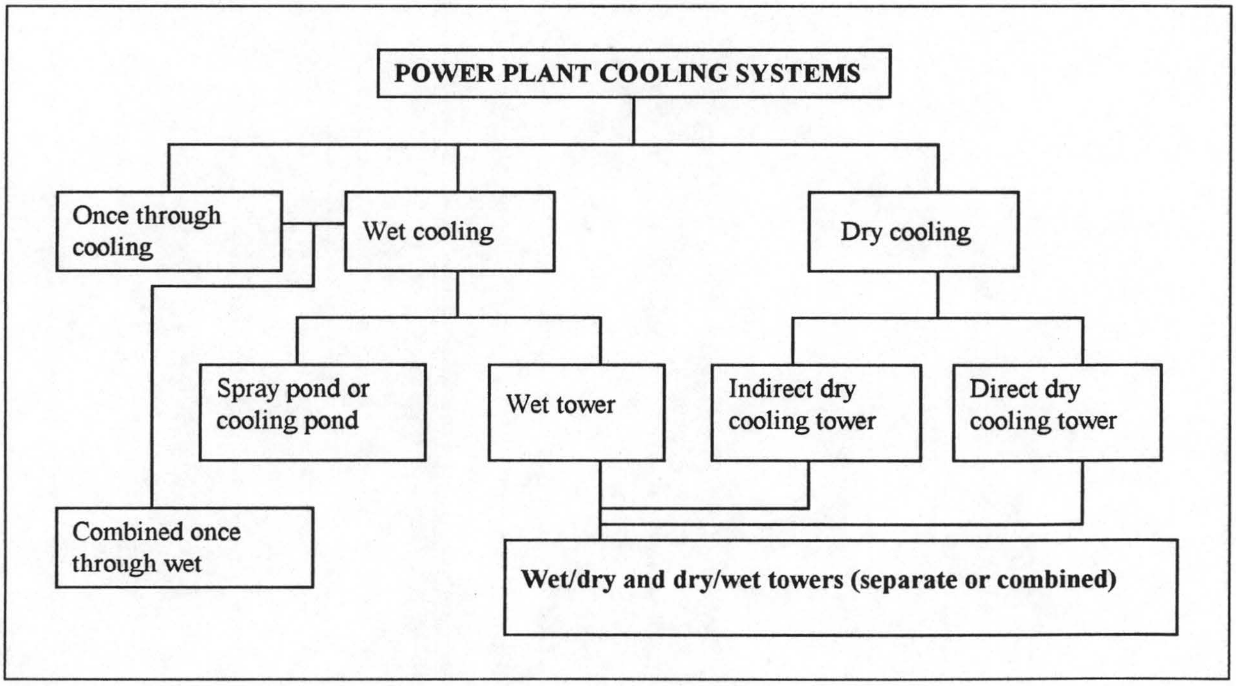

***Figure 1.1**: Power plant cooling system options.* [91SZ1]

With once-through cooling, water from a river, lake or the sea is brought into close contact with the heated substance by means of a condenser or heat exchanger and the waste heat is thereby transferred to the cooling water by means of conduction and convection. The heated water is then dumped back into the source. This method of cooling can have detrimental effects on the environment, because of the abnormal heating of the aquatic environment, especially if a river or lake is used as the source for the cooling water. Where the cooling requirement is close to the sea once-through cooling is still most often used. In regions where these cooling water sources did not exist cooling towers started to appear and they evolved from the earliest spraying ponds to the hybrid towers of today.

During the early seventies the world became more conscious of the environment and once-through cooling methods that were used extensively until then were becoming increasingly unpopular, especially where lakes or rivers were used as the cooling source. Wet cooling towers gradually started to replace once-through cooling systems. With wet cooling towers cooling is accomplished by the evaporation of water that is brought into direct contact with the atmospheric air over a large area, and to a lesser extent by the sensible energy transfer from the water to the air. Approximately 1 to 2 per cent of the cooling water evaporates during the cooling process. This implies that these cooling systems have a relatively high water consumption rate and are not practical in regions where water shortages occur or where water is expensive. To solve this problem dry cooling systems were introduced.

Dry cooling makes site selection of power plants and industrial works independent of water availability. Since areas containing coal and other fuel deposits are often short of water, dry cooling makes it possible to set up pithead power generating plants in such areas. Another advantage of using dry cooling towers is that since they emit only warm and clean air they have nearly no adverse effect on the environment. Dry cooling systems, however, have a very high capital outlay, are very large structures and on warm days are subject to a considerable reduction in cooling capacity. This led to the idea of a dry/wet system to bring down capital costs and to decrease the water consumption rate, while still allowing the cooling system to maintain its ability to reject heat on warm days. This kind of system can consist of a dry tower with one or more wet auxiliary towers, known as dry/wet-peaking systems, or the dry and wet sections can both be combined in the same tower, known as a dry/wet hybrid tower. The wet section of a dry/wet cooling system is usually used during periods of warm ambient temperatures to keep the cold water temperature from rising above the system's design cold water temperature, or they can be used to improve the efficiency of the system at times when water is abundant.

A problem with wet cooling towers that has received increasing attention in recent years is that of plume formation. In some densely populated countries where power stations and other industries have to be built near inhabited areas, the plume that rises from wet cooling towers is a matter of concern. When ambient air passes through a wet cooling tower the air absorbs water vapour as it removes latent heat from the hot cooling water. This causes the air to become very humid as it passes through the fill. As the air is discharged into the atmosphere it is cooled by the cooler atmospheric air and also as a result of the natural temperature lapse that occurs. This cooling of the humid plume air causes the water vapour in the plume to condense out of the plume air and to form a cloud of small water droplets, known as a visible vapour plume. On rising, the evaporation of droplets from the edge of the plume, further increases the rate and amount of cooling, causing more drops to form inside the plume. The plume thus becomes denser than the atmospheric air and as it moves downwind it edges towards the earth. Visible plume formation is often condemned and some of the negative aspects of visible plumes are:

- The plumes can produce a visibility hazard, especially if highways or airports are situated nearby, and icing on roads and landing strips can further increase the hazard.
- Corrosion of nearby steel structures may occur as a result of condensate from the plume.
- The vapour plumes are classified as visual pollution and produce shading (of gardens, houses, farming areas, etc.) from the sun, particularly in the prevailing downwind direction.
- Because of the visible plumes they produce and their size, wet cooling towers are perceived as a symbol of the negative impact of the power industry on the environment, particular by the media.

In many of the regions where these problems occur, wet/dry cooling towers became a popular option because of the capability of such towers to inhibit plume formation. In these towers, the combination of evaporative and dry cooling results in a lower humidity ratio for the air leaving the tower and this inhibits visible plume formation to a certain extent. The lower height of these structures is also visually more appealing to people living in close proximity. These specific wet/dry towers are also known as hybrid towers, because of the combination of both the wet and dry units in a single tower structure. The dry part is usually small and is mainly used to change the humidity ratio of the exhaust air so that plume formation is inhibited.

All these factors contributed to hybrid cooling towers becoming a subject of renewed interest in the 1980’s early 1990’s. Hybrid towers are already widely used in Europe and in Germany where they have been used for the past 20 years, the world's largest hybrid cooling tower has been in operation since 1988. [92AL1] The tower installed at the 1300 MWe Neckarwestheim nuclear power station, is situated in a wine growing area and it was therefore important to avoid the shading effects of the plume. Although hybrid cooling is rare in the UK it is gaining popularity there as well. According to Isles [94IS1] the majority of new power stations planned for the UK will be adopting hybrid technology.

It should be noted that if the main purpose of the dry part of a combined cooling system is to reduce plume formation, the system is classified as a wet/dry system, as opposed to the dry/wet system where the purpose of the wet part is that of supplementing the dry part during warm periods.

In this study a theoretical model is developed to determine the performance of a specific design wet/dry hybrid tower. This tower consists of separate wet and dry sections combined in one structure (hybrid) and is a parallel path air flow (PPAF) series path water flow (SPWF) design. In Chapter 2 the different wet/dry and dry/wet tower designs will be discussed in more detail and some existing towers will be considered.

CHAPTER
TWO

WET/DRY AND DRY/WET TOWERS

2.1 Classification of dry/wet and wet/dry systems

For every cooling requirement there is a unique cooling tower arrangement to optimally satisfy the cooling needs. In the search for this optimum cooling tower every possibility has to be considered, including all possible wet/dry and dry/wet systems. The wet/dry and dry/wet systems can consist of two separate towers for the wet and dry sections, or the wet and dry sections can be built into one structure, known as a hybrid tower. The separate systems can have series or parallel water flow paths while the hybrid towers can have series or parallel air and water flow configurations. A schematic classification of the different wet/dry and dry/wet systems is given in figure 2.1.

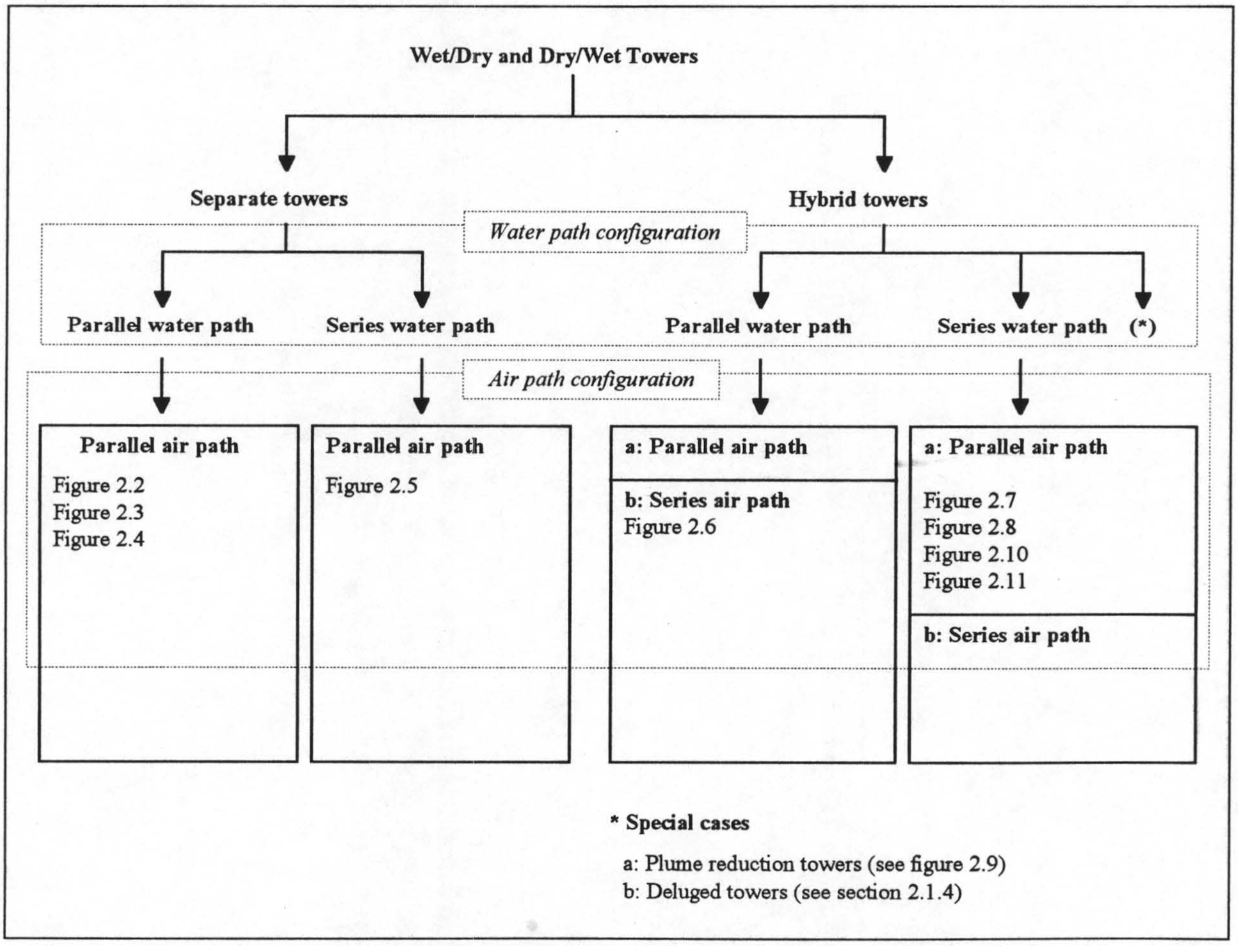

***Figure 2.1**: Schematic classification of the different Wet/Dry and Dry/Wet towers.*

Since both the hybrid as well as the separate tower configurations can have series or parallel water flow arrangements, such water flow arrangements will be discussed simultaneously for both these tower configurations in section 2.1.1. In sections 2.1.2 and 2.1.3 the different tower configurations will then be discussed, together with the different air flow arrangements.

2.1.1 Different water flow configurations

The *parallel path water flow configuration* (PPWF) can have two completely separate water circuits for the wet and dry sections, as shown in figure 2.2 for the separate tower design with a divided condenser, or the cooled water of both sections can be mixed before it goes to a common condenser, as shown in figure 2.4. It is also possible to feed the dry part with steam that is bled directly from the low pressure side of the turbine, as shown in figure 2.3. In this way the mean temperature difference of the air and the water through the dry section is kept as high as possible and it therefore operates more effectively.

In the parallel path water flow configuration where the condenser is divided, the dry section's water circuit is completely isolated and the water which flows in this circuit can be treated to make it non-corrosive. The heat exchanger tubes can therefore be manufactured from relatively low cost materials like mild steel. This is usually the best option in dry/wet cooling towers where the dry section is large and therefore has a high capital cost.

In the *series path water flow configuration* (SPWF) as shown in figure 2.5 for a separate tower design and in figures 2.7 and 2.8 for hybrid tower designs, cooling water first passes through the dry section and then through the wet section. It would be impractical to pass the water through the wet section first, because the dry section must always have the highest possible mean temperature difference through it. It has to be remembered that the dry section has a theoretical cooling limit equal to the dry bulb temperature while the wet section's cooling limit is the wet bulb temperature. As the water exits the dry section it is passed over the fill from where it is pumped back to the condenser. This is an open water system and since the water that passes through the dry section may cause corrosion, the dry heat exchangers have to be manufactured from high quality corrosion resistant materials like stainless steel, copper-nickel alloys or plastic. Heat exchangers manufactured from stainless steel and copper-nickel alloys are very expensive and are usually only economically viable in wet/dry cooling towers where the dry cooling section is relatively small. Gilbert [78GI1] states that although the thermal properties of plastic heat exchangers are distinctly less favourable than those made of stainless steel or copper-nickel alloys, plastic materials display considerable advantages with respect to corrosion and cost.

2.1.2 Separate tower configurations

The different separate wet/dry and dry/wet tower arrangements their advantages and disadvantages and their economics are discussed by various authors. Only an overview of the different tower arrangements is given in this section.

Separate towers are mostly of the dry/wet type where the purpose of the tower combination is to conserve makeup water and to maintain a low turbine back pressure when the atmospheric dry bulb temperature is too high for the dry part to cool the water sufficiently. In dry/wet systems the dry tower operates all year round and does the most work during the cooler weather, while the wet tower operates during warm weather, mostly during the summer. The advantages of the separate tower system over the combined system are the following: [75LA1] [76LA1] [76SM1] [77SM1]

- The separate tower arrangement is a simple and straightforward solution where two well known time proven systems are combined, while the single structure wet/dry tower with common fans does not allow the complete freedom of design and optimisation that the individual pieces of equipment do.
- Complete separation of the wet and dry systems prevent the heat exchangers and other components of the dry section from corroding or becoming clogged because of the dirt and drift from the wet section's air stream.
- It simplifies air flow control problems, compared to single fan hybrid towers, by eliminating the need for louvers or air damper doors since the wet tower is usually either operating or not. If both towers are of the mechanical draft type air flow can be controlled by the separate fans in the wet and the dry sections.
- Wet cooling tower icing problems are eliminated since the wet tower would normally not be operating in cold weather.
- Existing systems can easily be upgraded by simply adding the other system.
- Noise problems which can occur in hybrid towers because of the variable louvers and air damper doors are eliminated.

A computer program to optimise the performance of separate dry/wet towers was written by Brown et. al. [76BR1]. This program includes procedures to optimise dry/wet operation, provide estimates of water consumption over a year's operation and to identify the dry/wet tower arrangement that would yield the minimum total cost for a given water consumption. Conradie [93CO1] also wrote a computer program to determine the thermal performance of a separate dry/wet tower system.

The different configurations which are shown in figures 2.2 to 2.5 will now be discussed briefly. A comparison between the cooling systems shown in figure's 2.2, 2.4 and 2.5 is given by Smith [76SM1] [76SM2], while Von Cleve [75VO1] gives a comparison between ten different cooling tower arrangements, including dry and dry/wet systems. The possibilities regarding the cooling water supply to the wet and dry towers were already discussed in section 2.1.1. Although all the towers shown in figures 2.2 to 2.5 are induced draft towers it is only for illustrative purposes that induced draft towers were selected and natural draft or forced draft towers can also be used.

For the configuration shown in figure 2.2 the heat exchangers for the dry tower's water circuit can be made of relatively cheap mild steel tubes since the dry section's water circuit is closed and the water can therefore be treated to become non-corrosive. On the other hand the cost of the system is increased by the more expensive split condenser and duplicated water piping layout. Since both the wet and the dry sections receive hot water directly from the condenser the wet section has a higher cooling range than the wet section of a SPWF tower and the water flow is therefore less for a given heat load. Separate pumps are needed for the water circuits of the wet and the dry sections.

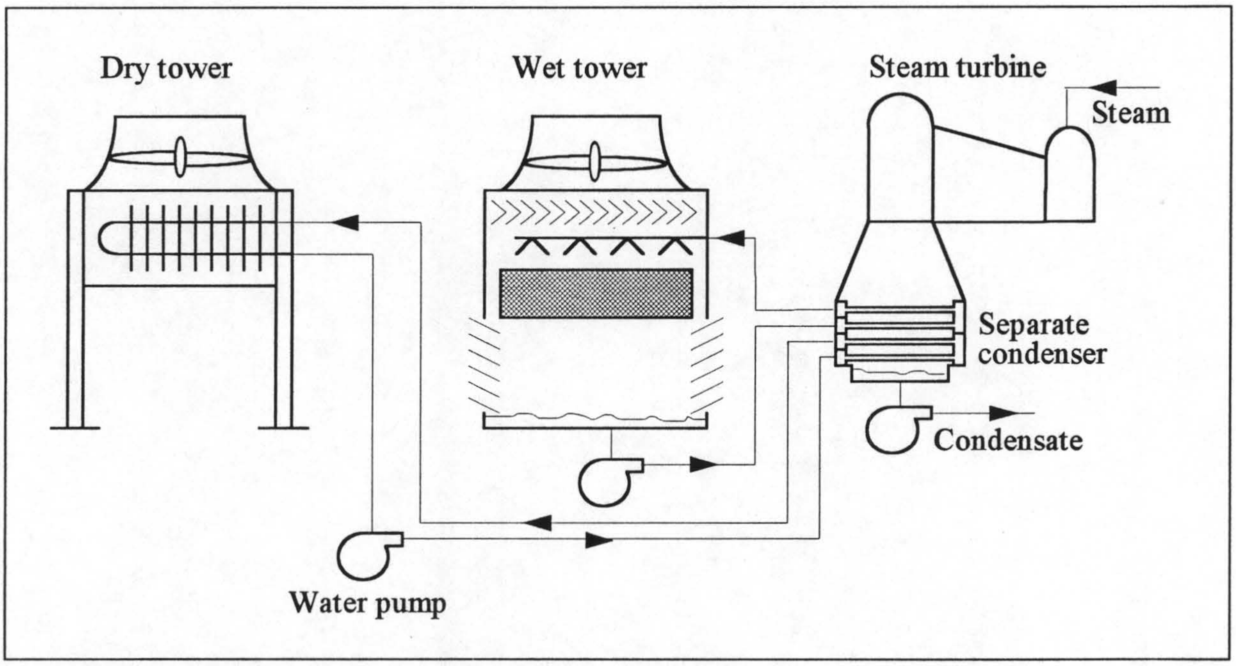

Figure 2.2: *Parallel water circuits with indirect dry cooling.*

The cooling system of the configuration shown in figure 2.3 works at a higher efficiency than the dry cooling systems used in the other configurations since the approach temperature difference for the dry tower is maximised by using direct dry cooling of the steam. The condenser for the configuration shown in figure 2.3 is not as expensive as that of the indirect dry cooling system but the thicker piping, leading from the turbine to the heat exchanger, increases the cost of the system.

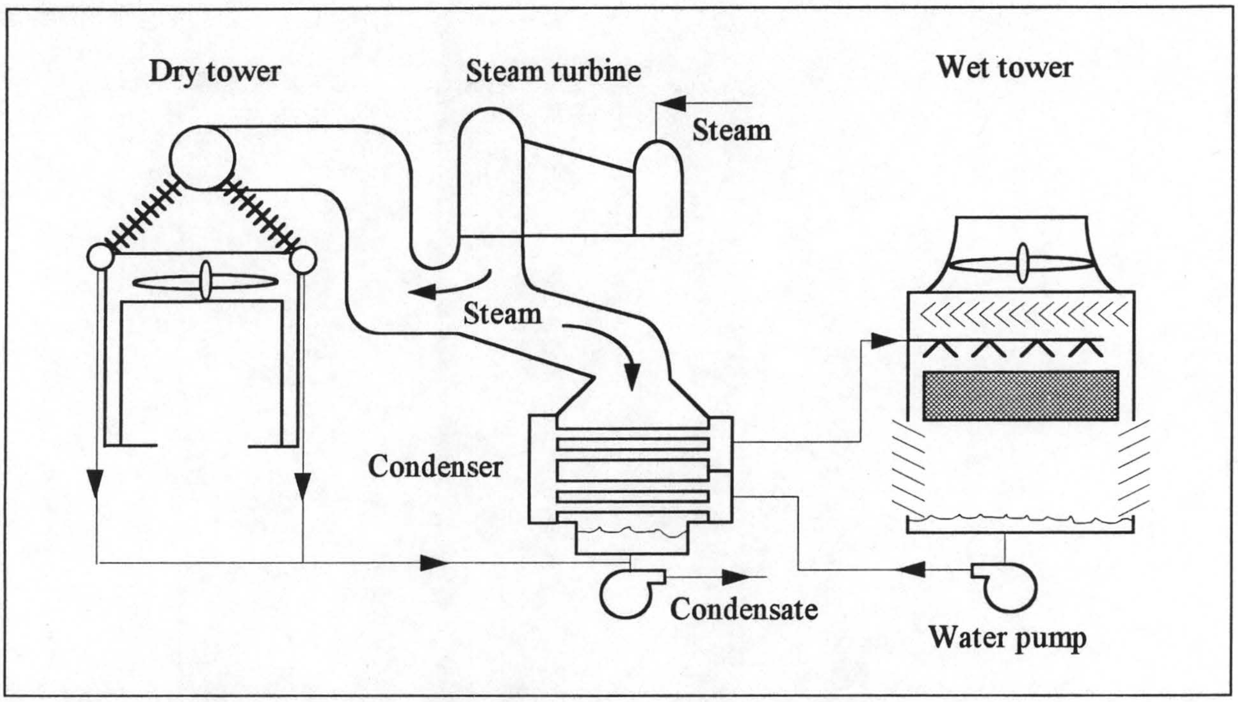

Figure 2.3: *Parallel water circuits with a direct air-cooled condenser.*

For the configuration shown in figure 2.4 the water from the two cooling towers is mixed in the water basin before it is pumped to a common condenser. The temperature of the cold water is not as low as for the series path water flow configuration shown in figure 2.5, since the water from the dry tower can only approach the ambient dry bulb temperature and the mean mixed water temperature is therefore higher. The water circuit is open and therefore the heat exchangers have to be manufactured from corrosion resistant materials. As already stated in section 2.1.1, this is usually not a viable option if the dry part is large because of the high cost of corrosion resistant metals and the poor conductive properties of plastic.

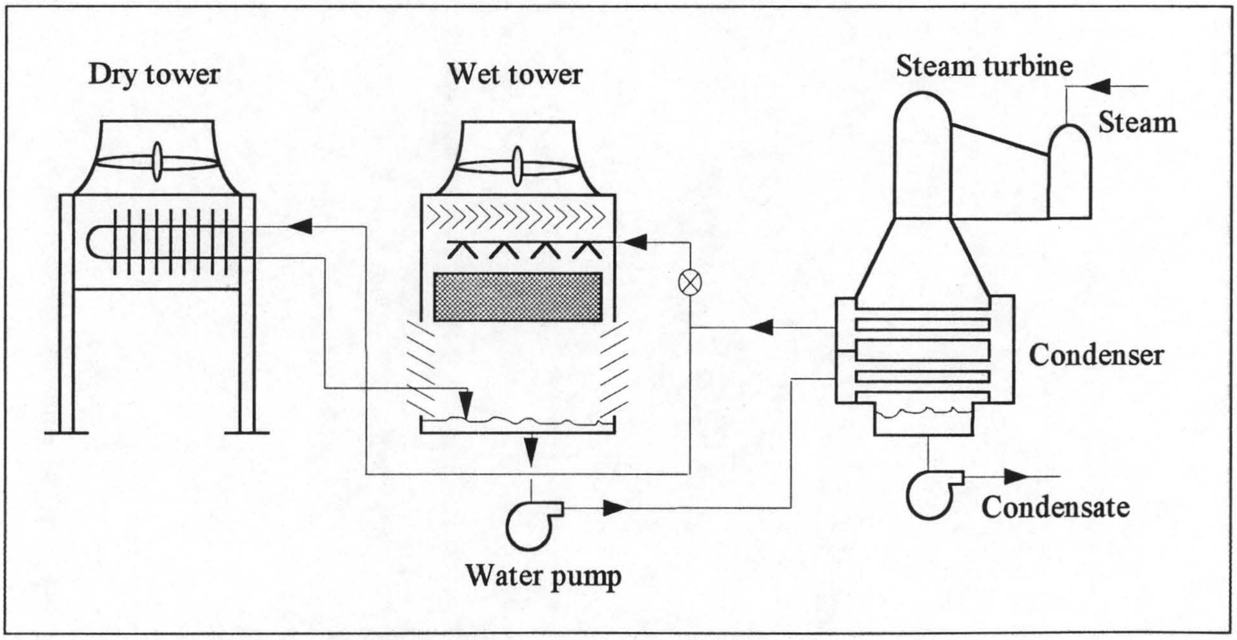

Figure 2.4: *Parallel path water flow with common condenser.*

In figure 2.5 a series path water flow configuration is shown. The water circuit is again completely open and the heat exchangers have to be manufactured from expensive non-corroding materials. The water first passes through the dry tower in order to keep the mean temperature difference through the dry section as high as possible. The amount of water that is passed through the wet section is controlled by means of a bypass valve system, in order to be able to control the amount of evaporative cooling. According to Lefevre [84LE1] this is the best arrangement for a separate dry/wet tower combination.

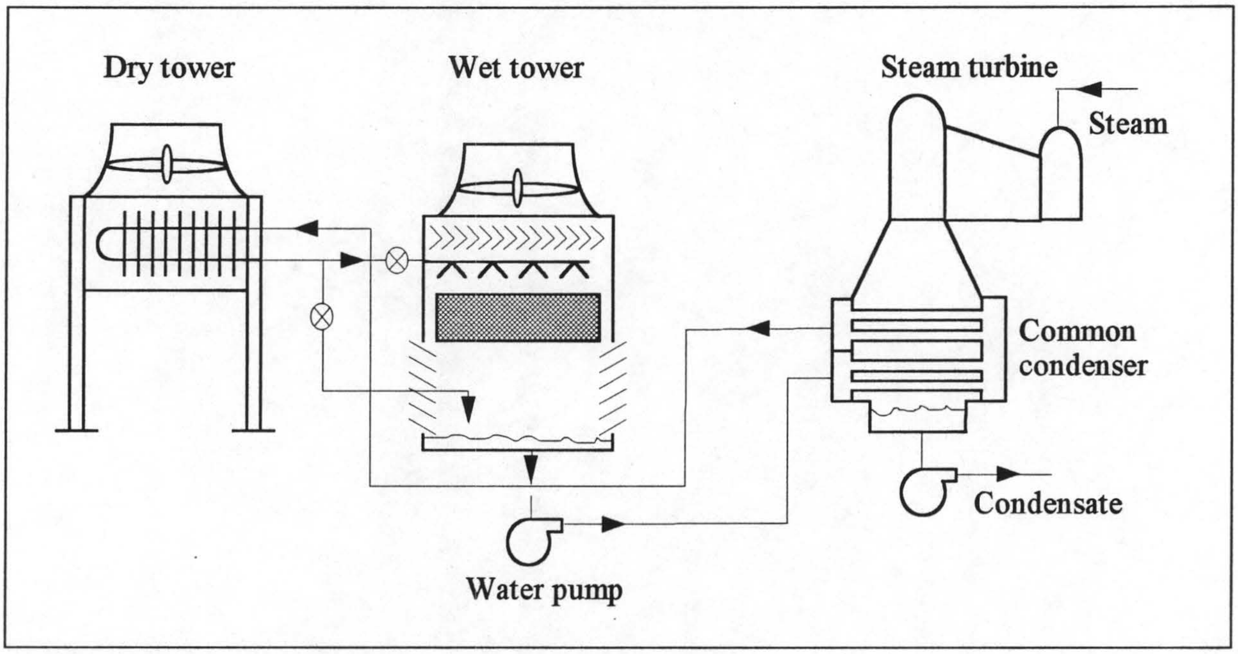

Figure 2.5: *Series path water flow with common condenser.*

2.1.3 Hybrid towers

A tower incorporating both dry and wet cooling systems in the same structure is known as a hybrid tower. The main advantage of incorporating both the wet and the dry cooling systems in the same tower is that it makes visible plume abatement possible. Another advantage of this kind of tower compared to an all-wet tower is the decrease in water consumption per MW of heat dissipated. This decrease in water consumption varies according to the amount of heat dissipated by the dry part of the tower. Hybrid towers can be of the wet/dry or dry/wet type while, as previously stated, separate tower systems are mostly of the dry/wet type.

It is possible to categorise hybrid towers as having either a parallel or series air flow and a parallel or series water flow configuration. Since the different water flow configurations were already discussed in section 2.2, only the different air flow configurations will now be investigated.

Series path air flow (SPAF) hybrid towers

Hybrid towers with series air flow arrangements employ dry sections either preceding or following the wet section. Figure 2.6 shows a series air flow hybrid tower where the dry section precedes the wet section. The series path air flow arrangement has the advantage of being of simple design and having a low total tower height.

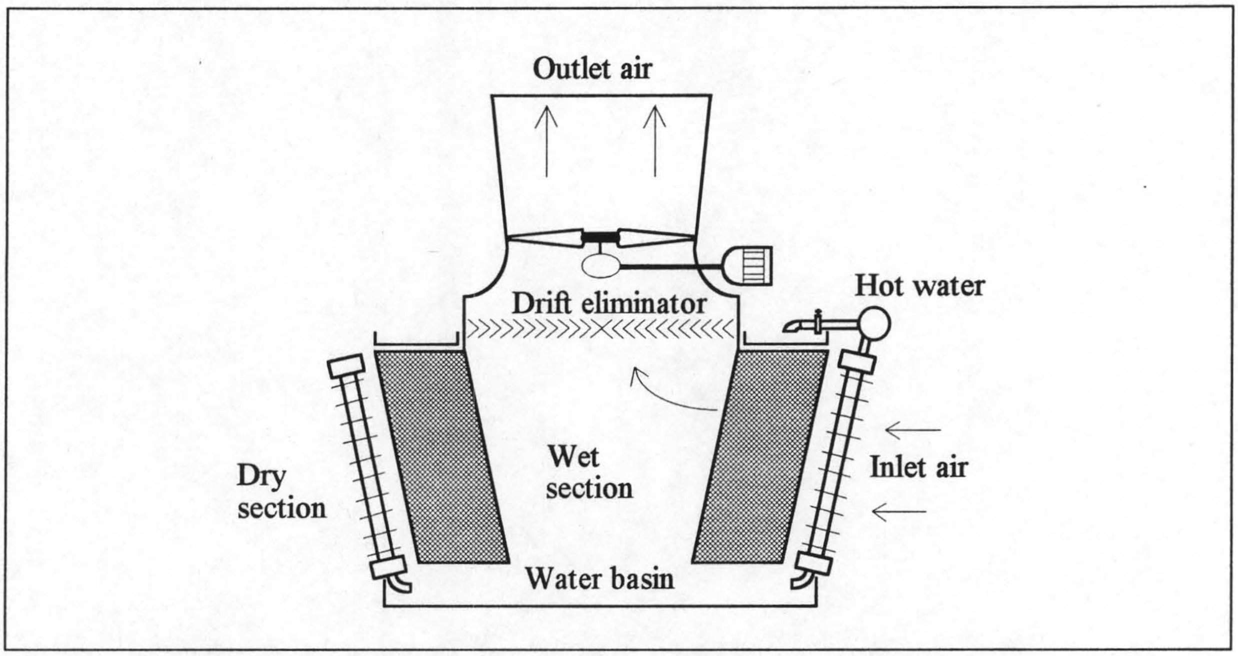

Figure 2.6: *Series air flow hybrid tower with dry section preceding the wet section.*

In the series path air flow tower the air flow through the dry and wet sections cannot be controlled separately. Because of this the optimum air flow rate for both sections cannot be achieved simultaneously and therefore plume abatement cannot be optimally controlled. Another drawback of the series air flow design is that the heat exchangers are always present in the air stream, thereby increasing the pressure drop through the tower whether or not plume abatement is required.

The tower design where the *dry section precedes the wet section*, as shown in figure 2.6, is in some respects a better option than the configuration where the heat exchangers are situated behind the fill. In this configuration the drift from the wet fill is directed away from the dry heat exchangers and therefore corrosion and clogging of the heat exchangers are not nearly as extensive as in the configuration where the dry section follows the wet section. Another advantage of this configuration is that the ambient air first comes into contact with the dry section providing it with cooler air and a higher average temperature difference therefore exists. The problem with this design, however, is that only a small amount of heat must be dissipated in the wet section otherwise the air will still become saturated and plume abatement will not be achieved. Only a prototype installation of this kind is known to exist. [93LI1] This prototype is situated at the Cliffside power station of the Duke Power Company in the USA.

For the case where the *heat exchangers are situated downstream of the fill* the temperature difference between the water and the air in the dry section will generally be too small to give sufficient heat to the air stream to prevent visible plume formation. Disadvantages of this design can be summarised as follows:

- Deposition of dissolved solids contained in the drift from the wet section occurs on the dry heat exchangers. This deposition causes clogging of the heat exchangers which leads to a reduced efficiency of the dry section.
- Corrosion of the dry section because of the drift from the wet section.
- A reduced driving potential for heat rejection in the dry section, since the warmer air that leaves the wet section causes a reduced average temperature difference in the dry section.

A potential advantage of the series air flow arrangement where the dry heat exchangers are situated after the fill is that the tower can be operated with a process fluid other than the circulating water in the heat exchangers and because the air is preheated after it leaves the wet section there is little or no risk of freezing. [78KU1] Potential application of this system would be in an electric power station where the dry part of the cooling tower is fed with steam that is bled directly from the low pressure side of the turbine. In this way a high average temperature difference will still exist in the dry section even though it receives warm air from the wet section.

In general the series air flow tower is not a very effective design for plume abatement and is suited for plume abatement only when there is an auxiliary fluid or steam, at a higher temperature than the main cooling water, that can be cooled in the dry section.

Parallel path air flow (PPAF) hybrid towers

Three different parallel path air flow series path water flow hybrid tower configurations can be seen in figures 2.7 and 2.8. Configurations where the water circuits are parallel can also be found but are less common. In the parallel path air flow series path water flow arrangements the hot water first passes through the dry section where it is cooled by a fraction of the total cooling range and is then passed through the wet section. In this kind of tower ambient air is directed over both the dry and the evaporative sections, resulting in a relatively low pressure drop on the air side. Both sections benefit thermally by receiving the cooler ambient air, with the wet and dry air streams mixing after exiting their respective sections.

The mixing of the two air streams in a PPAF hybrid cooling tower can be accomplished by the generation of intense air vortices. For mechanical draft cooling towers the mixing distance in the tower shell is usually very short and mixing has to be accomplished very rapidly. With this in mind, Henning [80HE1] proposes two mixing systems namely, mixing by means of vortex generator plates and mixing by means of cylindrical vortex generators. Variable length inlet ducts from the dry section into the wet section can also be used to obtain effective mixing of the two air streams. [92AL1] [94BI1]

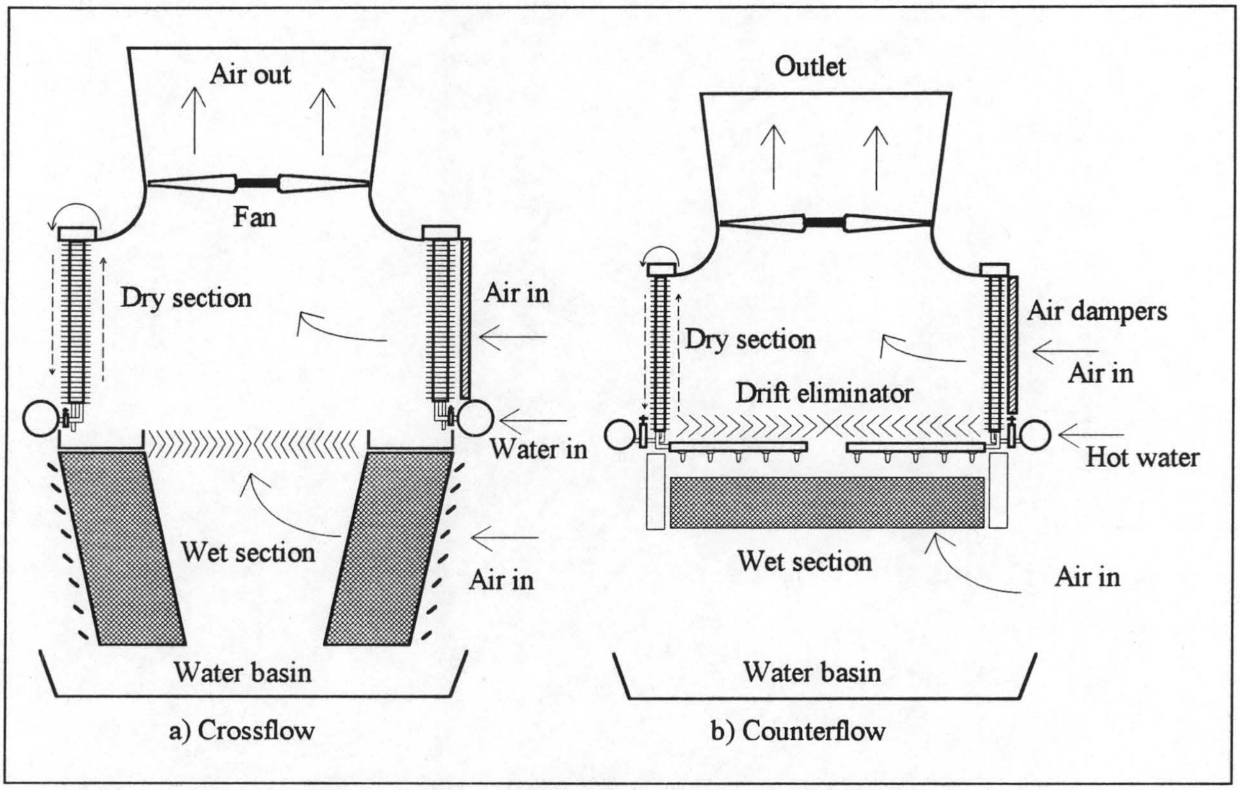

a) Crossflow b) Counterflow

Figure 2.7: *Parallel path air flow series path water flow hybrid towers.*

In contrast to the series air flow tower, the air flow through the wet and dry sections of these towers can be controlled separately through the use of adjustable louvers and/or air damper doors and the air flow rate through both parts can thus be optimised. In some instances, control of the air flow rates through the wet and the dry sections is obtained through the use of separate variable speed fans for the respective sections.

Since the wet section responds to the wet bulb and the dry section to the dry bulb temperature, the effects of changing ambient conditions on the thermal performance of both the wet and the dry sections of these towers are very complex. When the ambient conditions are favourable for plume formation more air is directed over the dry section and less through the wet section. This brings down the humidity ratio of the exit air and inhibits plume formation. In summer when the ambient temperatures are higher and the humidity of the air lower, the risk of plume formation is much less. During these warm conditions the performance of the cooling tower is also at its worst and in order to improve the tower performance more air is directed over the wet section and less through the dry section.

Increased pumping heads may occur in PPAF hybrid towers depending upon the equipment configuration. The pumping work for the heat exchangers can be minimised by using a siphon concept for vertically installed dry tubes. This siphon concept, however, places a constraint on the maximum height of the dry heat exchanger bundles since boiling in the top headers will start to occur if the bundles exceed a certain height. For large cooling towers where large dry sections are required this problem can partly be solved by sloping the heat exchanger bundles. An example of this is at the San Juan power station as described in section 2.2.1.

The most common series water path hybrid tower design has dry sections located physically above the wet sections as shown in figure 2.7. Either crossflow or counterflow cooling tower designs are used for the wet section. A crossflow arrangement is shown in figure 2.7a and a counterflow arrangement in figure 2.7b. The water leaving the dry section mostly flows into the fill of the wet section by gravity. Towers with this design are more likely to be influenced by recirculation of the hot outlet air since the inlet to the dry section is situated close to the outlet of the tower.

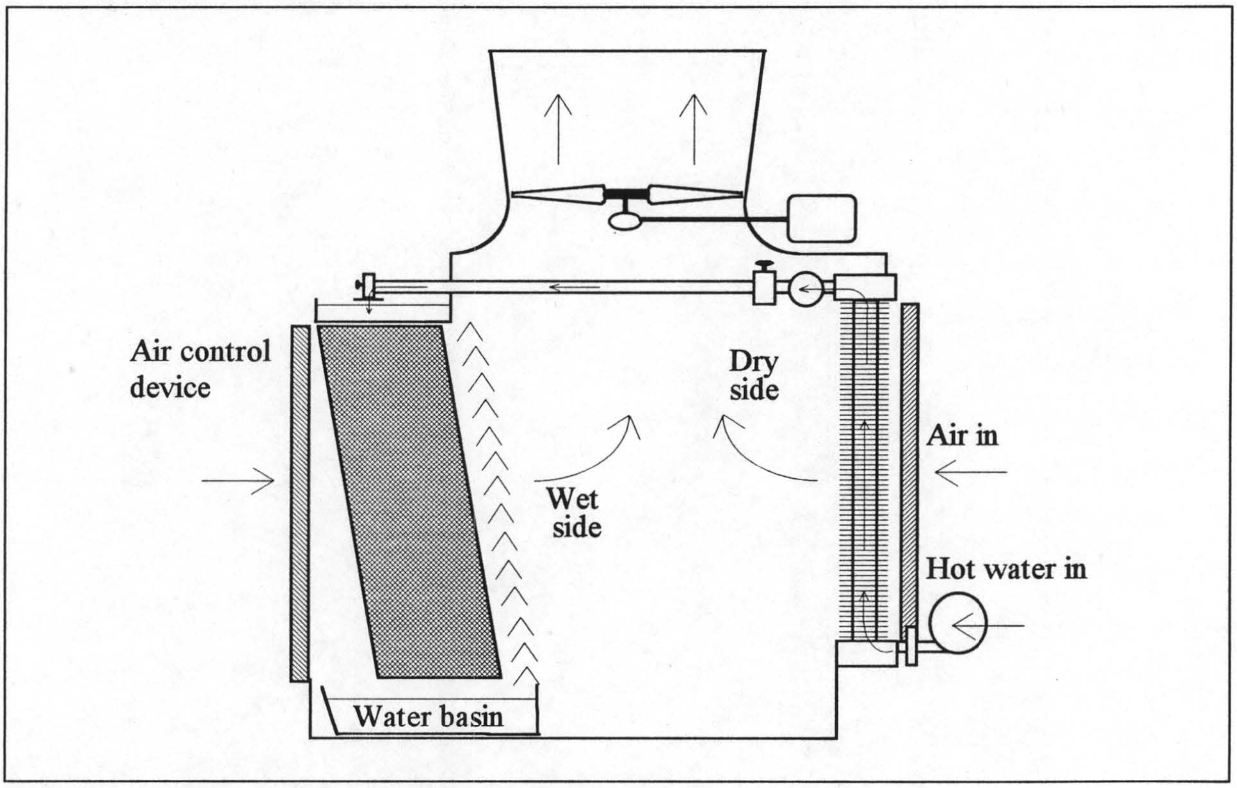

Figure 2.8: *Opposed path air flow hybrid tower.*

A variation on the design shown in figure 2.7 is shown in figure 2.8. In this tower configuration the dry section is located on one side of the tower and the wet section on the opposite side. The hot water enters the base of the dry section, rises through the heat exchanger bundles, crosses the tower plenum in piping and falls through the wet section on the other side of the tower. This variant of the series water path design is commonly referred to as an opposed path wet/dry tower. [93LI1] This arrangement is low in capital cost but results in longer towers than with the other configurations. With lower efficiency single water pass dry sections and the additional siting requirements, the opposed path hybrid tower is limited in flexibility to suit plume abatement needs. [93LI1]

Plume reduction tower [92BL1] [92BO1] [93LI1]

A particular kind of wet/dry cooling tower is the plume reduction tower. This system was originally proposed in 1978. Nearly 15 years later an enlarged fill was tested, suitable for cooling towers in power stations with some 100 MW output. [92BL1]

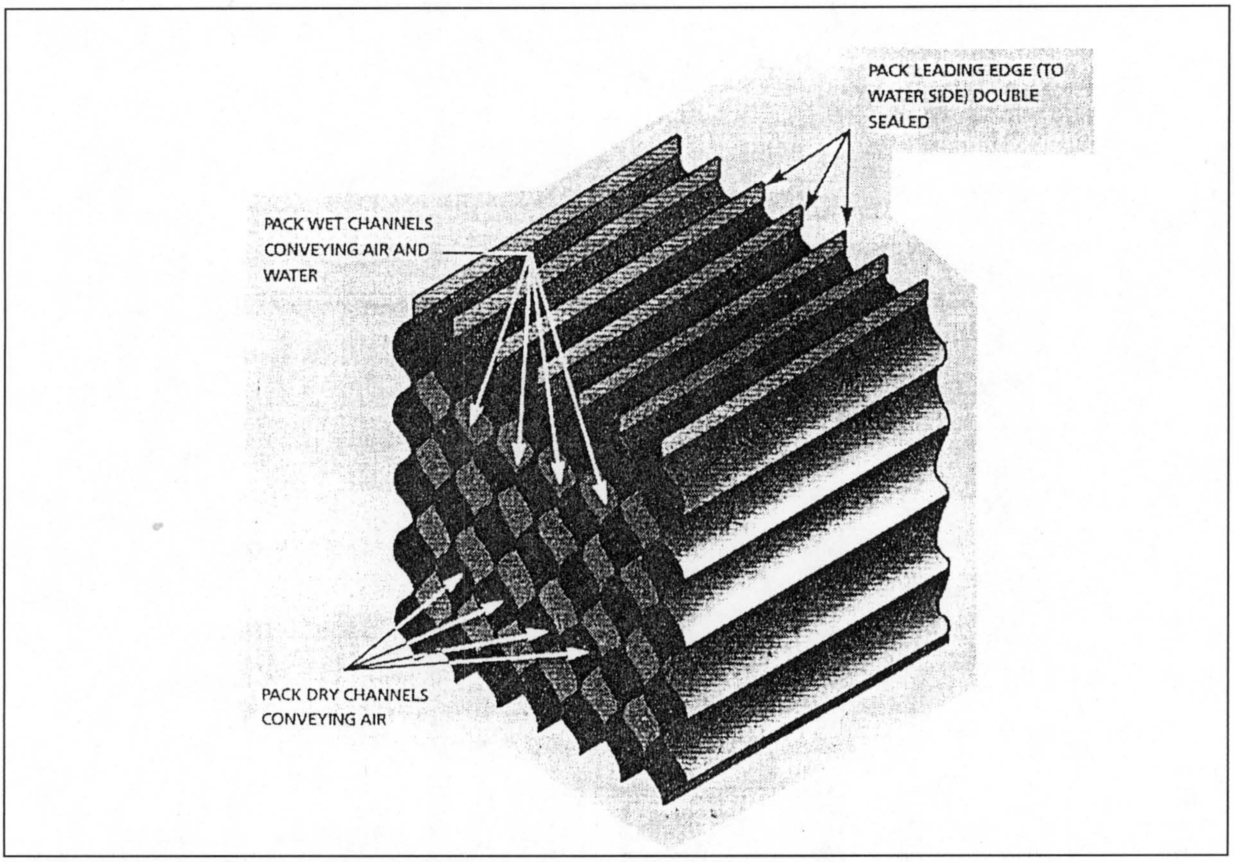

Figure 2.9: *Schematic representation of the plume reduction fill.*

This tower uses a special kind of crossflow fill which consists of wet and dry channels located side by side. The fill restricts the flow of water to alternate channels and consists of thin PVC sheets. Ambient air flows horizontally through this fill and cools the water through either wet or dry cooling, depending on which channel it flows through. The amount of plume reduction achieved by this tower cannot be controlled and is dependent on the operating conditions of the tower. Evaporative transfer occurs in 50% of the channels. The others act as dry heat exchangers where heat is transferred through the thin PVC walls from the neighbouring wet channels. A schematic representation of the fill can be seen in figure 2.9.

2.1.4 Dry/wet deluged towers

According to this concept the performance of a normally dry tower is enhanced during periods of high ambient temperatures and/or periods of high heat load by wetting the air side of the dry heat exchangers with water. This water forms a thin film over the heat exchangers, which is then evaporatively cooled by the air that flows over it. The cooled water film then cools the warmer process fluid inside the tube bundles through conduction and convection. Considerable increases in the performance of a tower can be obtained by deluging the heat exchangers, but problems with deposition on the heat exchangers and corrosion usually occur. The deluging principle is commonly practised in smaller cooling towers, known as evaporative coolers. However, this method can not be used for plume abatement purposes and is solely used to increase the effectiveness of dry heat exchangers.

A cooling tower system that uses the principle of deluging dry heat exchangers to increase tower performance and is used successfully in various cooling towers is the Heller system. [73HE1] [91SZ1] This system is described in section 2.2.7 as used in the Trakya cooling tower.

2.2 Existing wet/dry and dry/wet hybrid towers

2.2.1 The dry/wet cooling system at San Juan power station [88NO1] [93LI1]

The San Juan power station situated at Farmington, New Mexico, was commissioned in 1979. The hybrid cooling tower serving the system is shown in figure 2.10. Two of these dry/wet induced draught cooling towers serve a 500 MWe unit.

The cooling towers were designed and constructed by the Marley Cooling Tower Company Inc. They are constructed of galvanised steel with a corrugated iron casing. Each tower consists of five cells, each containing sixteen air cooled heat exchanger modules and two evaporative sections. The cooling water flows in series, first through the dry heat exchangers and then through the evaporative section. The dry sections are sloped so that the siphon loop in the tower is approximately 6 m high, allowing a comfortable margin against boiling in the upper headers of the dry heat exchangers. The tower is situated 1680 metres above sea level and the design hot water temperature is about 52 °C.

Air flows in parallel through the dry and evaporative sections of the tower. At the tower's design conditions (wet bulb temperature of 18.9 °C and dry bulb temperature of 35 °C) approximately 27% of the heat is dissipated as sensible heat. All the heat can however be dissipated as sensible heat at certain lower ambient temperatures, and at these temperatures the wet section can be completely bypassed for fully dry operation. Below the dry sections, between the wet sections, the tower has specially designed open areas to inhibit recirculation of warm air.

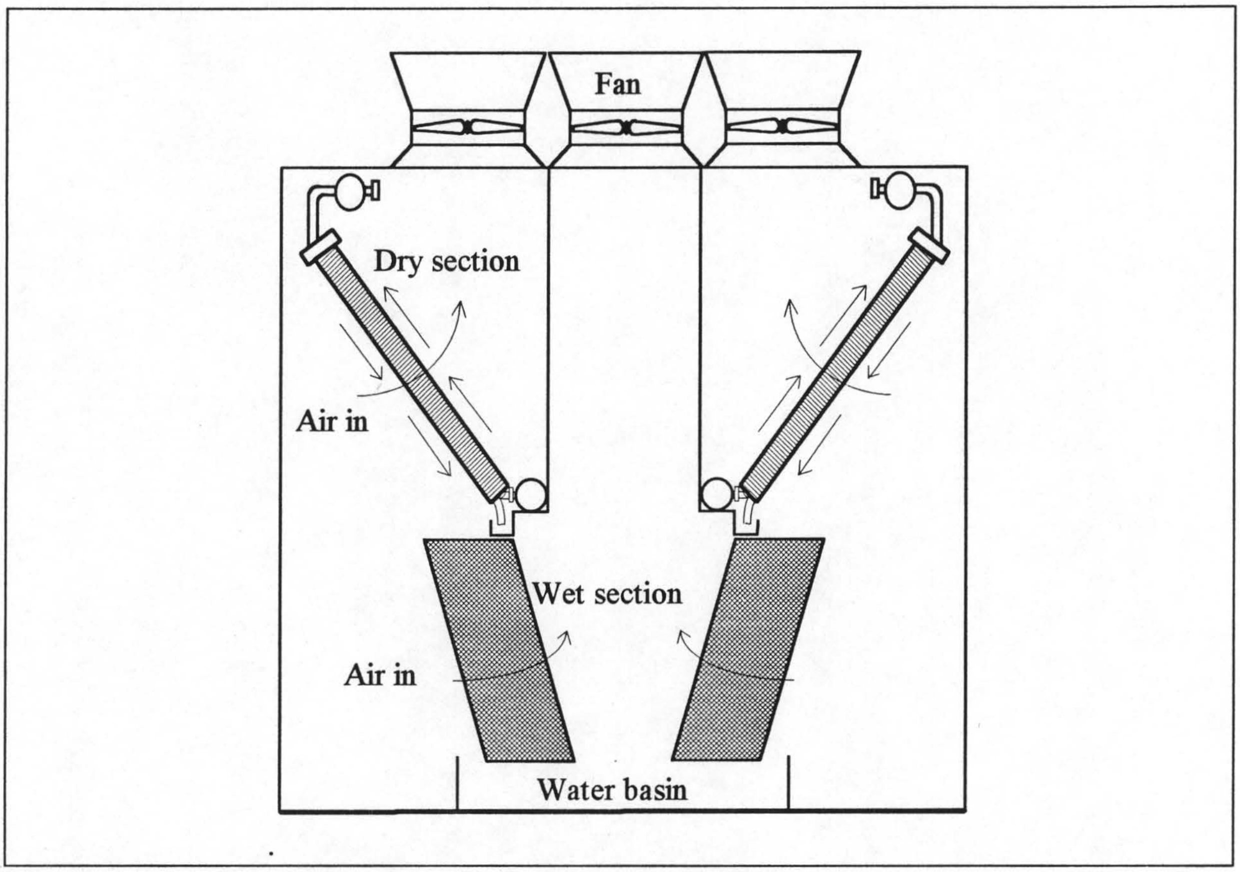

Figure 2.10: *The hybrid towers at the San Juan power station.*

Problems experienced with the system are the following:

- Corrosion and deposits due to incorrect material selection.
- Vibration of the fans caused cracks in the tower walls and loosening of the bolts and nuts.
- Because of poor maintenance service up to 15% of the fans were not operational at any one time. This caused recirculation of air through the non-operational fan ducts and this caused an outlet water temperature increase by up to 2 °C at times.
- The heat exchanger fin spacing of 1.59 mm proved to be too close causing dirt to block the air passages. Lack of provision for external cleaning of the heat exchangers together with lack of maintenance service worsened the situation.

The above problems do not disprove the correctness of the general design of the tower, but according to Nowosad [88NO1] they were rather caused by a lack of experience and show that the complexity of the system requires more preliminary studies during the design phase and better service during operation.

2.2.2 Wet/dry cooling system at Harvard power station [88NO1] [94BO1]

This hybrid tower was designed and constructed by Hamon Sobelco SA in order to reduce visible plumes and is situated in Boston, USA. This was the first plume reduction tower to be built and was commissioned in 1977.

The tower's cooling capacity is 245 MW. It consists of eight induced draft reinforced concrete cells, each equipped with a 9.1 m diameter fan. The water flow arrangement is parallel and the air flow is series. The wet section is of the counterflow type with the heat exchanger bundles situated horizontally behind them.

2.2.3 Wet/dry cooling systems at the BASF petrochemical plant [88NO1] [92BL1]

The BASF petrochemical plant is situated in Ludwigshafen, Germany. There are two hybrid towers serving the plant. The first tower which has a heat rejection capacity of 150 MW was designed and built by Hamon Sobelco SA in 1980.

The tower consists of a reinforced concrete structure containing four cells, each made up of wet and dry sections and served by a 44.5 kW fan. The cooling water flows in series, first through the dry and then through the wet sections and the air flow is parallel with mixing of the wet and the dry air prior to exit from the tower.

The dry cooling section consists of bare polyethylene tubes 16 mm in diameter and 6.4 m long. The air flow rate through the dry section is controlled by louvers while the wet cooling section is of a counterflow type. The layout of the tower is like the one shown in figure 2.7b. Although the system was built primarily for plume abatement the dry section is capable of rejecting up to 40 % of the total heat at an ambient wet bulb temperature of -6 °C.

The tower can be operated in the following three modes:

- Dry operation at low ambient temperatures. No plume will occur in this mode.
- Integrated operation at wet bulb temperatures up to about 12 °C, with various levels of plume abatement.
- Wet operation at ambient wet bulb temperatures above 12 °C. Only plumes of moderate intensity will occur at wet bulb temperatures above 12 °C.

In July 1990 another wet/dry cooling tower started operation at BASF Ludwigshafen. Boundary conditions for the design of this tower were:

- Operation in an open circuit throughout the year.
- Limited height.
- No impairment on surrounding installations by wet plumes.

These conditions lead to a cell-type wet/dry cooling tower.

2.2.4 Wet/dry cooling system at Altbach/Deizisau power station [87AL1] [87AL2] [88NO1]

This system was designed by W Alt, and constructed for the 420 MWe Altbach power station, situated in Germany, by Balcke-Dürr. The tower was commissioned in 1985. A schematic layout of the tower is shown in figure 2.11. The system with a heat rejection capacity of 558 MW is one of the largest of its kind in Europe. It was developed to eliminate the visible vapour plumes generated by evaporative cooling while avoiding the high cost of all dry cooling. It consists of a reinforced concrete cooling tower (base diameter 70 m, outlet diameter 38 m, tower height 45 m) of the forced-draft type.

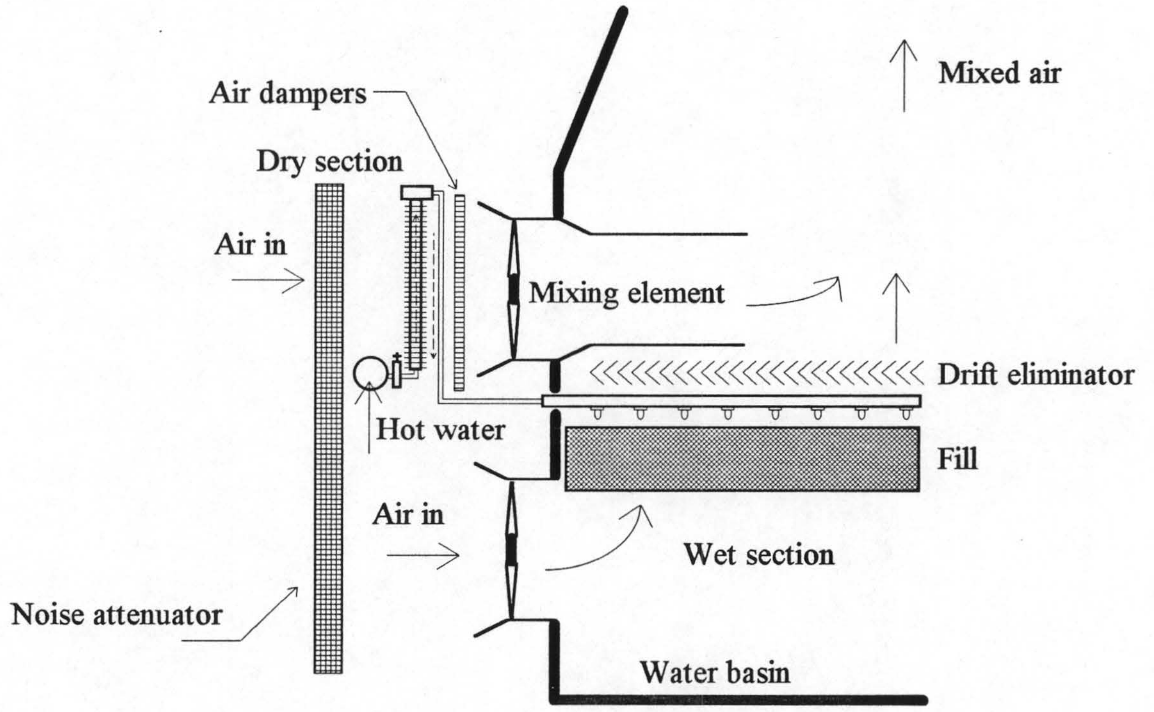

Figure 2.11: Section of Altbach cooling tower.

The air flow arrangement is parallel with separate fans for the dry and the wet sections. Variable length air inlet ducts are used to mix the wet and dry air streams prior to exit. These ducts are installed at the outlet of the dry section as shown in figure 2.11. The length of these ducts vary from once to twice the diameter of the fans, which is 6.3 m. The dry section is supplied with 20 of these axial flow fans, while the wet section is only supplied with 19 since space in the wet section is reduced by the presence of the cable and stair well, as well as the cooling water pump house.

The water flow is in series, first through the one pass dry heat exchangers, from where it is distributed over the counterflow evaporative section. A total of 78 dry heat exchanger elements, each 2.8 m wide and 8.5 m high, are evenly distributed on the periphery in a vertical arrangement. The tower was designed so that the dry section would reject 20 % of the total heat load. This proved to be sufficient for plume abatement purposes.

The tower can be operated in the following main modes:

- Wet operation at full fan capacity where the wet section dissipates 100 % of the heat load. The sliding doors downstream of the heat exchangers and upstream of the fans must be closed for this operating mode. The formation of a visible plume is only dependant on the prevalent ambient conditions.
- Wet operation at reduced fan capacity. This mode of operation can be used at reduced heat load especially during winter. There will nearly always be plume formation under this mode of operation.
- At design conditions of 10 °C dry bulb temperature and 70.8 % relative humidity, integrated operation at full fan capacity of both the wet and the dry sections will occur. The visible plume will be eliminated during this mode of operation.
- Integrated operation at reduced fan capacity. The fan speed can be reduced in both sections simultaneously or only in one of the two sections. This mode of operation must be used during reduced heat load periods when the plume must still be eliminated.
- Dry cooling operation. At an ambient air temperature of -15 °C with the heat load not exceeding 35 % of the design heat load, the tower can be operated using only the dry section. The wet section is bypassed by having the water flow directly from the heat exchangers to the water basin via a bypass line.

2.2.5 Gemeinschaftskernkraftwerk Neckar II (GKN II) [87AL1] [87AL2] [92AL1] [93CO1]

The building site for the Neckar II cooling tower is situated amongst beautiful vineyards in the countryside of Germany. The people of the area showed resistance to a large unsightly natural draft wet cooling tower from where plumes would cast shadows over the area. This necessitated a cooling tower which would not be harmful to the scenic beauty of the surrounding area and would not cause any large visible plumes to form. A 160 m diameter forced draft hybrid cooling tower with a cooling capacity of 2500 MW was built to satisfy these needs. The dry section was designed to dissipate a maximum of 500 MW in the hybrid mode of operation in order to prevent a plume from forming. A picture of the cooling tower is shown in figure 2.12 and a schematic cross section of the tower in figure 2.13.

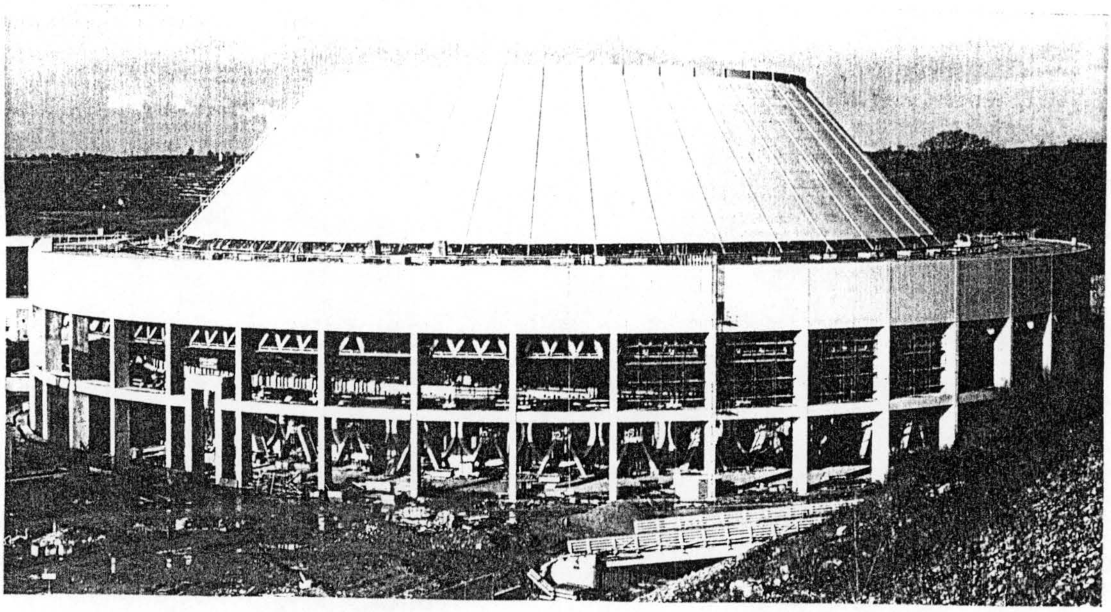

Figure 2.12: *Picture of the GKN II cooling tower.*

The dry and wet air streams are mixed inside the tower by blowing the dry air into the wet air stream through air ducts of varied length.

In principle this cooling tower differs only slightly from the Altbach/Deizisau tower described in section 2.2.4. The differences are:

- The dry cooling elements are arranged at an angle, compared to the vertical arrangement at the Altbach/Deizisau tower.
- Only one third of the cooling water passes through the dry section as compared to the total water flow. This water is drawn from the return channels of the condenser. The precooled water is then fed into the risers to the wet section again, as shown in figure 2.13.
- The dry cooling elements are provided with two water passes where those of the Altbach/Deizisau tower have only one water pass.

- The sliding gates of the dry section are situated downstream of the fans as opposed to the Altbach/Deizisau tower where they are situated upstream of the fans.
- The wet section and the dry section have a joint air inlet which is equipped with silencers, as opposed to the separate air inlets of the Altbach/Deizisau tower. This has the advantage of a lower inlet pressure drop during pure wet operation.

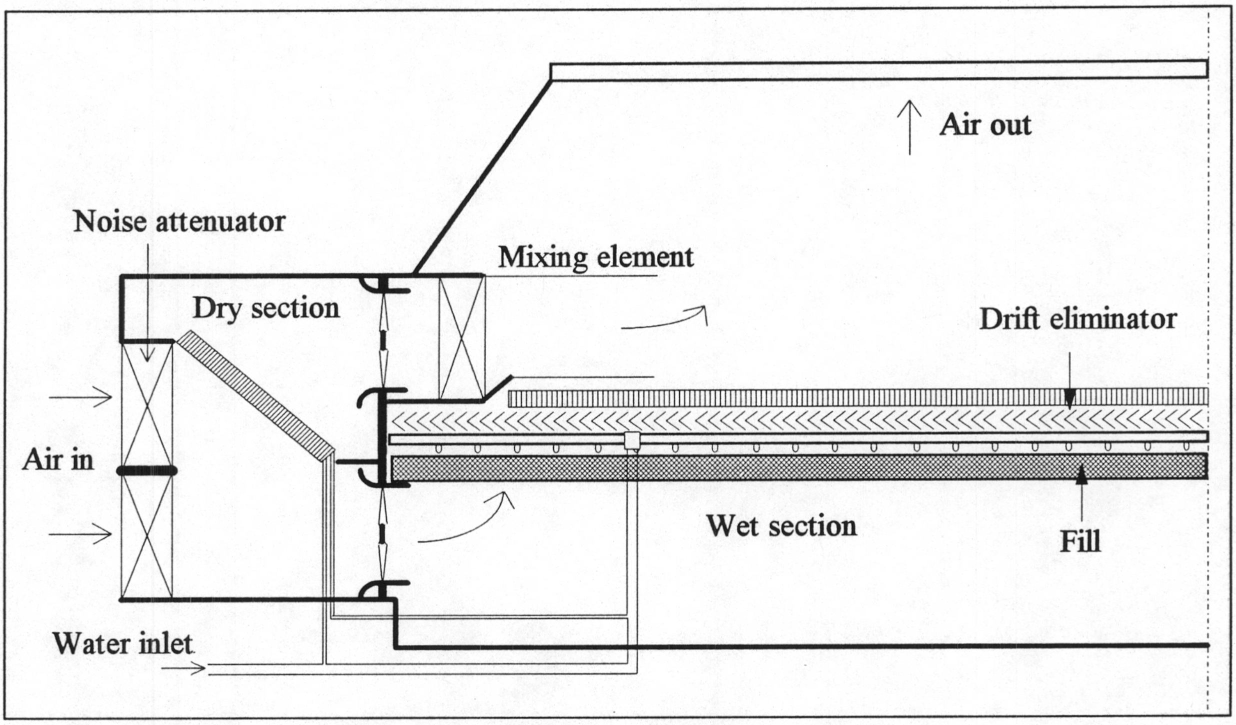

Figure 2.13: *Cross section through the GKN II cooling tower.*

2.2.6 Hybrid tower at Frankfurt power station, Germany [91MU1]

In 1983/84 it was decided to increase the size of the existing Frankfurt power station with two 69 MW electricity, 105 MW heating units. It was originally proposed that fresh water from the Main river should be used for the primary and secondary cooling cycles, but the temperature and water level changes of the river over a year period showed that it was not a viable option. It was decided not to use a wet cooling tower because the power station is situated in an inhabited area and visible vapour plumes are therefore unwanted. The best alternative was to use a hybrid tower.

In 1988 construction on the cooling system started and in 1989 a hybrid cooling tower with a thermal capacity of 91 MW was commissioned. The tower consists of six cells, each unit being served by three of them. The cells are of a PPAF-SPWF configuration as shown in figure 2.7b, with ground dimensions of 10.8 m by 10.8 m each. A unit must always be served by at least two cells at a time. Noise attenuators were installed to keep the maximum noise level below 25 dB(A) at a distance of 360 m.

The tower was designed so that the dry part would contribute 20 % to the cooling capacity of the tower and can be operated in dry mode, wet mode or hybrid mode. Roller doors were installed in the wet and the dry sections and the amount of air that flows through each of them is automatically controlled by these doors. Since the air mixing chamber is very short, the mixing of the wet and the dry air streams is enhanced by the creation of intense air vortices.

It was calculated that at a temperature of -5 °C, a visible plume would only start to appear at a height of 300 m. The tower can be considered as being plume free since there are only a few days per year with temperatures beneath 10 °C and since the tower would be mostly operated in dry mode during winter.

2.2.7 The Trakya cooling system [88SZ1] [86BÓ1]

The Trakya power station is situated in the central region of the European part of Turkey. The first phase of the power station was completed in 1987. EGI designed and supplied the dry/wet cooling system.

The system consists of one natural draft cooling tower which serves two steam turbines. Each turbine is served by a separate cooling installation, although they are both housed in the same tower shell. The cooling tower is 135 m high with a base diameter of 121.6 m and a throat diameter of 67 m. The tower uses the HEADd (Heller/EGI Advanced Dry/deluged) cooling system. This cooling system is an example of a dry/wet cooling system that uses deluging of heat exchangers to increase the tower's cooling capacity during warm periods. It uses delta shaped heat exchangers arranged around the circumference of the cooling tower with peak/preheater induced draft cooling units situated inside the tower.

The peak/preheater units normally take part in the cooling operation by means of the tower's natural draft, but during the hottest peak periods cooling capacity is enhanced by means of natural or induced draft deluged operation. Although these auxiliary units only comprise 5.1% of the total cooling area they can contribute up to 22% of the total cooling capacity. This means that the coolers, when deluged, reject 4.3 times more heat than when they are operated dry. In winter during start-up of the cooling tower the peak/preheater coolers are used to preheat the main coolers. This is done by shutting the louvers on the main heat exchangers and reversing the direction of fan rotation.

2.2.8 The Isfahan cooling system [88NO1] [84BÓ1]

The Isfahan power station was ordered by TAVANIR, the State Electricity Board of the Islamic Republic of Iran. Construction of the turbine units started in 1981 and commissioning of the first turboset took place in 1984. EGI supplied the four cooling towers for each of the four 200 MWe units.

Since the power station had to utilise residual oil from the Isfahan oil refinery for it's electric power generation and, since the high viscosity of the residual oil makes it difficult to transport the power station had to be build in the immediate vicinity of the oil refinery, which is situated in an arid area. This necessitated the use of dry cooling towers. It was calculated that the available water supply would exceed the power station's required water quantity during dry operation and it was therefore possible to use some water for wet cooling purposes during periods of high ambient temperatures. Consequently both the main and the auxiliary cooling towers were designed as combined dry/wet systems.

The power station is located at an altitude of 1590 m above sea level. At this high altitude, due to the low specific weight of the air, cooling tower dimensions had to be substantially increased. Since the region where the power station is situated is vulnerable to earthquakes, light steel structured natural draft towers with corrugated aluminium sheet cladding were used. The towers are of the same HEADd type as those used at the Trakya power station. Each cooling tower consists of 119 A-frame heat exchangers and 30 peak coolers. The cooling tower can be operated with the peak coolers working dry with the natural draft (up to 30.5°C), the peak coolers working dry with an induced draft (30.5-32.5°C), or with the peak coolers working with an induced draft while also being deluged (above 32.5°C).

2.2.9 The Deeside cooling system in the UK [94IS1]

The 500 MWe Deeside combined cycle power station in Wales was handed over to the National Power company in November 1994. The plant includes two 166 MW gas turbines and a 176 MW steam turbine for which steam is supplied by two heat recovery steam generators. Although cooling water from the river Dee was readily available a hybrid tower was still chosen as opposed to a conventional wet cooling tower. The most important reason for choosing a hybrid tower was to reduce the visible plume from the tower, since a motor-way bridge was due to be constructed close to the power station and the possibility of freezing on the bridge in winter had to be avoided.

The Deeside power plant uses a total of 12 hybrid cooling towers arranged in two blocks, each block housing six cells. Each cell is of a parallel path air flow, series path water flow configuration. Some, or all, of the water to be cooled is fed through finned tube heat exchangers and each cell has four of these finned tube bundles. The tubes are cooled by air drawn up through the tower by a 9.75 m diameter fan rotating at 70 r/min. This serves to remove about 10 % of the heat from the water, while the balance of the heat is removed by spraying the water over a special fill in the wet section. Drift eliminators are situated behind the fill and remove about 99 % of the drift from the wet section. Each cooling tower uses four vortex discs to mix the wet and dry air streams before leaving the tower. The average exit air humidity for the cooling tower is 85 %. The hybrid tower ensures that there is no visible plume at ambient conditions down to 5 °C and 90 % relative humidity, essentially covering climatic conditions for 85 % of the year.

As water from the river Dee is used to top up the system and this water varies in salt content from almost fresh to sea water, expensive non-corrosive materials had to be used in the cooling system. Water velocities in the pipes also have to be kept up to avoid settling of particles.

The Deeside cooling system operates uncontrolled, i.e. the dry part operates continuously throughout the year and the extent of plume abatement is fixed. Additional performance could be gained by controlling the dry air mass flow according to ambient conditions. The cost of such a system would be 20 percent of the cost of the cooling towers, but if it provides the station manager with the means to maximise station output it could be a worthwhile investment.

2.2.10 Other existing hybrid towers [94BO1]

Hybrid towers have also been erected at Hempstead, Detroit, Bergen and Hennepin all in the US and they all have vertical dry sections. Other towers with horizontal dry sections exists at Anyang and Bundang in Korea and at Connah's Quay power station in the UK. All these towers are equipped with air control devices in the dry section, in order to keep the benefit of maximum tower performance in summer when the plume is less critical. On the other hand air control devices are not always installed in the wet inlet sections, for example, they are installed in BASF, Detroit, Hempstead, Anyang, Bundang and Hennepin, but not in the towers of Bergen and Connah's Quay.

CHAPTER

THREE

VISIBLE PLUME FORMATION

3.1 Visible plume abatement methods and prediction criteria

There are two possible ways of reducing visible wet cooling tower plumes. The one method is to reduce the heat load on the wet cooling tower and the other method is to increase the temperature of the cooling tower outlet air without adding more moisture to the air. Although, by heating the exhaust air, visible plume formation will be reduced, the amount of water vapour in the plume still remains the same since the evaporation process is still the primary mode of heat removal. It should be remembered that the amount of evaporation is proportional to the heat load on the wet section of the tower and is relatively insensitive to tower design.

The outlet air temperature can be increased by either heating the tower's exhaust air with the aid of gas burners, or by using dry heat exchangers to further heat the exhaust air from the wet section. Depending on the tower configuration the use of dry heat exchangers in tandem with the wet section can however, make it possible to incorporate either one or both of the above mentioned methods of plume abatement. According to Reisman and Dolan [74RE1] gas burners have been used on a number of installations with reasonable success. Extreme fire hazards and high operating costs are disadvantages of this method.

The different psychrometric models for different hybrid tower configurations will be discussed in section 3.5, while the different hybrid tower configurations have already been discussed in Chapter 2.

In the cooling tower industry the suppliers of hybrid cooling towers must be able to specify the plume abatement capacity of the cooling tower under specific atmospheric conditions, for a given tower heat rejection rate. To be in a position to specify this the visible plume occurrence has to be quantified in some or other way. It may sometimes be acceptable if a visible plume of a moderate severity occurs and it is therefore necessary for suppliers to be able to specify the plume severity and not only to differentiate between a non-visible plume and a visible plume situation. The nature of a plume depends on the condition of the plume air at the tower outlet as well as the condition of the atmosphere, which makes it very difficult to predict the optical appearance of the plumes. From an optical point of view, a cooling tower can be defined as being plume free when no visible plume can be seen, which is incidentally very subjective since it is open to different interpretations. It is possible to define minor streaks of plume at the tower outlet or even virtually dissolved plumes some metres above the tower outlet as being plume free. A more definite criteria therefore has to be used to define the plume severity.

A further method of plume classification was proposed by Gilbert and Lemmens [78GI1]. They characterise a plume by its maximum condensed water content. According to them, plumes can be classified according to one of the following three categories:

- no plume (0 g/m^3 of condensed water)
- slight plume (less than 0.1 g/m^3 of condensed water)
- dense plume (more than 1 g/m^3 of condensed water).

The size of the visible plume, which depends on ambient conditions like temperature, wind speed, temperature lapse rate and turbulence, as well as the state of the outlet plume air, is a further characteristic of the plume. Several analytical methods to determine the density and size of cooling tower plumes exist and will be discussed in the literature survey of section 3.2. These methods are very complex and do not provide a relatively simple basis for comparison. Another way of predicting plume severity is by means of a psychrometric chart. For the purpose of this study only some of these more straightforward graphical prediction methods will be used, as will be discussed in section 3.4.

3.2 Literature survey on plume prediction models

Wessels and Wisse [71WE1] developed a nomogram to determine the length of the visible part of the plume. The conditions for which the plume reaches the ground are given in dependence of the Pasquill-stability-class and the effective source height. To determine the Pasquill-stability-class, the dispersion model developed by Pasquill and Gifford [61PA1] is used, with the enthalpy flow and the enthalpy excess taken as the source strength and the concentration respectively. This theoretical model is demonstrated for a fictitious 500 MW natural draft cooling tower using meteorological data of one winter season at De Bilt, The Netherlands.

Hanna [72HA1] gives analytical methods for determining the final plume rise and the levels of initial condensation of the plumes from cooling towers. Formulas for the derivation of height variation in buoyancy, volume and water vapour fluxes are derived for large wet cooling towers. The formulas developed by Briggs [69BR1] are suggested for estimating plume rise if the possibility of the release of latent heat is accounted for in the definition of the initial buoyancy flux. According to Hanna, condensation is strongly influenced by small variations in atmospheric conditions. Unavailability of accurately measured plume data hampered the verification of this theory.

Saame and Somers [72SA1] developed a model for predicting visible plumes from natural draft cooling towers. The model first predicts the condition of the cooling tower exit air as a function of the local ambient conditions and the cooling tower parameters and then it predicts the extent of visible plume formation as a function of the same ambient conditions. A computer program, called PLUME, was written in FORTRAN to solve the design equations described in Saame's thesis. Required input to the PLUME program consists of the following seven cooling tower parameters and five meteorological parameters:

Cooling tower design input:

- Total tower height
- Tower inlet height
- Inside diameter at the packing
- Inside diameter at the top
- Resistance to air flow
- Water mass flow rate
- Water cooling range

Meteorological input:

- Dry bulb temperature
- Relative humidity
- Atmospheric stability
- Wind speed at reference height
- Reference height above ground

This program was utilised in studying visible plume formation at existing natural draft cooling towers for typical and extreme ambient conditions and for studying the effects of variation in ambient conditions on the visible plume formation at such towers. Results show visible plume formation to be most severe for cold, humid and calm conditions, when associated with nocturnal inversions. During the afternoon the fog plumes are rapidly dissipated. This is explained by the fact that afternoon meteorological conditions are typically unstable with higher temperatures, lower specific humidities and greater wind speeds.

Biese and Gilbert [74BI1] examined plume formation by means of a mathematical model employing simple numerical techniques. They specifically investigated the immediate psychrometric behaviour of the sub-saturated plumes discharged by hybrid induced draft cooling towers. The results indicate that for any fixed set of environmental conditions, effects such as exit velocity, initial temperature and heat loss by radiation, are small compared to the effect of initial relative humidity.

For the sake of simplicity the following conditions are used in this mathematical model:

- The atmosphere is assumed to be still
- The plume rise is purely vertical
- Atmospheric conditions are constant
- The tower operating conditions are constant, like constant heat load and constant air flow
- Sufficient period of operation for equilibrium plume behaviour is assumed

The plume is treated as a free vertical jet with a half spread angle of 7.5 degrees. With the atmosphere at rest and turbulent flow in the plume, linked with the aforementioned assumptions, a one-dimensional flow system was developed by following the control volume approach. A computer program was written to solve this numerical model and a few runs at different conditions were done. From their results they predict that visible plumes will still occur with hybrid towers, but that the density and persistence of such plumes will be less than that for their counterpart all wet towers.

Sneck and Brown [74SN1] carried out an experimental study on the dry buoyant plume rise from a finite size source into a stable stratified atmosphere. According to them the existing point source solutions like the one proposed by Hanna [72HA1], which do not take into account the size of the source, cannot be applied with accuracy to cooling tower plumes. The test results from Sneck's experiments are correlated with published theory which is shown to be applicable to a wide range of discharge conditions. Methods for predicting the height of the stratified plume accumulation as well as the maximum rise height of the plume are presented.

Rubin and Klanian [75RU1] investigated the visibility of plumes at the full scale hybrid test tower, at the Duke Power Company's Cliffside Power Plant in Cliffside, North Carolina. In their visibility analysis they concluded that visibility in a fog is a function of liquid water content and droplet size distribution. Some experimental results are given. According to them, quite accurate plume visibility predictions were obtained by using the Houghton and Radford prediction model together with a droplet size correction factor. This correction factor accounts for the fact that droplets in a cooling tower plume are smaller than the droplets in the coastal fog, as used by Houghton and Radford in their study.

Mäule [80MÄ1] developed a code with which different plume severity's can be defined and compared. The code assigns mathematical values to the plume height, plume length and the place of condensation. The product of these values are then taken as an indication of plume severity under the specific operating conditions. For a certain tower, a number of these plume parameters must be determined under different operating conditions and the sum of these parameters then give an indication of the tower's plume abatement ability. However, to be able to implement this method the formation of the plume must still first be determined numerically.

3.3 Physics of plume formation

The outlet air, or plume, from a wet or hybrid cooling tower is essentially an air, water-vapour mixture at a temperature higher than that of the ambient air. For wet cooling towers, except in dry weather conditions, this air is usually already saturated or supersaturated on leaving the cooling tower. For hybrid cooling towers the humidity of the exit air can vary considerably, depending on the operating conditions of the tower and visible plume formation may or may not occur.

Wet cooling towers generate a visible plume under almost all atmospheric conditions. This visible plume consists of a cloud of small droplets that condenses out of the plume as it leaves the tower. Condensation takes place because the ambient air is at a lower temperature than the plume air and as the plume mixes with the ambient air it is cooled by this cooler air through convection as well as radiation. The drop in plume temperature causes the plume to become supersaturated and small droplets to form. It is these droplets that make the plume visible. As the dilution process further continues the droplets evaporate and the plume disappears, except of course if the atmosphere is already saturated.

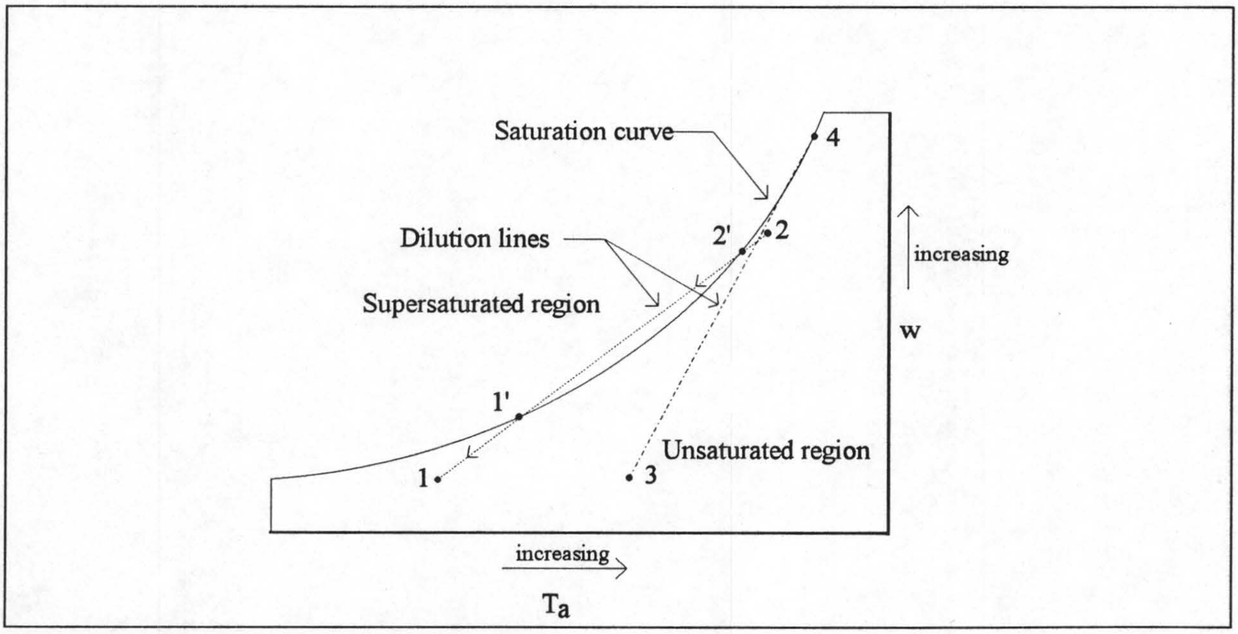

Figure 3.1: *Visible plume formation.*

The emission of hot, wet air from the cooling tower as well as the dilution of this air, can be illustrated on a psychrometric chart. The process of visible plume formation can be seen in figure 3.1.

Assume that on leaving the tower the plume air is at the state represented by point 2 on the psychrometric chart and the ambient air is at the state represented by point 1, as for typical winter conditions. As the plume rises and the exit air mixes with the ambient air, it is assumed that the dilution and cooling of the plume follows a straight line 2-1. If the dilution line enters the supersaturated region at point 2', condensation starts to occur and a visible plume forms. This plume will stay visible until the mixed air reaches the air state described by point 1'. At this point the plume will disappear, as the air again enters the unsaturated region on the psychrometric chart.

During warm summer conditions the dilution process is better described by the line that connects points 3 and 4 in figure 3.1. Point 4 represents the saturated tower exit air and point 3 the warm dry ambient air. Theoretically no visible plume will form during this dilution process since the dilution line never crosses the saturation curve. According to Reisman and Dolan [74RE1], in reality some visible plume usually exists immediately beyond the outlet point since the heat transfer between the two air masses initially occurs at a faster rate than the direct mixing. Hence, the dilution line from 4 to 3 would curve slightly to the left and a small portion of the line would enter the supersaturated region.

3.4 Visible plume severity

Several analytical plume prediction models do exist, as discussed in the literature survey. These models require much additional data on specific site and tower characteristics and if one of these models is used it would be very specific and limited. In this study visible plume formation considerations are limited to the questions of whether visible plumes occur and how severe they are. There are several ways of predicting visible plume severity with the help of a psychrometric chart by using the straight line mixing model. Three different prediction methods will be illustrated with the help of the psychrometric chart shown in figure 3.2.

- **Mix line ratio method** [72OL1] [73KL1]

In this method plume severity is simply defined as the ratio of the change in humidity between plume condensation and evaporation, divided by the total change in humidity during mixing from outlet to ambient conditions. This ratio is equal to the change in air dry bulb temperature from plume condensation to evaporation, divided by the total temperature change from outlet to ambient.

On the psychrometric chart in figure 3.2, the visible plume severity can be indicated by the ratios:

$$\frac{w_{2'} - w_{1'}}{w_2 - w_1} \text{ or } \frac{T_{2'} - T_{1'}}{T_2 - T_1}$$

A visible plume severity of zero, would produce no visible plume, since the mixing line would never intersect the saturation curve in figure 3.2. A plume severity of one, would occur if the outlet air as well as the ambient air is saturated and the mixing line would lie completely in the supersaturated region of figure 3.2. The latter condition would be an extreme case for an all wet cooling tower. According to Olesen and Budenholzer [72OL1] as well as Klanian and Noyes [73KL1], an annual average plume severity of 0.7 typifies most conventional towers in the north-eastern United States.

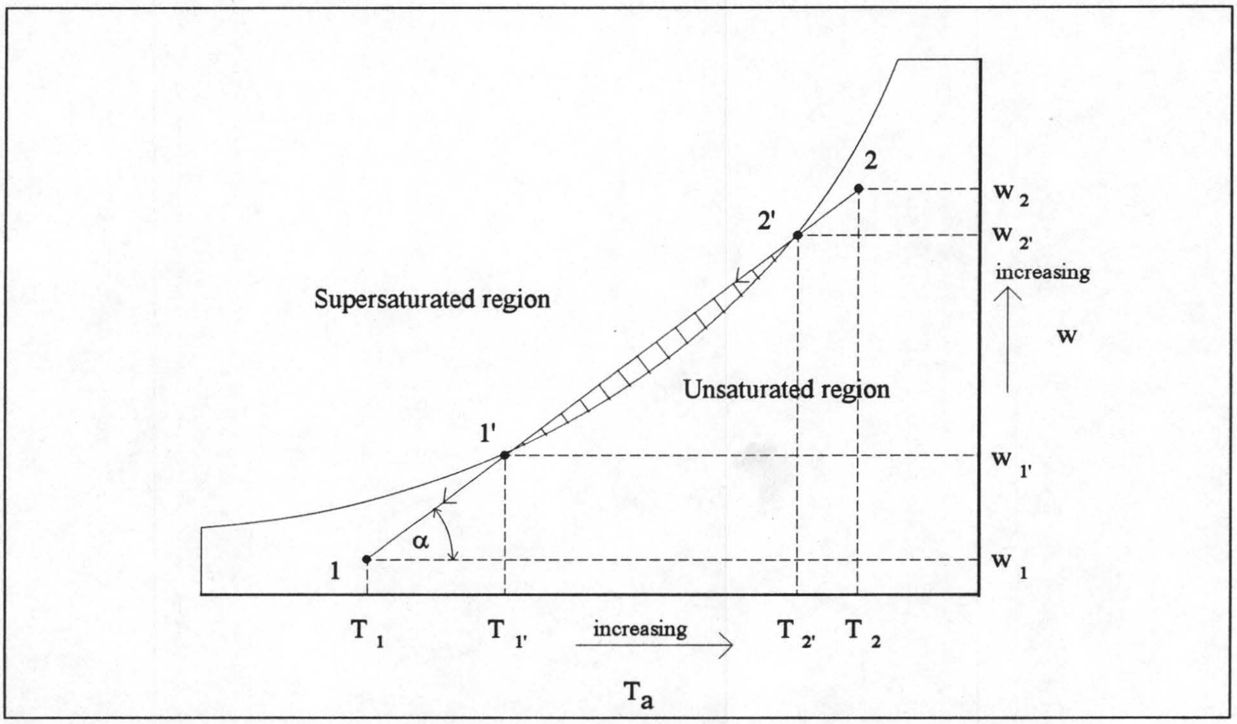

Figure 3.2: *Psychrometric chart illustrating methods for predicting plume severity.*

According to Croley, Patel and Mow-Soung Cheng, [76CR1] this method is not consistent in estimating the severity of the visible plume. According to them this method may predict heavy or light fogging for the same mix line ratio, depending on the actual length of the dilution line.

- **Plume abatement angle** [73LA1] [76CR1]

This is the angle between the dilution line and the horizontal. On the psychrometric chart of figure 3.2 this angle is indicated by the symbol α. The value of this parameter depends upon the ambient and tower outlet air conditions. This is not a consistent indicator of visible plume severity because for the same abatement angle, fogging may or may not occur, depending on the position of the dilution line on the psychrometric chart as well as the scale of the psychrometric chart on which it is plotted.

The smaller the plume abatement angle the better the plume abatement capability of the tower would be, since a dilution line with a small angle would not cross the saturation curve for as many atmospheric conditions as one with a large angle.

- **Enclosed area between dilution line and saturation curve** [76CR1]

In this method the visible plume severity is determined from the enclosed area between the saturation curve and the part of the dilution line that lies in the supersaturated region of the psychrometric chart. In figure 3.2 this is the part of the dilution line from point 2' to point 1'. Severe visible plume formation will be indicated by a large area, while no visible plume would form if the area is zero. According to Croley, Patel and Mow-Soung Cheng [76CR1], this appears to be the most consistent method in predicting visible plume severity. The visible plume severity can now be indicated by a value expressed in units of [kg/kg]×[°C].

3.5 Hybrid tower psychrometrics

For the different plume abatement hybrid tower configurations, different psychrometric models exist. In all of these models the result is basically the same, that is to decrease the plume abatement angle and thereby prevent the dilution line from crossing the saturation curve. The psychrometric models for some of the different hybrid tower configurations will briefly be discussed in sections 3.5.1 to 3.5.3.

3.5.1 Parallel path air flow configuration (PPAF hybrid tower)

Line 1-2 in figure 3.3 represents the fraction of air that flows through the wet section. As the air flows through the wet section its humidity and temperature increases. The fraction of air that flows through the dry section is sensibly heated along line 1-3. The humidity ratio of this air stays constant and only the temperature of the air increases. The air streams from the wet and dry sections mix along line 2-3, until the new homogeneous air state at point 4 is reached. The position of point 4 depends on the mass flow rates through the wet and dry sections respectively. It can be seen that the new dilution curve never crosses the saturation curve and therefore no visible plume will form.

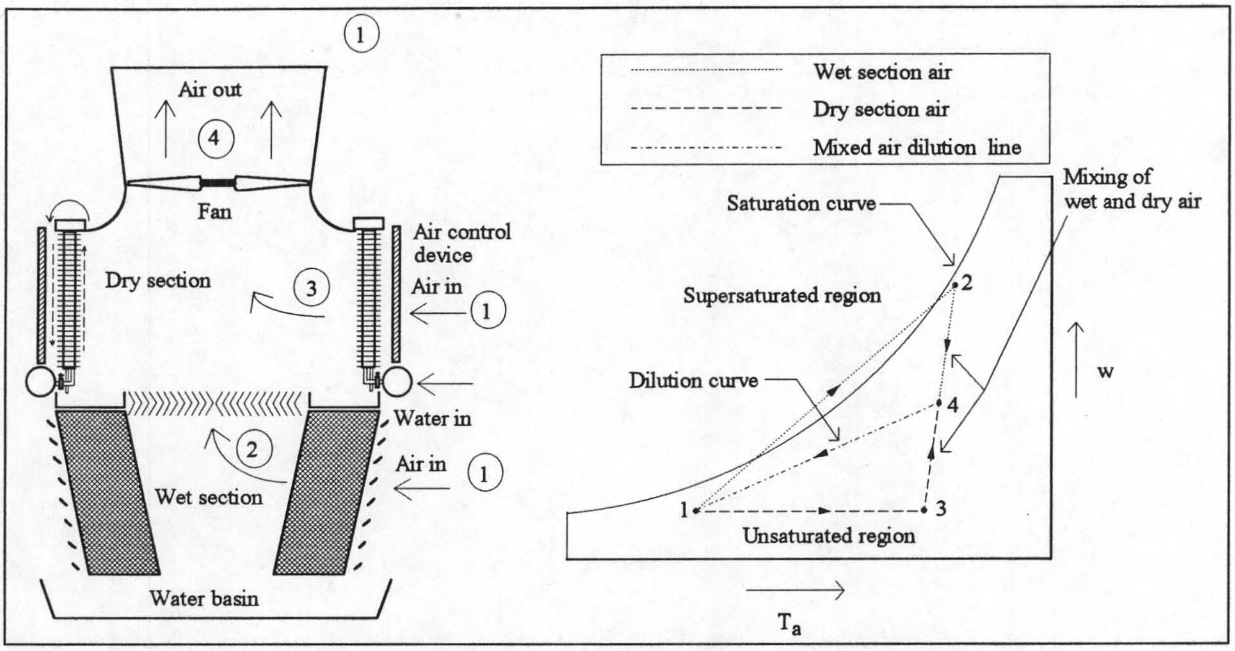

Figure 3.3: *Psychrometric representation of plume abatement for a PPAF tower.*

3.5.2 Series air flow configuration - Dry section before the wet section

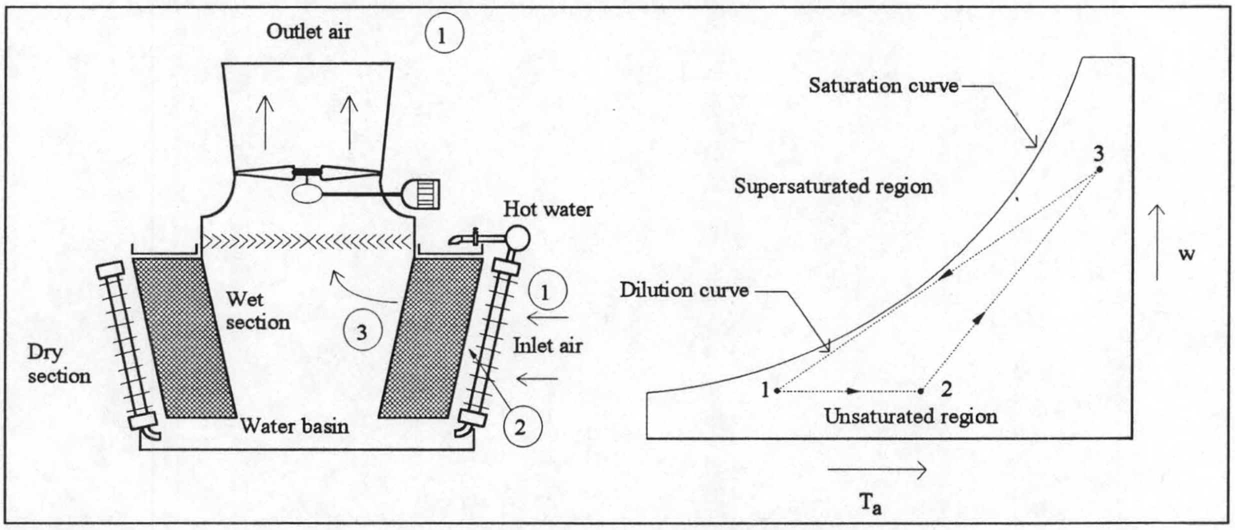

Figure 3.4: *Psychrometric representation for a SPAF tower with the dry section first.*

Line 1-2 in figure 3.4 represents the air flow through the dry section. The humidity ratio of the air stays constant and the temperature increases along this line. The air then flows through the wet section as indicated by line 2-3. The dilution process outside the tower is represented by line 3-1. Because of the dry cooling represented by line 1-2, the plume abatement angle is decreased and this prevents the dilution line from crossing the saturation curve. Visible plume formation is therefore prevented.

3.5.3 Series air flow configuration - Wet section before the dry section

For the tower shown in figure 3.5, the air flows through the wet section along line 1-2. Along this line both the humidity and the temperature of the air increase. It can be seen that the air at point 2 would still form a visible plume if it were released into the atmosphere. Line 2-3 represents sensible heating of the air through the dry section. This line again decreases the angle of the dilution line thereby preventing the dilution line from crossing the saturation curve into the supersaturated region, inhibiting visible plume formation.

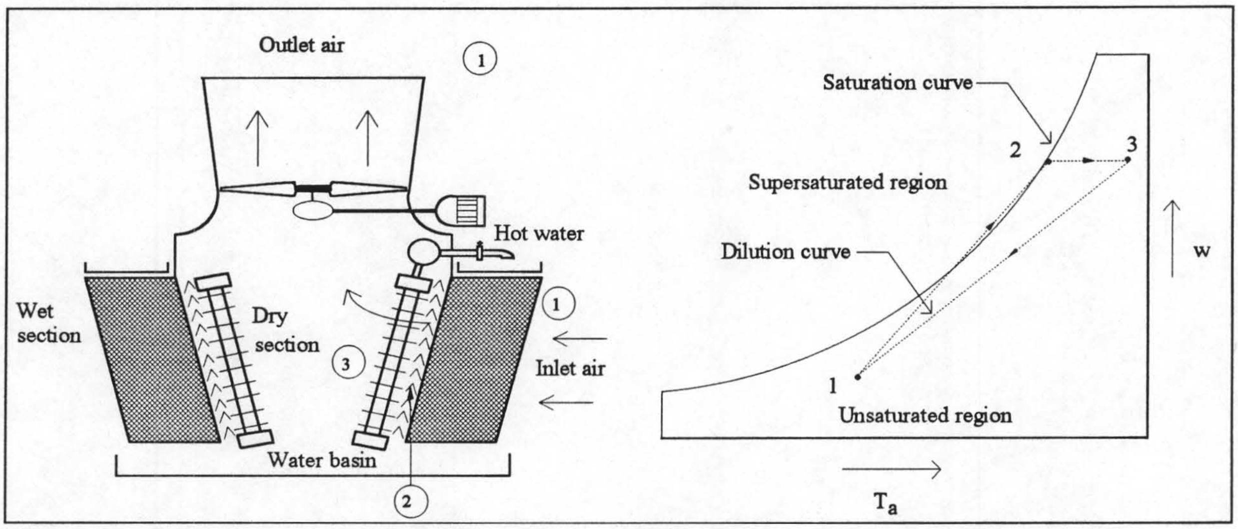

Figure 3.5: *Psychrometric representation for a SPAF tower with the wet section first.*

3.6 Mixing of wet and dry air inside the tower

In a parallel air flow hybrid tower, the air from the wet and dry tower sections have to be mixed before it is discharged into the atmosphere. If the air is not properly mixed before exit, the more humid air from the wet section can still form a visible plume, even if the homogeneous air state does not indicate visible plume formation on the psychrometric chart. To achieve efficient plume abatement it is therefore necessary to obtain proper mixing of the two air streams before exit. This mixing of the air can be achieved by several methods. One such method is to discharge the air from the dry section into the humid air stream of the wet section through varied length air ducts [92AL1] [94BI1]. The mixing of the two air streams can also be accomplished by the generation of intense air vortices. For mechanical draft cooling towers the mixing distance in the tower shell is usually very short and mixing has to be accomplished very rapidly. With this in mind, Henning [80HE1] proposes two vortex generation systems. The first system uses vortex generator plates and the second system uses cylindrical vortex generators.

If complete mixing is assumed, the quality of the discharge air can be predicted by simple psychrometric theory. In the following model, which can be used to predict the homogeneous outlet air state, the properties of the air from the dry section are indicated with a "d" as a subscript and the properties of the air from the wet section are indicated with a "w" as a subscript.

The humidity ratio of the mixed air stream can be obtained from the humidity ratios of the exit air from the wet and dry sections as follows:

$$w = \frac{w_w m_{aw} + w_d m_{ad}}{m_{aw} + m_{ad}} \tag{3.1}$$

From the exit air enthalpies of the wet and dry sections, the enthalpy of the mixed air stream can be determined as follows:

$$i_{ma} = \frac{i_{maw} m_{aw} + i_{mad} m_{ad}}{m_{aw} + m_{ad}} \tag{3.2}$$

The dry bulb temperature for completely mixed exit air can now be determined by solving equation (A.3.6) for T_a.

$$i_{ma} = c_{pa} T_a + w\left(i_{fgw0} + c_{pv} T_a\right)$$

This equation has to be solved iteratively, since c_{pa} and c_{pv} are both functions of T_a, and they must be evaluated at $\left(\frac{T_a}{2} + 273.15\right)$ K.

The determined homogeneous outlet air state can now be used to calculate the visible plume severity with one of the methods described in section 3.4. If the visible plume severity is too high, the ratio of cooling between the wet and the dry sections can be changed accordingly, until satisfactory plume abatement is achieved.

CHAPTER
FOUR

WET AND DRY ENTHALPY TRANSFER THEORY

In a hybrid cooling tower enthalpy transfer takes place in both the wet and dry cooling sections. To determine the enthalpy transfer from the water to the air in both these sections, already existing transfer theory can be used. In this chapter the equations that quantify the enthalpy transfer in both the wet and dry sections of a hybrid tower are given. The theory that is given is specifically applicable to an induced draft PPAF-SPWF hybrid tower. Application of the theory is shown in the hybrid tower sample calculation given in section 6.3.

4.1 Wet section

In a wet counterflow cooling section, as used in the hybrid tower shown in figure 2.7b, there are three regions where enthalpy transfer from the water to the air takes place, i.e. the rain zone, the fill, and the spray zone. The enthalpy transfer in each of these regions consists of a mass transfer and a heat transfer component. To accurately determine the amount of heat and mass transfer that occurs in each region, a heat and mass transfer coefficient for each of the three transfer regions have to be determined. However, if it is assumed that the Lewis factor is equal to unity, as is done in the Merkel theory [25ME1], the energy transfer equation is greatly simplified and the energy transfer can be determined from a transfer coefficient that combines both the heat and the mass transfer. The transfer coefficient has to be determined for each of the three regions and is then used in the transfer equation to determine the amount of cooling that the water undergoes through them.

Equation (4.1.1) is the simplified transfer equation for the mass and heat transfer in a wet cooling tower as derived by Merkel [25ME1], where h_d is the combined transfer coefficient.

$$\frac{(h_d a)_{fi} A_{fr} L_{fi}}{m_w} = \int_{T_{wo}}^{T_{wi}} \frac{c_{pw} dT_w}{(i_{mas} - i_{ma})} \tag{4.1.1}$$

The transfer equation is non-linear, and therefore it cannot be solved by normal analytical methods. One method of solving it is to use some kind of numerical integration technique. The methods that are most frequently used, are the fourth order Runga Kutta method [84GE1] and the Chebyshev numerical integration method [65FR1]. Another way of solving the equation is by linearizing it and then solving it analytically as was done by Jaber and Webb

[89JA1] in the ε-NTU method. These methods differ from one another in simplicity, computational speed and accuracy. A description of the Chebyshev numerical integration method is given in Appendix B and sample calculations where both the Chebyshev and ε-NTU methods are used to determine fill transfer characteristics are given in Appendix C.

It is stated in an EPRI report [89JO1] that the same theoretical model and computational method that were used to obtain the transfer coefficient for the fill, should also be used to predict the cooling tower performance. In this way the same simplifying assumptions and inaccuracies of the theory and method that were used to determine the fill transfer coefficient are used in computing the cooling tower performance and some of the inaccuracies are then cancelled out in the two computations.

4.1.1 The transfer coefficient for the rain zone

In any detailed study of the performance characteristics of a wet counterflow cooling tower, the transfer process in the rain zone may not be ignored. Conradie [93CO1] analysed the rain zone and from sets of analytically determined data he obtained empirical correlations for the transfer coefficient in both round and rectangular cooling towers.

The following function correlates the data for a rectangular cooling tower.

$$\frac{(h_d a)_{rz} H_3}{\rho_{av1} v_{av34}} = 340.76 \times 1.007^{\left(\frac{W_{fi}}{H_3}\right)} \times \left(\frac{\rho_{av1} v_{av34} H_3}{\mu_{av1}}\right)^{0.359} \left(\frac{D}{H_3 v_{av34}}\right)^{1.0986} \left(\frac{p_{a1}}{\rho_{av1} v_{av34}^2}\right) \times$$
$$0.409^{w_{sw3}} \times 0.365^{w_1} \times 0.9996^{\left(\frac{\rho_{w3}}{\rho_{av1}}\right)} \times \left(\frac{v_{w3}}{v_{av34}}\right) \left(\frac{v_{av34}^2}{R_v T_{w3}}\right)^{0.95} \left(\frac{\sigma_{w3}}{H_3 \rho_{av1} v_{av34}^2}\right)^{-0.165}$$
$$\times \exp\left[0.01835536\left(\ln\left(\frac{gH_3}{v_{av34}^2}\right) - 13.46\right)^2 + 0.1208605\left(\ln\left(\frac{d_d}{H_3}\right) - 0.0324\right)^2\right]$$

(4.1.2)

This correlation is valid for:

$0 \le T_{a1} \le 40$ °C
$0 \le T_{wb1} \le 22$ °C
$0 \le T_{w3} \le 40$ °C

$2 \leq d_d \leq 8$ mm
$80000 \leq p_{a1} \leq 101325 \text{ N/m}^2$
$9.7 \leq g \leq 10 \text{ m/s}^2$
$4 \leq W_{fi} \leq 40$ m
$2 \leq H_3 \leq 8$ m
$0.001 \leq v_{w3} \leq 0.006$ m/s
$1 \leq v_{av34} \leq 7.5$ m/s

4.1.2 The transfer coefficient for the fill

The transfer coefficient for a specific fill must be known, in order to determine the amount of cooling that the water will undergo through the fill. This fill characteristic can be obtained by testing the fill in an instrumented experimental cooling tower as described in Appendix C. The results from such a fill test can then be used to derive a correlation for the transfer coefficient of the particular fill. In these correlations the transfer coefficient for the specific fill is given as a function of the water and dry air mass fluxes. When using these correlations for cooling tower calculations it is important to remember that they were derived for a specific fill height and for specific operating conditions. Significant errors can therefore occur if the correlations are used to predict the transfer coefficient for a fill operating under totally different conditions, or having a different fill height.

The transfer coefficient is usually given by a correlation having either of the following forms:

$$\frac{(h_d a)_{fi} A_{fr} L_{fi}}{m_w} = a_h G_w^{b_h} G_a^{c_h} \tag{4.1.3}$$

or

$$\frac{(h_d a)_{fi} A_{fr} L_{fi}}{m_w} = a_h \left(\frac{G_w}{G_a} \right)^{b_h} \tag{4.1.4}$$

The first form is usually the more accurate one, since a more accurate curve fit can be made on the experimental data if three constants are used instead of two.

A set of experimental data for a 1.88 m high fill, as well as the transfer and pressure drop correlations for the fill are given in Appendix C. Sample calculations to show how the fill characteristics were obtained from the experimental data with both the Chebyshev and the ε-NTU methods are included.

4.1.3 The transfer coefficient for the spray zone

Conradie [93CO1] gives a correlation for the transfer coefficient in the spray zone. The correlation was obtained from a curve fit through data from Lowe and Christie [61LO1]. The correlation is:

$$\frac{(h_d a)_{sp}}{G_w} = 0.2\left(\frac{G_w}{G_a}\right)^{-0.5} \tag{4.1.5}$$

This correlation is only an approximation and since the actual size of the drops in the spray zone is not included in the correlation, it is a very general correlation.

4.2 Dry section

The dry section of a hybrid tower usually consists of finned tube heat exchanger bundles and normal dry cooling tower theory can therefore be used to solve the energy transfer in the dry section of a hybrid cooling tower. For the example PPAF-SPWF hybrid tower, the ε-NTU method [89HO1] (section 4.2.5) is used to solve the energy transfer equation in the dry section and the correlations of Gnielinski [75GN1] (section 4.2.4) and Ganguli et. al. [85GA1] (section 4.2.3) are used to determine the water side and air side heat transfer coefficients respectively.

4.2.1 Dry heat exchanger geometry

In most hybrid towers the dry heat exchanger bundles are situated above the wet section at the sides of the tower (as shown in figure 2.7), arranged in such a way that the water flows through them vertically. This arrangement is done in such a way that a siphon is created by the bundles, in order to assist the water in flowing through them. This decreases the required pumping head thereby lowering the energy consumption of the water pumps.

A typical heat exchanger tube is shown in figures 4.1 and a plan view of a heat exchanger bundle is shown in figure 4.2. The tube shown in figure 4.1 is an extruded bi-metallic E-fin tube and is recommended in applications where corrosion is a major consideration and fluid temperatures are below 200 °C. The finned surface is obtained by plastically deforming the outer aluminium muff onto an internal steel tube during a rolling process. In hybrid cooling towers where untreated water flows through the tubes, the core tube has to be manufactured of a corrosion resistant material like stainless steel or a copper-nickel alloy.

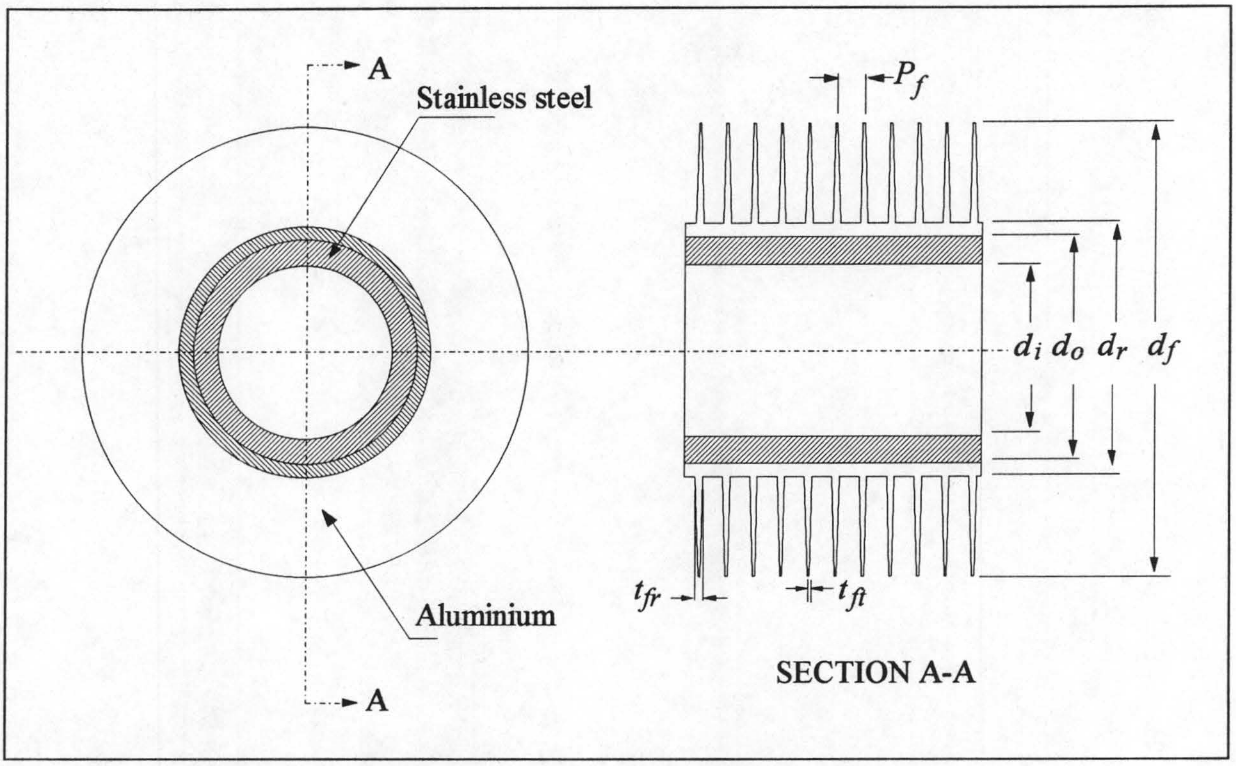

Figure 4.1: *Schematic layout of the extruded bi-metalic finned tube.*

The fin pitch must not be too small since this can cause clogging of the fins, leading to reduced performance for the dry section. Special cleaning devices must be installed to keep the inside and the outside tube surfaces clean and thereby preventing their thermal resistances from increasing too much. In open water circuit hybrid towers, rubber balls are mostly used to clean the insides of the tubes and it is therefore not possible to use the more effective elliptical heat exchanger tubes in such installations.

The bundle shown in figure 4.2 is a four pass bundle where mixing of the process fluid does not occur between the passes, since there are no headers between each pass. The process fluid flows in a counterflow fashion relative to the air, so that a high approach temperature difference is maintained between the air and the process fluid. The different tube and exchanger dimensions that are required to solve the enthalpy transfer in the dry section of a hybrid tower are shown in figures 4.1 and 4.2.

The heat exchangers that are used in the example PPAF hybrid tower, as solved in the tower simulation of section 6.3, are two pass exchangers with four tube rows. The tube bundle consists of finned tubes as shown in figure 4.1 with the tube core made out of stainless steel.

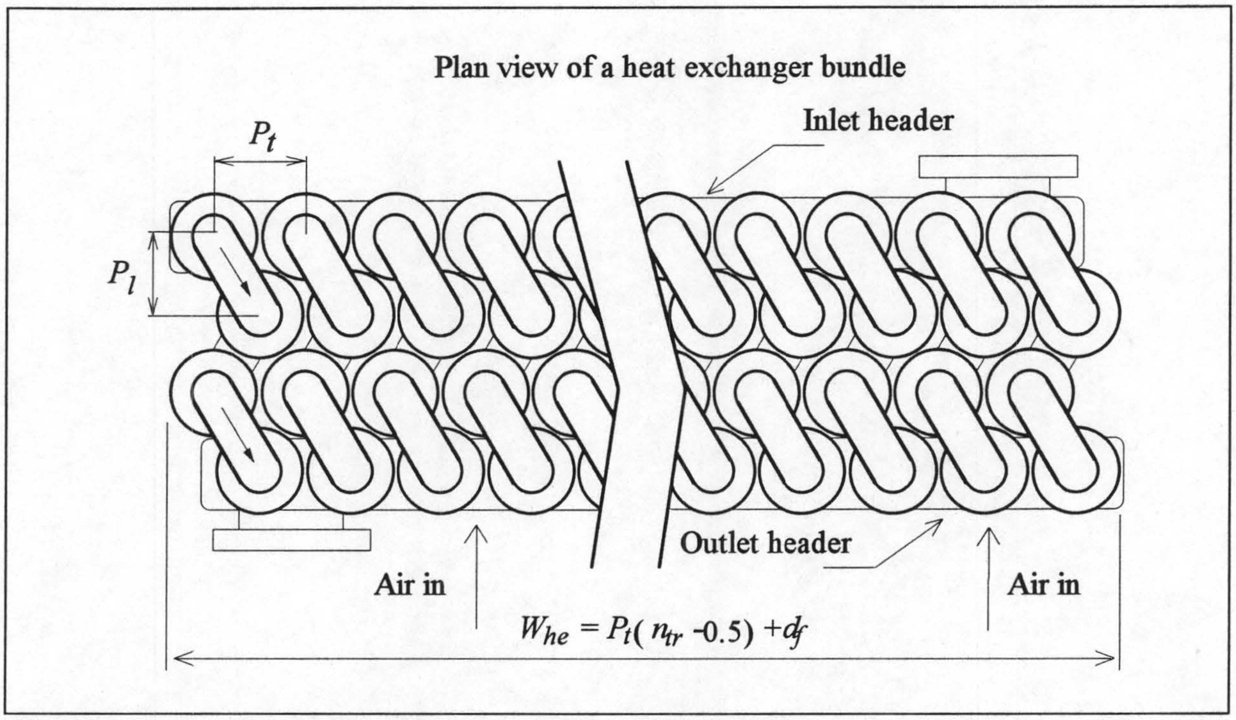

Figure 4.2: *Plan view of a four pass heat exchanger bundle.*

4.2.2 Overall heat transfer coefficient

For a combined conductive convective problem, as in the case with a dry heat exchanger bundle, it is convenient to express the heat transfer rate in terms of an overall heat transfer coefficient. According to Holman [89HO1], in the case of a hollow cylinder with convective boundaries, the overall heat transfer coefficient based on the inside area of the tube can be expressed as:

$$U_i = \left(\frac{1}{h_i} + \frac{A_i \ln(r_o/r_i)}{2\pi kL} + \frac{A_i}{A_o}\frac{1}{h_o} \right)^{-1} \tag{4.2.1}$$

and based on the outside area of the tube as:

$$U_o = \left(\frac{A_o}{A_i}\frac{1}{h_i} + \frac{A_o \ln(r_o/r_i)}{2\pi kL} + \frac{1}{h_o} \right)^{-1} \tag{4.2.2}$$

This formula for the overall heat transfer coefficient can also be used for a finned tube if the outside transfer coefficient (h_o) is replaced by the effective air side heat transfer coefficient of the finned tube. In section 4.2.3 it will be shown how this effective air side heat transfer coefficient (h_{ae}) can be obtained. For finned tubes it is sometimes also necessary to include the contact resistance between the fins and the tubes in equations (4.2.1) and (4.2.2).

4.2.3 The air side heat transfer coefficient

The air side performance characteristics of dry heat exchangers are usually determined under idealised conditions in specially designed wind tunnels. If no such facility is available, the air side heat transfer and pressure drop coefficients for the heat exchanger bundle have to be determined with one of the different correlations that are reported in the literature. These correlations were derived by different researchers and they differ from one another in their respective range of applicability and accuracy. One of these correlations, that gives good results, was derived by Ganguli et al. [85GA1]. This correlation will be used in the hybrid cooling tower calculations.

Ganguli et al. [85GA1] proposed the following correlation for the air side heat transfer coefficient for three or more rows of finned tubes:

$$\mathrm{Nu} = \frac{h_a d_r}{k} = 0.38\,\mathrm{Re}^{0.6}\,\mathrm{Pr}^{0.333}\left(\frac{A_a}{A_r}\right)^{-0.15} \tag{4.2.3}$$

where $\mathrm{Re} = G_c d_r / \mu$ and the ratio of the total air-side area to the root area (A_r), if no fins are present, is given by:

$$\frac{A_a}{A_r} = \frac{A_f + A_{re}}{A_r} = \left[\frac{\left(d_f^2 - d_r^2\right)}{2} + d_f t_{ft} + d_r\left(P_f - t_{fr}\right)\right] \Big/ \left(d_r P_f\right) \tag{4.2.4}$$

This correlation is valid for:

$11.176 < d_r < 50.8$ mm
$5.842 < \left(d_f - d_r\right)/2 < 19.05$ mm
$2.3 < P_f < 3.629$ mm
$0.254 < t_f < 0.559$ mm
$27.432 < P_t < 98.552$ mm
$1800 < \mathrm{Re} < 100000$
$1 < \left(A_f + A_{re}\right)/A_r < 50$

The air side heat transfer coefficient that is obtained from equation (4.2.3) must be multiplied by a surface effectiveness (e_f) to obtain the effective heat transfer coefficient. The surface effectiveness is defined as the actual heat transfer from the fin and free base surface, divided by the heat transfer from those surfaces when the entire fin is at the root or base temperature.

The surface effectiveness can therefore be given as:

$$e_f = \frac{h_a A_r (T_r - T_\infty) + h_a A_f \eta_f (T_r - T_\infty)}{h_a A_a (T_r - T_\infty)} = 1 - \frac{A_f (1 - \eta_f)}{A_a} \tag{4.2.5}$$

where η_f is the fin efficiency, which is defined as the ratio of the actual heat transferred by the fin, to the heat that would be transferred if the entire fin was at the root temperature. The analytically determined formulas for the efficiencies of radial fins are complex functions that are difficult to solve and an approximate method will therefore be used. The empirical method given by Schmidt [46SC1] is relatively simple but accurate enough for application in most practical cases.

For a radial fin of uniform thickness he finds:

$$\eta_f = \frac{\tanh\left(bd_r \frac{\phi}{2}\right)}{\left(bd_r \frac{\phi}{2}\right)} \tag{4.2.6}$$

where $b = \left(\frac{2h_a}{k_f t_f}\right)^{0.5}$ and

$$\phi = \left(\frac{d_f}{d_r} - 1\right)\left[1 + 0.35 \ln\left(\frac{d_f}{d_r}\right)\right]$$

The fin root diameter d_r is replaced by the outside tube diameter d_{to} if the fin has no shoulder at its root.

The effective air side heat transfer coefficient can now be defined as $h_{ae} = h_a e_f$.

4.2.4 The water side heat transfer coefficient

The heat transfer from the water to the duct is determined by the nature of the flow in the duct, i.e. laminar, transitional or turbulent. Furthermore, the flow may be fully developed, hydrodynamically or thermally, or it may be developing in one form or another. The heat transfer coefficients for laminar flow in ducts of various geometries have been determined analytically and numerically. In the region of transitional and turbulent flow, correlations based on experimental measurements are employed to predict heat transfer rates. For the application in hybrid towers, the flow would mostly be developed and in the turbulent region. Gnielinski [75GN1] proposed the following equation for turbulent flow:

$$\mathrm{Nu} = \frac{h_i d}{k} = \frac{(f_D/8)(\mathrm{Re}-1000)\,\mathrm{Pr}\left[1+(d/L)^{0.67}\right]}{1+12.7(f_D/8)^{0.5}\left(\mathrm{Pr}^{0.67}-1\right)} \tag{4.2.7}$$

where the D' Arcy friction factor is:

$$f_D = (1.82\log\mathrm{Re} - 1.64)^{-2} \tag{4.2.8}$$

This equation is valid for the following ranges:

$2300 < \mathrm{Re} < 10^6$

$0.5 < \mathrm{Pr} < 10^4$

$0 < \frac{d}{L} < 1$

4.2.5 Solving the energy equation with the ε-NTU method

In the calculation of the heat transfer in the dry section, only the water inlet and air inlet temperatures are known. The ε-NTU method is therefore used to solve the energy equation. The effectiveness is defined as the ratio of the actual heat transfer to the maximum possible heat transfer.

$$\text{Effectiveness} = \varepsilon = \frac{Q}{Q_{\max}} \tag{4.2.9}$$

To determine the maximum possible heat transfer for the exchanger it should be remembered that the maximum value can only be attained if one of the fluids was to undergo a temperature change equal to the maximum temperature difference present in the exchanger. The fluid that may undergo this maximum temperature difference is the one having the minimum heat capacity (mc_p). This minimum value for mc_p is called C_{min}, and the value of mc_p for the other fluid is then called C_{max}.

The effectiveness can also be expressed as:

$$\varepsilon = \frac{\Delta T(\text{minimum fluid})}{T_{wi} - T_{ai}}$$

For a crossflow configuration Holman [89HO1] gives the effectiveness relations, where $C_r = \frac{C_{\min}}{C_{\max}}$ and $NTU = \frac{U_o A_a}{C_{\min}}$, as follows:

For the C_{min} fluid unmixed and the C_{max} fluid mixed:

$$\varepsilon = \frac{1}{C_r}\left\{1 - \exp\left[-C_r\left(1 - e^{-NTU}\right)\right]\right\} \tag{4.2.10}$$

For the C_{min} fluid mixed and the C_{max} fluid unmixed:

$$\varepsilon = 1 - \exp\left\{-\frac{1}{C_r}\left[1 - \exp\left(-NTU \times C_r\right)\right]\right\} \tag{4.2.11}$$

For both fluids mixed:

$$\varepsilon = 1 - \exp\left[\frac{\exp\left(-NTU^{0.78} C_r\right) - 1}{NTU^{-0.22} C_r}\right] \tag{4.2.12}$$

Equations (4.2.10) and (4.2.11) are used for bare tube exchangers, while equation (4.2.12) is usually used for finned tube exchangers.

Since the heat exchanger bundles used in the hybrid tower have a multipass configuration a correction has to be used. Kays and London [64KA1] have derived an expression for a multipass cross-counterflow arrangement with mixing of the process fluid between passes and for mixed or unmixed flow on the air side. They derived the following expression:

$$\varepsilon = \frac{\left[\frac{1 - \varepsilon_p C_r}{1 - \varepsilon_p}\right]^{n_p} - 1}{\left[\frac{1 - \varepsilon_p C_r}{1 - \varepsilon_p}\right]^{n_p} - C_r} \tag{4.2.13}$$

where n_p is the number of identical passes and ε_p is the effectiveness per pass.

For the case of $C_r = 1$ they propose the following relation:

$$\varepsilon = \frac{n_p \varepsilon_p}{1 + \left(n_p - 1\right)\varepsilon_p} \tag{4.2.14}$$

The value for ε_p is determined by replacing NTU in the effectiveness equations with NTU_p where $NTU_p = NTU / n_p$.

From the determined effectiveness the heat transfer can now be determined from equation (4.2.9).

When a heat exchanger has four or more passes, the effectiveness for the heat exchanger can also be approximately determined with the counterflow equation as given by Holman [89HO1]. This equation is:

$$\varepsilon = \frac{1-\exp\left[-NTU\left(1-C_r\right)\right]}{1-C_r\exp\left[-NTU\left(1-C_r\right)\right]} \tag{4.2.15}$$

This can be done since a four pass heat exchanger bundle arrangement approaches the thermodynamic limit of a pure counterflow arrangement asymptotically. This asymptotic approach is depicted in figure 4.3.

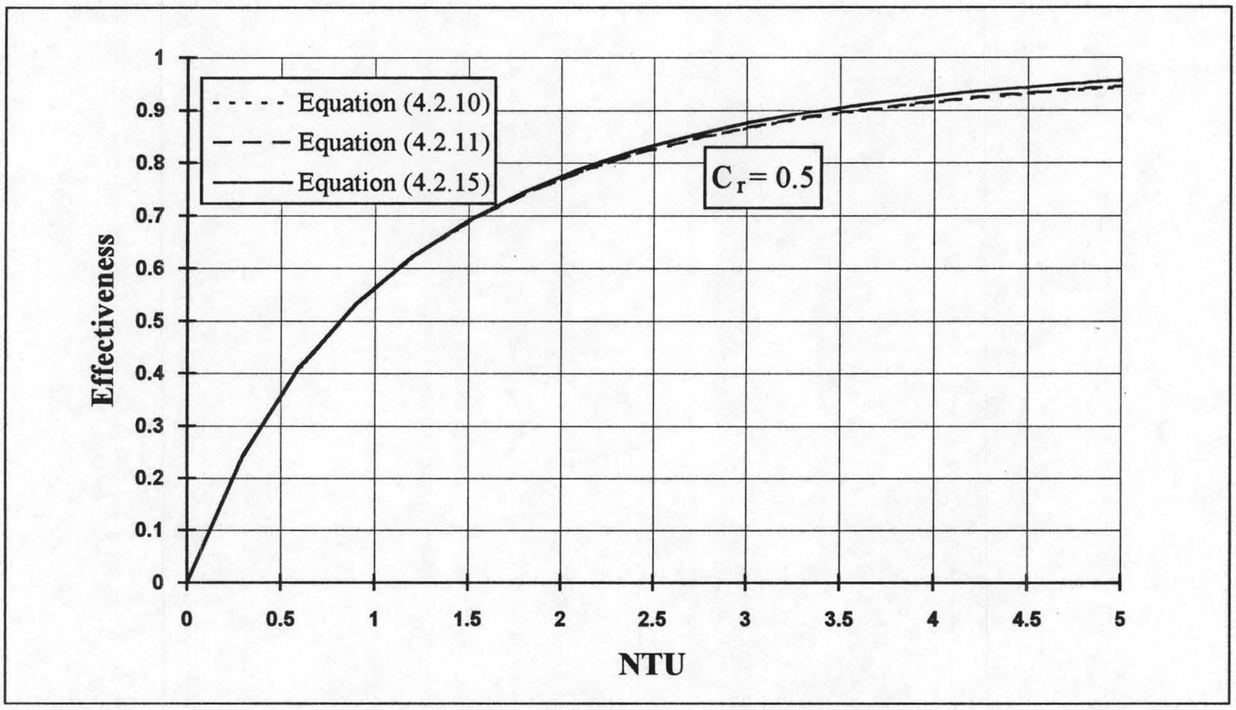

Figure 4.3: *Comparison between the effectiveness values determined from the corrected crossflow and the counterflow equations for a four pass configuration with $C_r = 0.5$.*

CHAPTER

FIVE

DRAFT CALCULATION

Depending on the geometry of the hybrid tower the air can follow series or parallel routes through it. For the parallel path air flow tower it is sometimes desirable to control the air flow through the wet and dry sections separately. To accomplish this, variable air restriction devices can be used in either one, or both of the wet and dry sections, or the wet and dry sections can each have their own variable speed fan. The method for solving the draft through a series path air flow hybrid tower is much the same as for solving the draft through a normal wet or dry cooling tower, with the exception that there are more restrictions in the path of the air flow. For a parallel path air flow tower, the method for solving the draft is somewhat different, and the draft equation is complicated by added constraints that have to be satisfied.

The draft in a PPAF hybrid tower is the result of a pressure difference over the tower's fan (forced or induced draft tower) and to a lesser extent the hydrostatic pressure difference that exists over the tower. This pressure potential causes air to flow through the tower in order to obtain a state of equilibrium. When the sumtotal of the pressure losses through the tower is equal to the pressure difference over the tower, equilibrium is established and the air mass flow rate through the tower stays constant. The pressure losses that occur through the tower are dependent on the air mass flow rates through the wet and dry sections, the tower geometry, the packing and heat exchanger characteristics and the various other flow resistances that are encountered through the tower. For a specific fan, the pressure potential delivered by the fan is dependent on the mass flow rate and density of the air flowing through it.

In this chapter the pressure losses that usually occur through a PPAF hybrid tower are discussed in section 5.1 and the pressure loss coefficients for each obstacle are given. The equations to determine the hydrostatic draft are given in section 5.2. Polynomials for the performance curves of the fan/diffuser used in the hybrid tower sample solution of section 6.3, along with a discussion of the relevant fan performance theory, are given in section 5.3.

5.1 Pressure loss coefficients for an induced draft PPAF hybrid tower

Pressure losses through a cooling tower are determined from loss coefficients that are usually given in terms of experimentally obtained correlations. If no correlation exists for a specific loss coefficient, or if the exact nature of the resistance that causes the loss is not yet known, values for these coefficients are estimated. The loss coefficients are based on certain air velocities and air densities, usually the velocity and the density of the air at the specific obstacle. With these loss coefficients the pressure drop can be determined as follows:

$$\Delta p = K\tfrac{1}{2}\rho v^2 \qquad (5.1.1)$$

Consider the schematic layout of the hybrid tower shown in figure 5.1. Different positions in the tower are indicated by the numbers 1 to 12. These numbers are used consistently throughout this thesis and are used to indicate all geometries and air properties relevant to that particular position in the example PPAF hybrid tower.

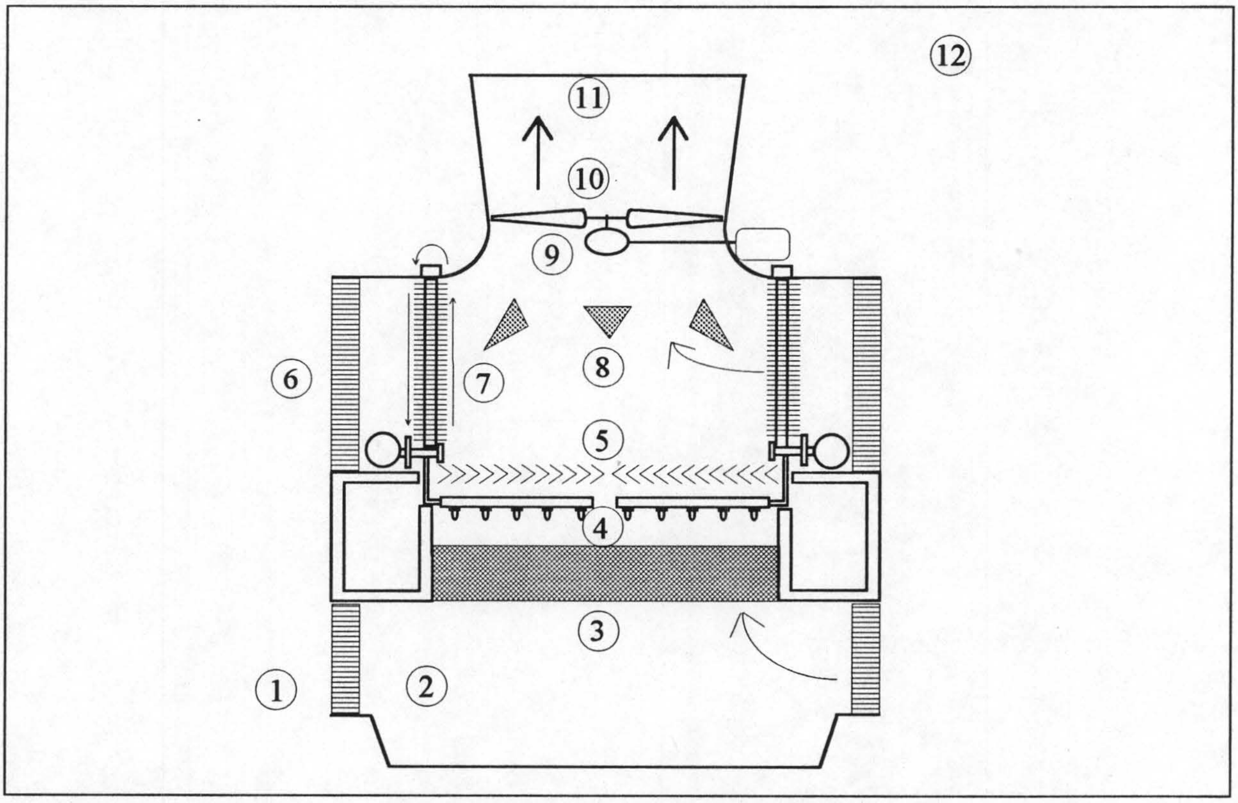

Figure 5.1: *Schematic representation of a PPAF hybrid tower.*

For comparative purposes, and simplification of the draft equation, the loss coefficients through the wet section will all be based on the mean air properties through the fill. The air density is taken as the mean harmonic density of the air through the fill and the air velocity through the fill is determined from the mean air mass flow rate and the mean harmonic air density through the fill. The mean harmonic density is determined as follows:

$$\rho_{av34} = 2\left[\frac{1}{\rho_{av3}} + \frac{1}{\rho_{av4}}\right]^{-1} \tag{5.1.2}$$

If it is assumed that the air mass flow rate through the wet section of the tower is constant ($m = m_{av34}$), the loss coefficient that is based on the mean air conditions through the fill (K_{ref}), is determined from the local loss coefficient as follows:

$$\begin{aligned} K_{ref} &= K\frac{\frac{1}{2}\rho v^2}{\frac{1}{2}\rho_{av34}v_{av34}^2} = K\frac{\rho m^2/\rho^2 A^2}{\rho_{av34}\, m_{av34}^2/\rho_{av34}^2 A_{fr}^{\;2}} \\ &= K\frac{\rho_{av34}}{\rho}\left[\frac{A_{fr}}{A}\right]^2 \end{aligned} \tag{5.1.3}$$

In the same way the loss coefficients for the dry section will all be based on the mean air conditions through the heat exchanger bundle and the loss coefficients for the losses that occur after the two air streams combine will be based on the air conditions through the fan.

The pressure losses that usually occur through hybrid towers as the one shown in figure 5.1 will now be discussed for each of the 3 regions, i.e. the wet region, the dry region and the mixed region.

5.1.1 The pressure losses through the wet section

Inlet louvers

Kelly [76KE1] suggests a value of $K_{il2} = 5$ for inlet louvers in crossflow towers, based on the air speed and density through the louvers. According to Jorgensen [61JO1] the value for K_{il2} varies from 2 to 5. He also states that a 30° louver with up to 80% open area can have a K_{il2} of as low as 2 and that the older type of louver with a 45° angle can have a K_{il2} of as high as 5.

If this coefficient is referred to the conditions through the fill it becomes

$$K_{il} = K_{il2}\frac{\rho_{av34}}{\rho_{av2}}\left[\frac{A_{fr}}{A_{il}}\right]^2 \approx K_{il2}\frac{\rho_{av34}}{\rho_{av1}}\left[\frac{A_{fr}}{A_{il}}\right]^2 \tag{5.1.4}$$

Noise attenuator elements

In most hybrid cooling towers silencing measures are required since the fans, the air damper doors and the inlet louvers all generate a lot of unwanted noise. Noise attenuator elements are therefore usually installed to comply with noise regulations. Typical values for the loss coefficients of such noise attenuator elements are from $K_{na2} = 2$ up to $K_{na2} = 3$. Referred to the conditions through the fill it becomes:

$$K_{na} = K_{na2}\frac{\rho_{av34}}{\rho_{av2}}\left[\frac{A_{fr}}{A_{na}}\right]^2 \approx K_{na2}\frac{\rho_{av34}}{\rho_{av1}}\left[\frac{A_{fr}}{A_{na}}\right]^2 \tag{5.1.5}$$

The rain zone

The following correlation for the pressure loss coefficient through the rain zone of a rectangular cooling tower was obtained by Terblanche [93TE1]:

$$\begin{aligned} K_{rz3} = {} & 148.4\left[\frac{W_{fi}/2}{H_3}\right]^{3.47} \times 227.7^{\frac{H_3}{W_{fi}/2}} \times \left[\frac{\rho_{w3}}{\rho_{av1}}\right]^{0.204} \\ & \times \exp\left[0.017544\left(\ln\left(\frac{d_d}{H_3}\right) - 10.56\right)^2 - 0.015074\left(\ln\left(\frac{v_w}{v_{av34}}\right) - 25.9\right)^2\right. \\ & +0.059172\left(\ln\left(\frac{\rho_{av1}v_{av34}H_3}{\mu_{av1}}\right) - 15.4\right)^2 + 0.206612\left(\ln\left(\frac{v_{av34}^2}{gH_3}\right) + 1.92\right)^2 \\ & \left. +0.037313\left(\ln\left(\frac{\rho_{av1}v_{av34}^2H_3}{\sigma_{w3}}\right) - 4.05\right)^2\right] \end{aligned} \tag{5.1.6}$$

The correlation is valid within the following limits.

$2 \le d_d \le 8$ mm
$2 \le H_3 \le 8$ m
$8 \le W_{fi} \le 80$ m
$0.001 \le v_w \le 0.006$ m/s
$1 \le v_{av} \le 5$ m/s
$0.8 \le \rho_{av} \le 1.3$ kg/m^3

$992.2 \leq \rho_w \leq 999.7 \text{ kg/m}^3$
$9.7 \leq g \leq 10 \text{ m/s}^2$
$0.0696 \leq \sigma_w \leq 0.0742 \text{ N/m}$
$0 \leq T_a \leq 40 \text{ °C}$
$10 \leq T_w \leq 40 \text{ °C}$

Even though this correlation gives a conservative value for the pressure drop through the rain zone it will still be used. If this correlation is referred to the conditions through the packing it becomes:

$$K_{rz} = K_{rz3}\left[\frac{\rho_{av34}}{\rho_{av3}}\right] \approx K_{rz3}\left[\frac{\rho_{av34}}{\rho_{av1}}\right] \tag{5.1.7}$$

Tower supports

The loss coefficient for the tower supports can be determined from the drag coefficient, C_{Dts}, of the supports. The force exerted on each support, is:

$$F_{Dts} = \tfrac{1}{2}\rho_{av2}v_{av2}^2 C_{Dts} L_{ts} d_{ts} \tag{5.1.8}$$

If the number of tower supports is n_{ts}, then the pressure drop coefficient for the tower supports is:

$$K_{ts2} = \frac{C_{Dts} L_{ts} d_{ts} n_{ts}}{2W_3 H_3} \tag{5.1.9}$$

Referred to the conditions through the fill it becomes:

$$K_{ts} = K_{ts2}\frac{\rho_{av34}}{\rho_{av2}}\left[\frac{A_{fr}}{A_{ts}}\right]^2 \approx K_{ts2}\frac{\rho_{av34}}{\rho_{av1}}\left[\frac{A_{fr}}{A_{ts}}\right]^2 \tag{5.1.10}$$

Fill supports

The fill is supported by pillars and cross bars. These support elements cause a significant pressure drop which is dependent on the type and geometry of these elements. The value for K_{fs} is usually taken in the range of 0.3 to 0.5.

Referred to the conditions through the fill, it becomes:

$$K_{fs} = K_{fs2}\frac{\rho_{av34}}{\rho_{av2}} \approx K_{fs2}\frac{\rho_{av34}}{\rho_{av1}} \tag{5.1.11}$$

Fill

A correlation for the pressure drop through the fill is obtained from experimental data. This correlation is usually in the following form:

$$K_{fi} = a_p G_w^{b_p} G_a^{c_p} \tag{5.1.12}$$

It should be noted that the correlation for the pressure loss coefficient was derived for a fill with a specific fill height, under specific operating conditions. Care must therefore be taken when the correlation is used for a fill having a different fill height, or when the fill is operating under totally different conditions.

An approximated static pressure loss where momentum effects are excluded, (Δp^*_{fi}), can be obtained from the measured static pressure loss by subtracting the change in momentum from it. If the correlation is based on the static pressure loss coefficients determined from the static pressure losses which exclude momentum effects, a pressure loss can be accurately predicted over a wider range of cooling tower operating conditions. For each specific tower operating point the momentum and dynamic pressure increase of the air is determined and incorporated into the pressure loss coefficient. The pressure loss coefficient must therefore be re-calculated during each iteration. The approximated static correlation is given as:

$$K^*_{fi} = \frac{\Delta p^*_{fi}}{\frac{1}{2}\rho v^2} = a_p G_w^{b_p} G_a^{c_p} \tag{5.1.13}$$

From the above static correlation, the pressure loss coefficient for a specific tower operating point can be determined as follows:

- First determine the static pressure loss where momentum effects are included. This can be determined from the approximated static pressure loss as follows:

$$\Delta p_{fi} = \Delta p^*_{fi} + \left(\rho_{avo} v_{avo}^2 - \rho_{avi} v_{avi}^2\right) \tag{5.1.14}$$

where Δp^*_{fi} is determined from equation (5.1.13).

- The total pressure loss over the fill is then:

$$\begin{aligned}\Delta p_{fitot} &= \Delta p_{fi} + \left(\tfrac{1}{2}\rho_{avi}v_{avi}^2 - \tfrac{1}{2}\rho_{avo}v_{avo}^2\right) \\ &= \Delta p_{fi}^* + \left(\rho_{avo}v_{avo}^2 - \rho_{avi}v_{avi}^2\right) + \left(\tfrac{1}{2}\rho_{avi}v_{avi}^2 - \tfrac{1}{2}\rho_{avo}v_{avo}^2\right) \\ &= \Delta p_{fi}^* + \left(\tfrac{1}{2}\rho_{avo}v_{avo}^2 - \tfrac{1}{2}\rho_{avi}v_{avi}^2\right)\end{aligned} \tag{5.1.15}$$

- The pressure loss coefficient is then:

$$K_{fi} = \frac{\Delta p_{fitot}}{\frac{1}{2}\rho v^2} = K_{fi}^* + \frac{\left(\rho_{avo}v_{avo}^2 - \rho_{avi}v_{avi}^2\right)}{\rho v^2} \approx K_{fi}^* + \frac{2(\rho_{avi} - \rho_{avo})}{(\rho_{avi} + \rho_{avo})} \tag{5.1.16}$$

if it is assumed that $m_{avi} \approx m_{avo} \approx m_{av34}$.

This coefficient can now be used in the cooling tower solution for the specific tower operating conditions.

Spray zone

The following correlation was obtained from measured data given by Cale [82CA1].

$$K_{sp4} = L_{sp}\left[0.4\frac{G_w}{G_a} + 1\right] \tag{5.1.17}$$

Referred to the conditions through the fill it becomes:

$$K_{sp} = K_{sp4}\left[\frac{\rho_{av34}}{\rho_{av4}}\right] \approx K_{sp4}\left[\frac{\rho_{av34}}{\rho_{av5}}\right] \tag{5.1.18}$$

Water distribution system

The spray is uniformly distributed by a system of pipes and spray nozzles. A typical value for the loss coefficient through such a system is 0.5. If based on the conditions through the fill, it becomes:

$$K_{wd} = K_{wd5}\left[\frac{\rho_{av34}}{\rho_{av5}}\right] \tag{5.1.19}$$

Tower inlet losses

Terblanche [93TE1] obtained the following correlation for the inlet losses of a rectangular counterflow cooling tower with sharp tower inlets:

$$K_{ct3}=\left[1.1+1.1\left(\frac{W_3/2}{H_3}\right)^3-0.05\left(\frac{W_3/2}{H_3}\right)\exp\left(\frac{W_3/2}{H_3}\right)\right]\times K_{he}^{\left[0.079\cos\left(\frac{W_3/2}{H_3}\right)+0.102\sin\left(\frac{W_3/2}{H_3}\right)-0.29\right]} \qquad (5.1.20)$$

where $K_{he}=K_{fs}+K_{fi}+K_{sp}+K_{wd}+K_{de}$.

This correlation is valid for:

$$0\le\frac{W_3}{H_3}\le 10$$

$$4\le K_{he}\le 80$$

If this loss coefficient is referred to the conditions through the fill, it becomes:

$$K_{ct}=K_{ct3}\left[\frac{\rho_{av34}}{\rho_{av3}}\right]\approx K_{ct3}\left[\frac{\rho_{av34}}{\rho_{av1}}\right] \qquad (5.1.21)$$

Drift eliminators

The losses for different types of drift eliminators may be expressed as follows:

$$K_{de}=a\left(Ry_{de}\right)^b\frac{\rho_{av34}}{\rho_{av5}} \qquad (5.1.22)$$

Kelly [76KE1] and Jorgenson [61JO1] both suggest a value of 5 for K_{de5}. Botes [95BO1] tested a few different types of drift eliminators under wet conditions in an experimental tower. He obtained correlations for the pressure loss coefficients of the form given in equation (5.1.22).

5.1.2 The pressure losses through the dry section

Noise attenuator elements

As for the wet section, the dry section also contains noise attenuator elements. The same value for K_{na6} applies as for the wet section.

Heat exchangers

The pressure loss through the heat exchanger can be determined experimentally and a correlation for each specific heat exchanger can be obtained from the experimental data. If such data is not available a general correlation can be used. A frequently used correlation is that of Ganguli et al. [85GA1]:

$$Eu = \frac{\rho \Delta p}{G_c^2} = 2n_r \left[1 + 2\exp\left(\frac{d_f - P_t}{4d_r} \right) \Big/ \left(1 + \frac{P_t - d_f}{d_r} \right) \right] \times \left[0.021 + \frac{13.6(d_f - d_r)}{\mathrm{Re}(P_f - t_f)} + 0.25246 \left(\frac{d_f - d_r}{\mathrm{Re}(P_f - t_f)} \right)^{0.2} \right] \tag{5.1.23}$$

where $\mathrm{Re} = G_c d_r / \mu$

The limits of applicability of this equation are similar to those of equation (4.2.3) with:

$$2.5 \le \frac{d_f - d_r}{2(P_f - t_f)} \le 12.5$$

as an extra limit.

Air damper doors

Air damper doors can be placed before or behind the dry heat exchangers, to prevent airflow through the dry exchangers when conditions require that only the wet section be operating. These damper doors can be either fully opened or fully closed. Although it can be assumed that some air leakage will still occur when the air damper doors are closed, this will be ignored and the loss coefficient for the air damper doors will therefore be either 0 or ∞.

5.1.3 The pressure losses through the mixed region

After the two air streams combine all further pressure losses have to be based on the combined air mass flow rate. For the sake of simplicity these loss coefficients are based on the air density and air velocity through the fan. The losses that can occur after the two air streams combine are the following:

Air mixing devices

According to Henning [80HE1] the most commonly used mixing devices are vortex generator plates and cylindrical vortex generators. For the vortex generator plates he specifies a pressure loss that is less than 2% of the total pressure loss through the tower and for the cylindrical vortex generators he specifies a pressure loss of less than 2% of the pressure loss through the fill. Pressure loss coefficients of 0.85 and 0.7 were assumed for the respective cases.

The pressure loss coefficient can therefore be expressed as:

$$K_{me8} = \frac{0.02 \times (\text{ Pressure loss through tower})}{0.5\rho_{av8} v_{av8}^2} \approx 0.85 \tag{5.1.24}$$

if vortex generator plates are used, and as:

$$K_{me8} = \frac{0.02 \times (\text{ Pressure loss through fill})}{0.5\rho_{av8} v_{av8}^2} \approx 0.7 \tag{5.1.25}$$

if cylindrical vortex generators are used.

Referred to the conditions through the fan they become:

$$K_{me} = K_{me8} \left[\frac{\rho_{av9}}{\rho_{av8}} \right] \left[\frac{A_{fan}}{A_{me}} \right]^2 \approx K_{me8} \left[\frac{A_{fan}}{A_{me}} \right]^2 \tag{5.1.26}$$

Fan suction and discharge losses

At the suction side of the fan further pressure losses occur as a result of structures like the fan supports and the fan driving mechanisms. These losses can all be encompassed in a single loss coefficient K_{fsuc9}. This loss coefficient is already based on the conditions through the fan and K_{fsuc} is therefore equal to K_{fsuc9}.

Fan discharge pressure losses usually occur as a result of obstacles such as screens, walkways and sound attenuators. These losses can all be combined into a single loss coefficient K_{fdis10}. The value of K_{fdis10} depends upon the kind and nature of the obstructions that occur. This value must also be referred to the air conditions through the fan. It then becomes:

$$K_{fdis} = K_{fdis10} \tag{5.1.27}$$

Venter and Kröger [91VE1] did some research on the fan suction and discharge losses. They found that for reasonably uniformly distributed resistances, the loss coefficients can be predicted satisfactorily with the so-called bulk method. With this method the loss coefficient is taken as a function of the projected area of the obstacle, the obstacle distance from the fan, the casing diameter and the cross sectional area, respectively.

Diffuser

A large part of the dynamic pressure component of the air that leaves the fan is regained by means of a diffuser. The rest of this dynamic pressure is lost through frictional losses in the diffuser, or dissipated into the atmosphere on exit.

For a well-designed diffuser, Kelly [76KE1] suggests that the angle between the diffuser wall and the centre line has to be about 7 °. With this angle the area ratio of the diffuser is relatively small. Patterson [38PA1] determined diffuser efficiencies. From a graph of his results, as given by Kröger [89KR1], the efficiency (η_{dif}) of a diffuser with a small area ratio and a 14° included angle is about 90 %. Salta [95SA1] carried out experiments to determine diffuser efficiencies for round to round and round to rectangular diffusers. For a round to round diffuser with a 13.7 ° included angle he found that his results compared well with a diffuser efficiency η_{dif} of 85 % as proposed by Wallis [83WA1] for a round to round diffuser with a 14° included angle.

According to Wallis [83WA1] and Kröger [89KR1], if the efficiency of the diffuser is known, the loss coefficient for the diffuser, based on the air conditions at the inlet of the diffuser and for air flow entering the diffuser with a uniform axial velocity, can be determined as follows:

$$K_{dif10} = \left(1-\eta_{dif}\right)\left[1-\left(\frac{A_{10}}{A_{11}}\right)^2\right] = \left(1-\eta_{dif}\right)\left[1-\left(\frac{d_{10}}{d_{11}}\right)^4\right] \qquad (5.1.28)$$

Referred to the conditions before the fan it becomes:

$$K_{dif} = K_{dif10}\left[\frac{\rho_{av9}}{\rho_{av10}}\right] \qquad (5.1.29)$$

Salta [95SA1] found that under practical working conditions where the air does not enter the diffuser with a uniform axial velocity, the actual pressure recovery is generally slightly greater than the expected pressure recovery for small blade angles (10 °, 12 °, 14 °) and slightly less for large blade angles (16 °, 18 °, 22 °, 26 °). It is therefore better to use combined fan/diffuser characteristic curves when solving a cooling tower as the one shown in figure 5.1. This was done in the sample calculation of section 6.3.

Tower exit

That part of the dynamic pressure that the diffuser does not regain is lost at the tower exit. Because the velocity distribution at the tower exit is not uniform, a correction factor α_e has to be used. The value for this correction factor differs for different diffuser and fan geometries.

For most large axial flow fans a correction factor of about 2 is a good approximation. If the correction factor is known the pressure loss at the tower exit becomes:

$$\Delta p_{loss} = \alpha_e \tfrac{1}{2} \rho_{av11} v_{av11}^2 \tag{5.1.30}$$

where $K_{e11} = \alpha_e$

Referred to the conditions before the fan it becomes:

$$K_e = \alpha_e \left[\frac{\rho_{av9}}{\rho_{av11}} \right] \left[\frac{A_{fan}}{A_{11}} \right]^2 \tag{5.1.31}$$

The exit loss coefficient can be ignored in the calculations if fan/diffuser characteristics as those obtained by Salta [95SA1] are used instead of the normal fan characteristics, since the exit loss is then already incorporated in the system characteristics.

5.2 Pressure lapse rate for saturated and dry ambient air

Dry atmosphere

For a temperature lapse rate of -0.00975 K/m, the pressure at any height z above a reference level in a dry atmosphere, can be determined as follows according to Kröger [89KR1]:

$$p_{az} = p_{a1} \left[1 - 0.00975 \left(\frac{z}{T_{a1}} \right) \right]^{3.5(1+w_1)[1-w_1/(w_1+0.62198)]} \tag{5.2.1}$$

where p_{a1}, T_{a1} and w_1 are the pressure, dry bulb temperature and humidity ratio of the atmosphere at the reference level ($z = 0$) respectively.

The pressure difference between the reference level and any height z is therefore:

$$p_{a1} - p_{az} = p_{a1} \left[1 - \left(1 - 0.00975 \left[\frac{z}{T_{a1}} \right] \right)^{3.5(1+w_1)[1-w_1/(w_1+0.62198)]} \right] \tag{5.2.2}$$

Saturated atmosphere

The temperature lapse rate for saturated air, according to Kröger [89KR1], is:

$$\frac{dT}{dz} = \xi_T = \frac{-(1+w)g}{c_{pma} + \frac{dw}{dT}\left[i_{fgw0} - \left(c_{pw} - c_{pv}\right)(T - 273.15)\right]} \tag{5.2.3}$$

where

$$\frac{dw}{dT} = \frac{7.966 \times 10^{14}\, e^{-\left(\frac{5406.1915}{T}\right)}}{pT^2} \tag{5.2.4}$$

In a saturated atmosphere, the pressure at any height z above a reference level can then be determined as follows [89KR1]:

$$p_{az} = p_{a1}\left[1 + \xi_{T_{a1}}\left(\frac{z}{T_{a1}}\right)\right]^{-(1+w_1)\left[1 - \frac{w_1}{(w_1+0.62198)}\right]\left[\frac{g}{(R\xi_{T_{a1}})}\right]} \tag{5.2.5}$$

where p_{a1}, T_{a1} and w_1 are the pressure, temperature and humidity ratio of the saturated atmosphere at the reference level ($z = 0$) respectively.

5.3 The fan characteristics

Fan manufacturers specify the performance of their fans by means of fan performance curves. These curves usually give fan static pressure and fan power consumption as a function of the volumetric flow rate through the fan. The curves are obtained from performance tests, either on the prototype fan or on a scale model. It should be noted that the performance of a fan is affected by the connections made to its inlet and outlet. The four fan test installation types are:

- Type A : Free inlet, free outlet
- Type B : Free inlet, ducted outlet
- Type C : Ducted inlet, free outlet
- Type D : Ducted inlet, ducted outlet.

The fan test data should, wherever possible, be obtained by the method that is most representative of the geometry of the real installation.

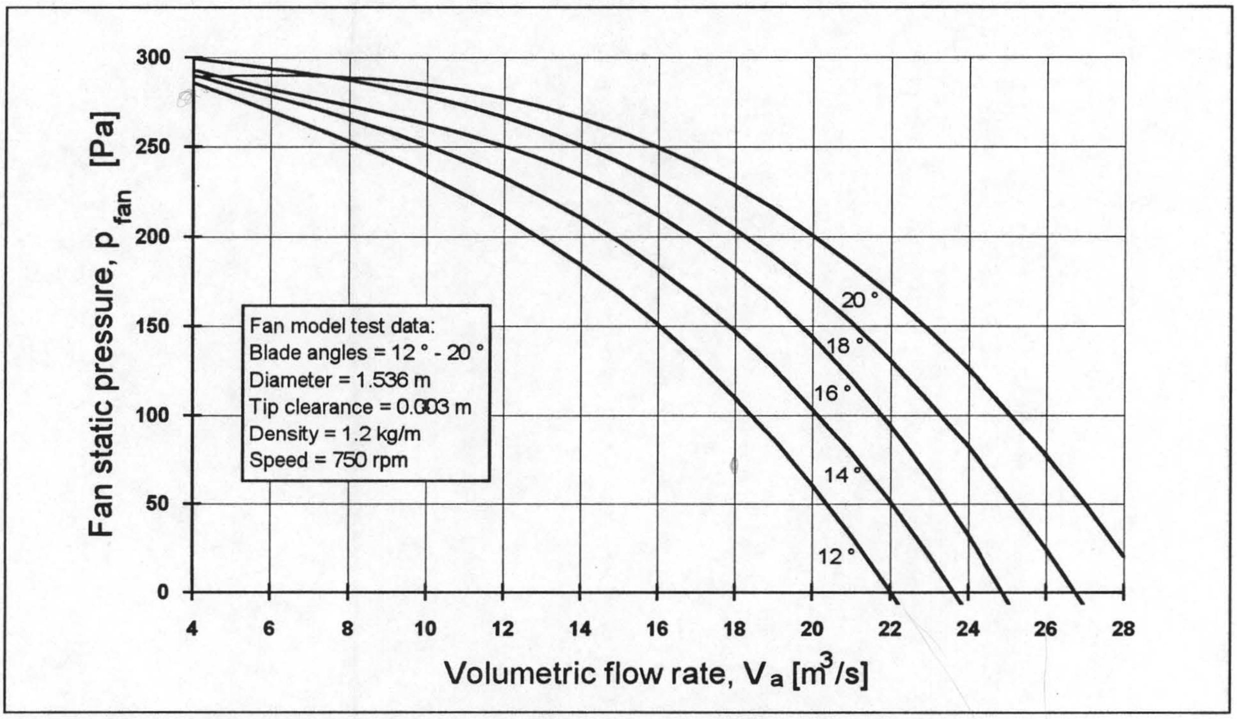

Figure 5.2: *Fan static pressure performance curves for fan model.*

The performance characteristics of a 1.536 m diameter, adjustable, 8-bladed axial flow fan model are given in figures 5.2, 5.3 and 5.6. All the performance characteristics are specified at a reference air density of 1.2 kg/m^3 and a fan rotational speed of 750 rpm. As noise can be a problem at fan installations, a limit of approximately 60 m/s is usually placed on the maximum speed for the fan blade tip. From the maximum allowable tip speed the maximum rotational speed of the prototype fan can be determined.

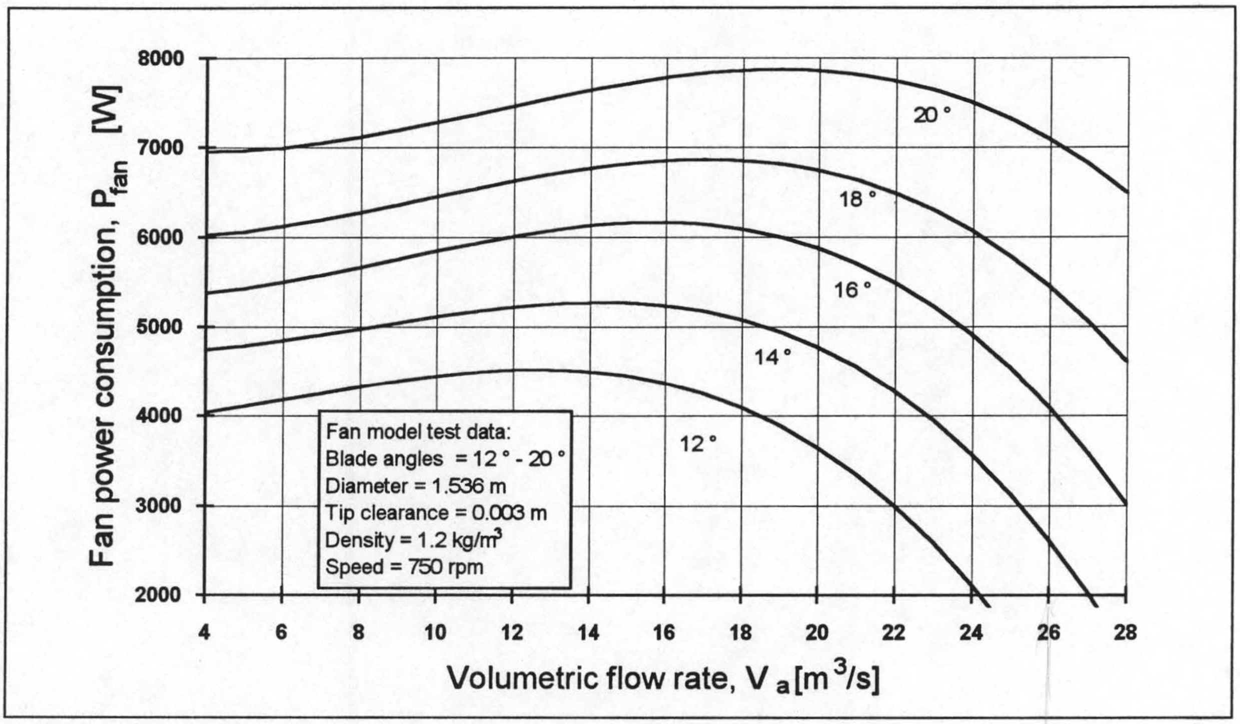

Figure 5.3: *Power consumption curves for fan model.*

Since the performance curves for the fan are given for a specific fan rotational speed, air density and fan size, the following conversion rules should be used to convert the model fan data to data that is applicable for the prototype fan, operating at its own specified conditions. In the conversion formulas the subscript "m" refers to the fan model. The conversion rules are as follows:

Volumetric flow rate:

$$\frac{V_{fan}}{V_{mfan}} = \left(\frac{n_{fan}}{n_{mfan}}\right)\left(\frac{d_{fan}}{d_{mfan}}\right)^3 \tag{5.3.1}$$

Fan static pressure rise:

$$\frac{p_{fan}}{p_{mfan}} = \left(\frac{n_{fan}}{n_{mfan}}\right)^2\left(\frac{d_{fan}}{d_{mfan}}\right)^2\left(\frac{\rho_{fan}}{\rho_{mfan}}\right) \tag{5.3.2}$$

Fan power consumption:

$$\frac{P_{fan}}{P_{mfan}} = \left(\frac{n_{fan}}{n_{mfan}}\right)^3\left(\frac{d_{fan}}{d_{mfan}}\right)^5\left(\frac{\rho_{fan}}{\rho_{mfan}}\right) \tag{5.3.3}$$

These conversion rules should also be used to determine the operating curves for different air densities. By using the above-mentioned conversion rules, the performance characteristics for a 9.7 m diameter, 8 bladed, axial flow prototype fan were obtained from the model fan data. The resulting performance characteristics can be seen in figures 5.4 and 5.5. The characteristics for this fan are given at an air density of 1.2 kg/m^3 and a fan rotational speed of 118 rpm.

Although it may be expected that the efficiency of the prototype is slightly higher than that of the model, no allowance is made for this effect and the efficiency of the prototype is considered the same as for the model fan. The efficiency curves for the model fan are given in figure 5.6.

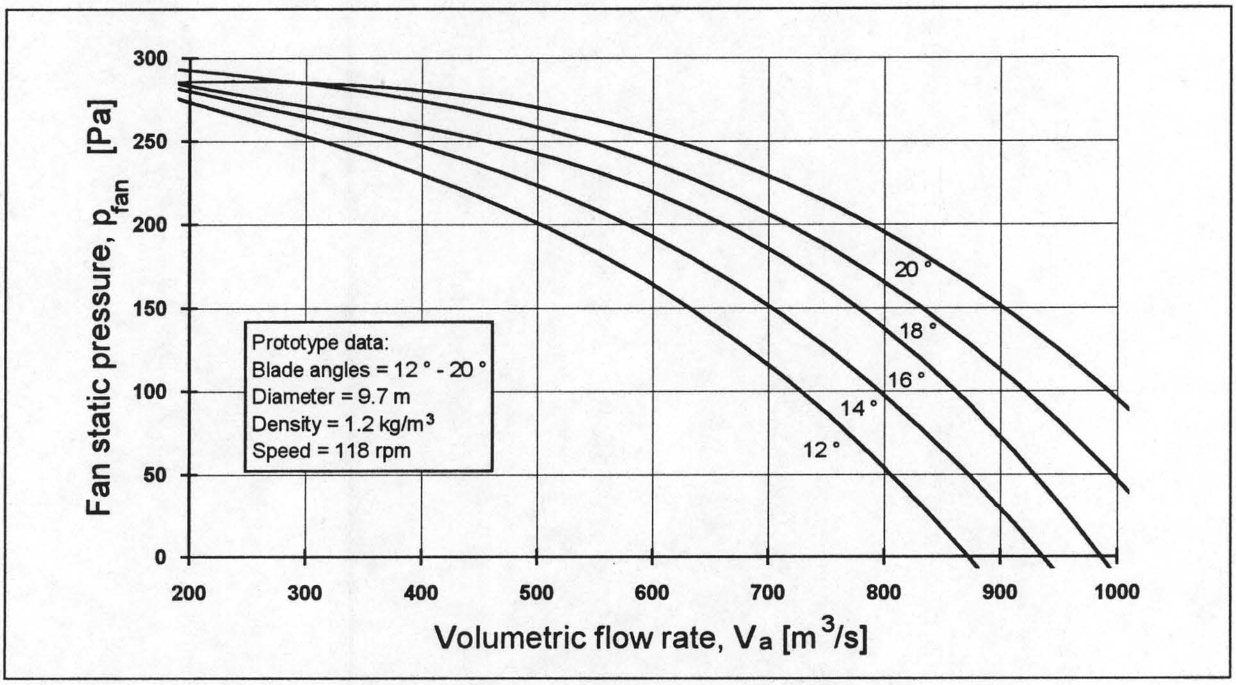

Figure 5.4: *Static pressure performance curves for the prototype fan.*

The tip clearance for the prototype fan that results in the same fan efficiency as for the model fan, can be obtained from the following equation as given by the VDI fan test code [66VD1].

$$\frac{s_{fan}}{s_{mfan}} = \left(\frac{d_{fan}}{d_{mfan}}\right)^{0.8}\left(\frac{p_{mfan}}{p_{fan}}\right)^{0.1} \qquad (5.3.4)$$

From the above equation the tip clearance for the prototype fan can be calculated. It was found to be approximately 0.013 m for the 9.7 m diameter prototype fan at an air density of 1.2 kg/m^3 and a fan rotational speed of 118 rpm.

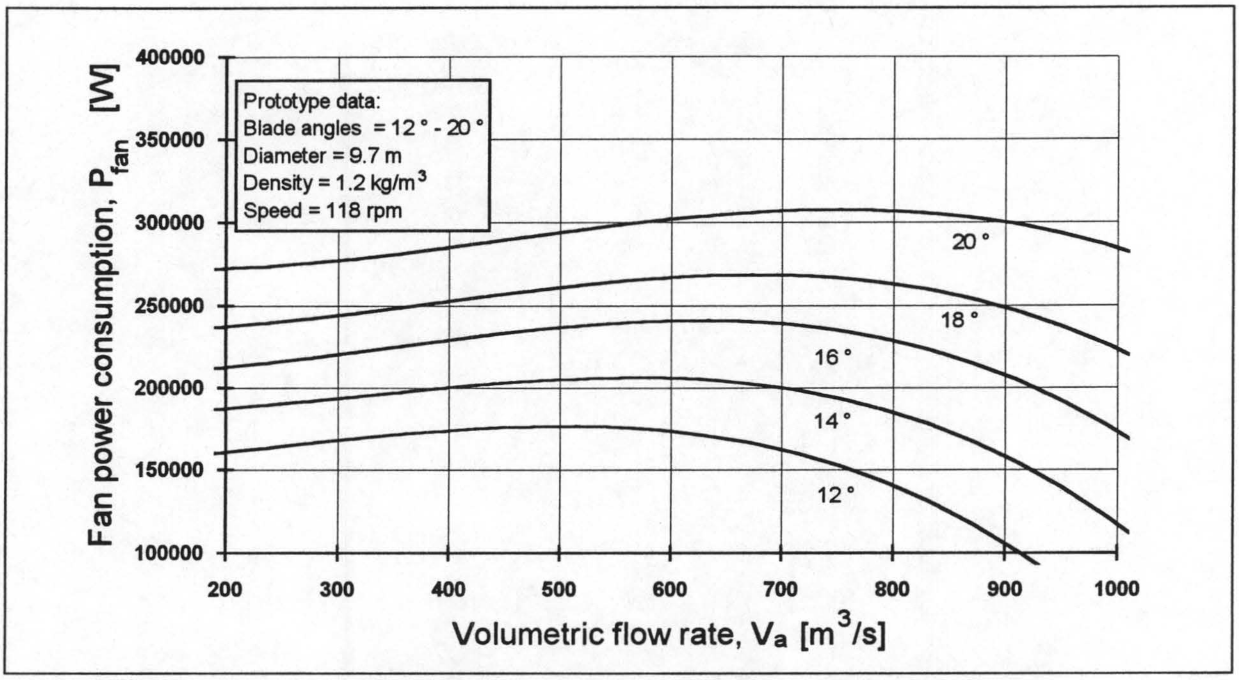

Figure 5.5: *Power consumption performance curves for the prototype fan.*

The fan operating point is determined from the fan static pressure curves, as shown in figure 5.4. For a required static pressure rise and volumetric flow rate, the correct fan blade angle can be determined from these curves. It is important that the operating point of the fan must be on the right hand side of the efficiency curve's maximum, as shown in figure 5.6. This is to ensure that the fan is able to overcome fluctuations in the system's resistance.

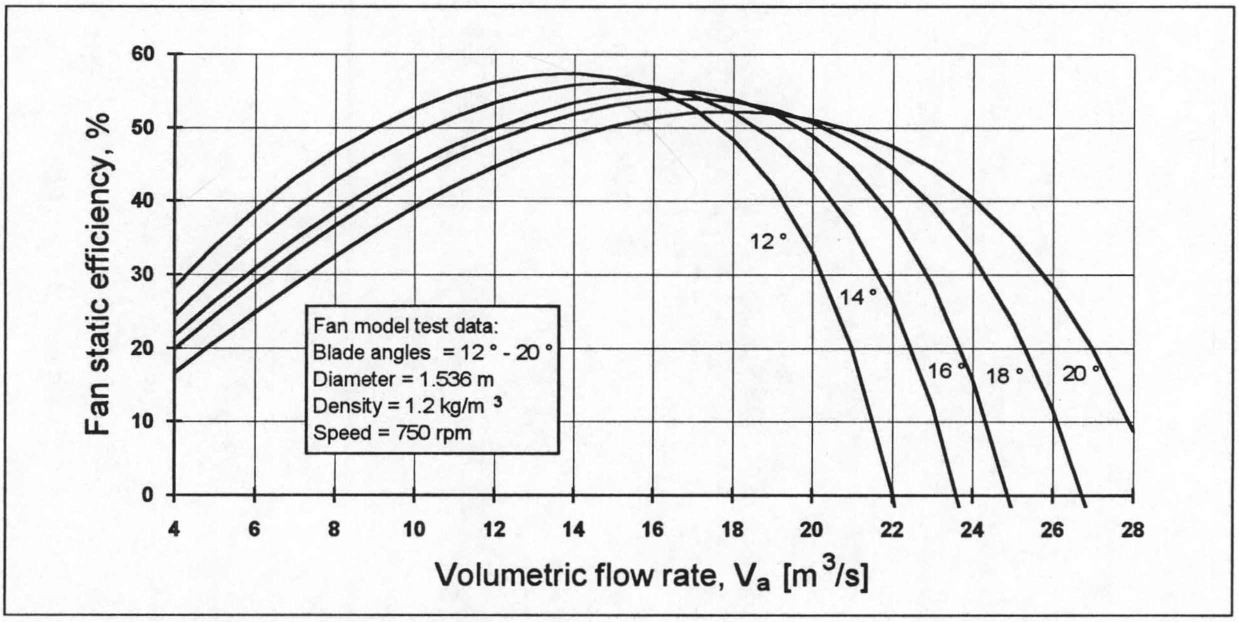

Figure 5.6: *Model fan static efficiency.*

The performance curves have to be approximated by polynomials before they can be used in the hybrid tower computer program.

Salta [95SA1] conducted a series of tests to determine the performance of a fan/(round to round diffuser) combination. The fan that he tested was a 1.536 m diameter, eight bladed variable pitch, axial flow fan and the diffuser had a half angle of 6.95 ° and was 1.542 m high. The fan casing had a diameter of 1.542 m which gives a tip clearance of 3 mm. From his measured results the following polynomials were obtained for the fan/diffuser performance characteristics at five different blade angles:

- The fan static pressure curves:

$$10°: p_{fan} = 320.85 - 6.9604V_{fan} + 0.31373V_{fan}^2 - 0.021393V_{fan}^3$$

$$12°: p_{fan} = 309.23 - 0.52081V_{fan} - 0.10376V_{fan}^2 - 0.010008V_{fan}^3$$

$$14°: p_{fan} = 306.25 + 1.5464V_{fan} - 0.14122V_{fan}^2 - 0.008432V_{fan}^3$$

$$16°: p_{fan} = 304.48 + 2.2925V_{fan} - 0.11339V_{fan}^2 - 0.008394V_{fan}^3$$

$$18°: p_{fan} = 336.14 - 7.1021V_{fan} + 0.64268V_{fan}^2 - 0.022945V_{fan}^3$$

- The fan power consumption curves:

$$10°: P_{fan} = 4245.1 - 64.134V_{fan} + 17.586V_{fan}^2 - 0.71079V_{fan}^3$$

$$12°: P_{fan} = 4761.1 - 37.29V_{fan} + 15.732V_{fan}^2 - 0.60598V_{fan}^3$$

$$14°: P_{fan} = 5484.3 - 59.613V_{fan} + 17.734V_{fan}^2 - 0.59297V_{fan}^3$$

$$16°: P_{fan} = 6265.7 - 96.842V_{fan} + 19.45V_{fan}^2 - 0.5801V_{fan}^3$$

$$18°: P_{fan} = 7829.2 - 256.67V_{fan} + 28.859V_{fan}^2 - 0.70876V_{fan}^3$$

- The fan efficiency curves:

$$10°: \eta_{fan} = -5.6511 + 10.996V_{fan} - 0.75481V_{fan}^2 + 0.035463V_{fan}^3 - 0.00083526V_{fan}^4$$

$$12°: \eta_{fan} = -6.3634 + 9.9845V_{fan} - 0.59598V_{fan}^2 + 0.023998V_{fan}^3 - 0.00051234V_{fan}^4$$

$$14°: \eta_{fan} = -5.8048 + 8.6499V_{fan} - 0.43624V_{fan}^2 + 0.015224V_{fan}^3 - 0.00031311V_{fan}^4$$

$$16°: \eta_{fan} = -4.6619 + 7.1085V_{fan} - 0.247V_{fan}^2 + 0.0057301V_{fan}^3 - 0.00013032V_{fan}^4$$

$$18°: \eta_{fan} = 1.1602 + 3.7369V_{fan} + 0.11649V_{fan}^2 - 0.01005V_{fan}^3 + 0.00012495V_{fan}^4$$

The above given polynomials were used in the PASWHY computer program (Chapter 6) to solve the example PPAF-SPWF hybrid tower of section 6.3. The computer program interpolates between the different fan static pressure curves to obtain the correct air mass flow rate for the specified fan blade angle.

5.4 Solving the draft through the PPAF hybrid tower

From the above information it is possible to determine a procedure for balancing the air flow through the PPAF hybrid tower shown in figure 5.1.

The following assumptions are made to simplify the solving procedure:

- The air is assumed completely mixed at point 8.
- The pressure at point 8 is the same for both air streams and is used to balance the air mass flow rates through the wet and dry sections respectively.

When calculating the cooling tower performance three different regions will be considered, i.e. the wet section, the dry section and the mixed airflow region. For each of these regions a local draft equation will be used.

The draft through the tower is determined as follows:

1. Estimate a value for the combined dry air mass flow rate through the wet and the dry sections and assign a certain fraction of this mass flow to the dry and the wet sections respectively.
2. For the air mass flow rate through the dry section, determine the pressure drop through the dry section up to point 8. The pressure lapse rate from ground level (1) up to the middle of the heat exchangers (6) and the pressure loss coefficients for the dry section as given in section 5.1.2 are used to calculate the pressure drop.
3. For the air mass flow rate through the wet section, determine the pressure drop through the wet section up to point 8. The pressure lapse rates from ground level to the middle of the fill and from the middle of the fill up to point 8, as well as the pressure loss coefficients for the wet section as given in section 5.1.1 are used to calculate the total pressure drop through the wet section.
4. Change the ratio of the air mass flow rates through the dry and wet sections until the pressure at point 8 for both these air streams are equal.
5. The pressure losses for the mixed air from point 8 onward are determined from the pressure loss coefficients given in section 5.1.3 and from the pressure lapse rate from point 8 to the tower exit (11).
6. For the mixed air properties at point 9 and the total air mass flow rate, determine from the fan static pressure curves what the blade angle of the fan should be, in order to deliver the required fan static pressure rise.
7. The total air mass flow rate through the tower is then iterated so that the specified fan blade angle is obtained.

It should be kept in mind that the draft equations through the wet and dry sections of the hybrid tower, are dependent on the energy transfer that takes place in each region and the draft equations must therefore be solved in conjunction with the energy equations. The wet and dry energy transfer equations as well as their solving methods were described in Chapter 4.

CHAPTER

SIX

COMPUTER SIMULATION AND SAMPLE SOLUTION

In this chapter the basic layout of a personal computer program with which the performance of a PPAF-SPWF induced draft hybrid tower can be predicted is described. The program that was written in Borland Pascal Version 7, uses the theory given in Chapters 4 and 5 to solve the energy and draft equations for the tower. A sample calculation of the final iteration of the program is given in section 6.3.

6.1 Program operation and limitations

The program can only be used to determine the cooling capacity of a cell type rectangular PPAF-SPWF induced draft hybrid tower, from where the name PASWHY (Parallel Air Series Water HYbrid) is derived. The program calculates the tower performance for a specified fan blade angle and must make use of extensive iteration processes to determine the air mass flow rate that will satisfy the specified blade angle. The convergence time of the program is therefore much longer than for other wet or dry cooling tower programs, since an extra outside iteration loop is required.

Since this kind of tower is very sensitive to variation in the size of either the wet section, the dry section or the fan, and these components must all be combined into a proportionally balanced unit, a good knowledge of the subject is a prerequisite for any person who would wish to use the program.

The kind of tower solved by the program is mostly used for plume abatement purposes and for this purpose it is usually required that the dry part dissipates about 20 per cent of the total heat dissipated by the tower. The size of the dry section compared to the wet section should therefore be chosen in such a way that this heat rejection ratio is obtained when the tower is operating in plume abatement mode.

The size of the fan is another critical variable since a wrongly sized fan would either be too small to deliver the required air flow rate or the air flow rate delivered by the fan would be too high. If the air speed through the wet section becomes too high the integration procedure becomes unstable and the program will not be able to converge. For a chosen blade angle a good estimate for the air's volume flow rate through the tower can be obtained from the fan efficiency curve, since the operating point for the fan must be to the right of the maximum on the curve.

6.2 Program structure

The program consists of a main program, three data files, three units and eight procedures. The main program calls up the three main procedures (which solve the wet section, the dry section and the mixed region respectively) and controls the convergence of the program as well as the input and the output. These three main procedures in turn uses the other sub-procedures and units. Units were written to determine the fluid properties, the fan characteristics and to do the plume evaluation. Each of these program components will now be discussed separately.

- **Main program (PASWHY)**

The main program calls four procedures, one for the dry section calculations, one for the wet section calculations, one for the calculations in the mixed region and one to test the program input (EVALINPUT).

By monitoring the pressures of the wet and dry air streams at point 8 as well as the convergence of the fan blade angle, the main program also controls the convergence of the program. The handling of the program input and output is also done by the main program. In figure 6.1 a flow diagram is given to show how the main program's different iteration loops are controlled.

- **Procedure DRYMAIN**

This procedure calculates the energy transfer and the pressure drop through the dry section of the tower. It makes use of procedure GANGULI to determine the transfer coefficient for the air side of the heat exchanger bundle, as well as the pressure drop over the heat exchanger bundle. The temperature of the air stream after the heat exchanger must be determined iteratively and this is done with the procedure T_ITER.

- **Procedure WETMAIN**

This procedure controls the energy and draft calculations for the wet section of the tower. The procedure CHEBYSHEV is used to numerically determine the enthalpy transfer through the three wet regions of the tower. This must be done iteratively since the water outlet temperature is required in the integration process, but is not known. The procedure

WETMAIN controls this iteration process by monitoring the convergence of the inlet water temperature to the wet section. The temperature of the air leaving the wet section must also be determined iteratively, and this is done with the procedure TEMP_5.

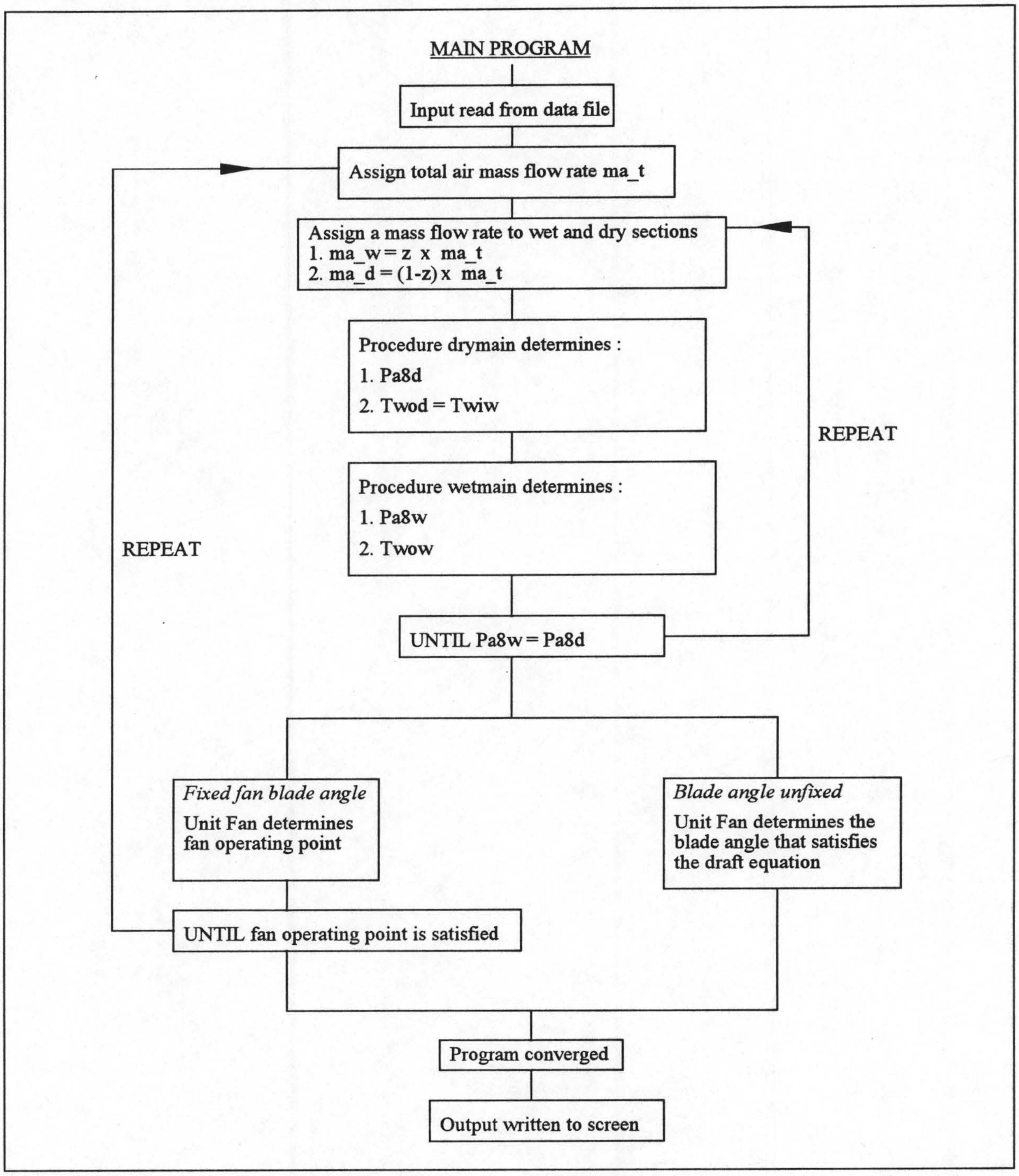

Figure 6.1: *Flow diagram of the main program's iteration structure.*

- **Procedure DRAFT_FAN**

Procedure DRAFT_FAN determines the pressure losses through the mixed region and the static pressure rise required from the fan. From unit FAN it then receives the fan blade angle that will deliver this pressure rise, for the specified air volume flow rate and air density through the fan.

- **Unit FAN**

This unit reads the model fan data from the specified data file. It then uses the fan conversion rules to obtain data for the prototype fan. From this data and the required static pressure rise, the blade angle that will deliver this pressure rise is obtained by interpolating between the different static pressure rise curves. After the blade angle is obtained the fan power consumption and fan efficiency is also calculated by interpolating between the relevant fan curves.

- **Unit PROPER**

This unit consists of various functions with which the fluid properties that are required by the program can be calculated. These include the properties for dry air, water vapour, water and an air/vapour mixture, as given in Appendix A.

- **Unit PLUMEEVAL**

From the properties of the air leaving the tower and the properties of the atmospheric air, this unit generates functions for the saturation curve, and the mixing line. These functions are then used to determine whether the mixing line crosses the saturation curve. The unit also determines where the two function curves cross, and from this it determines the mix line ratio as defined in section 3.4.

6.3 Sample solution

A sample calculation is done for an induced draft PPAF-SPWF hybrid tower as shown in figure 6.2.

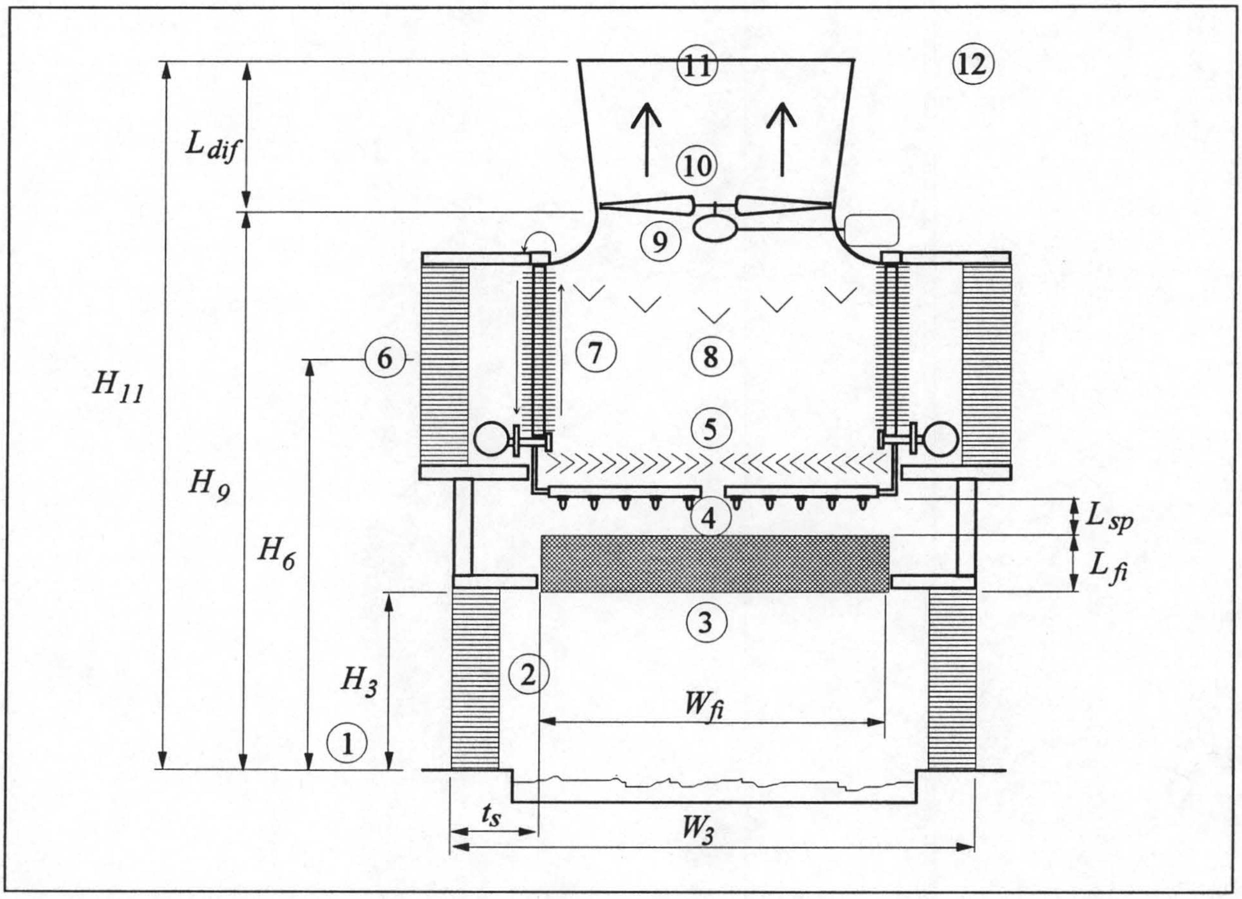

Figure 6.2: *Geometry of the example tower.*

6.3.1 Tower geometry and operating conditions

The tower geometry and the conditions under which the tower operates are the following:

Operating conditions

Water mass flow rate	m_w	= 450 kg/s
Water inlet temperature	T_{wi}	= 40 °C
Air dry bulb temperature at ground level	T_{a1}	= 15.45 °C
Air wet bulb temperature at ground level	T_{wb1}	= 11.05 °C
Atmospheric pressure at ground level	p_{atm}	= 84100 Pa

Tower geometry

Distance from outer inlet edge up to fill	t_s	= 1.5 m
Inlet width	W_3	= 18 m
Inlet breadth	B_3	= 12 m
Inlet height	H_3	= 3.5 m
Height to middle of dry bundles	H_6	= 8.38 m
Height to the fan	H_9	= 12.38 m
Total tower height	H_{11}	= 15.38 m

Wet section specifications

A splash pack type fill as shown in figure 6.3 is used. The fill's transfer coefficient is determined from the following correlation as given in Appendix C:

$$\frac{h_d a_{fi} L_{fi}}{G_w} = 0.5061 G_w^{-0.094} G_a^{0.6023}$$

The fill's static pressure loss coefficient in the absence of momentum effects is determined from equation (C.1.9).

$$K^*_{fiavm} = L_{fi} 1.9277 G_w^{1.2752} G_a^{-1.0356}$$

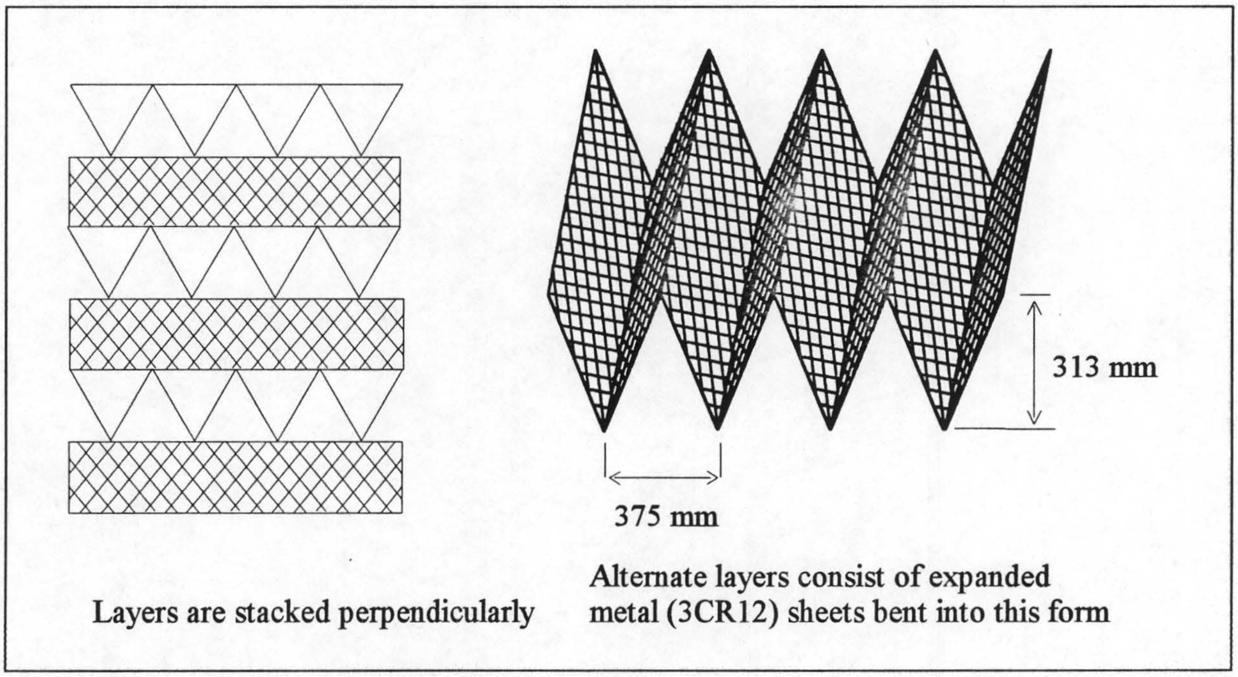

Figure 6.3: *Schematic representation of the fill that is used.*

Width of fill	$W_{fi} = 15$ m
Fill breadth	$B_{fi} = 12$ m
The depth of the fill	$L_{fi} = 1.88$ m
Spray zone height	$L_{sp} = 0.5$ m
Rain zone height	$L_{rz} = 3.5$ m
Drop diameter in the rain zone	$d_d = 0.0035$ m

Water distribution system pressure loss coefficient	$K_{wd5} = 0.5$
Noise attenuator pressure loss coefficient	$K_{na2} = K_{na6} = 3$
Fill support and contraction pressure loss coefficient	$K_{fs3} + K_{c3} = 0.5$
Drift eliminator pressure loss correlation	$K_{de5} = 27.4892\,\mathrm{Ry}^{-0.14247}$

Dry section specifications

Height of dry bundles	$L_t = 4$ m
Number of heat exchanger bundles	$n_b = 8$
Number of tube rows per bundle	$n_r = 4$
Number of tubes per row	$n_{tr} = 50$
Number of water passes	$n_p = 2$

Tube geometry (staggered tube arrangement)

Outside diameter	$d_{to} = 0.0254$ m
Inside diameter	$d_{ti} = 0.0216$ m
Thermal conductivity (stainless steel)	$k_t = 17$ W/mK
Transversal tube pitch	$P_t = 0.058$ m
Longitudinal tube pitch	$P_l = 0.05022$ m

Fin geometry (extruded aluminium E-fin)

Outside diameter	$d_f = 0.0572$ m
Root diameter	$d_{fr} = 0.0276$ m
Fin tip thickness	$t_{ft} = 0.00025$ m
Mean fin thickness	$t_{fm} = 0.0005$ m

Fin root thickness t_{fr} = 0.00075 m

Fin pitch P_f = 0.0028 m

Thermal conductivity (aluminium) k_f = 204 W/mK

The contact resistance of the fins is negligible

Mixed region specifications

It is assumed that the air flow area over the mixing devices is equal to the frontal area of the fill.

Air mixing elements pressure loss coefficient K_{me8} = 0.8

Fan suction side loss coefficient (drive shaft, support beams etc.) K_{fsuc9} = 0.2

Fan discharge side loss coefficient (walkway, screen etc.) K_{fdis10} = 0.2

Fan (8 bladed axial flow fan)

Fan diameter d_{fan} = 9.5 m

Rotational speed of fan n_{fan} = 118 rpm

Fan blade angle α_{fan} = 14 °

Fan casing diameter d_{fanc} = 9.5265 m

Diffuser (round to round geometry)

Height of diffuser L_{dif} = 3 m

Included diffuser angle α_{dif} = 14 °

Fan/diffuser performance curves at ρ_{av} = 1.2 kg/m^3 and n_{fan} = 120 rpm:

- Fan/diffuser static pressure:

$$p_{sfan} = 299.903 + 40.0071 \times 10^{-3} V_{sfan} - 96.5087 \times 10^{-6} V_{sfan}^2 - 152.2243 \times 10^{-9} V_{sfan}^3$$

- Fan power consumption:

$$P_{sfan} = 203302.6779 - 58.3775 V_{sfan} + 458.7692 \times 10^{-3} V_{sfan}^2 - 405.2315 \times 10^{-6} V_{sfan}^3$$

6.3.2 Performance evaluation

Values for the dry air mass flow rates through both the wet and the dry sections are assumed, and these values are then iterated until the pressure drop through the wet and dry sections balance up to point 8. The wet and the dry sections are solved iteratively for each mass flow rate. When the pressure drops through the wet and the dry sections balance, the total air mass flow through the tower is used to determine the fan blade angle that will deliver this air mass flow rate for the determined pressure drop through the tower. The total air mass flow rate is then iterated until the determined fan blade angle converges to the specified angle. Only the calculation for the last converged iteration is shown.

Since the dry section's outlet water temperature is the inlet water temperature for the wet section, the performance of the dry section must first be calculated.

Dry section calculations

The following values for the dry section's properties were obtained during the final iteration, and they will be used in further numerical calculations.

The dry air mass flow rate	m_{ad}	= 267.8392 kg/s
The air exit temperature	T_{a7}	= 305.9084 K
The water outlet temperature	T_{wod}	= 310.6171 K
The mean outlet air pressure	p_{a7}	= 83891.4308 Pa

The humidity ratio of the atmospheric air (T_{a1} = 288.6 K, T_{wb1} = 284.2 K, p_{a1} = 84100 Pa) as calculated from equation (A.3.5) is: w_{atm} = 0.008127 kg/kg. Since $w_{atm} = w_6 = w_1$, the air/vapour mass flow rate through the dry section is:

$$m_{avd} = m_{ad}(1+w_1) = 267.8392 \times (1+0.008127) = 270.0159 \text{ kg/s}$$

The geometric characteristics for the heat exchanger bundles are determined as follows:

- The total frontal area for the dry bundles:

$$A_{frd} = L_t n_b \left(P_t (n_{tr} - 0.5) + d_f \right)$$

$$= 4 \times 8 \left[0.058(50-0.5) + 0.0572 \right] = 93.7024 \text{ m}^2$$

- The minimum cross sectional flow area through the heat exchanger:

$$A_c = A_{frd} - n_b n_{tr} \frac{L_t}{P_f}\left[d_f t_{fm} + d_{fr}\left(P_f - t_{fm}\right)\right]$$

$$= 93.7024 - 8 \times 50 \times 4 / 0.0028\left[0.0572 \times 0.0005 + 0.0276\left(0.0028 - 0.0005\right)\right]$$

$$= 41.0853 \text{ m}^2$$

- The ratio of the total air-side area to the root area A_r, if no fins are present, as given by equation (4.2.4):

$$\frac{A_a}{A_r} = \frac{A_f + A_{re}}{A_r} = \left[\frac{\left(d_f^2 - d_{fr}^2\right)}{2} + d_f t_{ft} + d_{fr}\left(P_f - t_{fr}\right)\right] \Big/ \left(d_{fr} P_f\right)$$

$$= \frac{\left[\left(0.0572^2 - 0.0276^2\right)/2 + 0.0572 \times 0.00025 + 0.0276\left(0.0028 - 0.00075\right)\right]}{\left(0.0276 \times 0.0028\right)}$$

$$= 17.1573$$

- The ratio of the fin air side area to the total air side area:

$$\frac{A_f}{A_a} = \frac{\frac{1}{2}\left(d_f^2 - d_{fr}^2\right) + d_f t_{ft}}{\frac{1}{2}\left(d_f^2 - d_{fr}^2\right) + d_f t_{ft} + d_{fr}\left(P_f - t_{fr}\right)}$$

$$= \frac{\frac{1}{2}\left(0.0572^2 - 0.0276^2\right) + 0.0572 \times 0.00025}{\frac{1}{2}\left(0.0572^2 - 0.0276^2\right) + 0.0572 \times 0.00025 + 0.0276\left(0.0028 - 0.00075\right)}$$

$$= 0.95733$$

- The total air side area:

$$A_a = \pi\left[\frac{1}{2}\left(d_f^2 - d_{fr}^2\right) + d_f t_{ft} + d_{fr}\left(P_f - t_{fr}\right)\right] \times \left[L_t n_r n_{tr} n_b / P_f\right]$$

$$= \pi\left[\frac{1}{2}\left(0.0572^2 - 0.0276^2\right) + 0.0572 \times 0.00025 \times +0.0276\left(0.0028 - 0.00075\right)\right] \times$$

$$\left[4 \times 4 \times 50 \times 8 / 0.0028\right]$$

$$= 9521.1441 \text{ m}^2$$

The properties of the inlet air to the dry section can be determined as follows:

- The density correction factor for the atmospheric air:

$$\Omega_1 = (1+w_1)\left(1-\frac{w_1}{w_1+0.62198}\right) = (1+0.0081270)\left(1-\frac{0.0081270}{0.0081270+0.62198}\right)$$
$$= 0.99512$$

- The mean inlet air temperature:

$$T_{a6} = T_{a1} - 0.00975 \times H_6 = 288.6 - 0.00975 \times 8.38 = 288.5183 \text{ K}$$

- The mean air pressure at the inlet:

$$p_{a6} = p_{a1}\left(1-0.00975\frac{H_6}{T_{a1}}\right)^{3.5\Omega_1}$$
$$= 84100\left[1-0.00975\left(\frac{8.38}{288.6}\right)\right]^{3.5\times 0.99512}$$
$$= 84017.1026 \text{ Pa}$$

From Appendix A the following thermophysical properties for the inlet air to the dry section are determined at T_{a6} = 288.5183 K and p_{a6} = 84017.1026 Pa:

The air density:	ρ_{av6}	$= 1.0094$ kg/m^3	(A.3.1)
The air viscosity:	μ_{av6}	$= 1.7853\times10^{-5}$ kg/ms	(A.3.3)
The air enthalpy:	i_{ma6}	= 36031.2296 J/kgK	(A.3.6)

The mean air conditions through the dry section are:

Mean air temperature	T_{a67}	= 297.2133 K
Mean air pressure	p_{a67}	= 83954.2667 Pa

The air properties at these mean air conditions as determined from the equations given in Appendix A are:

Mean air viscosity	μ_{av67}	$= 1.8255\times10^{-5}$ kg/ms	(A.3.3)
The mean air density	ρ_{av67}	$= 0.97915$ kg/m^3	(A.3.1)
Mean air thermal conductivity	k_{av67}	= 0.025923 W/mK	(A.3.4)
The constant pressure specific heat	c_{pav67}	= 1013.9222 J/kgK	(A.3.2)

The mean air velocity based on the minimum cross sectional flow area through the heat exchanger can be determined as follows:

$$v_{av67c} = \frac{m_{avd}}{A_c \rho_{av67}} = \frac{270.0159}{41.0853 \times 0.97915} = 6.712 \text{ m / s}$$

The Prandtl and Reynolds numbers for the air through the heat exchanger are:

$$\mathrm{Pr}_a = \frac{\mu_{av67} c_{pav67}}{k_{av67}} = \frac{1.8255 \times 10^{-5} \times 1013.9222}{0.025923} = 0.714$$

$$\mathrm{Re}_a = \frac{\rho_{av67} v_{av67c} d_{fr}}{\mu_{av67}} = \frac{0.97915 \times 6.712 \times 0.0276}{1.8255 \times 10^{-5}} = 9936.5488$$

The Nusselt number for the heat exchanger can be determined from equation (4.2.3):

$$\mathrm{Nu_a} = \frac{h_a d_{fr}}{k_{av67}} = 0.38\,\mathrm{Re}_a^{0.6}\,\mathrm{Pr}_a^{0.333}\left(\frac{A_a}{A_r}\right)^{-0.15}$$
$$= 0.38 \times 9936.5488^{0.6} \times 0.714^{0.333} \times 17.1573^{-0.15} = 55.493$$

The air side heat transfer coefficient is then:

$$h_a = \mathrm{Nu_a}\frac{k_{av67}}{d_{fr}} = 55.493\frac{0.025923}{0.0276} = 52.1213 \text{ W / m}^2\text{K}$$

The air side heat transfer coefficient that was obtained from the above equations must still be multiplied by a surface effectiveness (e_f) to obtain the effective heat transfer coefficient.

The surface effectiveness is obtained as follows, where η_f is the fin efficiency as given by equation (4.2.6).

$$b = \left(\frac{2h_a}{k_f t_{fm}}\right)^{0.5} = \left(\frac{2 \times 52.1213}{204 \times 0.0005}\right)^{0.5} = 31.9685$$

$$\phi = \left(\frac{d_f}{d_{fr}} - 1\right)\left[1 + 0.35\ln\left(\frac{d_f}{d_{fr}}\right)\right] = \left(\frac{0.0572}{0.0276} - 1\right)\left[1 + 0.35\ln\left(\frac{0.0572}{0.0276}\right)\right] = 1.346$$

$$\eta_f = \frac{\tanh\left(b \times d_{fr} \frac{\phi}{2}\right)}{\left(b \times d_{fr} \frac{\phi}{2}\right)} = \frac{\tanh(31.9685 \times 0.0276 \times 1.346 / 2)}{(31.9685 \times 0.0276 \times 1.346 / 2)} = 0.89697$$

From equation (4.2.5) the surface effectiveness is:

$$e_f = \frac{h_a A_r (T_r - T_\infty) + h_a A_f \eta_f (T_r - T_\infty)}{h_a A_a (T_r - T_\infty)}$$

$$= 1 - \frac{A_f (1 - \eta_f)}{A_a} = 1 - 0.95733(1 - 0.89697) = 0.90137$$

The effective air side heat transfer coefficient is therefore:

$$h_{ae} = h_a e_f = 52.1213 \times 0.90137 = 46.9804 \text{ W / m}^2\text{K}$$

The mean water temperature through the dry section is:

$$T_{wm} = \frac{T_{wi} + T_{wod}}{2} = \frac{313.15 + 310.6171}{2} = 311.8836 \text{ K}$$

At this mean water temperature the properties of the water as determined from the equations in Appendix A are:

Constant pressure specific heat:	c_{pwm}	= 4176.7618 J/kgK	(A.4.2)
Thermal conductivity:	k_{wm}	= 0.62949 W/mK	(A.4.4)
Dynamic viscosity:	μ_{wm}	= 6.6744×10^{-4} kg/ms	(A.4.3)

The Reynolds and Prandtl numbers at these water properties are:

$$\text{Re}_w = \frac{4 m_w}{(n_{tr} n_b n_r / n_p) \mu_{wm} \pi d_i} = \frac{4 \times 450}{(50 \times 8 \times 4 / 2) \times 6.6744 \times 10^{-4} \pi 0.0216} = 49678.4373$$

$$\text{Pr}_w = \frac{\mu_{wm} c_{pwm}}{k_{wm}} = \frac{6.6744 \times 10^{-4} \times 4176.7618}{0.62949} = 4.4285$$

From equation (4.2.8) the D' Arcy friction factor is:

$$f_D = (1.82 \log \text{Re}_w - 1.64)^{-2} = [1.82 \log(49678.4373) - 1.64]^{-2} = 0.020961$$

The Nusselt number for the water flow on the inside of the tube as determined from equation (4.2.7) is:

$$\mathrm{Nu}_w = \frac{h_i d_{ti}}{k_{wm}} = \frac{(f_D/8)(\mathrm{Re}_w - 1000)\,\mathrm{Pr}_w\left[1+(d_{ti}/L)^{0.67}\right]}{1+12.7(f_D/8)^{0.5}\left(\mathrm{Pr}_w^{0.67}-1\right)}$$

$$= \frac{(0.020961/8)(49678.4373-1000)4.4285\left[1+\{0.0216/4\}^{0.67}\right]}{1+12.7(0.020961/8)^{0.5}\left(4.4285^{0.67}-1\right)}$$

$$= 275.5662$$

The heat transfer coefficient on the inside of the tube is then:

$$h_i = \mathrm{Nu}_w \frac{k_{wm}}{d_{ti}} = 275.5662\frac{0.62949}{0.0216} = 8030.8778\ \mathrm{W/m^2K}$$

The total inside tube area is:

$$A_i = \pi d_{ti} n_b n_r n_{tr} L_t = \pi \times 0.0216 \times 8 \times 4 \times 50 \times 4 = 434.2938\ \mathrm{m^2}$$

If the contact resistance of the fins is ignored, the overall heat transfer coefficient based on the inside area, as determined from equation (4.2.1) is:

$$U_i = \left(\frac{1}{h_i} + \frac{A_i \ln(d_{to}/d_{ti})}{2\pi k_t L_t n_r n_{tr} n_b} + \frac{A_i}{A_a}\frac{1}{h_{ae}}\right)^{-1}$$

$$= \left(\frac{1}{8030.8778} + \frac{434.2938 \ln(0.0254/0.0216)}{2\pi 17(4\times 4\times 50\times 8)} + \frac{434.2938}{9521.1441\times 46.9804}\right)^{-1}$$

$$= 834.46\ \mathrm{W/m^2K}$$

The heat capacities of the air and the water streams are respectively:

$$C_{av} = m_{avd} c_{pav67} = 270.0159 \times 1013.9222 = 273775.1185\ \mathrm{J/Ks}$$

$$C_w = m_w c_{pwm} = 450 \times 4176.7618 = 1879542.801\ \mathrm{J/Ks}$$

The heat capacity ratio is defined as:

$$C_r = \frac{C_{\min}}{C_{\max}} = \frac{273775.1185}{1879542.801} = 0.14566$$

The number of transfer units per pass is:

$$NTU_p = \frac{U_i A_i}{C_{\min} n_p} = \frac{834.46 \times 434.2938}{273775.1185 \times 2} = 0.66186$$

For both fluids unmixed the effectiveness per pass is according to equation (4.2.12):

$$\varepsilon_p = 1 - \exp\left[\frac{\exp\left(-NTU_p^{0.78} C_r\right) - 1}{C_r NTU_p^{-0.22}}\right] = 1 - \exp\left[\frac{\exp\left(-\left(0.66186^{0.78}\right) \times 0.14566\right) - 1}{0.14566 \times 0.66186^{-0.22}}\right]$$

$$= 0.46641$$

From equation (4.2.13) the corrected effectiveness is:

$$\varepsilon = \frac{\left[\dfrac{1-\varepsilon_p C_r}{1-\varepsilon_p}\right]^{n_p} - 1}{\left[\dfrac{1-\varepsilon_p C_r}{1-\varepsilon_p}\right]^{n_p} - C_r} = \frac{\left[\dfrac{1-0.46641 \times 0.14566}{1-0.46641}\right]^2 - 1}{\left[\dfrac{1-0.46641 \times 0.14566}{1-0.46641}\right]^2 - 0.14566} = 0.70596$$

The maximum amount of heat that can theoretically be transferred is:

$$Q_{\max} = C_{\min}\left(T_{wi} - T_{a6}\right) = 273775.1185(313.15 - 288.5183) = 6.743547 \times 10^6 \text{ W}$$

From the effectiveness the heat transfer can now be determined as follows from equation (4.2.9):

$$\varepsilon = \frac{Q_d}{Q_{\max}}$$

$$\therefore Q_d = \varepsilon Q_{\max} = 0.70596 \times 6.743547 \times 10^6 = 4.760678 \times 10^6 \text{ W}$$

The outlet water temperature and the outlet air enthalpy from the dry section is:

$$T_{wod} = T_{wi} - \frac{Q_d}{c_{pwm} m_w} = 313.15 - \frac{4.760678 \times 10^6}{4176.7618 \times 450} = 310.6171 \text{ K}$$

$$i_{ma7} = i_{ma6} + \frac{Q_d}{m_{ad}} = 36031.2296 + \frac{4.760678 \times 10^6}{267.8392} = 53805.621 \text{ J/kg}$$

From the outlet air enthalpy and humidity, the outlet temperature can be determined iteratively. The humidity of the air through the dry section stays constant, and is equal to the humidity of the atmospheric air.

To determine the air enthalpy at a dry bulb temperature of T_{a7} = 305.9084 K and a humidity ratio of w_7 = 0.008127 kg/kg, first determine c_{pa7m} and c_{pv7m} from equations (A.1.2) and (A.2.2) at T_{a7m} = (305.9084 + 273.15)/2 = 289.5292 K.

Constant pressure specific heat for dry air: c_{pa7m} = 1006.6291 J/kgK (A.3.2)
Constant pressure specific heat for water vapour: c_{pv7m} = 1876.5184 J/kgK (A.3.2)

The enthalpy is then:

$$\begin{aligned}i_{ma7} &= c_{pa7m}T_{a7} + w_7\left(i_{fgw0} + c_{pv7m}T_{a7}\right)\\ &= 1006.6291(305.9084-273.15)+0.008127\\ &\quad\left[2501598.5335+1876.5184(305.9084-273.15)\right]\\ &= 53805.621 \text{ J / kg}\end{aligned}$$

The determined enthalpy (i_{ma7}) is nearly equal to the correct one, and the temperature (T_{a7}) is therefore correct.

The density of the air leaving the dry section is:

$$\rho_{av7} = \frac{p_{a7}}{RT_{a7}}\Omega_1 = \frac{83891.4308}{287.08\times 305.9084}0.99512 = 0.95061 \text{ kg / m}^3$$

The pressure loss through the dry section can be determined as follows:

- The air mass flux based on the minimum cross sectional flow area is:

$$G_c = \frac{m_{avd}}{A_c} = \frac{270.0159}{41.0853} = 6.5721 \text{ kg / m}^2\text{s}$$

- The mean air velocity based on the frontal area of the dry bundles is:

$$v_{av67} = \frac{m_{avd}}{\rho_{av67}A_{frd}} = \frac{270.0159}{0.97915\times 93.7024} = 2.943 \text{ m / s}$$

- **The outlet air velocity based on the frontal area of the dry bundles is:**

$$v_{av7}=\frac{m_{avd}}{\rho_{av7}A_{frd}}=\frac{270.0159}{0.95061\times 93.7024}=3.0314\ \text{m/s}$$

- **From equation (5.1.23) the Euler number is:**

$$\begin{aligned}Eu=\frac{\rho_{av67}\Delta p}{G_c^2}&=2n_r\left[1+2\exp\left(\frac{d_f-P_t}{4d_{fr}}\right)\Bigg/\left(1+\frac{P_t-d_f}{d_{fr}}\right)\right]\times\\&\quad\left[0.021+\frac{13.6\left(d_f-d_{fr}\right)}{\mathrm{Re}_a\left(P_f-t_{fm}\right)}+0.25246\left(\frac{d_f-d_{fr}}{\mathrm{Re}_a\left(P_f-t_{fm}\right)}\right)^{0.2}\right]\\&=2\times 4\left[1+2\exp\left(\frac{0.0572-0.058}{4\times 0.0276}\right)\Bigg/\left(1+\frac{0.058-0.0572}{0.0276}\right)\right]\times\\&\quad\left[0.021+\frac{13.6(0.0572-0.0276)}{9936.5488(0.0028-0.0005)}+0.25246\left(\frac{0.0572-0.0276}{9936.5488(0.0028-0.0005)}\right)^{0.2}\right]\\&=2.4702\end{aligned}$$

- **The static pressure drop through the heat exchanger and noise attenuator of the dry section is therefore:**

$$\begin{aligned}\Delta p_{a6-7}&=Eu\frac{G_c^2}{\rho_{av67}}+\left(K_{na6}\frac{\rho_{av67}}{\rho_{av6}}\right)\times\tfrac{1}{2}\rho_{av67}v_{av67}^2+\tfrac{1}{2}\rho_{av7}v_{av7}^2\\&=2.4702\frac{6.5721^2}{0.97915}+\left(3\frac{0.97915}{1.0094}\right)\times\tfrac{1}{2}\times 0.97915\times 2.943^2+\tfrac{1}{2}\times 0.95061\times 3.0314^2\\&=125.6717\ \text{Pa}\end{aligned}$$

The mean static pressure after the dry section is therefore:

$$p_{a7}=p_{a6}-\Delta p_{a6-7}=84017.1026-125.6717=83891.4308\ \text{Pa}$$

Wet section calculations

The fill is located horizontally at the bottom inlet of the tower. The Merkel theory is used in solving the wet section of the tower. An iterative solving procedure must be used, since the equations governing the energy transfer in the wet section cannot be solved explicitly.

A dry air mass flow rate of m_{aw} = 482.345 kg/s was obtained after a number of iterations, and will be used in this calculation. Other values that were also obtained during the final iteration are:

Water outlet temperature	T_{wo} = 296.014 K
Mean air velocity through the fill	$v_{av34} \approx v_{av15}$ = 2.7656 m/s
Air pressure after the drift eliminators	p_{a5} = 83931.5803 Pa
The combined pressure loss coefficient	K_{he} = 11.2404

The thermophysical properties of the air entering the wet section (T_{a1} = 288.6 K, T_{wb1} = 284.2 K, p_{a1} = 84100 Pa) as calculated with the equations given in Appendix A are:

Density	ρ_{av1}	= 1.0101 kg/m^3	(A.3.1)
Dynamic viscosity	μ_{av1}	= 1.7857x10^{-5} kg/ms	(A.3.3)
Enthalpy	i_{ma1}	= 36114.7173 J/kg	(A.3.6)
Diffusivity	D_1	= 2.2963×10^{-5} m^2/s	(A.3.8)

Since the entrance to the wet section contains noise attenuators, and the air is forced to enter the rain zone horizontally, the entrance of the tower can be assumed to be rounded. From equation (D.1.4) the ratio of effective inlet width to inlet width for a tower with a rounded inlet is:

$$\frac{W_{fie}}{W_{fi}} = 1.0487 - 0.17408\ln\left(\frac{W_{fi}}{H_3}\right) + 0.09\ln\left(K_{he}\right)$$
$$= 1.0487 - 0.17408\ln\left(\frac{15}{3.5}\right) + 0.09\ln\left(11.2404\right)$$
$$= 1.0131$$

Since W_{fie} cannot be greater than W_{fi} it follows that $W_{fie} = W_{fi}$.

The frontal area of the wet fill is $A_{fr} = B_{fi}W_{fi} = 12 \times 15 = 180$ m^2.

The dry air mass flux is then:

$$G_a = \frac{m_{aw}}{A_{fr}} = \frac{482.345}{180} = 2.6797 \text{ kg / m}^2\text{s}$$

and the water mass flux is:

$$G_w = \frac{m_w}{A_{fr}} = \frac{450}{180} = 2.5 \text{ kg / m}^2\text{s}$$

The wet section's inlet water temperature is equal to the outlet water temperature of the dry section i.e. $T_{wiw} = T_{wod} = 310.6171$ K.

<u>The transfer coefficients for the *rain zone*, *fill* and *spray zone* must now be determined.</u>

For the rain zone the correlation given in equation (4.1.2) is used. To evaluate this equation, the properties of the water at the inlet to the rain zone are required. Since the integration through the wet section is done in one step, the temperature at point 3 is not known. The temperature of the water at this point is therefore assumed equal to the water outlet temperature ($T_{w3} \approx T_{wo} = 296.014$ K).

At T_{wo} = 296.014 K the following properties are determined from the equations given in Appendix A:

Density of the water	ρ_{w3}	$= 997.5455$ kg/m^3	(A.4.1)
Surface tension of the water	σ_{w3}	$= 0.072339$ N/m	(A.4.7)
Humidity ratio of saturated air at this temperature	w_{sw3}	$= 0.021414$ kg/kg	(A.3.5)

The mean velocity of the water at 3, based on the frontal area of the fill is:

$$v_{w3} = \frac{m_w}{\rho_{w3} A_{fr}} = \frac{450}{997.5455 \times 180} = 0.0025062 \text{ m / s}$$

The transfer coefficient for the *rain zone* as determined from equation (4.1.2) is:

$$\begin{aligned}
\frac{(h_d a)_{rz} H_3}{\rho_{av1} v_{av34}} &= 340.76 \times 1.007^{\left(\frac{W_{fi}}{H_3}\right)} \times \left(\frac{\rho_{av1} v_{av34} H_3}{\mu_{av1}}\right)^{0.359} \left(\frac{D}{H_3 v_{av34}}\right)^{1.0986} \left(\frac{p_{a1}}{\rho_{av1} v_{av34}^2}\right) \times \\
&\quad 0.409^{w_{sw3}} \times 0.365^{w_1} \times 0.9996^{\left(\frac{\rho_{w3}}{\rho_{av1}}\right)} \times \left(\frac{v_{w3}}{v_{av34}}\right) \left(\frac{v_{av34}^2}{R_v T_{w3}}\right)^{0.95} \left(\frac{\sigma_{w3}}{H_3 \rho_{av1} v_{av34}^2}\right)^{-0.165} \times \\
&\quad \exp\left[0.01835536\left(\ln\left(\frac{gH_3}{v_{av34}^2}\right) - 13.46\right)^2 + 0.1208605\left(\ln\left(\frac{d_d}{H_3}\right) - 0.0324\right)^2\right] \\
&= 340.76 \times 1.007^{(15/3.5)} \times \left(\frac{1.0101 \times 2.7656 \times 3.5}{1.7857 \times 10^{-5}}\right)^{0.359} \left(\frac{2.2963 \times 10^{-5}}{3.5 \times 2.7656}\right)^{1.0986} \times \\
&\quad \left(\frac{84100}{1.0101 \times 2.7656^2}\right) \times 0.409^{0.021414} \times 0.365^{0.008127} \times 0.9996^{\left(\frac{997.5455}{1.0101}\right)} \times \\
&\quad \left(\frac{0.0025062}{2.7656}\right) \left(\frac{2.7656^2}{461.52 \times 296.014}\right)^{0.95} \left(\frac{0.072339}{3.5 \times 1.0101 \times 2.7656^2}\right)^{-0.165} \times \\
&\quad \exp\left[0.01835536\left(\ln\left(\frac{9.8 \times 3.5}{2.7656^2}\right) - 13.46\right)^2 + 0.1208605\left(\ln\left(\frac{0.0035}{3.5}\right) - 0.0324\right)^2\right] \\
&= 0.19507
\end{aligned}$$

The heat transfer coefficient for the rain zone can now be written as:

$$\frac{(h_d a)_{rz} H_3}{G_w} = \frac{(h_d a)_{rz} H_3}{\rho_{av1} v_{av34}} \times \frac{\rho_{av1} v_{av34}}{G_w} = 0.19507 \times 1.0101 \times 2.7656 / 2.5 = 0.21798$$

From equation (C.1.1) the transfer coefficient for the *fill* is:

$$\begin{aligned}
\frac{(h_d a)_{fi} L_{fi}}{G_w} &= 0.5061 G_w^{-0.094} G_a^{0.6023} = 0.5061 \times 2.5^{-0.094} \times 2.6797^{0.6023} \\
&= 0.84074
\end{aligned}$$

From equation (4.1.5) the transfer coefficient for the *spray zone* is:

$$\frac{(h_d a)_{sp} L_{sp}}{G_w} = L_{sp} \times 0.2\left(\frac{G_w}{G_a}\right)^{-0.5} = 0.5 \times 0.2\left(\frac{2.5}{2.6797}\right)^{-0.5} = 0.10353$$

The Merkel equation (equation (4.1.1)) is used to solve the energy transfer in the wet section of the tower.

With the Chebyshev numerical integration method, as described in Appendix B, the Merkel equation can be approximated by equation (B.6) as follows:

$$\frac{(h_d a)L}{G_w} = \int_{T_{wo}}^{T_{wi}} \frac{c_{pw} dT_w}{(i_{mas} - i_{ma})} \approx \frac{c_{pwm}(T_{wi} - T_{wo})}{4}\left[\frac{1}{\Delta i_{(1)}} + \frac{1}{\Delta i_{(2)}} + \frac{1}{\Delta i_{(3)}} + \frac{1}{\Delta i_{(4)}}\right]$$

where the numerical subscripts refer to the positions in the wet region where the temperatures are equal to those determined from the Chebyshev interval values.

It is possible to combine the transfer coefficients of the three wet regions. This combined heat transfer coefficient can then be used to integrate through the whole wet section in one step. The combined heat transfer coefficient is:

$$\begin{aligned}(h_d a)_{combined} &= \frac{G_w\left[(h_d a)_{rz} H_3 / G_w + (h_d a)_{fi} L_{fi} / G_w + (h_d a)_{sp} L_{sp} / G_w\right]}{H_3 + L_{fi} + L_{sp}} \\ &= \frac{2.5(0.21798 + 0.84074 + 0.10353)}{3.5 + 1.88 + 0.5} \\ &= 0.49415 \ \ \mathrm{kg/m^3s}\end{aligned}$$

The combined Merkel value is:

$$\frac{(h_d a)_{combined}(H_3 + L_{fi} + L_{sp})}{G_w} = \frac{0.49415(3.5 + 1.88 + 0.5)}{2.5} = 1.1622$$

To perform the numerical integration, both the air and water properties must be known at either the top or the bottom of the region over which the integration has to be performed. In this case only the water inlet properties at the top of the spray zone, and the air inlet properties at the bottom of the rain zone are known. A water outlet temperature is therefore guessed at the bottom of the rain zone, and the integration is simultaneously performed through the entire wet region until the determined water temperature at the top of the spray zone, converges to the correct one.

The final iteration where the determined water inlet temperature has converged will now be given to show how the integration is performed.

The conditions at which the numerical integration is performed are:

Inlet air dry bulb temperature: $T_{a1} = 288.6$ K

Inlet air wet bulb temperature: $T_{wb1} = 284.2$ K

Dry air mass flow rate: $m_{aw} = 482.345$ kg/s

Water mass flow rate: $m_w = 450$ kg/s

Water inlet temperature: $T_{wiw} = 310.6171$ K.

The guessed water outlet temperature is $T_{wo} = 296.014$ K.

The mean pressure through the wet section is:

$p_{a15} = (p_{a1} + p_{a5})/2 = (84100 + 83931.5803)/2 = 84015.7902$ Pa.

For the approximated Chebyshev values (0.1, 0.4, 0.6, 0.9), the temperatures at which the enthalpies have to be evaluated are the following:

$$T_{w(1)} = T_{wo} + 0.1(T_{wiw} - T_{wo}) = 296.014 + 0.1(310.6171 - 296.014) = 297.4743 \text{ K}$$
$$T_{w(2)} = T_{wo} + 0.4(T_{wiw} - T_{wo}) = 301.8552 \text{ K}$$
$$T_{w(3)} = T_{wo} + 0.6(T_{wiw} - T_{wo}) = 304.7758 \text{ K}$$
$$T_{w(4)} = T_{wo} + 0.9(T_{wiw} - T_{wo}) = 309.1567 \text{ K}$$

To calculate the enthalpy of the saturated air at condition (1), the point where the water temperature $T_{w(1)} = 297.4743$ K, the following properties must first be determined at (273.15 + 297.4743)/2 = 285.3122 K:

Specific heat for dry air: $c_{paw(1)m} = 1006.528$ J/kgK (A.1.2)

Specific heat for water vapour: $c_{pvw(1)m} = 1872.9247$ J/kgK (A.2.2)

From equation (A.3.5) the humidity ratio for saturated air at 297.4743 K and at p_{a15} = 84015.7902 Pa is $w_{sw(1)} = 0.023483$.

The enthalpy of saturated air per kg dry air at point (1), can now be determined from equation (A.3.6) as follows:

$$\begin{aligned} i_{masw(1)} &= c_{paw(1)m}\left(T_{w(1)} - 273.15\right) + w_{sw(1)}\left[i_{fgw0} + c_{pvw(1)m}\left(T_{w(1)} - 273.15\right)\right] \\ &= 1006.528(297.4743 - 273.15) + 0.023483 \\ &\quad (2501598.5335 + 1872.9247(297.4743 - 273.15)) \\ &= 84297.3326 \text{ J / kg dry air} \end{aligned}$$

The enthalpy of the inlet air per kg dry air is $i_{ma1} = 36114.7173$ J / kg

From equation (A.4.2) the constant pressure specific heat at the mean water temperature through the wet section is:

$$T_{wm} = \frac{T_{wiw} + T_{wo}}{2} = \frac{310.6171 + 296.014}{2} = 303.3155 \text{ K}$$

$$\begin{aligned} c_{pwm} &= 8.15599 \times 10^3 - 2.80627 \times 10(303.3155) + 5.11283 \times 10^{-2}(303.3155)^2 \\ &\quad - 2.17582 \times 10^{-13}(303.3155)^6 \\ &= 4178.5265 \text{ J / kgK} \end{aligned}$$

The enthalpy of the air at point (1) in the fill, can be determined from the following equation (as given in Appendix B):

$$\begin{aligned} i_{ma(1)} &= \frac{m_w}{m_a} c_{pwm}\left(T_{w(1)} - T_{wo}\right) + i_{ma1} \\ &= \frac{450}{482.345} \times 4178.5265(297.4743 - 296.014) + 36114.7173 = 41807.4357 \text{ J / kg} \end{aligned}$$

From the above determined enthalpies it follows that the enthalpy difference is:

$$\Delta i_{(1)} = \left[i_{masw(1)} - i_{ma(1)}\right] = 84297.3326 - 41807.4357 = 42489.8968 \text{ J / kg}$$

In the same way the other required enthalpy differences were calculated and is:

$$\begin{aligned} \Delta i_{(2)} &= 107452.3836 - 58885.591 = 48566.7926 \text{ J / kg} \\ \Delta i_{(3)} &= 125759.1774 - 70271.0278 = 55488.1496 \text{ J / kg} \\ \Delta i_{(4)} &= 158562.7279 - 87349.183 = 71213.5449 \text{ J / kg} \end{aligned}$$

It is now possible to determine the inlet water temperature that satisfies the Merkel equation. From the Chebyshev approximation [equation (B.6)] the water inlet temperature is:

$$\begin{aligned} T_{wiw} &= \frac{(h_d a)_{combined}\left(H_3 + L_{fi} + L_{sp}\right)}{G_w} \Bigg/ \left[\left(\frac{1}{\Delta i_{(1)}} + \frac{1}{\Delta i_{(2)}} + \frac{1}{\Delta i_{(3)}} + \frac{1}{\Delta i_{(4)}}\right)\frac{c_{pwmw}}{4}\right] + T_{wo} \\ &= 1.1622 \Bigg/ \left[\left(\frac{1}{42489.8968} + \frac{1}{48566.7926} + \frac{1}{55488.1496} + \frac{1}{71213.5449}\right)\frac{4178.5265}{4}\right] + 296.014 \\ &= 310.6171 \text{ K} \end{aligned}$$

This temperature compares well with the real water inlet temperature to the wet section T_{w5} and convergence is therefore satisfied.

The properties of the air at point 5 must now be determined, since they are required for solving the draft through the wet section.

The enthalpy of the air leaving the wet section is:

$$\begin{aligned} i_{mas5} &= \frac{m_w}{m_{aw}} c_{pwm}\left(T_{wiw} - T_{wo}\right) + i_{ma1} \\ &= \frac{450}{482.345} 4178.5265(310.6171 - 296.014) + 36114.7173 \\ &= 93041.8847 \text{ J / kgK} \end{aligned}$$

Since it is assumed that the air is saturated after the drift eliminators, the outlet air temperature can be determined iteratively from equation (A.3.6). For this iteration the lower temperature limit can be taken as the atmospheric wet bulb temperature, and the upper limit can be taken as the water inlet temperature. The temperature that was obtained after a few iterations is T_{a5} = 299.2212 K

The thermophysical properties of saturated air at T_{a5} = 299.2212 K and p_{a5} = 83931.5803 Pa, as determined from the equations in Appendix A are:

Humidity ratio	w_{s5}	= 0.026191 kg/kg	(A.3.5)
Specific heat of air at (T_{a5}+273.15)/2	c_{pa5m}	= 1006.5475 J/kgK	(A.1.2)
Specific heat of water vapour at (T_{a5}+273.15)/2	c_{pv5m}	= 1873.6637 J/kgK	(A.2.2)
Specific heat of water at (T_{a5}+273.15)/2	c_{pw5m}	= 4192.8305 J/kgK	(A.4.2)
Density of mixed air at T_{a5}	ρ_{av5}	= 0.96216 kg/m^3	(A.3.1)
Dynamic viscosity	μ_{av5}	= 1.8162x10^{-5} kg/ms	(A.3.3)

The specific heat of the air/vapout mixture is:

$$c_{pav5m} = c_{pa5m} + w_{s5}\, c_{pv5m} = 1006.5475 + 0.026191 \times 1873.6637 = 1055.6215 \text{ J/kgK}$$

The enthalpy of the saturated air can now be determined to see if the determined temperature is correct.

$$\begin{aligned} i_{mas5} &= c_{pa5m}\left(T_{a5} - 273.15\right) + w_{s5}\left(i_{fgw0} + c_{pv5m}\left(T_{a5} - 273.15\right)\right) \\ &= 1006.5475 \times \left(299.2212 - 273.15\right) + \\ &\quad 0.026191\left(2501598.5335 + 1873.6637 \times \left(299.2212 - 273.15\right)\right) \\ &= 93041.8847 \text{ J / kg} \end{aligned}$$

This value compares well with the one obtained from the Chebyshev numerical integration, and the iterated temperature T_{a5} is therefore correct.

An approximate mean air density through the fill can be determined from equation (5.1.2) as follows:

$$\rho_{av34} = 2\left[\frac{1}{\rho_{av3}} + \frac{1}{\rho_{av4}}\right]^{-1} \approx \rho_{av15} = 2\left[\frac{1}{\rho_{av1}} + \frac{1}{\rho_{av5}}\right]^{-1}$$
$$= 2\left[\frac{1}{1.0101} + \frac{1}{0.96216}\right]^{-1} = 0.98556 \text{ kg/m}^3$$

The mean air mass flow rate through the fill is approximately:

$$m_{av34} \approx m_{av15} = \frac{m_{aw}(2 + w_1 + w_5)}{2} = \frac{482.345(2 + 0.008127 + 0.026191)}{2} = 490.6216 \text{ kg/s}$$

The air mass flow rate at 1 is:

$$m_{av1} = m_a(1 + w_1) = 482.345(1 + 0.008127) = 486.2867 \text{ kg/s}$$

The air mass flow rate at 5 is:

$$m_{av5} = m_a(1 + w_5) = 482.345(1 + 0.026191) = 494.9783 \text{ kg/s}$$

The mean air velocity across the fill can now be determined as follows:

$$v_{av34} = \frac{m_{av34}}{\rho_{av34} A_{fr}} = \frac{490.6216}{0.98556 \times 180} = 2.7656 \text{ m/s}$$

It is now possible to determine the static pressure drop through the wet section up to point 8. In order to determine this static pressure drop, the different *pressure loss coefficients* and the *hydrostatic pressure drop* through the wet section should be calculated.

Calculation of the pressure loss coefficients

The pressure loss coefficients are determined from the correlations given in Chapter 5 or values for the loss coefficients are assumed. In Chapter 5 the change in the air mass flow rate through the wet section were not taken into account when the correlations were referred to the mean air conditions through the fill, but it is taken into account in this sample calculation.

- Noise attenuators

Both the losses through, and the inlet losses to the noise attenuators are incorporated in this loss coefficient.

The frontal area of the wet section's noise attenuators is:

$$A_{na} = 2B_3H_3 = 2 \times 12 \times 3.5 = 84 \text{ m}^2$$

From equation (5.1.5) and taking into consideration small changes in the air mass flow rate, the loss coefficient for the noise attenuators is:

$$K_{na} = K_{na2}\frac{\rho_{av34}}{\rho_{av1}}\left[\frac{A_{fr}}{A_{na}}\right]^2\left[\frac{m_{av1}}{m_{av34}}\right]^2 = 3\frac{0.98556}{1.0101}\left[\frac{180}{84}\right]^2\left[\frac{486.2867}{490.6216}\right]^2 = 13.2028$$

- The rain zone

The loss coefficient for the rain zone can be determined from equation (5.1.6):

$$\begin{aligned}K_{rz3} = {} & 148.4\left[\frac{W_{fi}/2}{H_3}\right]^{3.47} \times 227.7^{\frac{H_3}{W_{fi}/2}} \times \left[\frac{\rho_{w3}}{\rho_{av1}}\right]^{0.204} \\ & \times \exp\left[0.017544\left(\ln\left(\frac{d_d}{H_3}\right) - 10.56\right)^2 - 0.015074\left(\ln\left(\frac{v_w}{v_{av34}}\right) - 25.9\right)^2\right. \\ & + 0.059172\left(\ln\left(\frac{\rho_{av1}v_{av34}H_3}{\mu_{av1}}\right) - 15.4\right)^2 + 0.206612\left(\ln\left(\frac{v_{av34}^2}{gH_3}\right) + 1.92\right)^2 \\ & \left. + 0.037313\left(\ln\left(\frac{\rho_{av1}v_{av34}^2H_3}{\sigma_{w3}}\right) - 4.05\right)^2\right] \\ = {} & 148.4\left[\frac{15/2}{3.5}\right]^{3.47} \times 227.7^{\frac{3.5}{15/2}} \times \left[\frac{997.5455}{1.0101}\right]^{0.204} \times \exp\left[0.017544\left(\ln\left(\frac{0.0035}{3.5}\right) - 10.56\right)^2\right. \\ & - 0.015074\left(\ln\left(\frac{0.0025062}{2.7656}\right) - 25.9\right)^2 + 0.059172\left(\ln\left(\frac{1.0101 \times 2.7656 \times 3.5}{1.7857 \times 10^{-5}}\right) - 15.4\right)^2 \\ & \left. + 0.206612\left(\ln\left(\frac{2.7656^2}{9.8 \times 3.5}\right) + 1.92\right)^2 + 0.037313\left(\ln\left(\frac{1.0101 \times 2.7656^2 \times 3.5}{0.072339}\right) - 4.05\right)^2\right] \\ = {} & 2.9016\end{aligned}$$

If this correlation is referred to the conditions through the fill it becomes:

$$K_{rz} = K_{rz3}\left[\frac{\rho_{av34}}{\rho_{av3}}\right]\left[\frac{m_{av3}}{m_{av34}}\right]^2 \approx K_{rz3}\left[\frac{\rho_{av34}}{\rho_{av1}}\right]\left[\frac{m_{av1}}{m_{av34}}\right]^2$$

$$= 2.9016\left[\frac{0.98556}{1.0101}\right]\left[\frac{486.2867}{490.6216}\right]^2 = 2.781$$

- Fill support and contraction losses

The value for K_{fs} that includes the contraction loss, is taken as 0.5. Referred to the conditions through the fill it becomes:

$$K_{fs} = K_{fs2}\frac{\rho_{av34}}{\rho_{av2}}\left[\frac{m_{av2}}{m_{av34}}\right] \approx K_{fs2}\frac{\rho_{av34}}{\rho_{av1}}\left[\frac{m_{av1}}{m_{av34}}\right]^2$$

$$= 0.5 \times \frac{0.98556}{1.0101}\left[\frac{486.2867}{490.6216}\right]^2 = 0.47921$$

- Fill

The mean air velocity at the outlet of the fill, based on the fill frontal area and the conditions at 5 is:

$$v_{av5} = \frac{m_a(1+w_5)}{\rho_{av5}A_{fr}} = \frac{482.345(1+0.026191)}{0.96216 \times 180} = 2.858 \text{ m/s}$$

The mean air velocity at the inlet to the fill, based on the fill frontal area and the conditions at 1 is:

$$v_{av3} \approx v_{av1} = \frac{m_a(1+w_1)}{\rho_{av1}A_{fr}} = \frac{482.345(1+0.008127)}{1.0101 \times 180} = 2.6744 \text{ m/s}$$

The static pressure drop through the fill as obtained from equation (C.1.9) is:

$$K^*_{fiavm} = L_{fi}\,1.9277 G_w^{1.2752} G_a^{-1.0356} = 1.88 \times 1.9277 \times 2.5^{1.2752} \times 2.6797^{-1.0356} = 4.2007$$

If the momentum effects are included, the pressure loss coefficient through the fill for these specific operating conditions is:

$$K_{fi} = K_{fi}^* + \frac{\left(\rho_{av4} v_{av4}^2 - \rho_{av3} v_{av3}^2\right)}{\rho_{av34} v_{av34}^2} \approx K_{fi}^* + \frac{\left(\rho_{av5} v_{av5}^2 - \rho_{av1} v_{av1}^2\right)}{\rho_{av34} v_{av34}^2}$$

$$= 4.2007 + \frac{\left(0.96216 \times 2.858^2 - 1.0101 \times 2.6744^2\right)}{0.98556 \times 2.7656^2}$$

$$= 4.2849$$

- Spray zone

From equation (5.1.17) the pressure loss coefficient through the spray zone can be determined as follows:

$$K_{sp} = L_{sp}\left[0.4\left(\frac{G_w}{G_a}\right)+1\right]\left[\frac{\rho_{av34}}{\rho_{av4}}\right]\left[\frac{m_{av4}}{m_{av34}}\right]^2 \approx L_{sp}\left[0.4\left(\frac{G_w}{G_a}\right)+1\right]\left[\frac{\rho_{av34}}{\rho_{av5}}\right]\left[\frac{m_{av5}}{m_{av34}}\right]^2$$

$$= 0.5\left[0.4\left(\frac{2.5}{2.6797}\right)+1\right]\left[\frac{0.98556}{0.96216}\right]\left[\frac{494.9783}{490.6216}\right]^2 = 0.71583$$

- Water distribution system

The loss coefficient through the water distribution system is taken as 0.5. Based on the conditions through the fill it becomes

$$K_{wd} = K_{wd5} \frac{\rho_{av34}}{\rho_{av5}}\left[\frac{m_{av5}}{m_{av34}}\right]^2 = 0.5 \times \frac{0.98556}{0.96216}\left[\frac{494.9783}{490.6216}\right]^2 = 0.5213$$

- Drift eliminators

The loss coefficient through the drift eliminators is determined from a correlation given by Botes [95BO1]. Based on the conditions through the fill it becomes:

$$K_{de} = 27.4892\left(Ry_{de}\right)^{-0.14247} \frac{\rho_{av34}}{\rho_{av5}} = 27.4892\left(\frac{m_a\left(1+w_5\right)}{\mu_{av5} A_{fr}}\right)^{-0.14247} \frac{\rho_{av34}}{\rho_{av5}}\left[\frac{m_{av5}}{m_{av34}}\right]^2$$

$$= 27.4892\left(\frac{482.345(1+0.026191)}{1.8162 \times 10^{-5} \times 180}\right)^{-0.14247} \frac{0.98556}{0.96216}\left[\frac{494.9783}{490.6216}\right]^2 = 5.2392$$

- Tower inlet losses

For a rectangular cooling tower with sharp tower inlets, the inlet pressure loss coefficient can be obtained from equation (5.1.20).

The heat exchanger pressure loss coefficient that is used in equation (5.1.20) is:

$$K_{he} = K_{fs} + K_{fi} + K_{sp} + K_{wd} + K_{de}$$
$$= 0.47921 + 4.2849 + 0.71583 + 0.5213 + 5.2392 = 11.2404$$

Because of the horizontal air inflow through the sound attenuators, it can again be assumed that the tower has rounded inlets with a width equal to the width of the fill. From data given by Terblanche [94TE1] it can be seen that the difference between the losses for a tower with a rounded and a sharp inlet is very small for small *W/H* ratios, and for the tower under consideration ($W_{fi}/2H_3 = 2.14$) the correlation for sharp inlets can be used for rounded inlets without causing a significant error. The inlet loss coefficient is therefore:

$$K_{ct3} = \left[1.1 + 1.1\left(\frac{W_{fi}/2}{H_3}\right)^3 - 0.05\left(\frac{W_{fi}/2}{H_3}\right)\exp\left(\frac{W_{fi}/2}{H_3}\right)\right] K_{he}^{\left[0.079\cos\left(\frac{W_{fi}/2}{H_3}\right) + 0.102\sin\left(\frac{W_{fi}/2}{H_3}\right) - 0.29\right]}$$
$$= \left[1.1 + 1.1\left(\frac{15/2}{3.5}\right)^3 - 0.05\left(\frac{15/2}{3.5}\right)\exp\left(\frac{15/2}{3.5}\right)\right] 11.2404^{\left[0.079\cos\left(\frac{15/2}{3.5}\right) + 0.102\sin\left(\frac{15/2}{3.5}\right) - 0.29\right]}$$
$$= 6.0569$$

Referred to the conditions through the fill it becomes:

$$K_{ct} = K_{ct3}\frac{\rho_{av34}}{\rho_{av3}}\left[\frac{m_{av3}}{m_{av34}}\right]^2 \approx K_{ct3}\frac{\rho_{av34}}{\rho_{av1}}\left[\frac{m_{av1}}{m_{av34}}\right]^2 = 6.0569\frac{0.98556}{1.0101}\left[\frac{486.2867}{490.6216}\right]^2 = 5.8051$$

The sum of all the pressure loss coefficients through the wet section is:

$$K_{tot} = K_{he} + K_{na} + K_{rz} + K_{ct} = 11.2404 + 13.2028 + 2.781 + 5.8051 = 33.0293$$

Calculation of the hydrostatic pressure drop

The density correction factor for the air leaving the spray zone is:

$$\Omega_5 = (1 + w_5)\left(1 - \frac{w_5}{w_5 + 0.62198}\right) = (1 + 0.026191)\left(1 - \frac{0.026191}{0.026191 + 0.62198}\right)$$
$$= 0.98472$$

From equation (5.2.2) the hydrostatic pressure difference between ground level and the middle of the fill is:

$$\begin{aligned}(\Delta p_{a1-34})_{hydrostatic} &= p_{a1}\left[1-\left(1-0.00975\left[\frac{H_3+L_{fi}/2}{T_{a1}}\right]\right)^{3.5\Omega_1}\right] \\ &= 84100\left[1-\left(1-0.00975\left[\frac{3.5+1.88/2}{288.6}\right]\right)^{3.5\times 0.99512}\right] \\ &= 43.929 \text{ Pa}\end{aligned}$$

From equations (5.2.4) and (5.2.3), the temperature lapse rate for the saturated air leaving the wet section is:

$$\begin{aligned}\left(\frac{dw}{dT}\right)_5 &= \frac{7.966\times 10^{14}\,\mathrm{e}^{-\left(\frac{5406.1915}{T_{a5}}\right)}}{p_{a5}T_{a5}^2} \\ &= \frac{7.966\times 10^{14}\exp\left[-\left(\frac{5406.1915}{299.2212}\right)\right]}{83931.5803\times 299.2212^2} = 1.5089\times 10^{-3}\ \mathrm{K}^{-1}\end{aligned}$$

$$\begin{aligned}\left(\frac{dT}{dz}\right)_5 = \xi_{T_{a5}} &= \frac{-(1+w_5)g}{c_{pavm5}+\left(\frac{dw}{dT}\right)_5\left[i_{fgw0}-\left(c_{pwm5}-c_{pvm5}\right)\left(T_{a5}-273.15\right)\right]} \\ &= \left[-(1+0.026191)9.8\right]/\{1055.6215+1.5089\times 10^{-3}\times \\ &\quad \left[2501598.5335-(4192.8305-1873.6637)(299.2212-273.15)\right]\} \\ &= -0.0021221\ \mathrm{K/m}\end{aligned}$$

The hydrostatic pressure change from the middle of the fill up to point 8 ($H_8 = H_6$, immediately before the air mixers) can now be determined from equation (5.2.5) as follows:

$$\begin{aligned}(\Delta p_{a34-8})_{hydrostatic} &= p_{a5}\left\{1-\left[1+\xi_{T_{a5}}\left(\frac{H_8-H_3-L_{fi}/2}{T_{a5}}\right)\right]^{-\Omega_5\left[\frac{g}{R\xi_{T_{a5}}}\right]}\right\} \\ &= 83931.5803\left\{1-\left[1-0.0021221\left(\frac{8.38-3.5-1.88/2}{299.2212}\right)\right]^{\frac{-0.98472\times 9.8}{287.08\times -0.0021221}}\right\} \\ &= 37.143 \text{ Pa}\end{aligned}$$

The hydrostatic pressure differential through the wet section is:

$$\left(\Delta p_{a1-8}\right)_{hydrostatic} = \left(\Delta p_{a1-34}\right)_{hydrostatic} + \left(\Delta p_{a34-8}\right)_{hydrostatic} = 43.929 + 37.143 = 81.0721 \text{ Pa}$$

The static pressure drop through the wet section up to point 8 is:

$$\begin{aligned}\Delta p_{a1-8} &= K_{tot}\,\tfrac{1}{2}\rho_{av34}v_{av34}^2 + \tfrac{1}{2}\rho_{av8}v_{av8}^2 + \left(\Delta p_{a1-8}\right)_{hydrostatic}\\ &\approx K_{tot}\,\tfrac{1}{2}\rho_{av34}v_{av34}^2 + \tfrac{1}{2}\rho_{av5}v_{av5}^2 + \left(\Delta p_{a1-8}\right)_{hydrostatic}\\ &= 33.0293\times\tfrac{1}{2}\times 0.98556\times 2.7656^2 + \tfrac{1}{2}\times 0.96216\times 2.858^2 + 81.0721 = 209.4923 \text{ Pa}\end{aligned}$$

The static pressure after the wet section is therefore:

$$p_{a8w} = p_{a1} - \Delta p_{a1-8} = 84100 - 209.4923 = 83890.5077 \text{ Pa}$$

This pressure is in good agreement with p_{a7} = 83891.4308 Pa determined after the dry section.

The static pressure at point 5 can now be determined, to see if the assumed value for p_{a5} was correct. If the hydrostatic pressure drop is calculated up to the middle of the fill by using the dry adiabatic lapse rate and if the dynamic pressure component at 5 is ignored, the approximated static pressure at point 5 is:

$$\begin{aligned}p_{a5} &= p_{a1}\left[1 - 0.00975\left(\frac{H_3 + L_{fi}/2}{T_{a1}}\right)\right]^{3.5\Omega_1}\\ &\quad -\left(K_{he} + K_{rz} + K_{ct} + K_{na}\right)\times\left(\tfrac{1}{2}\rho_{av34}v_{av34}^2\right)\\ &= 84100\left[1 - 0.00975\left(\frac{3.5 + 1.88/2}{288.6}\right)\right]^{3.5\times 0.99512} - \left(11.2404 + 2.781 + 5.8051 + 13.2028\right)\\ &\quad \times\left(0.5\times 0.98556\times 2.7656^2\right)\\ &= 83931.5803 \text{ Pa}\end{aligned}$$

The determined value for p_{a5} compares well with the value that was assumed in the beginning of the sample calculation, and convergence is therefore satisfied. Although the pressure p_{a5} is actually the total pressure it differs only slightly from the static pressure, and it is used as a static pressure in the calculations. If the dynamic term $\left(\tfrac{1}{2}\rho_{av5}v_{av5}^2 = 3.9296 \text{ Pa}\right)$ is not ignored the obtained pressure is p_{a5} = 83927.6507 Pa. This pressure is only 0.0047 % lower than the obtained one, and the assumption that $p_{at5} = p_{a5}$ is therefore accurate enough.

The cooling performance of the wet section as determined from an energy balance on the cooling water is:

$$Q_w = m_w c_{pwm}(T_{wiw} - T_{wo}) = 450 \times 4178.5265(310.6171 - 296.014)/1000000$$
$$= 27.4585 \text{ MW}$$

The amount of water that is lost through evaporation is approximately

$$m_{wlost} = m_a(w_5 - w_1) = 482.345(0.026191 - 0.008127) = 8.7131 \text{ kg/s}$$

Mixed region calculations

If it is assumed that complete mixing of the wet and the dry air streams has occurred at point 8, the properties of the mixed air at point 8 can be determined as follows:

The total air mass flow rate through the mixed region is:

$$m_{avt} = m_{aw}(1 + w_5) + m_{ad}(1 + w_7)$$
$$= 482.345(1 + 0.026191) + 267.8392(1 + 0.008127)$$
$$= 764.994 \text{ kg/s}$$

- The humidity ratio of the mixed air is:

$$w_8 = \frac{w_5 m_{aw} + w_7 m_{ad}}{m_{aw} + m_{ad}}$$
$$= \frac{0.026191 \times 482.345 + 0.008127 \times 267.8392}{482.345 + 267.8392}$$
$$= 0.019742 \text{ kg/kg dry air}$$

- The enthalpy of the mixed air stream can be determined with the following equation:

$$i_{ma8} = \frac{i_{ma5} m_{aw} + i_{ma7} m_{ad}}{m_{aw} + m_{ad}}$$
$$= \frac{93041.8847 \times 482.345 + 53805.621 \times 267.8392}{482.345 + 267.8392}$$
$$= 79033.3124 \text{ J/kg}$$

- The dry bulb temperature of the mixed air at 8.

The dry bulb temperature T_{a8}, is solved iteratively by using equation (A.3.6). It was found that a dry bulb temperature of T_{a8} = 301.5588 K satisfies the enthalpy equation. The following constant pressure specific heats were determined at (301.5588+273.15)/2 = 287.3544 K.

Specific heat of air	c_{pa8m} = 1006.5748 J/kgK	(A.1.2)
Specific heat of water vapour	c_{pv8m} = 1874.6565 J/kgK	(A.2.2)

The enthalpy is then:

$$\begin{aligned} i_{ma8} &= c_{pam8}T_{a8} + w_8\left(i_{fgw0} + c_{pvm8}T_{a8}\right) \\ &= 1006.5748(301.5588 - 273.15) + \\ &\quad 0.019742\left[2501598.5335 + 1874.6565(301.5588 - 273.15)\right] \\ &= 79033.3124 \text{ J / kg} \end{aligned}$$

This determined enthalpy is in good agreement with the obtained one, and the iterated temperature (T_{a8}) is therefore correct.

- The density of the mixed air at 8.

The density correction is:

$$\begin{aligned} \Omega_8 &= (1+w_8)\left[1 - \frac{w_8}{w_8 + 0.62198}\right] = (1+0.019742)\left[1 - \frac{0.019742}{0.019742 + 0.62198}\right] \\ &= 0.98837 \end{aligned}$$

The air density is then:

$$\rho_{av8} = \frac{p_{a8}}{RT_{a8}}\Omega_8 = \frac{83891.4308}{287.08 \times 301.5588}0.98837 = 0.95777 \text{ kg / m}^3$$

The fan casing area is:

$$A_{fanc} = \pi d_{fanc}^2 / 4 = \pi 9.5265^2 / 4 = 71.2784 \text{ m}^2$$

The velocity of the combined air stream at 8 is:

$$v_{av8} = \frac{m_{avt}}{\rho_{av8} A_{fr}} = \frac{764.994}{0.95777 \times 180} = 4.4373 \text{ m/s}$$

The fan that is used is a still fan and noise attenuators are therefore not installed at the tower exit. The loss coefficients through the mixed region are all being based on the fan casing area. If it is assumed that the density of the air does not change from point 8 onward, the pressure loss coefficients in the mixed region can be determined as follows:

- Air mixing devices

Based on the fan casing area it becomes:

$$K_{me} = K_{me8}\left(\frac{A_{fanc}}{A_8}\right)^2 \approx K_{me8}\left(\frac{A_{fanc}}{A_{fr}}\right)^2 = 0.8\left(\frac{71.2784}{180}\right)^2 = 0.12545$$

- The fan discharge and suction losses

The fan discharge and suction losses are both based on the fan casing area, and can therefore be combined in a single loss coefficient $K_{fsuc} + K_{fdis} = 0.4$.

The approximate mean air velocity through the fan with $\rho_{av9} \approx \rho_{av8}$ is:

$$v_{av9} = \frac{m_{avt}}{\rho_{av9} A_{fanc}} = \frac{764.994}{0.95777 \times 71.2784} = 11.2057 \text{ m/s}$$

The hydrostatic pressure drop through the mixed region is:

$$\begin{aligned}(\Delta p_{a8-11})_{hydrostatic} &= p_{a8}\left[1-\left(1-0.00975\left[\frac{H_{11}-H_6}{T_{a8}}\right]\right)^{3.5\Omega_8}\right] \\ &= 83891.4308\left[1-\left(1-0.00975\left[\frac{15.38-8.38}{301.5588}\right]\right)^{3.5\times 0.98837}\right] \\ &= 65.6622 \text{ Pa}\end{aligned}$$

The total pressure drop through the mixed region is therefore:

$$\begin{aligned}\Delta p_{at8-11} &= \left(K_{me} + K_{fsuc} + K_{fdis}\right) \times \tfrac{1}{2}\rho_{av9} v_{av9}^2 + (\Delta p_{a8-11})_{hydrostatic} \\ &= (0.12545 + 0.2 + 0.2) \times \tfrac{1}{2} \times 0.95777 \times 11.2057^2 + 65.6622 \\ &= 97.2586 \text{ Pa}\end{aligned}$$

The pressure losses through the mixed region are now referred to the region before the fan where the cross-sectional area is still equal to the frontal area of the fill. The imaginary point where this referred pressure drop is incorporated is indicated by 8'. The total pressure at this point if it is assumed that the resistances of the mixed region are all moved to the region between point 8 and point 8' (a small distance downstream from point 8) is:

$$\begin{aligned}\left(p_{a8'}+\tfrac{1}{2}\rho_{av8'}v_{av8'}^{2}\right) &= p_{a8}+\tfrac{1}{2}\rho_{av8}v_{av8}^{2}-\Delta p_{at8-11}\\ &= 83891.4308+\tfrac{1}{2}0.95777\times 4.4373^{2}-97.2586\\ &= 83803.6015\ \text{Pa}\end{aligned}$$

The atmospheric pressure at the outlet height of the tower is according to equation (5.2.1):

$$\begin{aligned}p_{a12} &= p_{a1}\left[1-0.00975\left(\frac{H_{11}}{T_{a1}}\right)\right]^{3.5\Omega_1}\\ &= 84100\left[1-0.00975\left(\frac{15.38}{288.6}\right)\right]^{3.5\times 0.99512}\\ &= 83947.9012\ \text{Pa}\end{aligned}$$

The atmospheric pressure at the top of the tower must be equal to the static pressure at the outlet of the tower ($p_{a12}=p_{a11}$), and the fan must therefore deliver the pressure rise to obtain this equilibrium. From the definition of the fan static pressure, the static pressure that the fan must deliver is:

$$p_{fan}=p_{a12}-\left(p_{a8'}+\tfrac{1}{2}\rho_{av8'}v_{av8'}^{2}\right)=83947.9012-83803.6015=144.2997\ \text{Pa}$$

The volume flow rate through the fan is:

$$V_{fan}=\frac{m_{avt}}{\rho_{av9}}=\frac{764.994}{0.95777}=798.7221\ \text{m}^3/\text{s}$$

The static pressure rise at this volume flow rate and air density, can now be determined with the help of the fan conversion rules given in equations (5.3.1) and (5.3.2).

From equation (5.3.1) the matching volume flow rate for the specified fan/diffuser is:

$$V_{sfan}=\frac{V_{fan}}{\left(n_{fan}/n_{sfan}\right)}=\frac{798.7221}{(118/120)}=812.2598\ \text{m}^3/\text{s}$$

For this volume flow rate the specified fan/diffuser static pressure can be determined, from the given fan/diffuser static pressure curve. For a 14 ° blade angle at the specified volume flow rate, the fan/diffuser static pressure is:

$$\begin{aligned}p_{sfan} &= 299.903 + 40.0071\times10^{-3}V_{sfan} - 96.5087\times10^{-6}V_{sfan}^2 - 152.2243\times10^{-9}V_{sfan}^3\\ &= 299.9 + 40.0071\times10^{-3}\times812.2598 - 96.5087\times10^{-6}\\ &\quad\times812.2598^2 - 152.2243\times10^{-9}\times812.2598^3\\ &= 187.1489 \text{ Pa}\end{aligned}$$

From this fan/diffuser static pressure, the static pressure delivered by the working fan at the same blade angle can be determined from equation (5.3.2) as follows:

$$\begin{aligned}p_{fan} &= \left(n_{fan}/n_{sfan}\right)^2\left(\rho_{fan}/\rho_{sfan}\right)p_{sfan}\\ &= (118/120)^2(0.95777/1.2)\times187.1489\\ &= 144.1547 \text{ Pa}\end{aligned}$$

The obtained static pressure rise for the 14 ° blade angle, agrees well with the required static pressure rise.

For a 14 ° blade angle at the determined volume flow rate, the power consumption of the specified fan can be determined from the relevant polynomial as follows:

$$\begin{aligned}P_{sfan} &= 203302.6779 - 58.3775V_{sfan} + 458.7692\times10^{-3}V_{sfan}^2 - 405.2315\times10^{-6}V_{sfan}^3\\ &= 203302.6779 - 58.3775\times812.2598 + 458.7692\times10^{-3}\\ &\quad\times812.2598^2 - 405.2315\times10^{-6}\times812.2598^3\\ &= 241.4012 \text{ kW}\end{aligned}$$

The power consumption of the working fan can now be determined from equation (5.3.3) as follows:

$$\begin{aligned}P_{fan} &= P_{sfan}\left(\frac{n_{fan}}{n_{sfan}}\right)^3\left(\frac{\rho_{fan}}{\rho_{sfan}}\right)\\ &= 241.4012\left(\frac{118}{120}\right)^3\left(\frac{0.95777}{1.2}\right)\\ &= 183.1984 \text{ kW}\end{aligned}$$

The efficiency of the working fan for a 14 ° blade angle is:

$$\eta_{fan} = \frac{p_{fan}V_{fan}}{P_{fan}} = \frac{144.1547 \times 798.7221}{183198}$$
$$= 0.6285 \text{ or } 62.85 \text{ \%}$$

The operating point is to the right of the maximum on the efficiency curve.

The tip speed of the fan blades is:

$$v_{fant} = \pi d_{fan} rpm / 60 = \pi 9.5 \times 118 / 60 = 58.6954 \text{ m / s}$$

This speed is under the recommended maximum speed of 60 m/s above which noise levels become too high.

Determination of the extent of plume formation

If it is assumed that the temperature of the air stays constant from point 8 onward, the temperature and the humidity ratio of the air leaving the tower is T_{a11} = 301.5588 K and w_{11} = 0.019742 kg/kg dry air.

If it is assumed that the dilution of the exit air would follow a linear path, the equation for this line can be determined as follows for this specific case:

$$w = \left(\frac{w_{11} - w_1}{T_{a11} - T_{a1}}\right) T_a + \left(\frac{T_{a11}w_1 - T_{a1}w_{11}}{T_{a11} - T_{a1}}\right)$$
$$= \left(\frac{0.019742 - 0.008127}{301.5588 - 288.6}\right) T_a + \left(\frac{301.5588 \times 0.008127 - 288.6 \times 0.019742}{301.5588 - 288.6}\right)$$
$$= 8.963 \times 10^{-4} T_a - 0.25055$$

The equation for the saturation curve as obtained from equation (A.3.5) is:

$$w_s = \left[\frac{0.62509 p_{vs}}{p_{atm} - 1.005 p_{vs}}\right]$$

where p_{vs} is determined from equation (A.2.1).

The points where the dilution line cross the saturation curve can now be obtained from these two equations by subtracting them from one another and finding the roots of the difference equation.

For this specific tower operating point, the two curves never cross, and according to the visible plume formation criteria given in section 3.4 visible plume formation will not occur. In figure E.3 it is shown that the dilution line stays in the unsaturated region.

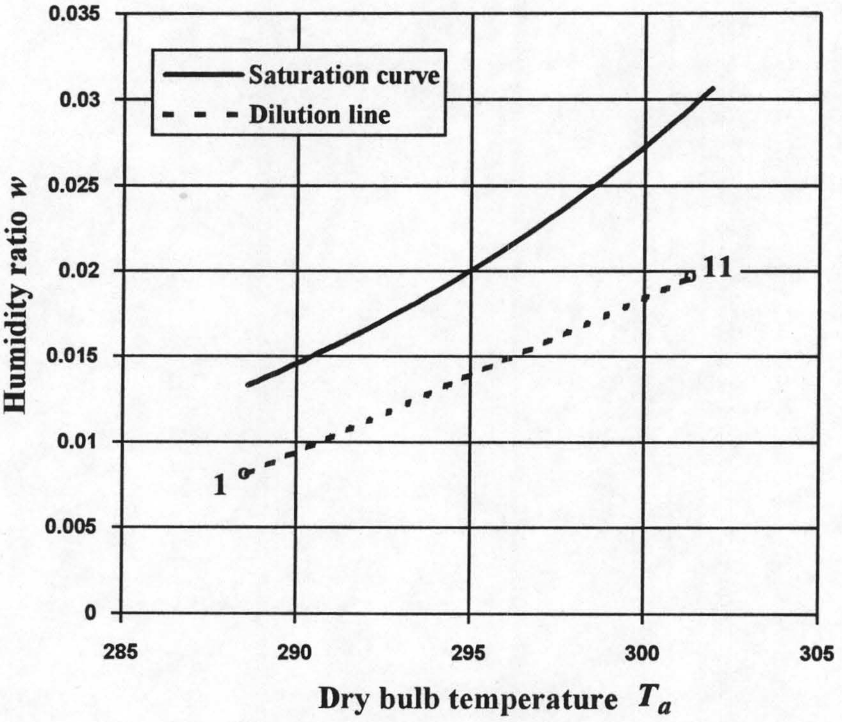

Figure E.3: *Psychrometric representation of the plume dilution line.*

CHAPTER
SEVEN

CONCLUSIONS AND RECOMMENDATIONS

Conclusions

From the study of the different hybrid tower geometries it was concluded that the parallel path air flow, series path water flow (PPAF-SPWF) tower was the most practical and commonly used one and therefore the rest of the work was aimed at developing a sample solution for this kind of tower. A theoretical model with which the heat rejection rate and plume abatement capability of a rectangular PPAF-SPWF hybrid tower can be predicted was developed and a computer program was written to implement this theoretical model for determining the performance of such a tower.

If visible plumes are unwanted at a certain cooling tower locality, hybrid cooling towers can be used to successfully control the formation of such a plume. An increase in a cooling tower's plume abatement capability is usually proportional to an increase in the cooling tower's cost, since this capability is only limited by the size of the tower's dry section and dry cooling is more expensive than wet cooling. Somewhere between an all-dry and an all-wet tower an optimum tower configuration must therefore be found.

Most of the existing hybrid towers are situated in Europe where extremely low winter temperatures occur and where the towers have to be built in densely populated areas. In South Africa the need for hybrid towers is not as great and since the climatic conditions are less favourable for visible plume formation, most of the large wet cooling towers are built in areas that are not so densely populated. However, instead of all dry cooling towers dry/wet hybrid towers such as the ones built at San Juan (section 2.2.1) or Trakya (section 2.2.7) can be used in areas where water supplies are limited. In this way optimal use can be made of the water resources that are available for cooling.

The experiments that were done to determine the extent of flow separation in cooling tower inlets indicated that this could have a measurable effect on the performance of a cooling tower and that this effect may not be ignored in cooling tower design. This effect is especially large in cooling towers with low heat exchanger or fill pressure loss coefficients and with a large inlet width or inlet diameter to inlet height ratio.

Evaluation of the fill test data given in Appendix C showed that a more accurate pressure loss correlation can be obtained if the momentum effects of the air and the hydrostatic pressure in the measuring pipes are also considered in the pressure loss calculations. The error that can occur if these influences are ignored is especially large for small air and water mass flow rates.

Recommendations

The computer program that was developed is only applicable for rectangular PPAF-SPWF hybrid towers and further work can be done in developing computer programs for solving hybrid towers with different geometries.

In this thesis the straight mixing line theory is used to quantify the severity of visible plume formation (section 3.4). However, this is a greatly simplified approach and a method that takes more factors into consideration would be better. To accurately quantify the severity of a visible plume, the exact nature of the plume that forms must first be calculated numerically. Various existing numerical methods are briefly discussed in section 3.2. It is recommended that a program to predict the visible plume formation be developed and that a method such as the one proposed by Mäule [80MÄ1] be used to quantify the severity of plume formation from the information obtained from the program. If this is done over a range of climatic conditions for a specific cooling tower site, a good indication of a cooling tower's plume abatement capability can be obtained and various cooling towers can then be realistically compared.

The experiments that were done to determine the extent of flow separation in the cooling tower should be extended for different inlet rounding diameters, and a better method of quantifying the size of the ineffective fill area should be considered. It is also recommended that a numerical analysis should be done to verify the experimental results.

Since no performance data for a PPAF-SPWF rectangular hybrid tower could be found, the accuracy of the mathematical model could not be confirmed and it is recommended that some data be collected from an existing tower to confirm that the results generated by the computer program are accurate.

REFERENCES

[25ME1] Merkel F.: *Verdunstungskühlung*, VDI-Zeitschrift, vol. 70, no. 70, pp. 123-128, 1925.

[38PA1] Patterson G.N.: *Modern Diffuser Design*, Aircraft Eng., vol. 10, pp. 267, 1938.

[46SC1] Schmidt T.E.: *La Production Calorifique des Surfaces Munies Dailettes*, Annexe Du Bulletin De L'Institut International Du Froid, Annex G-5, 1945 - 1946.

[61BE1] Berman L.D.: *Evaporative Cooling of Circulating Water*, 2nd Edition, Henryck Sawistowski, ed., Permagon Press, New York, Chapter 2, pp. 94-99, 1961. Translated from Russian by R. Hardbottle.

[61JO1] Jorgensen R.: *Fan Engineering*, Buffalo Forge Co., Buffalo, New York, 1961.

[61LO1] Lowe H.J. and Christie D.G.: *Heat Transfer and Pressure Drop Data on Cooling Tower Packings, and Model Studies of the Resistance of Natural Draft Towers to Airflow*, Proceedings of the International Heat Transfer Conference, Boulder, Colorado, Part V, Paper 113, pp. 933-950, 1961.

[61PA1] Pasquill F.: *The estimation of the dispersion of windborne material*, Met. Mag., vol. 90, pp. 33-49, 1961.

[64KA1] Kays W.M. and London A.L.: *Compact Heat Exchangers*, 2nd Ed., McGraw-Hill, New York, 1964.

[65FR1] Fröberg C.E.: *Introduction to Numerical Analysis*, Addison-Wesley Publishing Company Inc., pp. 190-194, 1965.

[66VD1] Verein Deutscher Ingenieure, VDI-Richtlinien, Abname - und Leistungsversuche an Ventilatoren, VDI 2044, Berlin und Köln, 1966.

[69BR1] Briggs G.A.: *Plume Rize*, AEC Criterical Review Series, TID-25075, Clearinghouse for Federal Scientific and Technical Info., N.B.S., U.S. Department of Commerce, 1969.

[71WE1] Wessels H.R.A. and Wisse J.A.: *A Method for Calculating the Size of Cooling Tower Plumes*, Atmospheric Environment, vol. 5, pp. 743-750, 1971.

[72AN1] *Are wet/dry cooling towers the answer?*, Electrical world, pp. 80-83, September 15, 1972.

[72HA1] Hanna S.R.: *Rise and Condensation of Large Cooling Tower Plumes*, Journal of Applied Meteorology, vol. 11, pp. 793-799, 1972.

[72OL1] Olesen K.A. and Budenholzer R.J.: *Economics of Wet/Dry Cooling Tower Show Promise*, Electrical World, pp. 32-34, December 15, 1972.

[72SA1] Saame J. and Somers E.V.: *The Formation and Dispersion of Fog Plumes From a Natural Draft Water Cooling Tower for Various Meteorological Conditions*, International Clean Air Conference Proceedings, pp. 53-59, 1972.

[73HA1] Hansen E.P.: *Dry Towers and Wet-Dry towers for the Indirect Power Plant Cycle*, ASME Heat Transfer Division, vol. 6, pp. 109-117, 1973.

[73HE1] Heller L.: *Heller Discusses Hybrid Wet/Dry Cooling*, Electrical World, pp. 74-77, March 15, 1973.

[73KL1] Klanian P.S. and Noyes E.G.: *Economics of Wet/Dry Cooling Towers for Utility Power Plants*, Combustion, vol. 45, no. 4, pp. 31-34, October, 1973.

[73LA1] Landon R.D. and Houx J.R.: *Plume Abatement and Water Conservation with the Wet-Dry Cooling Tower*, Proceedings of the American Power Conference, vol. 35, pp.726-742, 1973.

[74BI1] Biese R.J.: *The Generation of Visible Plumes by Wet Dry Cooling Towers*, Presented to the Cooling Tower Institute, New Orleans, Louisiana, January 28-30, 1974.

[74PA1] Patel V.C., Croley T.E. and Cheng M.-S.: *Optimum Design of Dry Wet Combination Cooling Towers for Power Plants*, Proceedings of the Symposium on Cooling Tower Environment, College Park, pp. 24-57, 1974.

[74RE1] Reisman J.I. and Dolan N.E.: *The Wet/Dry Cooling Tower: An Effective Plume Control Method*, ASME paper 74-WA/HT-57, 1974.

[74SN1] Sneck H.J. and Brown D.H.: *Plume Rise From Large Thermal Sources Such as Dry Cooling Towers*, Transactions of the ASME, Journal of Heat Transfer, May 1974, pp. 232-238, 1974.

[75CR1] Croley T.E., Patel V.C. and Cheng M.-S.: *The Water and Total Optimization of Wet and Dry-Wet Cooling Towers for Electric Power Plants*, Iowa Institute of Hydraulic Research Report no. 163, The University of Iowa, Iowa City, Iowa, January, 1975.

[75GN1] Gnielinski, V.: *Forsch Ing. Wesen*, vol. 41, no. 1, 1975.

[75LA1] Larinoff M.W. and Di Pace D.: *Performance Characteristics of Dry and Wet-Dry Cooling Systems for Nuclear Power Plants*, Nuclex-75, Basel, Switzerland, October 7-11, 1975.

[75MA1] Maze R.W.: *Air Cooler or Water Tower-Which for Heat Disposal?*, Chemical Engineering, pp. 106-114, January 6, 1975.

[75RU1] Rubin A.M. and Klanian P.S.: *Visible Plume Abatement with the Wet/Dry Cooling Tower*, Power Engineering, March 1975.

[75VO1] Von Cleve H.H.: *Comparison of Different Combinations of Wet and Dry Cooling Towers*, ASME paper 75-WA/PWR-10, 1975.

[76BR1] Brown C.A., Fay H.P., Yao M.S. and Molina R.A.: *Advanced Techniques Minimise Wet-Dry Tower Costs and Water Consumption*, Presented at American Power Conference, Chicago, Illinois, April 20-22, 1976.

[76CH1] Cheng M.-S., Croley T.E. and Patel V.C.: *Analysis of Different Types of Dry-Wet Cooling Towers*, Iowa Institute of Hydraulic Research Report no. 191, The University of Iowa, Iowa City, Iowa, July, 1976.

[76CR1] Croley T.E., Patel V.C. and Cheng M.-S.: *Economics of Dry/Wet Cooling Towers*, Journal of the Power Division, ASCE, vol. 102, no. PO2, pp. 147-163, November, 1976.

[76CR2] Croley T.E. Patel V.C. and Cheng M.-S.: *Thermodynamic Models of Dry Wet Cooling Towers*, Journal of the Power Division, ASCE, vol. 102, no. PO1, pp. 1-20, January, 1976.

[76CR3] Croley T.E. Patel V.C. and Cheng M.-S.: *Dry-Wet Tower Evaporation and Fog Psychrometrics*, Journal of the Power Division, ASCE, vol. 102, no. PO1, pp. 21-33, January, 1976.

[76KE1] Kelly N.W.: *Kelly's Handbook of Crossflow Cooling Tower Performance*, Niel W. Kelly and Associates, Kansas City, Missouri, 1976.

[76LA1] Larinoff M.W. and Forster L.L.: *Dry and Wet Peaking Tower Cooling Systems for Power Plant Application*, Engineering for Power, vol. 98, no. 3, July, 1976.

[76SM1] Smith E.C. and Larinoff M.W.: *Alternative Arrangements and Designs for Wet/Dry Cooling Towers*, Power Engineering, pp. 58-61, May, 1976.

[76SM2] Smith E.C. and Larinoff M.W.: *Analyzing Wet/Dry Cooling Towers*, Power, pp. 78-80, May, 1976.

[76CH1] Cheng M.-S., Croley T.E. and Patel V.C.: *Analysis of Different Types of Dry-Wet Cooling Towers*, Iowa Institute of Hydraulic Research Report no. 191, The University of Iowa, Iowa City, Iowa, July, 1976.

[77SM1] Smith E.C. and Larinoff M.W.: *Alternative Arrangements and Designs Wet/Dry Cooling Towers for Power Plant Applications*, Combustion, pp. 23-27, May, 1977.

[78GI1] Gilbert J. and Lemmens F.: *Wet/Dry-Type Cooling Towers with Reduced Plume*, Presented at Conference on Modern Electric Power Stations, 1978.

[78KU1] Kunesch T.: *Keep Your Cool When Selecting the Right Tower*, Process Engineering, pp. 164-167, September, 1978.

[78KU2] Kunesch T.: *Environmental Aspects of Cooling Tower Selection*, Process Engineering, pp. 86-91, November, 1978.

[78LA1] Larinoff M.W.: *Performance and Capital Costs of Wet/Dry Cooling Towers in Power Plant Service*, Combustion, vol. 49, no. 11, pp. 9-19, May, 1978.

[80HE1] Henning H. and Ruscheweyh H.: *Air Flow Conditions in a Cooling Tower and Means of Control*, Balcke-Dürr technical paper, 1980.

[80GI1] Giaquinta A.R., Croley T.E., Hsu T.-D.: *Hybrid Cooling System Thermodynamics and Economics*, Journal of the Energy Division, ASCE, vol. 106, no. EY1, April, 1980.

[80MÄ1] Mäule R.: *Studies for Design of a Dry-Wet-Type Cooling Tower,* Paper Presented at the 2nd IAHR Cooling Tower Workshop, San Francisco, California, U.S.A., September 22 - 25, 1980.

[82CA1] Cale S.A.: *Development of Evaporative Cooling Packing*, Commission of European Communities, Report EUR 7709 EN, Luxemburg, 1982.

[83SI1] Singham J.R.: *Heat Exchanger Design Handbook*, Chapter 3.12, Section 3.12.5: Hybrid Towers, pp. 3.12.5:1-3.12.5:5, Hemisphere Publishing Company, 1983.

[83WA1] Wallis R.A.: *Axial Flow Fans and Ducts*, A Wiley-Interscience Publication, John Wiley and Sons, New York, 1983.

[84BÓ1] Bódás J.: *"Heller" Dry Cooling Towers in Iran*, Paper Presented at the 4th Cooling Tower Workshop of the IAHR, Interlaken, Switzerland, October 2nd-5th, 1984.

[84ER1] Ernst G. and Moussiopoulos N.: *Hybrid Cooling Towers (Wet-Dry Cooling)*, VGB Congress on Power Plants, Den Haag, 1984.

[84ER2] Ernst G. and Moussiopoulos N.: *Thermal Performance of Fan-Assisted Hybrid Cooling Towers,* Paper Presented at the 4th IAHR Cooling Tower Workshop, Interlaken, Switzerland, October 1-5, 1984.

[84GE1] Gerald C.F. and Wheatly P.O.: *Applied Numerical Analysis*, Addison-Wesley Publishing Co., California, 1984.

[84LE1] Lefevre M.R.: *Heat Transfer Technology, Atmospheric Cooling Equipment, Water Consumption*, Heat Transfer-Niagara Falls 1984, AIChE Symposium Series, vol. 80, no. 236, pp. 361-370.

[84TE1] Tesche W.: *Present Day Hybrid Cooling and Dry Cooling Technology Illustrated in the Example of a 1300 MW Power Generating Unit*, Paper Presented at the 4th IAHR Cooling Tower Workshop, Interlaken, Switzerland, October 2-5, 1984.

[85GA1] Ganguli A., Tung S.S. and Taborek J.: *Parametric Study of Air-Cooled Heat Exchanger Finned Tube Geometry*, Heat Transfer Research, Inc., vol. 81, no. 245, 1985.

[86AL1] Alt W.: *Concept, Design, Construction and Commissioning of the First Hybrid Cooling Tower for a Heating Power Station with a Net Power Generating Unit Capacity of 420 MW*, 5th IAHR Cooling Tower Workshop, Monterey, California, U.S.A., September 29 - October 3, 1986.

[86BÓ1] Bódás J and Szabó Z.: *A Wet/Dry Cooling System for a 600/1200 MW Combined Cycle Power Plant in Turkey*, Paper Presented at the 5th Cooling Tower Workshop of the International Association for Hydraulic Research, Monterey, California, U.S.A., September 29 - October 3, 1986.

[86MÄ1] Mäule R., Ernst G. and Bräuning G.: *Results of Experiments on the Performance and the Emission of the Hybrid Cooling Tower of the Altbach-Deizisau Plant of Neckarwerke*, 5th IAHR Cooling Tower Workshop, Monterey, California, U.S.A., September 29 - October 3, 1986.

[86SC1] Schrey H.G.: *Reduction of Make Up Water in Wet Cooled Power Stations by Adding Dry Cooling Systems,* Balcke-Dürr Ratingen, March 23, 1986.

[87AL1] Alt W. and Mäule R.: *Hybridkühltürme im Wirtschaftlichen Vergleich zu Naß- und Trockenkühltürmen*, VGB Kraftswerkstechnik, vol. 8, pp. 763-768, 1987.

[87AL2] Alt W.: *Design and Operation of Hybrid Cooling Towers*, VGB Kraftwerkstechnik, vol. 1, 1987.

[87GE1] Geldenhuys J.D.: *Ontwerpsfaktore by Natuurlike Konveksie Droë Koeltorings*, M.Eng. thesis, University of Stellenbosch, Stellenbosch, November, 1987.

[88BR1] British Standard 4485, Water Cooling Towers, Part 2: Methods for Performance Testing, 1988.

[88ME1] Menzel K.W.: *Cooling Towers the "Environmentalists", Development of Wet Cooling Towers*, Energy, vol. 40, no. 6, June, 1988.

[88NO1] Nowosad R.M.: A *Review of the Development and Application of Industrial Dry/Wet Cooling*, CSIR Report O/DPT 1, December 1988.

[88SZ1] Szabó Z and Szentgyörgyi I: *Main Design Features and Operation Results of the Heller-Type Wet/Dry Cooling System Serving the 1200MWe Trakya CCPP*, Paper Presented at the 6th Cooling Tower Workshop of the International Association for Hydraulic Research, Pisa, Italy, October 4 - October 7, 1988.

[89AN1] *Survey of Water Conserving Heat Rejection Systems*, EPRI Final Report, Research Project 1260-59, March 1989.

[89HO1] Holman J.P.: *Heat Transfer*, McGraw-Hill, New York, 1989.

[89JA1] Jaber H. and Webb R.L.: *Design of Cooling Towers by the Effectiveness-NTU Method*, Journal of Heat Transfer, vol. 111, pp. 837-843, November, 1989.

[89JO1] Johnson B.M.: *Cooling Tower Performance Prediction and Improvement*, Vol's 1 and 2, EPRI Report GS-6370, 1989.

[89KR1] Kröger D.G.: *Cooling Towers - Performance Evaluation and Design*, University of Stellenbosch, Stellenbosch, 1989.

[89MI1] Mitchell R.D.: *Survey of Water-Conserving Heat Rejection Systems*, EPRI GS-6252, Project 1260-59, Final Report, March, 1989.

[90HO1] Hofmann J.E. and Kröger D.G.: *Analysis of Heat Mass and Momentum Transfer in the Rain Zone of a Natural Draft Counterflow Cooling Tower*, 7th IAHR Cooling Tower and Spraying Pond Symposium, Leningrad, USSR, 1990.

[91MU1] Münch S. and Fichtner H.: *Der Hybridkühlturm für das 2×60-MW-Heizkraftwerk West der Stadwerke Frankfurt am Main,* VGB Kraftwerkstechnik 71, Heft 6, 1991.

[91SC1] Schwickert M.: *Hybridkühltürme für die Chemische Industrie*, Chemie-Technik, Heidelberg, vol. 20, no. 11, pp. 64-69, 1991.

[91VE1] Venter S.J. and Kröger D.G.: *An evaluation of the Methods to Predict the System Effect Present in Air-Cooled Heat Exchangers*, Heat Recovery Systems and CHP, vol. 11, no. 5, pp. 431-440, 1991.

[91SZ1] Szabó Z.: *Why use the 'Heller System'? Circuitry, Characteristics & Special Features*, EGI Contracting and Engineering, Hungary, March, 1991.

[92AL1] Alt W. and Damjakob H.: *Große Hybrid und Trockenkühltürme an den Beispielen GKN II und KW KENDAL*, Source unknown.

[92BL1] Blanck D. and Münch S.: *Design and Construction of Wet/Dry Cooling Towers-Examples form Industry and Power Plants*, International Association for Hydraulic Research, 8th Cooling Tower and Spraying Pond Symposium, Karlsruhe Germany, October 5-9, 1992.

[92BO1] Bouton F.: *Mechanical-Draught Wet Cooling Towers with Plume Abatement*, International Association of Hydraulic Research, 8th Cooling Tower and Spraying Pond Symposium, Karlsruhe, Germany, October 5-9, 1992.

[92HE1] Henley J.: *Maximise Tower Power*, Chemical Engineering, pp. 74-82, February, 1992.

[92MI1] Mirsky G., Bryant K. and Libert J.-P.: *Latest Worldwide Technology in Environmentally Designed Cooling Towers*, CTI Journal, vol. 13, no. 2, pp. 20-28, 1992.

[92WI1] Willa J.L.: *Evolution of the Water Cooling Tower*, CTI Journal, vol. 13, no. 1, pp. 40 & 45-49, 1992.

[93CO1] Conradie C.F.G.: *Die Verkoelingsvermoë van Nat Koeltorings en Droë/Nat Stelsels by Kragstasies*, M.Eng. thesis, University of Stellenbosch, Stellenbosch, June, 1993.

[93LI1] Lindahl P.A. and Jameson R.W.: *Plume Abatement and Water Conservation with the Wet/Dry Cooling Tower*, CTI Journal, vol. 14, no. 2, pp. 20-36, 1993.

[93TE1] Terblanche J.E.: *Inlaatverliese by Koeltorings*, M.Eng. thesis, University of Stellenbosch, Stellenbosch, June, 1993.

[94BI1] Billet W., Bräuning G., Ernst G., Tesche W. and Wirbser H.: *Model Experiments on the Mixing of Dry and Wet Air in the Planned Hybrid Cooling Tower of the Power Plant HKW2 of the Neckarwerke in Altbach-Deizisau*, International Association for Hydraulic Research, 9th Cooling Tower and Spraying Pond Symposium, von Karman Institute for Fluid Dynamics, Rhode-Saint-Genése, Belgium, September 20-23, 1994.

[94BO1] Bouton F. and Monjoie M.: *Testing Procedure for Wet/Dry Plume Abatement Cooling Towers*, International Association for Hydraulic Research, 9th Cooling

Tower and Spraying Pond Symposium, von Karman Institute for Fluid Dynamics, Rhode-Saint-Genése, Belgium, September 20-23, 1994.

[94IS1] Isles J.: *Hybrid Cooling Towers Keep Deeside Plume Free*, Modern Power Systems, vol. 14, no. 6, pp.53-57, June 1994.

[94KR1] Kröger D.G.: *Fan Performance in Air-Cooled Steam Condensers*, Heat Recovery Systems & CHP, vol. 14, no. 4, pp. 391-399, 1994.

[94TE1] Terblanche J.E. and Kröger D.G.: *Experimental Evaluation of the Aerodynamic Inlet Losses in Cooling Towers*, R & D Journal, vol. 10, no. 2, pp. 41-44, 1994.

[94TE2] Tesche W.: *Minimizing Power Consumption of Hybrid Cooling Towers by Process-Controlled Mode of Operation*, International Association for Hydraulic Research, 9th Cooling Tower and Spraying Pond Symposium, von Karman Institute for Fluid Dynamics, Rhode-Saint-Genése, Belgium, September 20-23, 1994.

[95BO1] Botes H.: *An Investigation Into the Practical Application of Adiabatic Pre-Cooling of the Inlet Air to an Air-Cooled Heat Exchanger*, M.Eng. thesis, University of Stellenbosch, Stellenbosch, January, 1995.

[95SA1] Salta C.A.: *The Effect of Plenum Configuration on the Performance of Air-Cooled Heat Exchangers*, M.Eng. thesis, University of Stellenbosch, Stellenbosch, January, 1995.

APPENDIX

A

PROPERTIES OF FLUIDS

NOTE:

All the temperatures in the equations must be given in Kelvin.

All the properties given, are from [89KR1].

A.1 The thermophysical properties of dry air from 220 K to 380 K at standard atmospheric pressure (101325 N/m²)

Density:

$$\rho_a = \frac{p_a}{287.08T} \quad [\mathrm{kg/m^3}] \tag{A.1.1}$$

Specific heat:

$$c_{pa} = 1.045356\times10^{3} - 3.161783\times10^{-1}T + 7.083814\times10^{-4}T^2 - 2.705209\times10^{-7}T^3 \quad [\mathrm{J/kgK}] \tag{A.1.2}$$

Dynamic viscosity:

$$\mu_a = 2.287973\times10^{-6} + 6.259793\times10^{-8}T - 3.131956\times10^{-11}T^2 + 8.15038\times10^{-15}T^3 \quad [\mathrm{kg/ms}] \tag{A.1.3}$$

Thermal conductivity:

$$k_a = -4.937787\times10^{-4} + 1.018087\times10^{-4}T - 4.627937\times10^{-8}T^2 + 1.250603\times10^{-11}T^3 \quad [\mathrm{W/mK}] \tag{A.1.4}$$

A.2 The thermophysical properties of saturated water vapour from 273.15 K to 380 K

Vapour pressure:

$$p_v = 10^z \quad [\mathrm{N/m^2}] \tag{A.2.1}$$

$$z = 10.79586(1-x) + 5.02808\log_{10}(x) + 1.50474\times10^{-4}\left[1-10^{-8.29692(1/x-1)}\right]$$
$$+4.2873\times10^{-4}\left[10^{4.76955(1-x)}-1\right] + 2.786118312$$

$$x = \frac{273.16}{T}$$

Specific heat:

$$c_{pv} = 1.3605\times10^{3} + 2.31334T - 2.46784\times10^{-10}T^{5} + 5.91332\times10^{-13}T^{6} \quad [\mathrm{J/kgK}] \tag{A.2.2}$$

Dynamic viscosity:

$$\mu_{v} = 2.562435\times10^{-6} + 1.816683\times10^{-8}T + 2.579066\times10^{-11}T^{2} - 1.067299\times10^{-14}T^{3} \quad [\mathrm{kg/ms}] \tag{A.2.3}$$

Thermal conductivity:

$$k_{v} = 1.3046\times10^{-2} - 3.756191\times10^{-5}T + 2.217964\times10^{-7}T^{2} - 1.111562\times10^{-10}T^{3} \quad [\mathrm{W/mK}] \tag{A.2.4}$$

Vapour density:

$$\rho_{v} = -4.062329056 + 0.10277044T - 9.76300388\times10^{-4}T^{2} + 4.475240795\times10^{-6}T^{3} - 1.004596894\times10^{-8}T^{4} + 8.9154895\times10^{-12}T^{5} \quad [\mathrm{kg/m^{3}}] \tag{A.2.5}$$

Saturation temperature:

$$T_{v} = 164.630366 + 1.832295\times10^{-3}p_{v} + 4.27215\times10^{-10}p_{v}^{2} + 3.738954\times10^{3}p_{v}^{-1} - 7.01204\times10^{5}p_{v}^{-2} + 16.161488\ln p_{v} - 1.437169\times10^{-4}p_{v}\ln p_{v} \quad [\mathrm{K}] \tag{A.2.6}$$

A.3 The thermophysical properties of mixtures of air and water vapour

Density:

$$\rho_{av} = (1+w)\left[1 - \frac{w}{w+0.62198}\right]\left[\frac{p_a}{287.08T}\right] \ [\mathrm{kg/m^3}] \qquad \text{(A.3.1)}$$

Specific heat per unit mass of air/vapour:

$$c_{pav} = \frac{c_{pa} + wc_{pv}}{1+w} \ [\mathrm{J/kgK}] \qquad \text{(A.3.2)}$$

Dynamic viscosity:

$$\mu_{av} = \frac{\left(X_a \mu_a M_a^{0.5} + X_v \mu_v M_v^{0.5}\right)}{\left(X_a M_a^{0.5} + X_v M_v^{0.5}\right)} \ [\mathrm{kg/ms}] \qquad \text{(A.3.3)}$$

where $M_a = 28.97$ g/mole, $M_v = 18.016$ g/mole, $X_a = 1/(1+1.608w)$ and $X_v = w/(w+0.622)$.

Thermal conductivity:

$$k_{av} = \frac{\left(X_a k_a M_a^{0.33} + X_v k_v M_v^{0.33}\right)}{\left(X_a M_a^{0.33} + X_v M_v^{0.33}\right)} \ [\mathrm{W/mK}] \qquad \text{(A.3.4)}$$

Humidity ratio:

$$\begin{aligned} w = &\left[\frac{1}{2501.6 + 1.8577(T-273.15) - 4.184(T_{wb} - 273.15)}\right] \\ &\times\left[\frac{\{2501.6 - 2.3263(T_{wb} - 273.15)\} \times 0.62509\, p_{vwb}}{p_{abs} - 1.005\, p_{vwb}}\right. \\ &\left. -1.00416(T - T_{wb})\right] \ [\mathrm{kg\ /\ kg\ dry\ air}] \end{aligned} \qquad \text{(A.3.5)}$$

Enthalpy per unit mass of dry air:

$$i_{ma} = c_{pa}(T - 273.15) + w\left[i_{fgw0} + c_{pv}(T - 273.15)\right] \ [\mathrm{J/kg\ dry\ air}] \qquad \text{(A.3.6)}$$

where c_{pa} and c_{pv} are evaluated at $(T - 273.15)/2$ °C and i_{fgw0} is evaluated at 0 °C.

Diffusivity of water vapour in air: **[89HO1]**

$$D = 435.7 \times 10^{-4} \frac{T_a^{1.5}}{p_a\left(V_a^{1/3} + V_v^{1/3}\right)^2} \sqrt{\frac{1}{M_a} + \frac{1}{M_v}} \quad [\mathrm{m^2 / s}] \tag{A.3.7}$$

where the molecular volumes and weights are: $V_a = 29.9$, $V_v = 18.8$, $M_a = 28.9$ g/mole and $M_v = 18$ g/mole. If you replace these constants in the above equation it becomes:

$$D = 0.0003939 \frac{T_a^{1.5}}{p_a} \quad [\mathrm{m^2 / s}] \tag{A.3.8}$$

A.4 The thermophysical properties of saturated water liquid from 273.15 K to 380 K

Density:

$$\begin{aligned}\rho_w = \big[&1.49343 \times 10^{-3} - 3.7164 \times 10^{-6} T + 7.09782 \times 10^{-9} T^2 \\ &-1.90321 \times 10^{-20} T^6\big]^{-1} \quad [\mathrm{kg / m^3}]\end{aligned} \tag{A.4.1}$$

Specific heat:

$$\begin{aligned}c_{pw} = {}&8.15599 \times 10^3 - 2.80627 \times 10 T + 5.11283 \times 10^{-2} T^2 \\ &- 2.17582 \times 10^{-13} T^6 \quad [\mathrm{J / kgK}]\end{aligned} \tag{A.4.2}$$

Dynamic viscosity:

$$\mu_w = 2.414 \times 10^{-5} \times 10^{[247.8/(T-140)]} \quad [\mathrm{kg / ms}] \tag{A.4.3}$$

Thermal conductivity:

$$\begin{aligned}k_w = {}&-6.14255 \times 10^{-1} + 6.9962 \times 10^{-3} T - 1.01075 \times 10^{-5} T^2 \\ &+ 4.74737 \times 10^{-12} T^4 \quad [\mathrm{W / mK}]\end{aligned} \tag{A.4.4}$$

Latent heat of vaporisation:

$$\begin{aligned}i_{fgw} = {}&3.4831814 \times 10^6 - 5.8627703 \times 10^3 T + 12.139568 T^2 \\ &- 1.40290431 \times 10^{-2} T^3 \quad [\mathrm{J / kg}]\end{aligned} \tag{A.4.5}$$

Critical pressure:

$$p_{wc} = 22.09 \times 10^{6} \quad [\mathrm{N/m^2}] \tag{A.4.6}$$

Surface tension:

$$\begin{aligned}\sigma_w = {} & 5.148103 \times 10^{-2} + 3.998714 \times 10^{-4}\, T - 1.4721869 \times 10^{-6}\, T^2 \\ & + 1.21405335 \times 10^{-9}\, T^3 \quad [\mathrm{N/m}]\end{aligned} \tag{A.4.7}$$

APPENDIX

B

THE CHEBYSHEV METHOD OF NUMERICAL INTEGRATION

Various numerical integration methods can be used to solve the differential equations that govern the heat and mass transfer process at an air-water interface. The different methods vary considerably when it comes to accuracy and computation time. For every problem the time and accuracy requirements are different, and the numerical method that best suits that problem, must be found. To solve the above mentioned differential equations, the Chebyshev numerical integration method is recommended by various scientists [82CA1] [88BR1] because of its computational speed and ease of use. The method is named after the Russian mathematician, Chebyshev (1821-1894).

The Chebyshev method is the special case of the Gaussian quadrature formula, where the weighting factors are all equal. The following is a representation of the Chebyshev formula [65FR1], where R_n is the error function.

$$\int_{-1}^{+1} f(x)dx = \frac{2}{n} \cdot \sum_{r=1}^{n} f(x_r) + R_n \tag{B.1}$$

This formula is valid for $n = 2$ to 7 and $n = 9$. For other values of n, complex values occur. The higher the value of n the more accurate the integration will be, but the longer the computation time will become.

For $n = 4$:

$$\int_{-1}^{+1} f(x)dx \approx \frac{1}{2}[f(x_1) + f(x_2) + f(x_3) + f(x_4)]$$

where the function values $f(x_r)$ are determined at x values of ± 0.1875924741 and ± 0.7946544723.

For the Chebyshev formula to be more applicable for computational use it is necessary to change the integration interval from [-1,1] to a more general interval [a,b]. To do this the following substitution can be made:

$$x = \alpha t + \beta$$

where $t = a$ when $x = -1$ and $t = b$ when $x = 1$, thus:

$$x = \frac{1}{(b-a)}\left[2t - (a+b)\right] \tag{B.2}$$

and

$$dx = \frac{2}{(b-a)}dt \tag{B.3}$$

Substitution of equations (B.2) and (B.3) into equation (B.1) gives:

$$\int_a^b f\left[\frac{1}{(b-a)}\left[2t-(a+b)\right]\right]\frac{2}{(b-a)}dt = \frac{2}{n}\cdot\sum_{r=1}^{n} f\left[\frac{1}{(b-a)}\left[2t_r-(a+b)\right]\right] + R_n$$

For $f\left[\frac{1}{(b-a)}\left[2t-(a+b)\right]\right] = F(t)$ and $n = 4$ the equation becomes:

$$\int_a^b F(t)dt \approx \frac{b-a}{4}\left[F(t_1)+F(t_2)+F(t_3)+F(t_4)\right] \tag{B.4}$$

The values for t_r where the function values $F(t_r)$ must be determined, are:

$$t_r = \frac{x_r(b-a)+(a+b)}{2}$$

If the integration interval $(b-a) = h$, t_r can be written as:

$$t_r = a + h/2(1+x_r)$$

and for the case where $n = 4$

$$t_1 = a + 0.10267276h$$

$$t_2 = a + 0.40620376h$$

$$t_3 = a + 0.59379624h$$

$$t_4 = a + 0.89732724h$$

To simplify the Chebyshev equation these factors are sometimes approximated as 0.1, 0.4, 0.6 and 0.9. For the Merkel equation these approximated values are accurate enough, since the Merkel equation is also an approximation of a more complex equation.

From equation (B.4) the Chebyshev formula for the Merkel equation is:

$$\frac{(h_d a) A_{fr} L}{m_w} = \int_{T_{wo}}^{T_{wi}} \frac{c_{pw} dT_w}{(i_{mas} - i_{ma})} = \frac{(T_{wi} - T_{wo})}{4}\left[\frac{c_{pw1}}{\Delta i_1} + \frac{c_{pw2}}{\Delta i_2} + \frac{c_{pw3}}{\Delta i_3} + \frac{c_{pw4}}{\Delta i_4}\right]$$

where Δi_1 is the value of $(i_{mas1} - i_{ma1})$, with i_{mas1} evaluated at $T_{w1} = T_{wo} + 0.1(T_{wi} - T_{wo})$ and:

$$i_{ma1} = \frac{m_w}{m_a} c_{pw} (T_{w1} - T_{wo}) + i_{mai} \qquad \text{(B.5)}$$

as derived from the energy balance at point 1.

In equation (B.5), c_{pw} must be calculated at $(T_{w1} - T_{wo})/2$ for the calculation of i_{ma1}.

The value of c_{pw1} is calculated at T_{w1} from equation (A.4.5).

Equally Δi_2, Δi_3 and Δi_4 as well as c_{pw2}, c_{pw3} and c_{pw4} are all calculated at those T_w values corresponding to positions 0.4, 0.6 and 0.9 of the water temperature interval respectively.

With only a small loss in accuracy, it is possible to replace the specific heat capacities of the water at the different states, with the mean heat capacity through the integration interval. The following equation is then obtained, and is most commonly used.

$$\frac{h_d a_{fi} A_{fr} L_{fi}}{m_w} = \int_{T_{wo}}^{T_{wi}} \frac{c_{pw} dT_w}{(i_{mas} - i_{ma})} = \frac{c_{pwm}(T_{wi} - T_{wo})}{4}\left[\frac{1}{\Delta i_1} + \frac{1}{\Delta i_2} + \frac{1}{\Delta i_3} + \frac{1}{\Delta i_4}\right] \qquad \text{(B.6)}$$

The points in the fill where the air states must be calculated for the Chebyshev equation are shown schematically in figure B.1. It can be seen that it is the four points in the fill where the water temperatures are as obtained from the factors 0.1, 0.4, 0.6 and 0.9 respectively. The positions of the points is therefore a function of water temperature and not of the geometry of the fill.

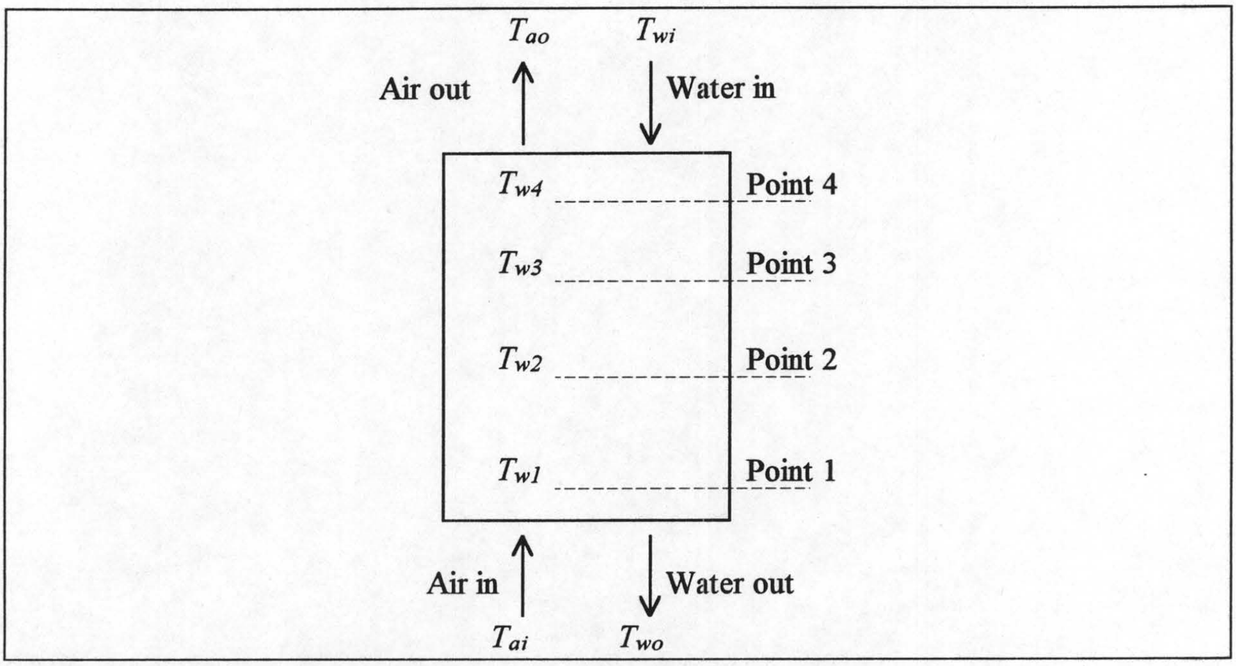

Figure B.1: *Points in fill where air states must be evaluated.*

APPENDIX

C

SPLASH PACK CHARACTERISTICS

The performance characteristics of an expanded metal fill has been determined experimentally. A numerical example is presented to illustrate the procedures followed in obtaining correlations for the fill's transfer and pressure loss coefficients. The transfer coefficient for each test is obtained from the Merkel theory, by employing both the Chebyshev numerical integration method [See Appendix B] and the ε-NTU method [89JA1]. A description of the experimental testing facility and the testing procedures are given.

C.1 Testing facility and experimental results

C.1.1 Cooling tower test facility

The splash pack tests were performed in a small cooling tower test facility shown schematically in figure C.1.

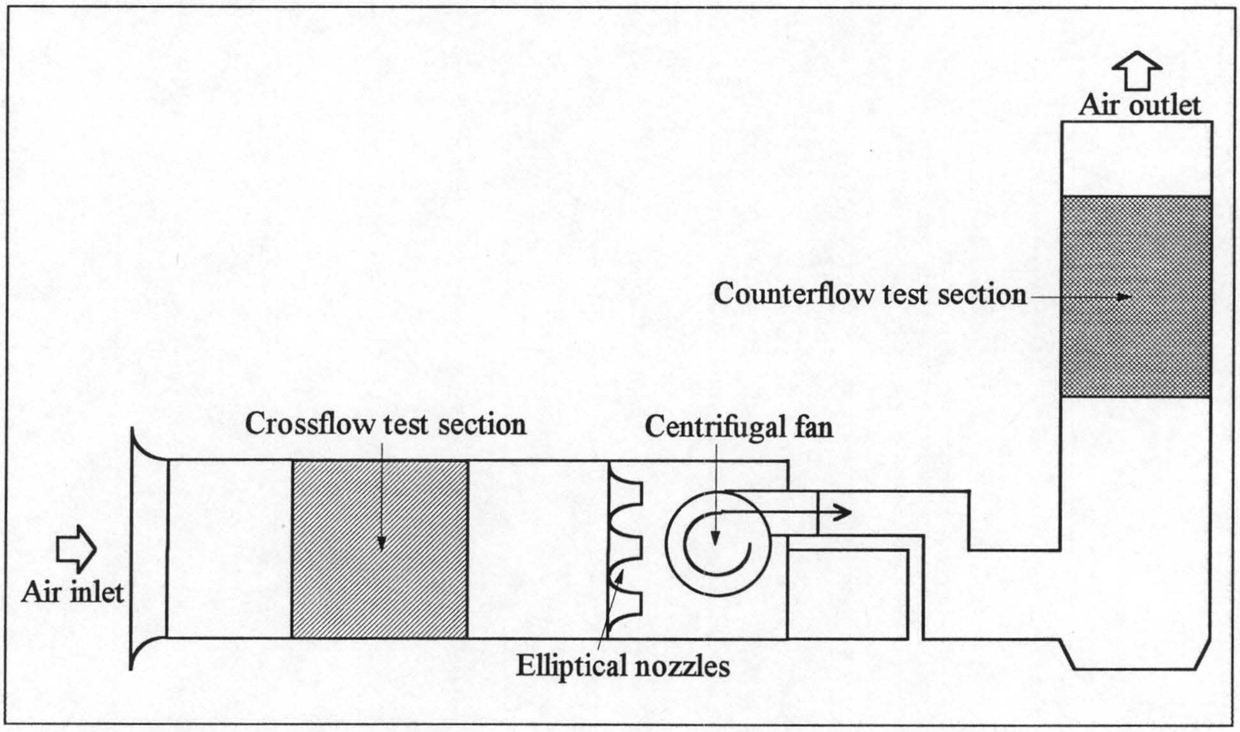

Figure C.1: *Fill testing facility.*

The tower test facility was designed to enable both the testing of counterflow and crossflow packings. The counterflow test section that was used in the test, described in this appendix, is shown schematically in figure C.2. This test section has a plan area of 1.5 m by 1.5 m and is 2.25 m high with a swing door to facilitate the loading of packing material. The tower is insulated with 25 mm closed cell polyurethane foam sheets, to minimise heat loss to the environment.

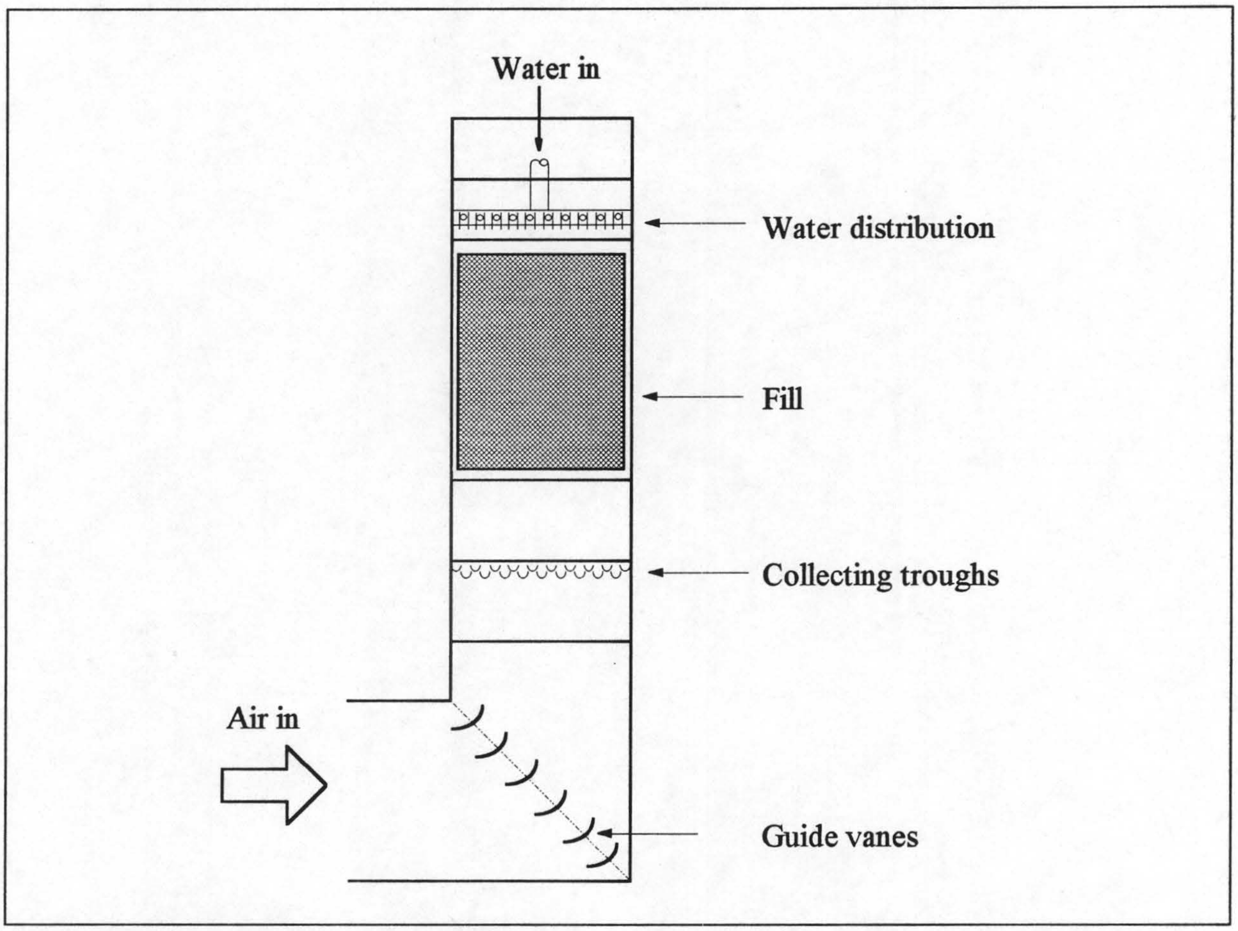

Figure C.2: *Counter flow test section.*

Hot water is supplied to the test section by a distributing spray frame as shown schematically in figure C.3. The spray frame consists of 20 drip plates, each 1.5 m long. These drip plates are supplied with water by water distribution pipes from where water jets are issuing out of small openings, as shown in figure C.3. The lower edge of each plate is cut into a 45° sawtooth pattern. This configuration ensures an even distribution of water, since the water drips from the points of the sawtooth pattern. The inlet water mass flow rate is calculated from the pressure drop across an orifice plate, designed according to the BS 1042 standard.

The water is collected by a staggered trough system made of PVC to minimise heat transfer in the troughs. The water flow is drained selectively from the trough system, which is divided into two water collecting areas. Dividing plates in the troughs separate the collecting areas in such a way that water collected in the central area is drained away separately. This set-up eliminates the effect of water accumulation and cooling on the walls of the test section by isolating a part of the water flow that has not been in contact with the walls. The water from this test area is collected in a basin and the outlet water flow rate is measured by a V-notch arrangement, before flowing into a 200 litre sump and being pumped back to the underground water reservoir. The water from outside the test area is drained directly into the sump, before being pumped away. The water pipes of the manifold collecting the water from the troughs have a 360° bend. This ensures that part of the pipes will always be filled with water, thereby preventing air from being drawn into the tunnel from the outside, as well as ensuring that the thermocouples, measuring water outlet temperature, are always covered with water.

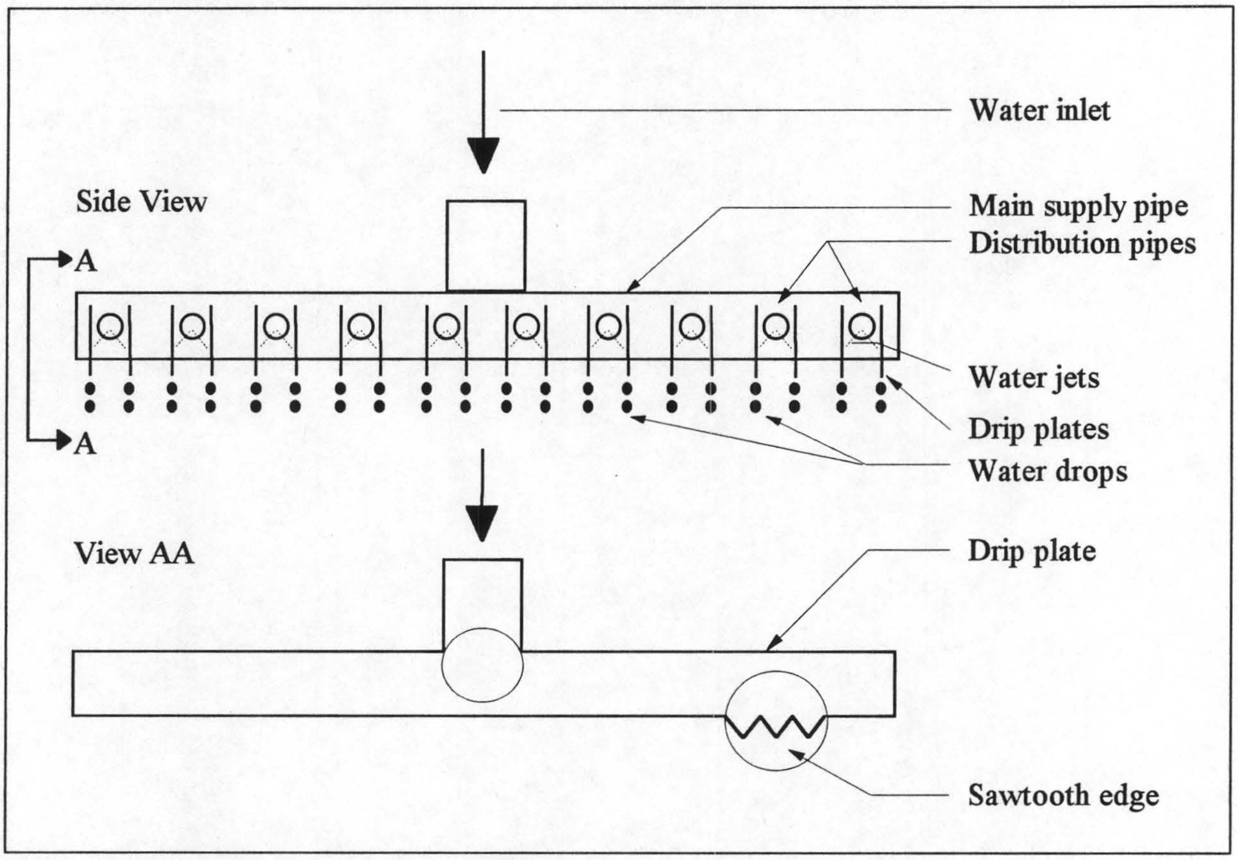

Figure C.3: *Water distribution spray frame.*

Hot water for testing is supplied from a 40 m^3 underground reservoir. This water is heated to the required inlet temperature by means of a 150 kW diesel burning boiler. Water is drawn by pump from just below the reservoir surface and returned through a narrow slot at the bottom of the reservoir. This ensures that the water in the reservoir stays stratified, thereby preventing excessive fluctuation in water temperature.

A centrifugal fan with a variable speed motor is used to supply the air flow through the test section at speeds up to 4.5 m/s. The air volume flow rate to the test section is calculated from the pressure drop measured across a set of ASHRAE 51-75 elliptical flow nozzles. The dry and wet bulb temperatures are also measured at this point to determine the humidity of the air and the dry air mass flow rate.

All temperature readings are made with calibrated copper-constantan thermocouples. The thermocouples are calibrated by determining the thermocouple readings at the melting point of ice and the water boiling point, at atmospheric pressure. Each temperature reading is hence corrected according to its calibration curve.

The water temperatures are recorded by calibrated thermocouples, placed in the inlet water pipe and the outlet water manifold (three measuring positions), respectively.

The inlet air temperatures to the test section are measured below the water collection system, and the outlet air temperatures above the drift eliminators. Both inlet and outlet air conditions are measured by a set of four ventilated psychrometric probes. In order to obtain a good representative thermocouple reading, the probes are evenly spaced over the cross-section of the tower. The probes located at the air outlet side are protected with radiation shields to avoid direct sunlight influencing temperature measurement. All the thermocouples are directly coupled to a Schlumberger data logging system.

The ambient pressure is recorded before every test with a mercury column barometer. The pressure drop across the fill zone is measured with a Betz micro-manometer. Due to the high water flow rate and the slight over-pressure, conventional wall pressure tappings cannot be used to measure the local static pressure in the test section. This necessitated the use of special pressure measuring probes to be able to facilitate measuring the local static pressure. These probes consist of two flat perspex plates, connected by a 20 mm PVC tube. The static pressure point is located on the top part in the middle of the tube. The probes were found to be insensitive to slight inclinations relative to the air flow direction. Any water entering the tube runs out the other side without blocking the pressure point. The pressure readings (for determining the air and water mass flow rates) are obtained from differential pressure transducers connected to the data logging system. These pressure transducers were individually calibrated.

All thermocouples and pressure transducers are directly connected to a multiplexing data logger, which is capable of reading all channels once per second. The data logger has an internal electronic ice point which eliminates the need for an ice bath for temperature measurement purposes. It is programmed to convert all temperature readings from millivolts to degrees Celsius before transferring them to a personal computer. The pressure transducers prdoce a current signal, which is converted to a voltage signal. The data logger is programmed to convert this voltage signal to a pressure reading in Pascal, by means of the transducer's calibration curve. The personal computer receives all temperature and pressure drop readings in the units of degrees Celsius and Pascal, respectively, from the data logger. This data is then used for further mass flow and energy balance calculations.

A Turbo Pascal program is used to read the data from the data loggers and process it immediately. The program can also display time traces of the temperatures, energy balance, mass flow rates and transfer characteristics. The real-time processing of the test data makes it possible to see when the steady-state has been reached. Once steady-state conditions are reached the data can be stored on magnetic disk for further processing.

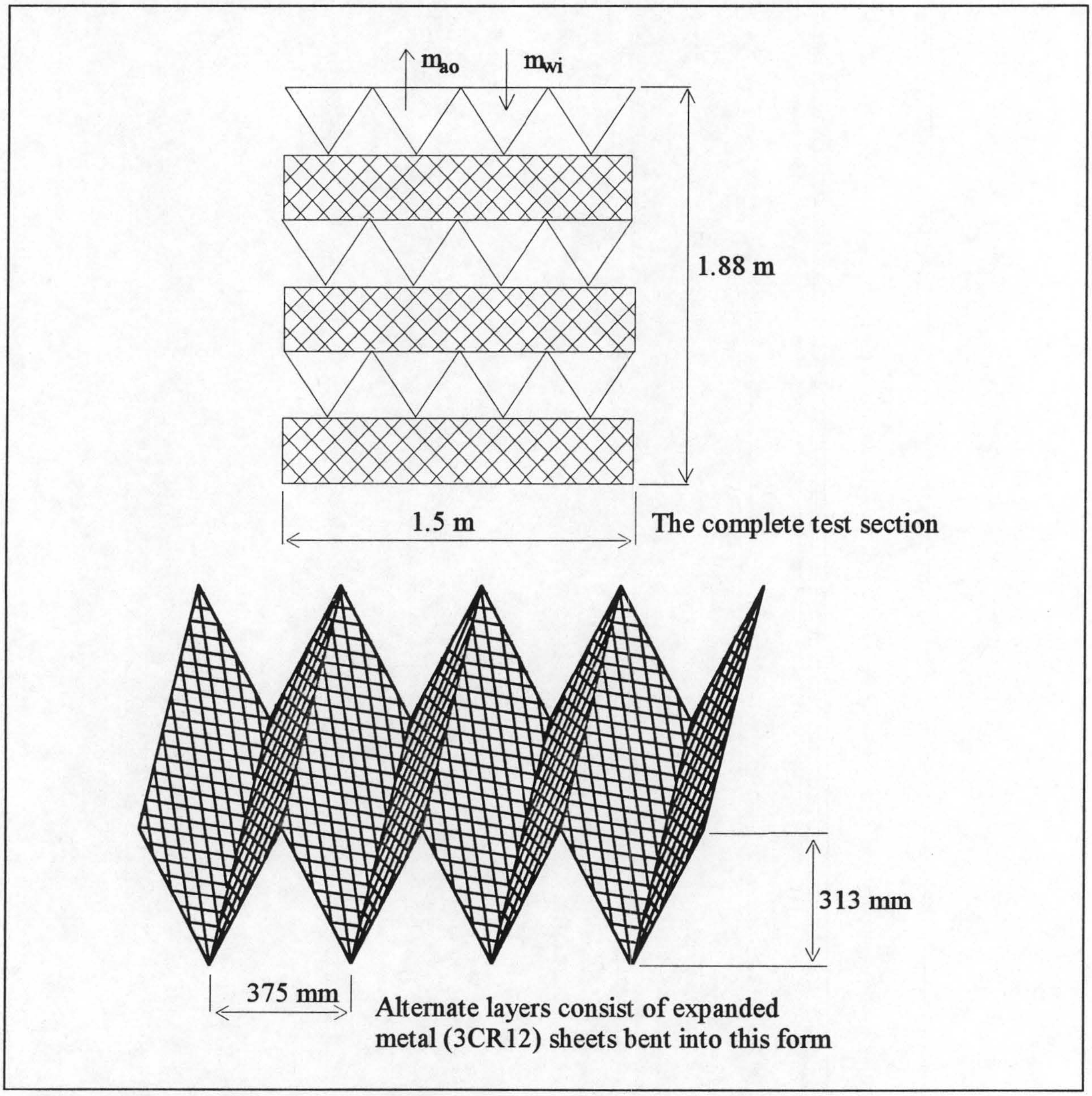

Figure C.4: *Schematic representation of the fill that was tested.*

A schematic drawing of the fill that was tested can be seen in figure C.4. The main dimensions of the fill that was tested are as follows:

Height of the fill = 1.88 m
Width of the fill = 1.5 m
Depth of the fill = 1.5 m
Frontal area of the fill = 2.25 m^2

C.1.2 Test results

The data and results obtained from the fill tests and fill performance calculations, are given in table C.1 with the fill transfer coefficients calculated with the Merkel theory by both the *ε-NTU* and the *Chebyshev* numerical integration methods.

Table C.1: *Data obtained from fill test.*

Atmospheric Pressure = 101712.27 Pa

Test no.	T_{ai} °C	T_{aiwb} °C	T_{wi} °C	T_{wo} °C	m_a kg/s	m_w kg/s	Δp_{fi} Pa	$\frac{(h_d a)_{fi} L_{fi}}{G_w}$ ε-NTU	$\frac{(h_d a)_{fi} L_{fi}}{G_w}$ CHEBY	$\frac{K^*_{fiavm}}{L_{fi}}$ 1/m
1	9.57	8.23	40.33	29.71	2.912	3.999	3.0	0.5865	0.5922	2.722
2	9.70	8.23	39.67	27.77	4.134	3.999	4.5	0.6771	0.6847	1.835
3	9.79	8.13	39.29	25.82	5.691	4.040	8.0	0.8032	0.8139	1.619
4	10.24	8.34	38.87	24.41	6.982	4.023	10.5	0.9118	0.9251	1.384
5	10.75	8.62	38.41	22.93	8.494	4.014	13.5	1.0496	1.0659	1.186
6	11.02	8.92	38.27	24.03	8.426	5.955	20.0	1.0026	1.0187	1.769
7	10.97	8.94	37.59	25.15	6.893	5.954	15.5	0.8740	0.8856	2.072
8	10.98	9.03	37.22	26.12	5.590	5.963	12.5	0.7886	0.7974	2.575
9	11.39	9.67	36.60	27.53	4.142	5.932	8.5	0.6668	0.6721	3.276
10	11.95	10.24	35.94	29.05	2.761	5.936	6.0	0.5439	0.5466	5.427
11	12.41	10.70	35.27	29.74	2.706	7.899	10.0	0.4871	0.4890	9.038
12	12.37	10.48	35.00	27.76	4.047	7.880	13.0	0.6348	0.6386	5.132
13	12.03	10.12	34.62	26.23	5.333	7.888	16.5	0.7372	0.7427	3.703
14	12.38	10.24	34.32	24.83	6.810	7.859	21.0	0.8588	0.8669	2.858
15	12.93	10.45	34.03	23.36	8.452	7.861	28.0	1.0267	1.0388	2.454
16	13.26	10.60	33.63	23.91	8.388	9.548	34.0	0.9897	0.9999	3.015
17	13.35	10.65	32.70	24.56	6.849	9.544	26.5	0.8684	0.8752	3.550
18	13.23	10.64	32.15	25.46	5.269	9.513	21.0	0.7418	0.7459	4.799
19	13.57	11.10	31.75	26.39	4.033	9.490	16.5	0.6276	0.6301	6.496
20	14.00	11.35	31.32	27.60	2.641	9.499	13.0	0.4645	0.4658	12.097

From a curve fit through the fill transfer coefficients that were obtained with the Merkel theory and the *Chebyshev* numerical integration method, the following two correlations were obtained:

$$\frac{(h_d a)_{fi} L_{fi}}{G_w} = 0.5061 G_w^{-0.094} G_a^{0.6023} \tag{C.1.1}$$

or

$$\frac{(h_d a)_{fi} L_{fi}}{G_w} = 0.8267 \left[\frac{G_w}{G_a}\right]^{-0.395} \tag{C.1.2}$$

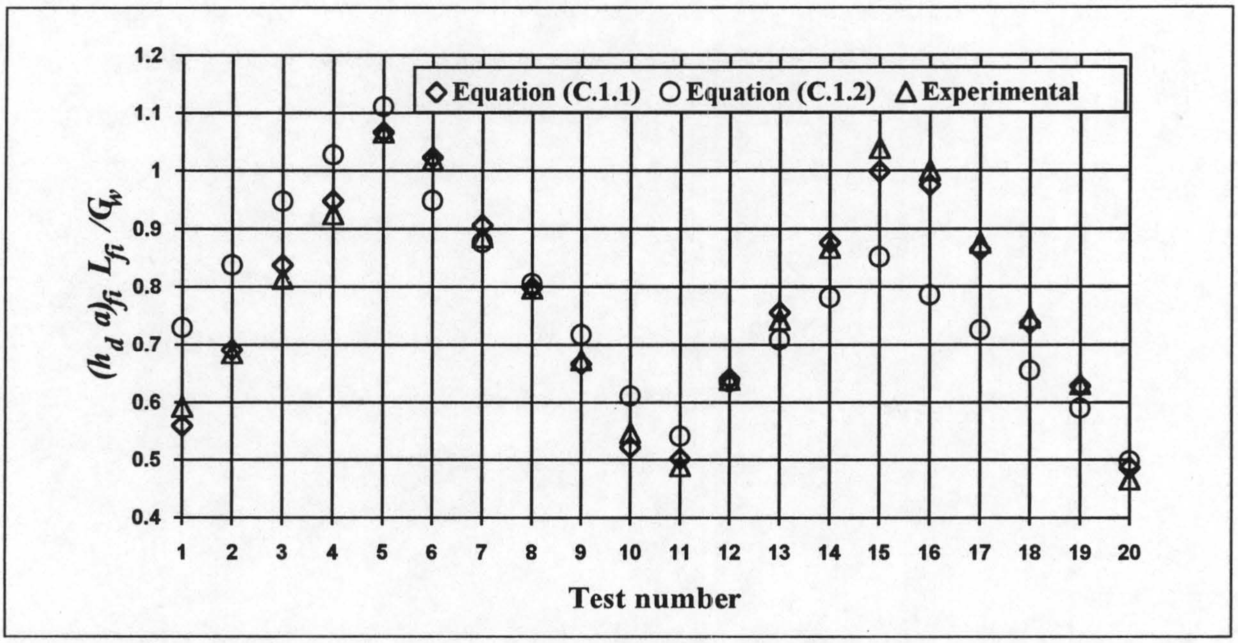

Figure C.5: *Comparison between the values obtained from equations (C.1.1) and (C.1.2) and the experimental values.*

The above correlations can also be given per unit depth of fill. They then become:

$$\frac{(h_d a)_{fi}}{G_w} = 0.2692 G_w^{-0.094} G_a^{0.6023} \tag{C.1.3}$$

or

$$\frac{(h_d a)_{fi}}{G_w} = 0.4397 \left[\frac{G_w}{G_a}\right]^{-0.395} \tag{C.1.4}$$

The first correlation [equation (C.1.1)] is the more accurate one, as can be seen in figure C.5, and is generally preferred to the second one [equation (C.1.2)]. The absolute mean deviation for the first correlation is 2 %, while the absolute mean deviation for the second correlation is 10.6 %

For the fill transfer data obtained with the Merkel theory and the ε-*NTU* method, the following correlations were obtained for the fill's transfer coefficient:

$$\frac{(h_d a)_{fi} L_{fi}}{G_w} = 0.5004 G_w^{-0.0864} G_a^{0.5951} \tag{C.1.5}$$

or

$$\frac{(h_d a)_{fi} L_{fi}}{G_w} = 0.8177 \left[\frac{G_w}{G_a} \right]^{-0.3878} \tag{C.1.6}$$

The above correlation's can also be given per unit depth of fill. They then become:

$$\frac{(h_d a)_{fi}}{G_w} = 0.2661 G_w^{-0.0864} G_a^{0.5951} \tag{C.1.7}$$

or

$$\frac{(h_d a)_{fi}}{G_w} = 0.4349 \left[\frac{G_w}{G_a} \right]^{-0.3878} \tag{C.1.8}$$

The following correlation was obtained for the approximated static pressure drop coefficient, where momentum effects are excluded:

$$K^*_{fiavm} / L_{fi} = 1.9277 G_w^{1.2752} G_a^{-1.0356} \tag{C.1.9}$$

This correlation is also given per unit depth of fill height and is based on the mean air properties through the fill. The agreement between the experimentally obtained pressure loss coefficients, and those determined by equation (C.1.9) are shown in figure C.6. It can be seen from figure C.6 that a fair agreement between the experimental values, and the values obtained with the pressure drop correlation was found. The absolute mean deviation for this correlation is 6.6 %.

Although the above correlations are given per unit depth of fill height, it should be noted that these are only really applicable for a 1.88 m high fill. Accurate predictions of fill characteristics can only be made if the data for the specific fill was obtained under conditions similar to the operating conditions of the real tower. The fact that the tests were conducted in a small cooling tower test facility, could also effect the accuracy of the obtained transfer characteristics, since wall effects tend to be more significant than in a large cooling tower.

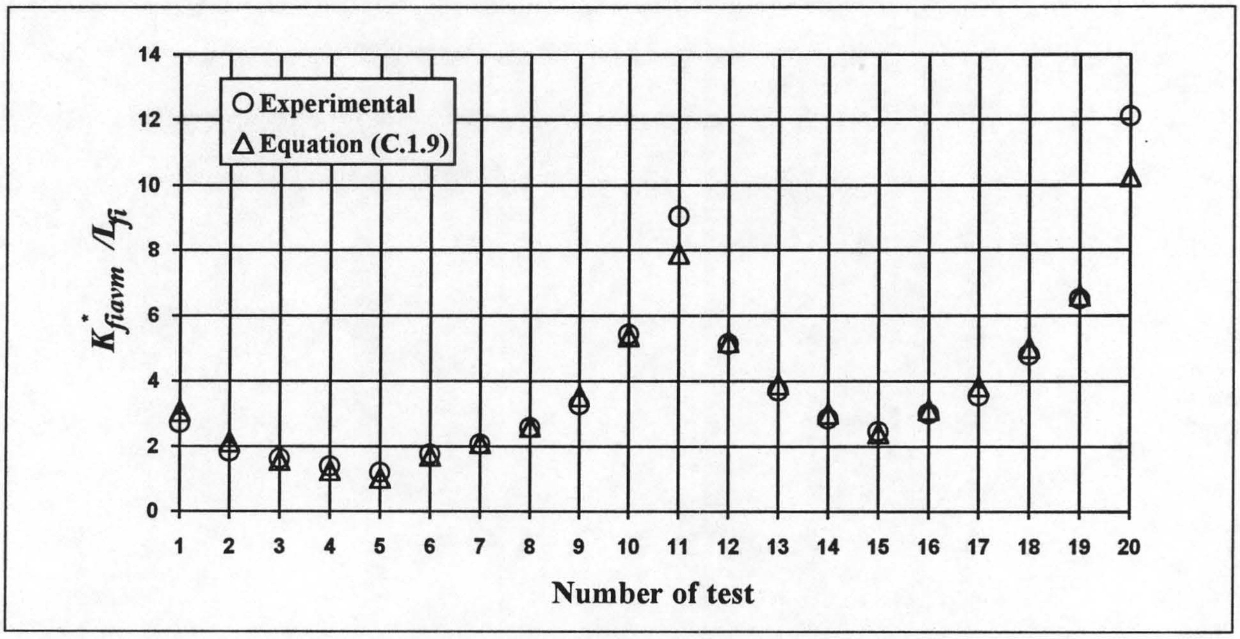

Figure C.6: *Comparison between the experimental and the correlated values for the pressure loss coefficient.*

In the determination of the correlations, G_w is taken as the inlet water mass flow rate per unit area, and G_a as the dry air mass flow rate per unit area. For the same dry air mass flow rate and water mass flow rate, the determined values for the fill transfer coefficient and the pressure drop can vary, depending on the air inlet conditions. This implies that a certain margin of error will occur if the dry air mass flow rate is used in the correlations, depending on the humidity of the inlet air. This is investigated in section C.2.3, to show what the effect of different inlet air humidities would be on the pressure drop coefficient.

C.2 Sample calculations

C.2.1 Transfer coefficient calculated from the Merkel theory with Chebyshev's numerical integration method

A sample calculation is done to show how the values of $\frac{(h_d a)_{fi} L_{fi}}{G_w}$ in table C.1 are determined with the Merkel theory by using the numerical integration method of Chebyshev.

For test number 2 in table C.1 the following measurements were made:

Atmospheric pressure	p_{atm}	= 101712.27 Pa
Inlet air dry bulb temperature:	T_{ai}	= 9.7 °C
Inlet air wet bulb temperature:	T_{aiwb}	= 8.23 °C
Water inlet temperature:	T_{wi}	= 39.67 °C
Water outlet temperature:	T_{wo}	= 27.77 °C
Dry air mass flow rate:	m_a	= 4.134 kg/s
Inlet water mass flow rate:	m_w	= 3.999 kg/s
Pressure drop across the fill:	Δp_{fi}	= 4.5 Pa

The ambient atmospheric pressure p_{atm} = 101712.27 Pa, is used in the calculations. Even though the pressure in the fill is a little lower than atmospheric pressure, the fluid properties are not very pressure sensitive and atmospheric pressure can therefore be used with high accuracy, to determine the fluid properties in the sample calculations.

From the Chebyshev numerical integration method described in Appendix B, the Merkel equation can be approximated by equation (B.6) as follows:

$$\frac{(h_d a)_{fi} L_{fi}}{G_w} = \int_{T_{wo}}^{T_{wi}} \frac{c_{pw} dT_w}{(i_{mas} - i_{ma})} \approx \frac{c_{pwm}(T_{wi} - T_{wo})}{4}\left[\frac{1}{\Delta i_1} + \frac{1}{\Delta i_2} + \frac{1}{\Delta i_3} + \frac{1}{\Delta i_4}\right]$$

where the numerical subscripts refer to the positions in the fill where the temperatures are equal to those determined from the Chebyshev interval values. These positions are shown in figure C.7 for a section of a counterflow fill.

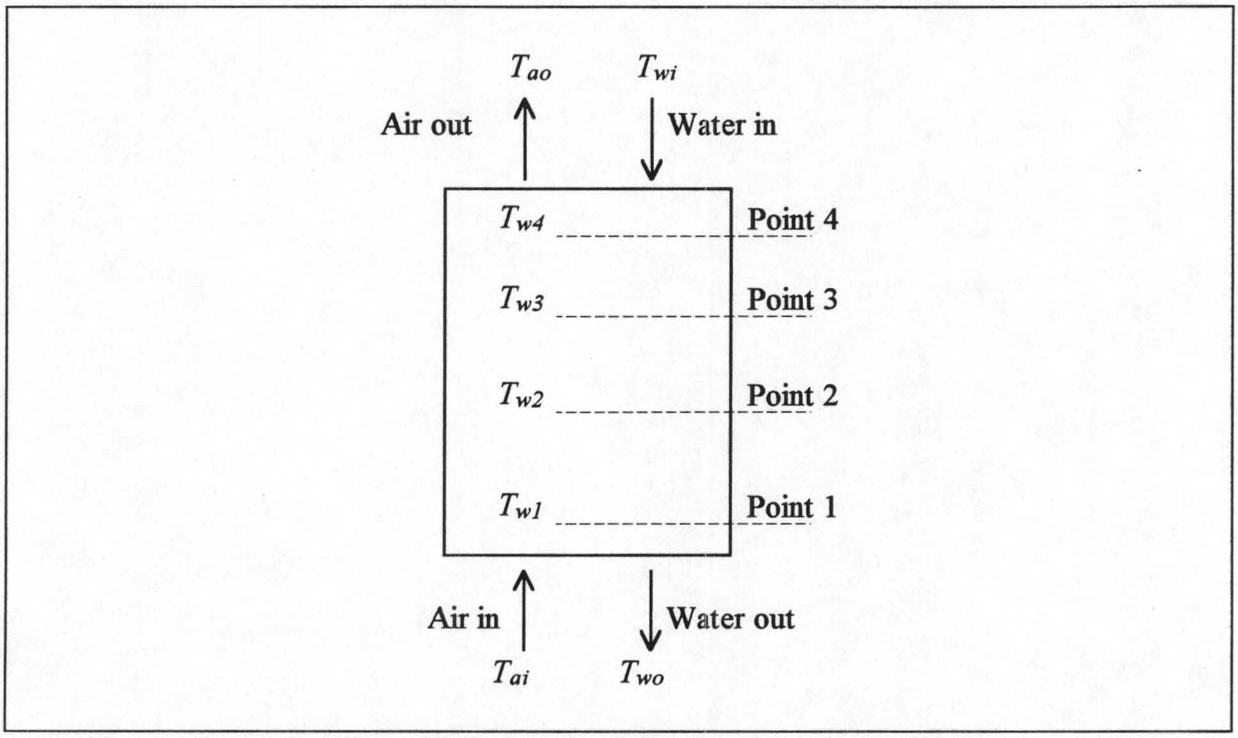

Figure C.7: *Schematic representation of a section from a counterflow fill.*

For the approximated Chebyshev values (0.1, 0.4, 0.6, 0.9), the temperatures at which the enthalpies have to be evaluated are the following:

$$T_{w1} = T_{wo} + 0.1(T_{wi} - T_{wo}) = 27.77 + 0.1(39.67 - 27.77) = 28.96\ ^\circ\mathrm{C}$$

$$T_{w2} = T_{wo} + 0.4(T_{wi} - T_{wo}) = 32.53\ ^\circ\mathrm{C}$$

$$T_{w3} = T_{wo} + 0.6(T_{wi} - T_{wo}) = 34.91\ ^\circ\mathrm{C}$$

$$T_{w4} = T_{wo} + 0.9(T_{wi} - T_{wo}) = 38.48\ ^\circ\mathrm{C}$$

To calculate the enthalpy of the saturated air at point 1, the point where the water temperature $T_{w1} = 28.96\ ^\circ\mathrm{C}$, the following properties must first be determined:

- The latent heat of evaporation at 0 °C from equation (A.4.5):

$$\begin{aligned} i_{fgw0} &= 3.4831814 \times 10^{6} - 5.8627703 \times 10^{3} \times 273.15 \\ &\quad + 12.139568 \times 273.15^{2} - 1.40290431 \times 10^{-2} \times 273.15^{3} \\ &= 2501598.53345\ \mathrm{J/kg} \end{aligned}$$

- Specific heat for dry air at 28.96/2 °C from equation (A.1.2):

$$c_{pawlm} = 1.045356\times10^{3} - 3.161783\times10^{-1}\left(\frac{T_{w1}}{2}+273.15\right)$$
$$+7.083814\times10^{-4}\left(\frac{T_{w1}}{2}+273.15\right)^{2} - 2.705209\times10^{-7}\left(\frac{T_{w1}}{2}+273.15\right)^{3}$$
$$= 1006.5815 \text{ J / kgK}$$

- Specific heat for water vapour at 28.96/2 °C from equation (A.2.2):

$$c_{pvwlm} = 1.3605\times10^{3} + 2.31334\left(\frac{T_{w1}}{2}+273.15\right) - 2.46784\times10^{-10}\left(\frac{T_{w1}}{2}+273.15\right)^{5}$$
$$+5.91332\times10^{-13}\left(\frac{T_{w1}}{2}+273.15\right)^{6}$$
$$= 1874.8913 \text{ J / kgK}$$

- Saturated vapour pressure at 28.96 °C from equation (A.2.1):

$$x = \frac{273.16}{T_{w1}+273.15} = 0.904174$$

$$z = 10.79586(1-x) + 5.02808\log_{10}(x) + 1.50474\times10^{-4}\left[1-10^{-8.29692(1/x-1)}\right]$$
$$+4.2873\times10^{-4}\left[10^{4.76955(1-x)}-1\right] + 2.786118312$$
$$= 3.6016$$

$$p_{vsw1} = 10^{z} = 3995.8041 \text{ N / m}^2$$

- Humidity ratio for saturated air at 28.96 °C from equation (A.3.5):

$$w_{sw1} = \left[\frac{2501.6 - 2.3263T_{w1}}{2501.6 + 1.8577T_{w1} - 4.184T_{w1}}\right]\left[\left(\frac{0.62509\,p_{vsw1}}{p_{abs} - 1.005\,p_{vsw1}}\right)\right] = 0.0255663 \text{ kg / kg dry air}$$

The enthalpy of saturated air per kg dry air at point 1, can now be determined from equation (A.3.6):

$$i_{masw1} = c_{pawlm}T_{w1} + w_{sw1}\left[i_{fgw0} + c_{pvwlm}T_{w1}\right]$$
$$= 1006.5815\times28.96 + 0.0255663(2501598.5335 + 1874.8913\times28.96)$$
$$= 94495.37386 \text{ J / kg dry air}$$

The enthalpy of the inlet air per kg of dry air, can also be determined from the equations in Appendix A. The following properties must first be determined:

- Specific heat of dry air at $T_{ai}/2 = 9.7/2$ °C from equation (A.1.2):

$$c_{paim} = 1.045356\times10^{3} - 3.161783\times10^{-1}\left(\frac{T_{ai}}{2}+273.15\right)$$
$$+7.083814\times10^{-4}\left(\frac{T_{ai}}{2}+273.15\right)^{2} - 2.705209\times10^{-7}\left(\frac{T_{ai}}{2}+273.15\right)^{3}$$
$$= 1006.39285 \text{ J / kgK}$$

- Specific heat of water vapour at $T_{ai}/2 = 9.7/2$ °C from equation (A.2.2):

$$c_{pvim} = 1.3605\times10^{3} + 2.31334\left(\frac{T_{ai}}{2}+273.15\right) - 2.46784\times10^{-10}\left(\frac{T_{ai}}{2}+273.15\right)^{5}$$
$$+5.91332\times10^{-13}\left(\frac{T_{ai}}{2}+273.15\right)^{6}$$
$$= 1866.79847 \text{ J / kgK}$$

- Saturated vapour pressure at $T_{aiwb} = 8.23$ °C from equation (A.2.1):

$$x = \frac{273.16}{T_{aiwb}+273.15} = 0.97079$$

$$z = 10.79586(1-x) + 5.02808\log_{10}(x) + 1.50474\times10^{-4}\left[1-10^{-8.29692(1/x-1)}\right]$$
$$+4.2873\times10^{-4}\left[10^{4.76955(1-x)}-1\right] + 2.786118312$$
$$= 3.036985$$

$$p_{vsi} = 10^{z} = 1088.89333 \text{ N / m}^{2}$$

- Humidity ratio of the inlet air from equation (A.3.5):

$$w_i = \left[\frac{2501.6 - 2.3263T_{wb}}{2501.6 + 1.8577T_{ai} - 4.184T_{wb}}\right]\left[\left(\frac{0.62509\,p_{vsi}}{p_{abs} - 1.005\,p_{vsi}}\right)\right]$$
$$-\left[\frac{1.00416(T_{ai} - T_{wb})}{2501.6 + 1.8577T_{ai} - 4.184T_{wb}}\right]$$
$$= 0.00616336 \text{ kg / kg dry air}$$

The enthalpy of the inlet air per kg dry air, can now be determined from equation (A.3.6):

$$i_{mai} = c_{paim}T_{ai} + w_i\left[i_{fgw0} + c_{pvim}T_{ai}\right] = 25291.87496 \text{ J / kg}$$

The water's constant pressure specific heat is calculated from equation (A.4.2) at the mean water temperature $T_{wm} = \dfrac{T_{wi} + T_{wo}}{2} = \dfrac{39.67 + 27.77}{2} = 33.72\ °\text{C}$, it is:

$$\begin{aligned} c_{pwm} &= 8.15599 \times 10^3 - 2.80627 \times 10\left(T_{wm} + 273.15\right) + 5.11283 \times 10^{-2}\left(T_{wm} + 273.15\right)^2 \\ &\quad - 2.17582 \times 10^{-13}\left(T_{wm} + 273.15\right)^6 \\ &= 4177.40244 \text{ J / kgK} \end{aligned}$$

The enthalpy of the air at point 1 in the fill, can be determined from the following equation (as given in Appendix B):

$$\begin{aligned} i_{ma1} &= \frac{m_w}{m_a} c_{pwm}\left(T_{w1} - T_{wo}\right) + i_{mai} \\ &= \frac{3.999}{4.134} \times 4177.40244(28.96 - 27.77) + 25291.875 = 30100.6472 \text{ J / kg} \end{aligned}$$

where the water's specific heat is evaluated at the mean water temperature through the fill, although it would be more accurate if it was evaluated at the mean water temperature through the specific interval, $T_{wm} = (T_{w1}+T_{wo})/2$. This kind of accuracy is however not required.

From the above determined enthalpies it follows that the required enthalpy difference is:

$$\Delta i_1 = \left(i_{masw1} - i_{ma1}\right) = 94495.37386 - 30100.6472 = 64394.727 \text{ J / kg}$$

In the same way the other required enthalpy differences were calculated and are:

$$\Delta i_2 = 113825.4307 - 44526.964 = 69298.4667 \text{ J / kg}$$

$$\Delta i_3 = 128582.7344 - 54144.5085 = 74438.2259 \text{ J / kg}$$

$$\Delta i_4 = 154048.0124 - 68570.8253 = 85477.1871 \text{ J / kg}$$

It is now possible to evaluate the Merkel equation with the Chebyshev method, this gives:

$$\frac{(h_d a)_{fi} L_{fi}}{G_w} = \frac{c_{pwm}(T_{wi} - T_{wo})}{4}\left[\frac{1}{\Delta i_1} + \frac{1}{\Delta i_2} + \frac{1}{\Delta i_3} + \frac{1}{\Delta i_4}\right]$$

$$= \frac{4177.4024(39.67 - 27.77)}{4}\left[\frac{1}{64394.727} + \frac{1}{69298.4667} + \frac{1}{74438.2259} + \frac{1}{85477.1817}\right]$$

$$= 0.68468$$

If the accurate Chebyshev values are used, the value for $\frac{(h_d a)_{fi} L_{fi}}{G_w}$ is found to be equal to 0.68485. This gives a difference of 0.0254 % between the values obtained with the accurate and the approximated Chebyshev values. From this it can be seen that the approximated values are adequate for application in cooling tower problems.

Per unit depth of fill the value for the transfer coefficient becomes:

$$\frac{(h_d a)_{fi}}{G_w} = \frac{0.68468}{1.88} = 0.3642 \text{ m}^{-1}$$

C.2.2 Transfer coefficient calculated with the effectiveness-NTU method based on the Merkel theory

The *effectiveness-NTU* method, as used for calculating the transfer coefficient of the fill in this sample calculation, was developed by Jaber and Webb [89JA1] for application in wet cooling towers.

The calculations are based on the test data obtained for test 2 in table C.1.

An iterative procedure is used to calculate the fill's transfer coefficient. A value for the fill's transfer coefficient is estimated and iterated until the correct water outlet temperature is found. In the sample calculation, only the last iteration is shown.

Take $\frac{(h_d a)_{fi} L_{fi}}{G_w} = 0.67709$

The mean water temperature is $T_{wm} = (T_{wi}+T_{wo})/2 = (39.67+27.77)/2 = 33.72$ °C.

The enthalpy of the inlet air as determined in section C.2 is:

$$i_{mai} = c_{pai}T_{ai} + w_i\left[i_{fgw0} + c_{pvi}T_{ai}\right] = 25291.87496 \text{ J / kg}.$$

To calculate the enthalpy of the saturated air at the water outlet temperature, $T_{wo} = 27.77\ ^\circ\text{C}$, the following properties first have to be determined:

- The latent heat of evaporation at 0 °C from equation (A.4.5):

$$\begin{aligned} i_{fgw0} &= 3.4831814\times10^6 - 5.8627703\times10^3\times273.15 \\ &\quad + 12.139568\times273.15^2 - 1.40290431\times10^{-2}\times273.15^3 \\ &= 2501598.5334 \text{ J / kg} \end{aligned}$$

- Specific heat of dry air at 27.77/2 °C from equation (A.1.2):

$$\begin{aligned} c_{pawom} &= 1.045356\times10^3 - 3.161783\times10^{-1}\left(\frac{T_{wo}}{2}+273.15\right) \\ &\quad + 7.083814\times10^{-4}\left(\frac{T_{wo}}{2}+273.15\right)^2 - 2.705209\times10^{-7}\left(\frac{T_{wo}}{2}+273.15\right)^3 \\ &= 1006.5672 \text{ J / kgK} \end{aligned}$$

- Specific heat of water vapour at 27.77/2 °C from equation (A.2.2):

$$\begin{aligned} c_{pvwom} &= 1.3605\times10^3 + 2.31334\left(\frac{T_{wo}}{2}+273.15\right) - 2.46784\times10^{-10}\left(\frac{T_{wo}}{2}+273.15\right)^5 \\ &\quad + 5.91332\times10^{-13}\left(\frac{T_{wo}}{2}+273.15\right)^6 \\ &= 1874.3847 \text{ J / kgK} \end{aligned}$$

- Saturated vapour pressure at 27.77 °C from equation (A.2.1):

$$x = \frac{273.16}{T_{wo} + 273.15} = 0.90775$$

$$\begin{aligned} z &= 10.79586(1-x) + 5.02808\log_{10}(x) + 1.50474\times10^{-4}\left[1 - 10^{-8.29692(1/x-1)}\right] \\ &\quad + 4.2873\times10^{-4}\left[10^{4.76955(1-x)} - 1\right] + 2.786118312 \\ &= 3.5716 \end{aligned}$$

$$p_{vswo} = 10^z = 3728.8246 \text{ Pa}$$

- Humidity ratio for saturated air at 27.77 °C from equation (A.3.5):

$$w_{swo} = \frac{0.62509\, p_{vso}}{p_{abs} - 1.005 p_{vso}} = \frac{0.62509 \times 3728.8246}{101712.27 - 1.005 \times 3728.8246} = 0.0237927 \text{ kg / kg dry air}$$

The enthalpy of saturated air per kg dry air at T_{wo}, can now be determined from equation (A.3.6)

$$\begin{aligned} i_{maswo} &= c_{pawom} T_{wo} + w_{swo}\left[i_{fgw0} + c_{pvwom} T_{wo}\right] \\ &= 1006.5672 \times 27.77 + 0.0237927(2501598.5334 + 1874.3847 \times 27.77) \\ &= 88710.7054 \text{ J / kg} \end{aligned}$$

In the same way the enthalpy of saturated air at the inlet water temperature T_{wi}, and at the mean water temperature T_{wm} can be calculated to get:

$$\begin{aligned} i_{maswi} &= c_{pawim} T_{wi} + w_{swi}\left[i_{fgw0} + c_{pvwim} T_{wi}\right] \\ &= 1006.7245 \times 39.67 + 0.04798(2501598.5334 + 1879.5264 \times 39.67) \\ &= 163546.9337 \text{ J / kg} \end{aligned}$$

and

$$\begin{aligned} i_{maswm} &= c_{pawmm} T_{wm} + w_{swm}\left[i_{fgw0} + c_{pvwmm} T_{wm}\right] \\ &= 1006.6417 \times 33.72 + 0.033942(2501598.5334 + 1876.933 \times 33.72) \\ &= 121000.7923 \text{ J / kg} \end{aligned}$$

In the *effectiveness-NTU* method the saturated air enthalpy-temperature curve is taken as a straight line over the control volume. An analytical method was developed by Berman [61BE1] to improve this approximation. He proposed a correction factor δ given by:

$$\begin{aligned} \delta &= \left(i_{maswo} + i_{maswi} - 2 i_{maswm}\right) / 4 \\ &= (88710.7054 + 163546.9337 - 2 \times 121000.7923) / 4 = 2564.0136 \text{ J / kg} \end{aligned}$$

The gradient of the saturated air enthalpy-temperature curve between the water inlet and outlet temperatures is:

$$\frac{di_{mas}}{dT_w} = \frac{i_{maswi} - i_{maswo}}{T_{wi} - T_{wo}} = \frac{163546.9337 - 88710.7054}{39.67 - 27.77} = 6288.7587 \text{ J / kgK}$$

The equivalent capacity rate of the air (cold fluid) is:

$$C_{\max} = m_a = 4.134 \text{ kg/s}$$

The specific heat of water at T_{wm} can be determined from equation (A.4.2), and is:

$$\begin{aligned} c_{pwm} &= 8.15599 \times 10^3 - 2.80627 \times 10(T_{wm} + 273.15) + 5.11283 \times 10^{-2}(T_{wm} + 273.15)^2 \\ &\quad - 2.17582 \times 10^{-13}(T_{wm} + 273.15)^6 \\ &= 4177.4024 \text{ J/kgK} \end{aligned}$$

The equivalent water capacity rate (hot fluid) is:

$$C_{\min} = \frac{m_w c_{pwm}}{(di_{mas}/dT_w)} = \frac{3.999 \times 4177.4024}{6288.7587} = 2.6564 \text{ kg/s}$$

The evaporative capacity rate ratio is:

$$C_{re} = \frac{C_{\min}}{C_{\max}} = \frac{2.6564}{4.134} = 0.6426$$

The maximum possible amount of heat that can be exchanged is:

$$\begin{aligned} Q_{\max} &= C_{\min}(i_{maswi} - \delta - i_{mai}) \\ &= 2.6564(163546.9337 - 2564.0136 - 25291.875) = 360449.1272 \text{ W} \end{aligned}$$

The *NTU* equation for a counterflow wet cooling system is:

$$NTU = \frac{(h_d a)_{fi} V_{fi}}{C_{\min}} = \frac{(h_d a)_{fi} L_{fi}}{G_w} \times \frac{m_w}{C_{\min}} = \frac{0.67709 \times 3.999}{2.6564} = 1.0193$$

From the *effectiveness-NTU* equation for a counterflow heat exchanger it follows that:

$$e_e = \frac{1 - \exp[-NTU(1 - C_{re})]}{1 - C_{re}\exp[-NTU(1 - C_{re})]} = \frac{1 - \exp[-1.0193(1 - 0.6426)]}{1 - 0.6426\exp[-1.0193(1 - 0.6426)]} = 0.55152$$

The heat exchanger effectiveness is defined as:

$$e_e = \frac{Q}{Q_{\max}}$$

therefore:

$$Q = e_e Q_{\max} = 0.55152 \times 360449.1272 = 198794.66 \text{ W}$$

From this the water inlet temperature can be found, and is:

$$T_{wi} = \frac{Q}{m_w c_{pwm}} + T_{wo} = \frac{198794.66}{3.999 \times 4177.4024} + 27.77 = 39.67 \text{ °C}$$

The determined inlet water temperature is correct, and the estimated value for the fill transfer coefficient is therefore also correct. The transfer coefficient is:

$$\frac{(h_d a)_{fi} L_{fi}}{G_w} = 0.67709$$

or

$$\frac{(h_d a)_{fi}}{G_w} = 0.36015 \text{ m}^{-1}$$

C.2.3 Calculation of the approximate static pressure loss coefficient where momentum effects are ignored

When determining the pressure loss coefficient from an experimentally determined pressure drop, it is possible to base the pressure loss coefficient on different reference air velocity heads. In the relevant literature it was found that the pressure loss coefficient is based on the mean air/vapour, the dry inlet air, and the mean dry air velocity pressure heads. It is important that the same air velocity pressure head that was used to determine the pressure loss coefficient, must be used to determine the pressure loss from the pressure loss coefficient, otherwise large errors can occur. For practical considerations, in this study the pressure loss coefficients used to obtain the correlation given in equation (C.1.9) will be based on the mean air/vapour velocity pressure head.

Mean air/vapour velocity pressure head

To determine the mean air/vapour velocity pressure head, the mean air density and the mean air velocity through the fill must first be determined.

The calculations are based on the test data obtained for test 2 in table C.1.

- *The properties of the inlet air are first determined.*

The humidity ratio of the inlet air is determined as shown in section C.2.1 and is:

$$w_i = 0.00616336 \text{ kg / kg dry air}$$

The density of the inlet air can be determined from equation (A.3.1) and is:

$$\begin{aligned}\rho_{avi} &= (1+w_i)\left[1-\frac{w_i}{w_i+0.62198}\right]\left[\frac{p_{ai}}{287.08T_{ai}}\right]\\ &= (1+0.00616336)\left[1-\frac{0.00616336}{0.00616336+0.62198}\right]\left[\frac{101712.27}{287.08(9.7+273.15)}\right]\\ &= 1.248 \text{ kg / m}^3\end{aligned}$$

The inlet air mass flow rate can be determined as follows:

$$m_{avi} = m_a + w_i m_a = 4.134 + 0.00616336 \times 4.134 = 4.1595 \text{ kg / s}$$

The enthalpy of the inlet air as determined section C.2.1 is:

$$i_{mai} = 25291.875 \text{ J / kg dry air}$$

- *The properties of the outlet air can now be determined.*

According to the conservation of energy:

$$m_a(i_{avo} - i_{avi}) = m_w c_{pwm}(T_{wi} - T_{wo})$$

The enthalpy of the outlet air can be determined as follows:

$$\begin{aligned}i_{mao} &= \frac{m_w}{m_a} c_{pwm}(T_{wi} - T_{wo}) + i_{mai}\\ &= \frac{3.999}{4.134} \times 4177.4024(39.67-27.77) + 25291.875 = 73379.5976 \text{ J / kg dry air}\end{aligned}$$

where the specific heat of water at T_{wm} as determined in section C.2.1 is $c_{pwm} = 4177.4024$ J / kgK.

The temperature of the outlet air can now be solved iteratively if the outlet air is assumed to be saturated i.e. $i_{mao} = i_{maso}$.

An outlet air temperature is estimated, and the saturated air enthalpy for this estimated temperature is calculated with equation (A.3.6). The temperature is then iterated until the determined air enthalpy agrees with the correct value for the outlet air enthalpy as determined from the energy balance.

The determined air outlet temperature T_{ao} = 24.278 °C.

To determine the saturated air enthalpy at 24.278 °C, the following properties should first be determined:

- Specific heat for dry air at 24.278/2 °C from equation (A.1.2):

$$\begin{aligned} c_{paom} &= 1.045356\times10^{3} - 3.161783\times10^{-1}\left(\frac{T_{ao}}{2}+273.15\right) \\ &\quad +7.083814\times10^{-4}\left(\frac{T_{ao}}{2}+273.15\right)^{2} - 2.705209\times10^{-7}\left(\frac{T_{ao}}{2}+273.15\right)^{3} \\ &= 1006.5274 \text{ J / kgK} \end{aligned}$$

- Specific heat for water vapour at 24.278/2 °C from equation (A.2.2):

$$\begin{aligned} c_{pvom} &= 1.3605\times10^{3} + 2.31334\left(\frac{T_{ao}}{2}+273.15\right) - 2.46784\times10^{-10}\left(\frac{T_{ao}}{2}+273.15\right)^{5} \\ &\quad +5.91332\times10^{-13}\left(\frac{T_{ao}}{2}+273.15\right)^{6} \\ &= 1872.9051 \text{ J / kgK} \end{aligned}$$

- Saturated vapour pressure at 24.278 °C from equation (A.2.1):

$$x = \frac{273.16}{T_{ao}+273.15} = 0.9184$$

$$\begin{aligned} z &= 10.79586(1-x) + 5.02808\log_{10}(x) + 1.50474\times10^{-4}\left[1-10^{-8.29692(1/x-1)}\right] \\ &\quad +4.2873\times10^{-4}\left[10^{4.76955(1-x)}-1\right] + 2.786118312 \\ &= 3.4819 \end{aligned}$$

$$p_{vso} = 10^{z} = 3032.9647 \text{ Pa}$$

- Humidity ratio for saturated air at 24.278 °C from equation (A.3.5):

$$w_{so} = \frac{0.62509 p_{vso}}{p_{abs} - 1.005 p_{vso}} = \frac{0.62509 \times 3032.9647}{101712.27 - 1.005 \times 3032.9647} = 0.019215 \text{ kg / kg dry air}$$

The enthalpy of saturated air per kg dry air at T_{ao}, can now be determined from equation (A.3.6), as follows:

$$\begin{aligned} i_{maso} &= c_{pao} T_{ao} + w_{so}\left[i_{fgw0} + c_{pvo} T_{ao} \right] \\ &= 1006.5274 \times 24.278 + 0.019215(2501598.5334 + 1872.9051 \times 24.278) \\ &= 73379.597 \text{ J / kg} \end{aligned}$$

This value is equal to the correct value as determined earlier on, and the estimated outlet temperature is therefore also correct.

The density of the outlet air as determined from equation (A.3.1) is:

$$\begin{aligned} \rho_{avo} &= (1 + w_{so})\left[1 - \frac{w_{so}}{w_{so} + 0.62198}\right]\left[\frac{p_{ao}}{287.08 T_{ao}}\right] \\ &= (1 + 0.019215)\left[1 - \frac{0.019215}{0.019215 + 0.62198}\right]\left[\frac{101712.27}{287.08(24.278 + 273.15)}\right] \\ &= 1.1777 \text{ kg / m}^3 \end{aligned}$$

The outlet air mass flow rate can be determined as follows:

$$m_{avo} = m_a + w_{so} m_a = 4.134 + 0.019215 \times 4.134 = 4.2134 \text{ kg / s}$$

◆ *The mean air properties can now be determined*

The mean air mass flow rate is:

$$m_{avm} = \frac{m_{avi} + m_{avo}}{2} = \frac{4.1595 + 4.2134}{2} = 4.1865 \text{ kg / s}$$

The harmonic mean air density is:

$$\rho_{avm} = 2\left(\frac{1}{\rho_{avi}} + \frac{1}{\rho_{avo}}\right)^{-1} = 2\left(\frac{1}{1.248} + \frac{1}{1.1777}\right)^{-1} = 1.2118 \text{ kg / m}^3$$

The mean air velocity is:

$$v_{avm} = \frac{m_{avm}}{\rho_{avm} A_{fi}} = \frac{4.1865}{1.2118 \times 2.25} = 1.5354 \text{ m/s}$$

The mean air velocity pressure head can now be determined as follows:

$$\tfrac{1}{2}\rho_{avm} v_{avm}^2 = 0.5 \times 1.2118 \times 1.5354^2 = 1.428 \text{ Pa}$$

If the momentum equation is considered for the air control volume over the fill, an approximated static pressure loss, without momentum effects, can be determined from the measured static pressure loss as follows:

$$\Delta p_{fi}^* = \Delta p_{fi} - \left(\rho_{avo} v_{avo}^2 - \rho_{avi} v_{avi}^2\right) + g L_{fi}\left(\rho_{avi} - \rho_{avm}\right)$$

where $\left(\rho_{avo} v_{avo}^2 - \rho_{avi} v_{avi}^2\right)$ is the momentum increase of the air over the control volume, and $g L_{fi}\left(\rho_{avi} - \rho_{avm}\right)$ is the term that compensates for the measuring error that occurs because of the buoyancy effects in the measuring pipes.

The velocities of the air at the inlet and at the outlet of the fill are:

$$v_{avi} = \frac{m_{avi}}{\rho_{avi} A_{fr}} = \frac{4.1595}{1.248 \times 2.25} = 1.481 \text{ m/s}$$

and

$$v_{avo} = \frac{m_{avo}}{\rho_{avo} A_{fr}} = \frac{4.2134}{1.1777 \times 2.25} = 1.59 \text{ m/s}$$

The approximated static pressure loss, without momentum and gravity effects, is therefore:

$$\Delta p_{fi}^* = 4.5 - \left(1.1777 \times 1.59^2 - 1.248 \times 1.481^2\right) + 9.81 \times 1.88(1.248 - 1.2118) = 4.9274 \text{ Pa}$$

From the above, the pressure loss coefficient, for the static pressure drop without momentum and gravity effects, based on the mean air conditions is:

$$K_{fiavm}^* / L_{fi} = \frac{\Delta p_{fi}^*}{\tfrac{1}{2}\rho_{avm} v_{avm}^2 L_{fi}} = \frac{4.9274}{1.428 \times 1.88} = 1.8348 \text{ m}^{-1}$$

For test 2 in table C.1, the value for the above static pressure loss coefficient was also determined for the extreme cases of completely dry and completely saturated air entering the tower. The maximum error that can occur if the dry air mass flow rate is used in the correlation, would be the difference between these two extreme cases.

A comparison of the static pressure loss coefficients obtained in the absence of momentum effects, for the three different air inlet conditions is shown in table C.2. From table C.2 it can be seen that there is a 0.3 % difference between the two extreme cases.

Table C.2: *Approximated static pressure loss coefficients based on the mean mixed air velocity head for various air inlet conditions.*

Case	Inlet air condition	K^*_{fiavm} / L_{fi} [m^{-1}]
1	Completely dry air (T_{wb} = 273.325 K)	1.8294
2	Real air conditions for test 2	1.8348
3	Completely saturated air	1.8350

Dry inlet air velocity head

To determine the approximated static pressure loss coefficient, based on the dry inlet air velocity head, the following air properties must first be obtained:

The density of dry air at the inlet air temperature is:

$$\rho_{ai} = \frac{p_{ai}}{R_a\left(T_{ai}+273.15\right)} = \frac{101712.27}{287.08\times\left(9.7+273.15\right)} = 1.2526 \text{ kg/m}^3$$

The dry inlet air velocity is then:

$$v_{ai} = \frac{m_a}{\rho_{ai}A_{fr}} = \frac{4.134}{1.2526\times 2.25} = 1.46681 \text{ m/s}$$

The dry air velocity pressure head can now be determined as follows

$$\tfrac{1}{2}\rho_{ai}v_{ai}^2 = 0.5\times 1.2526\times 1.46681^2 = 1.3475 \text{ Pa}$$

From the above, the isothermal static pressure loss coefficient based on the dry inlet air conditions can be determined as follows:

$$K^*_{fiai} / L_{fi} = \frac{\Delta p^*_{fi}}{\frac{1}{2}\rho_a v_a^2 L_{fi}} = \frac{4.9274}{1.3475\times 1.88} = 1.9451 \text{ m}^{-1}$$

Velocity head for dry air at the mean air temperature

This is the method used by Johnson [89JO1] to determine the pressure loss coefficients for the different fill test results as given in the 1989 EPRI report.

If the properties of the dry air, at the mean air temperature were used, the value for the approximated static pressure loss coefficient is:

$$K^*_{fiam} / L_{fi} = 1.8955 \text{ m}^{-1}$$

Comparison

A comparison between the pressure loss coefficients obtained for the three different reference air velocity heads are given in table C.3.

Table C.3: *Approximated static pressure loss coefficients based on the three different air velocity heads.*

Case	Reference air velocity head	K^*_{fi} / L_{fi} [m^{-1}]
1	Mean air/vapour conditions	1.8348
2	Dry inlet air conditions	1.9451
3	Dry mean air conditions	1.8955

From table C.3 it can be seen that large differences in the pressure loss coefficient occur for the different air velocity heads. Large errors can therefore occur if the reference velocity head is not used consistently in all the calculations.

APPENDIX

D

EFFECTIVE FILL FRONTAL AREA

In many cooling towers, breakaway of the air at the inlet of the tower causes turbulence and results in the formation of circulating eddies near the tower shell, as shown in figure D.1. This effect is more prominent in wet cooling towers, where the pressure loss coefficient of the fill is lower than for the heat exchangers in a dry tower. As a result of this circulation, a certain area of the fill does not receive a continuous stream of cold air from the atmosphere, and this causes a decrease in the performance of the tower. In the wet cooling tower performance prediction models, this can be taken into consideration by using a reduced fill frontal area in the cooling tower calculations.

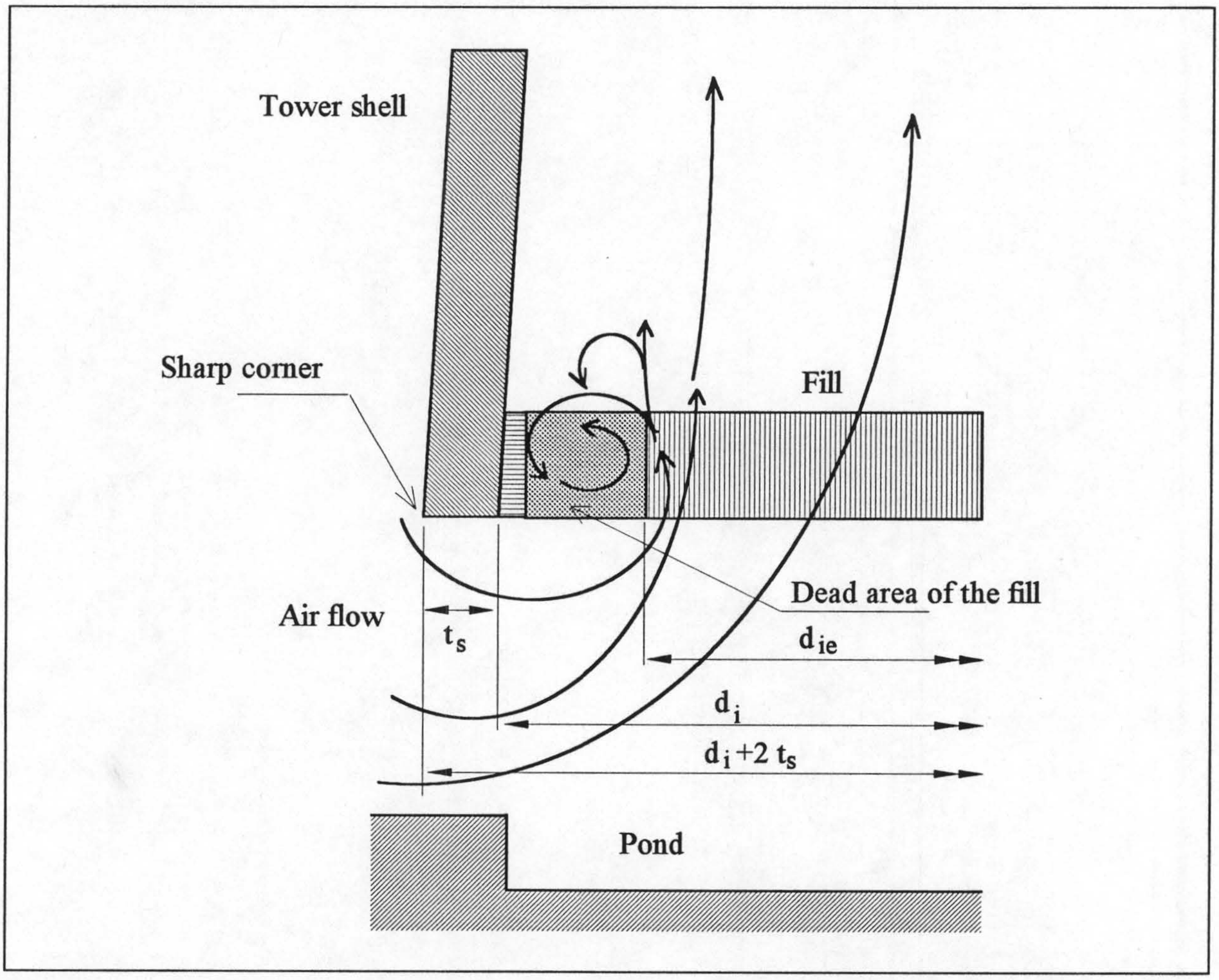

Figure D.1: *Section near the wall of a cooling tower illustrating the circulation that occurs.*

The size of this ineffective area is dependent on the inlet width or inlet diameter to inlet height ratio of the cooling tower (W/H or d/H) as well as the loss coefficient of the fill or heat exchanger and other obstacles in their immediate vicinity referred to as K_{he}. The geometry of the heat exchanger or fill also plays a role in the size of the ineffective area, although this effect was ignored in this experiment. To determine the approximate size of this ineffective area, a series of experiments were conducted. The experimental apparatus, testing procedure, and experimental results are discussed in section D.1, and some sample calculations are given in section D.2.

D.1 Test facility, procedures and experimental results

D.1.1 Model tower section test facility

The test facility that was used is shown in figure D.2 for a cylindrical tower configuration and in figure D.3 for a rectangular tower configuration. This test facility was originally used by Geldenhuys [87GE1] to determine the inlet pressure losses for counterflow cylindrical cooling towers. It was later also used by Terblanche [93TE1] to determine the air inlet losses for counterflow and crossflow cylindrical towers, as well as for counterflow rectangular towers. The tests conducted by them were done for different inlet diameter and inlet width to height ratios, as well as for different heat exchanger pressure loss coefficients.

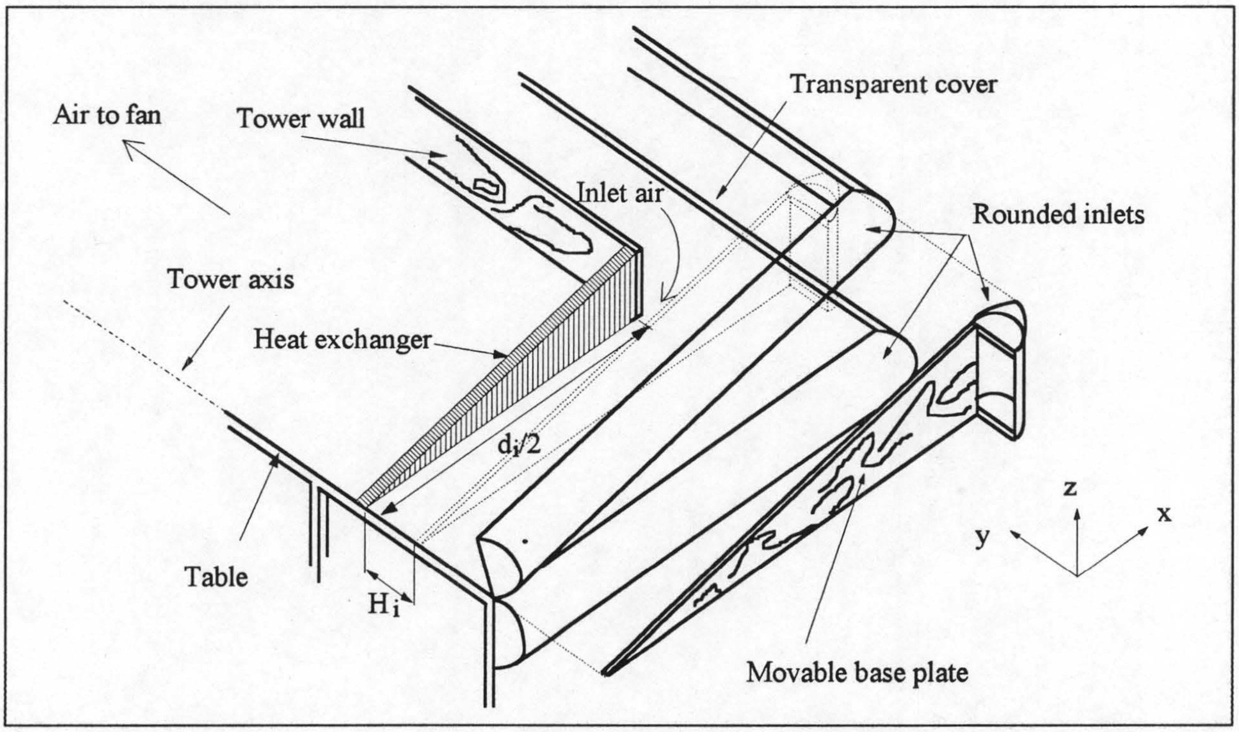

Figure D.2: *The test facility representing a section of a model cylindrical cooling tower.*

A wind tunnel that is connected to the tower section is used to draw air through it by means of a variable speed fan. The mass flow rate of the air through the wind tunnel can be measured by different sized nozzles, situated in a special chamber inside the wind tunnel.

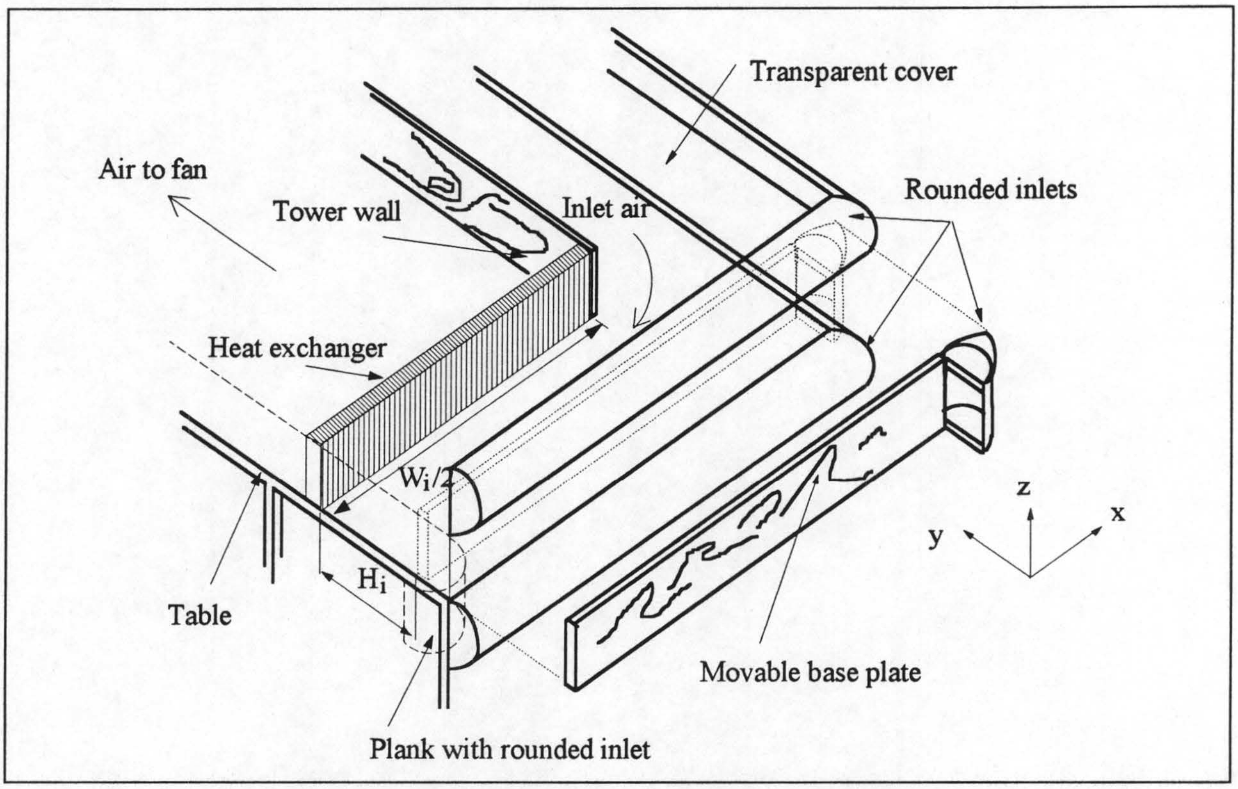

Figure D.3: *The test facility representing a section of a model rectangular cooling tower.*

The test facility set-up as shown in figure D.2, represents a sector of a model cylindrical cooling tower were the cooling tower sector is placed on its side. A section of a model rectangular cooling tower is shown in figure D.3. This tower section represents a rectangular cooling tower where the air is drawn in from two opposing sides, while the other two sides are not open to air flow. Both the experimental set-ups shown in figures D.2 and D.3 consist of a horizontal table with a transparent perspex cover on top of it. The ground is represented by a movable plank that enables one to vary the inlet diameter or width to height ratio of the tower. The tower wall is represented by a plank inserted between the table surface and the perspex cover, as shown in figures D.2 and D.3. The edge of the plank can be either sharp (90°) or rounded. Another plank is also inserted at the left hand side of the rectangular tower set-up, as shown in figure D.3, to represent the symmetry plane of the rectangular tower. Integrally finned tube heat exchangers (radiators) were used to simulate the cooling tower fill. Since these heat exchangers have directional properties, it is more suited to simulate dry heat exchangers and film fills than it is to simulate trickle grids and splash packs. All the inlets of the experimental apparatus are well rounded to eliminate breakaway of the incoming air. Each test was duplicated with an inlet rounding attached to the lower edge of the plank representing the tower wall. The inlet rounding consisted of a quarter piece of PVC pipe, attached at a 90 ° angle onto the bottom outside edge of the plank representing the tower wall.

D.1.2 Testing procedure

All the dry bulb and wet bulb temperature readings were measured with glass bulb thermometers, and the atmospheric pressures were measured with a mercury column manometer. All the other pressure readings were measured with a Betz micro-manometer.

As already mentioned, during testing, air is drawn through the tower section by a fan situated in the wind tunnel, and therefore the static pressure from the tower section inlet up to the fan is lower than atmospheric. Since the experimental apparatus is not completely air tight, a certain amount of air leaks into the experimental apparatus during operation. The air flow rate that is measured by the nozzle is therefore not the same as the air flow rate through the inlet of the tower section. To determine the true flow rate of the air through the heat exchanger bundle, the air leakage for each experimental set-up and for each testing condition had to be determined. To do this, the inlet to the tower where the heat exchanger is usually situated was sealed with a plank. The pressure drop over the nozzle and the difference between atmospheric pressure and the static pressure in front of the nozzle were then measured for different fan speeds. From the pressure drop over the nozzle, the air leakage mass flow rate for each static pressure difference (atmospheric to static in front of the nozzle) was determined, and a correlation for the air leakage mass flow rate against the static pressure drop up to the nozzle was obtained from these data. Figures D.9 and D.10 show the air leakage data for both the cylindrical tower and the rectangular tower set-ups respectively. From the figures it can be seen that a linear fit on the data was accurate enough for use in the calculations, since the tests were all done in the regions where the data tended to be linear. In figure D.10 the small discontinuity in the experimentally determined pressure loss coefficients, at a pressure difference of about 420 Pa, occurred because a larger nozzle was used to determine the air leakage mass flow rate from there onward. This change in nozzle size caused a change in Reynolds number through the nozzle, and this caused the deviation. For the data points in figure D.10 the curve fit was only done on the last four data points, since all the tests were done in that pressure difference region.

The pressure loss coefficient for the each heat exchanger set-up had to be determined. To do this, normal air flow conditions had to be created at the bundle inlet. This was done by extending the plank representing the cooling tower wall to the edge of the table. Different heat exchanger and perforated plate combinations were used to achieve different air flow resistances. The pressure drop over the heat exchanger, the pressure drop over the nozzle, and the static pressure drop to the inlet of the nozzle was measured for each heat exchanger bundle set-up, over a range of air velocities. From these pressure readings, the pressure loss coefficient for each bundle was obtained for a series of air velocities, as shown in the sample calculation of section D.2. For a certain heat exchanger bundle, the pressure loss coefficient varies as the air velocity through the bundle is changed. Figure D.4 shows the variation of the pressure loss coefficient against the air velocity for one of the cylindrical tower tests. It is seen from figure D.4 that the pressure loss coefficient approaches a constant value at high air velocities. The tests to predict the extent of the ineffective area, were therefore done at high air velocities to maintain a constant loss coefficient. A typical interval at which the tests were conducted lies between the arrows shown in figure D.4.

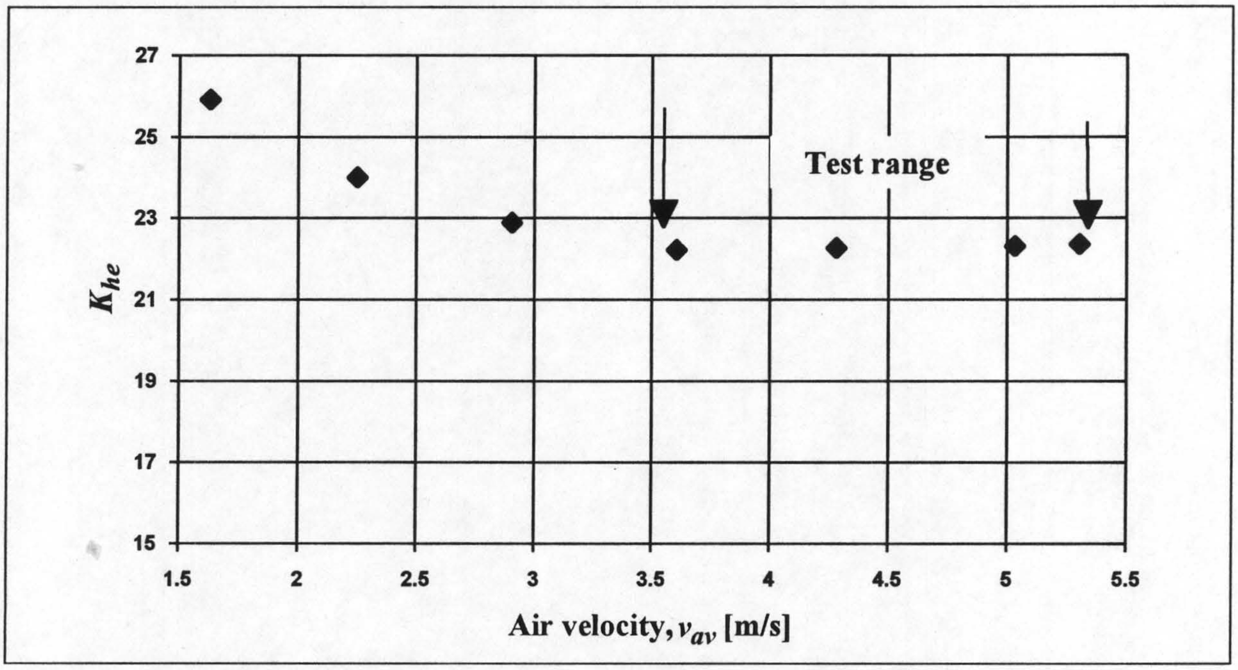

Figure D.4: *Variation of the pressure loss coefficient with changing air velocity.*

The flow patterns of the air through the fill were determined visually. A nylon string with pieces of wool attached to it was fastened behind the fill to give an indication of where circulation started to occur and of the general flow pattern just behind the heat exchanger bundle. A steel rod with a piece of wool attached to its tip was then used to more accurately determine the distance over which the ineffective area extends. This distance was measured from the inside of the tower wall up to a point where a definite decrease in air velocity could be noticed. The steel rod was inserted into the cooling tower section through a hole in the plank representing the tower wall, just behind the heat exchanger bundle. When using the rod to make measurements, care was taken not to stand too close to the inlet of the tower test section, since this influenced the air flow patterns and changed the size of the circulation area.

There was usually a very sudden decrease in air velocity, and backward flow of air through the fill could be seen in most cases. For each test the static pressure drop to the front of the nozzle and the pressure drop over the nozzle were measured. These pressures were then used to determine the air mass flow rate through the bundle for each test. The graph of pressure loss coefficient against air velocity as shown in figure D.4, was then used to determine the pressure loss coefficient of the bundle for each of these air mass flow rates. After all the pressure loss coefficients were determined, a mean pressure loss coefficient was taken to represent all the tests done for that specific heat exchanger bundle and tower inlet edge characteristics. This was done to simplify the curve fitting process. Since a variation in air speed did not cause a noticeable change in the size of the ineffective area, doing this did not influence the accuracy of the tests.

The plank representing the ground was moved to different positions to vary the tower's inlet diameter or inlet width to height ratio for each of the different bundles tested, and for a sharp or rounded tower inlet. The positions to where the plank was moved were marked out on the table surface, and were kept the same for all the cylindrical tower tests and then again for all the rectangular tower tests.

D.1.3 Experimental results

In the experimental tests the tower wall thickness was ignored since it is relatively small compared to the ineffective region. In practical towers, however, the wall thickness is usually not small enough to ignore, and must be taken into consideration. If no inlet rounding is present, the outer edge of the wall is where the breakaway of the air starts to occur, and the wall thickness should therefore be incorporated in the correlations for the effective tower diameter. For a tower with an inlet rounding, the inlet width or diameter is used, and the wall thickness is ignored. As a result of this, the form of the correlations for the towers with inlet roundings differs from the form used for the towers with sharp inlets.

From curve fits done on the test data, the following correlations were obtained from the cylindrical tower data.

- For a cylindrical cooling tower with no inlet rounding the correlation is:

$$\begin{aligned}\frac{d_{ie}}{d_i} \approx \frac{d_{ie}}{(d_i+2t_s)} &= 1.2349 - 0.21069\ln\left(\frac{d_i+2t_s}{H_i}\right) \\ &+ \left(5.0673\times10^{-2}\ln\left(\frac{d_i+2t_s}{H_i}\right) - 5.2085\times10^{-2}\right)\ln(K_{he})\end{aligned} \tag{D.1.1}$$

This correlations is valid for:

$$5.35 < \frac{d_i + 2t_s}{H_i} < 16$$

and

$$3.6 < K_{he} < 49$$

- For a cylindrical cooling tower with an inlet rounding of $r_{ir}/d_i = 0.01$ the correlation is:

$$\frac{d_{ie}}{(d_i + 2t_s)} \approx \frac{d_{ie}}{d_i} = 1.2477 - 0.16722\ln\left(\frac{d_i}{H_i}\right) + \left(4.3653\times10^{-2}\ln\left(\frac{d_i}{H_i}\right) - 6.2658\times10^{-2}\right)\ln(K_{he}) \tag{D.1.2}$$

This correlations is valid for:

$$5.35 < \frac{d_i}{H_i} < 16$$

and

$$3.6 < K_{he} < 49$$

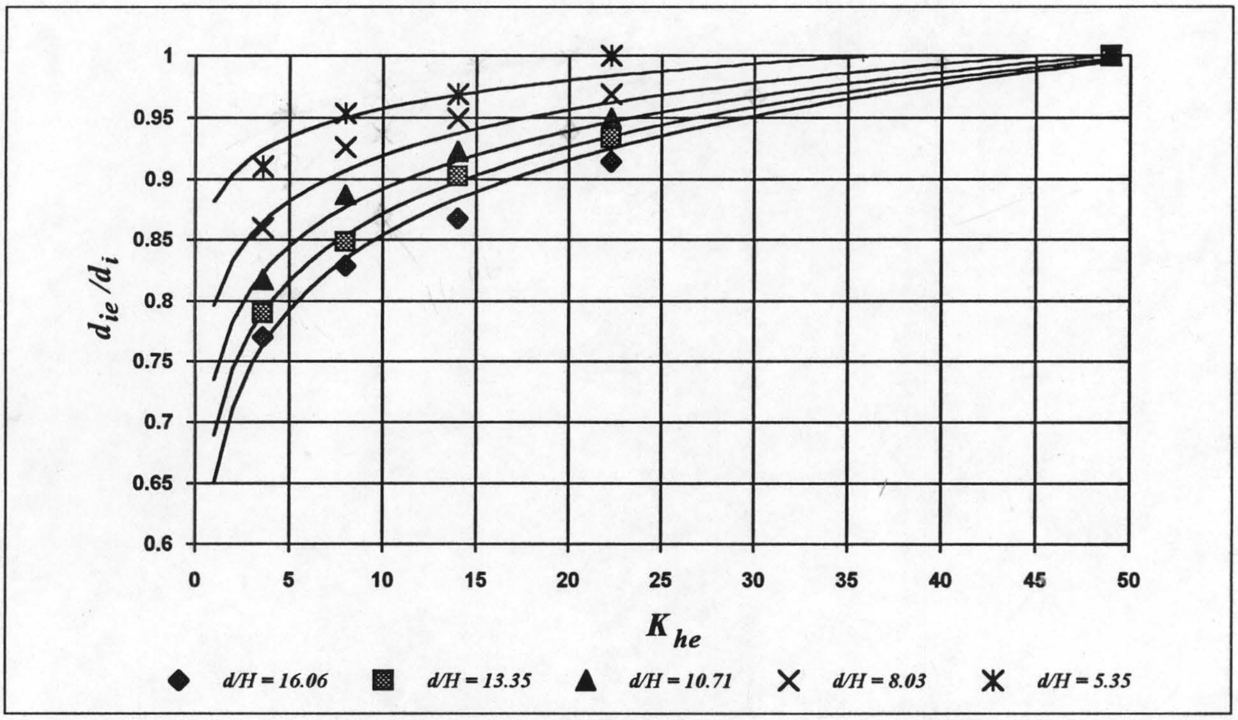

Figure D.5: *Agreement between correlation and experimental results for a cylindrical tower with no inlet rounding.*

For the cylindrical tower tests, the agreement between the correlations and the experimental results are depicted in figures D.5 and D.6. The correlation for the cylindrical tower without an inlet rounding agrees better with the experimental results than the correlation for the cylindrical tower with an inlet rounding. It would appear as if a curve with an inflexion point is needed to fit the data for the test with the inlet rounding. That kind of curve is difficult to simulate with a simple equation form, and since all the other test data could be nicely approximated with the natural logarithmic equation form, it was decided to keep all the equations in that form.

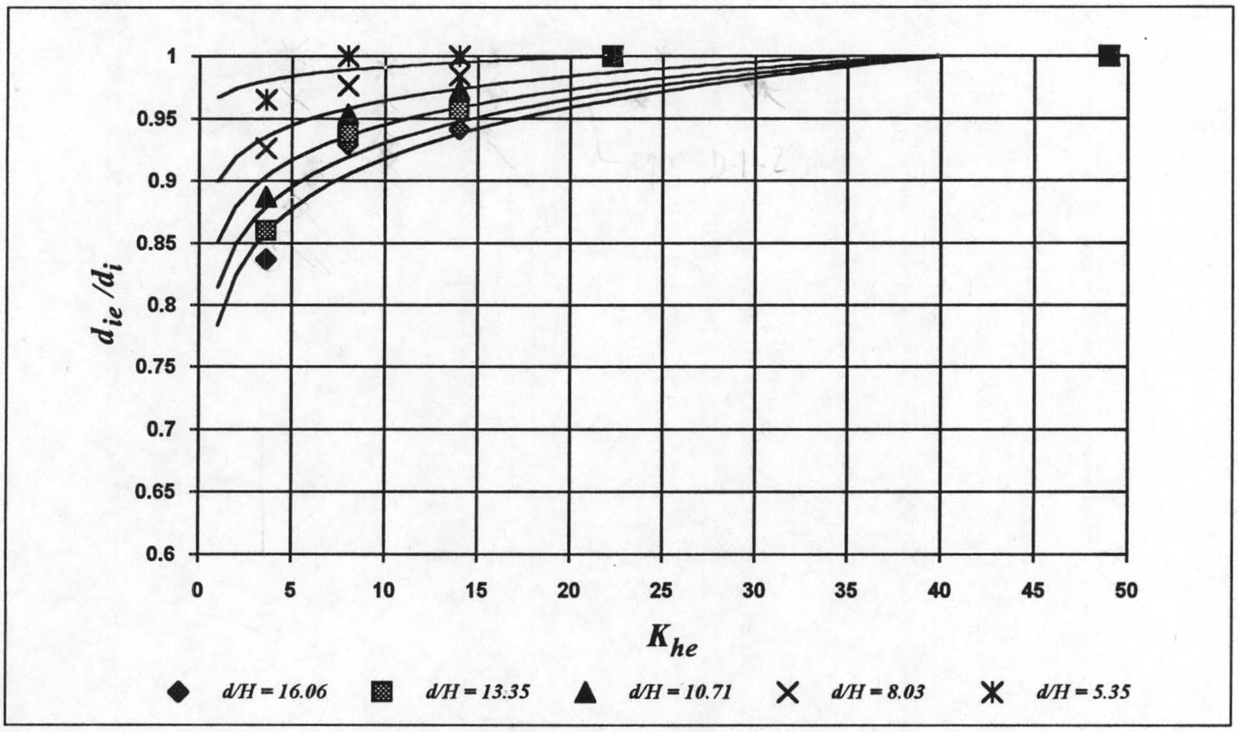

Figure D.6: *Agreement between the correlation and the experimental results for a cylindrical tower with an inlet rounding of* $r_{ir}/d_i = 0.01$.

From the rectangular tower data the following correlations were obtained.

- The correlation for a rectangular tower with no inlet rounding is:

$$\frac{W_{ie}}{W_i} \approx \frac{W_{ie}}{(W_i + 2t_s)} = 0.9366 - 0.12786 \ln\left(\frac{W_i + 2t_s}{H_i}\right) + 0.073 \ln(K_{he}) \qquad \text{(D.1.3)}$$

This correlations is valid for:

$$5 < \frac{W_i + 2t_s}{H_i} < 16.13$$

and

$$2.5 < K_{he} < 20.2$$

- The correlation for a rectangular cooling tower with an inlet rounding of $r_{ir}/W_i = 0.014$ is:

$$\frac{W_{ie}}{W_i} = 1.0487 - 0.17408 \ln\left(\frac{W_i}{H_i}\right) + 0.09 \ln\left(K_{he}\right) \tag{D.1.4}$$

This correlations is valid for:

$$5 < \frac{W_i}{H_i} < 16.13$$

and

$$2.5 < K_{he} < 20.2$$

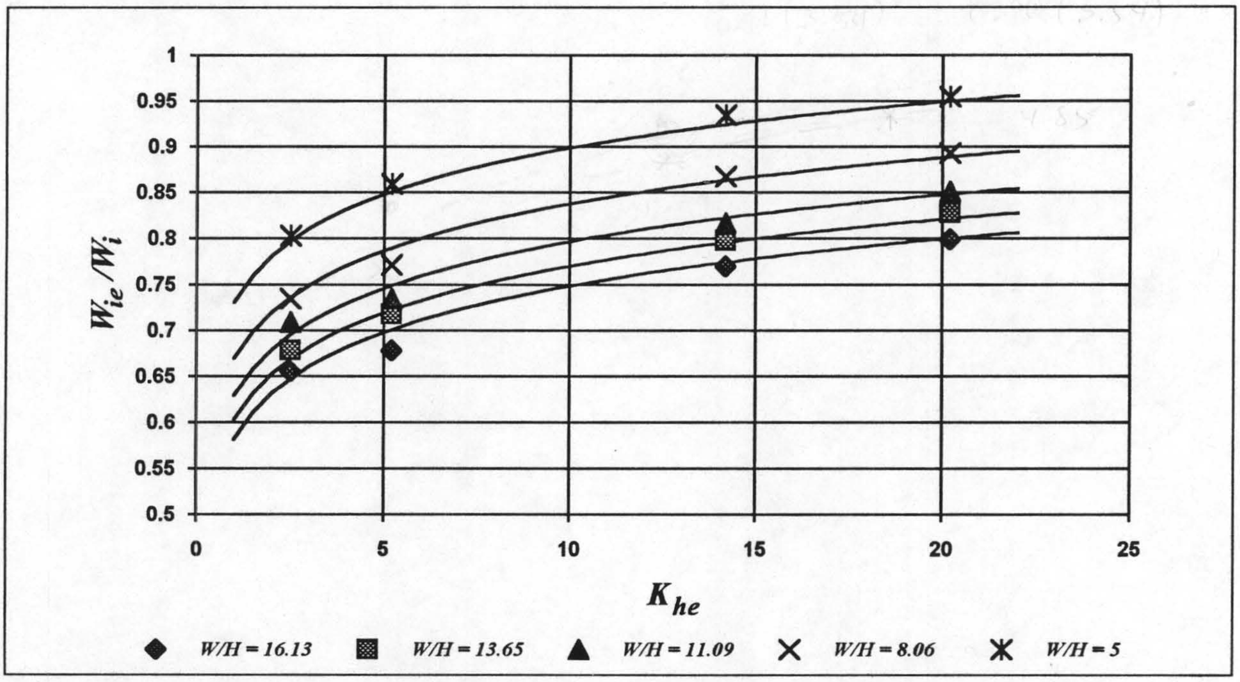

Figure D.7: *Agreement between the correlation and the experimental results for a rectangular tower with no inlet rounding.*

For the rectangular tower tests, the agreement between the obtained correlations and the experimental results are depicted in figures D.7 and D.8. Both the correlations are in good agreement with the experimentally determined values, and the general form of the equation can be assumed to be a good representation of the observed trends in circulation growth.

To determine the effective frontal area of the fill from the above correlations, the blocked area at the tower inlet, i.e. the area where no fill is present, must also be taken into consideration. Since most of this blocked area is usually situated at the outer edge of the tower, it can be assumed that this area is completely situated at the outer edge of the tower inlet region. The size of this area can be approximated as the difference in area between the tower inlet area and the fill frontal area. If the calculated effective fill frontal area is therefore larger than the specified frontal area of the packing, the ineffective area would coincide with this blocked area, and no ineffective fill area would therefore occur. In such a case the frontal area of the packing should be used in the calculations.

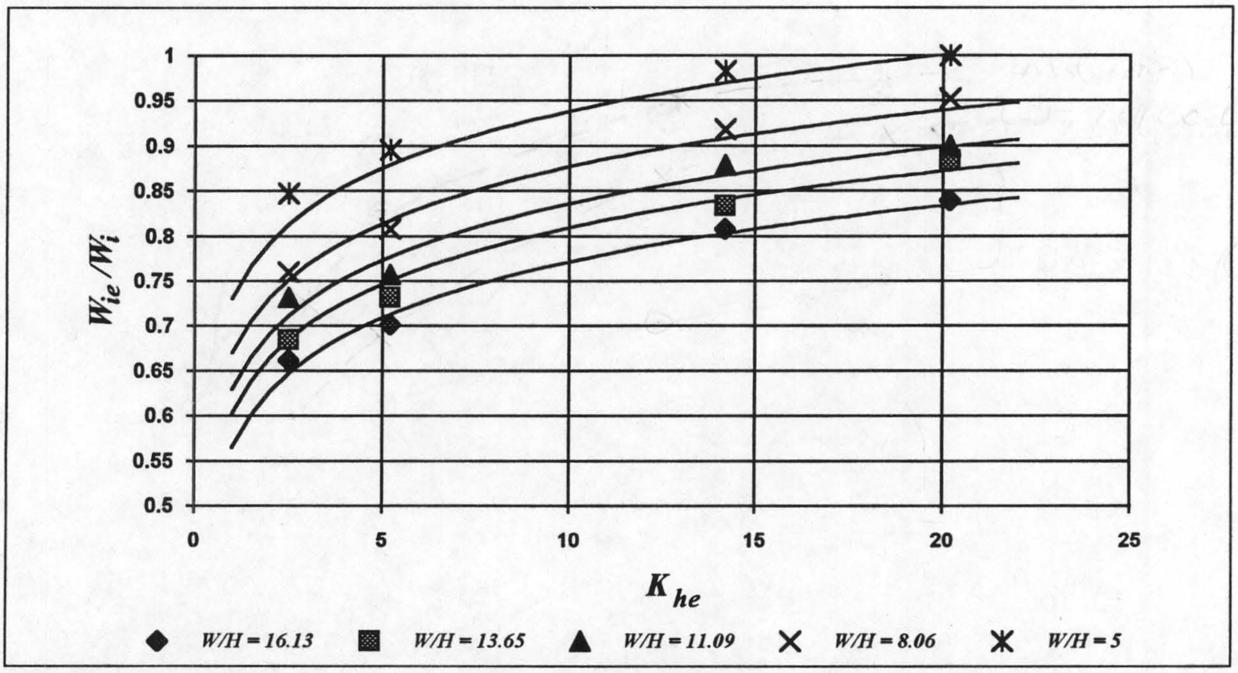

Figure D.8: *Agreement between the correlation and the experimental results for a rectangular tower with an inlet rounding of* $r_{ir}/W_i = 0.014$

For a cylindrical cooling tower the new effective fill frontal area is:

$$A_{fre} = \frac{\pi d_{ie}^2}{4} \tag{D.1.5}$$

where d_{ie} can be obtained from either equation D.1.1 or D.1.2.

For a rectangular cooling tower the new effective fill frontal area is:

$$A_{fre} = W_{ie} B_i \tag{D.1.6}$$

where W_{ie} can be obtained from either equation D.1.3 or D.1.4.

This new effective frontal area must now be used in the tower performance calculations. The increased air velocity through the fill will increase the heat transfer through the effective fill area, but the decrease in the fill frontal area will decrease the overall tower performance. As the resultant increase in fill pressure loss is already included in the tower's inlet pressure loss coefficient, the effect of the effective area reduction on pressure loss is therefore already included in the calculations.

D.2 Sample calculations

D.2.1 Sample calculation for cylindrical tower

Calculation of air leakage correlation

The air leakage test procedure was described in section D.1. From the prevailing atmospheric conditions, the measured pressure drop data, and the nozzle characteristics, a set of air leakage data was generated with the computer program "Massflow". For the cylindrical cooling tower set-up, the air leakage mass flow rate against the static pressure difference is shown in figure D.9.

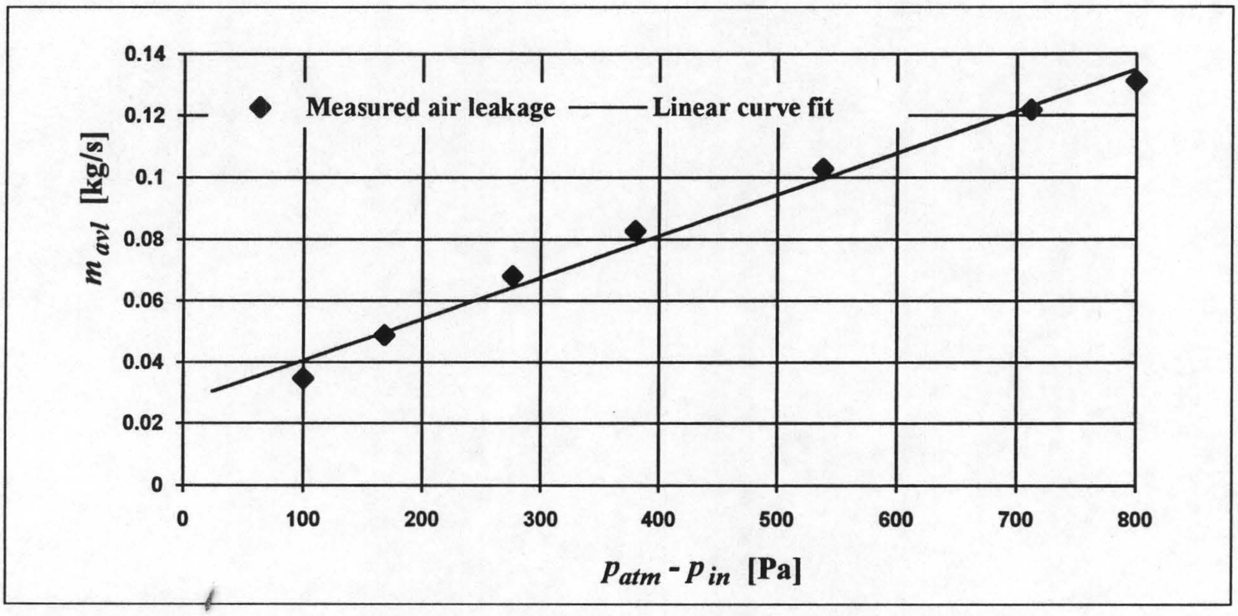

Figure D.9: *Correlation for the air leakage mass flow rate of the cylindrical tower set-up.*

A linear curve fit on the air leakage data shown in figure D.9, gives the following correlation:

$$m_{avl} = 0.027095 + 0.00013484(p_{atm} - p_{in}) \tag{D.2.1}$$

Determination of the pressure loss coefficient for one of the heat exchanger configurations

The atmospheric conditions are:

Atmospheric pressure	p_{atm}	= 100670 Pa
Dry bulb temperature	T_a	= 20 °C
Wet bulb temperature	T_{wb}	= 17.5 °C

The data obtained for perpendicular inflow conditions are:

Pressure drop over nozzle $p_{ain} - p_{aon}$ = 582 Pa
Pressure drop up to nozzle $p_{atm} - p_{ain}$ = 1193 Pa
Pressure drop over heat exchanger bundle $p_{ai} - p_{ao}$ = 336 Pa

The air mass flow rate through the nozzle is determined with the "Massflow" computer program. An air mass flow rate of m_{avt} = 1.8782 kg/s is obtained.

From equation (D.2.1), the air leakage mass flow rate is:

$$m_{avl} = 0.027095 + 0.00013484(1193) = 0.18796 \text{ kg / s}$$

The corrected mass flow rate, which is the mass flow through the heat exchanger bundle is then:

$$m_{av} = m_{avt} - m_{avl} = 1.8782 - 0.18796 = 1.6902 \text{ kg / s}$$

The frontal area of the triangular heat exchanger can be determined as follows:

$$A_{fr} = \frac{d_i H_{he}}{4} = \frac{5.14 \times 0.22}{4} = 0.2827 \text{ m}^2$$

where H_{he} is the maximum height of the heat exchanger bundle.

From equation (A.2.1) the saturated vapour pressure at T_{wb} = 17 °C is:

$$x = \frac{273.16}{17 + 273.15} = 0.94144$$

$$\begin{aligned} z &= 10.79586(1-x) + 5.02808\log_{10}(x) + 1.50474 \times 10^{-4}\left[1 - 10^{-8.29692(1/x-1)}\right] \\ &\quad + 4.2873 \times 10^{-4}\left[10^{4.76955(1-x)} - 1\right] + 2.786118312 \\ &= 3.287 \end{aligned}$$

$$p_{vs} = 10^z = 1936.458 \text{ Pa}$$

From equation (A.3.5) the humidity ratio of the air is:

$$\begin{aligned} w &= \left[\frac{2501.6-2.3263T_{wb}}{2501.6+1.8577T_a-4.184T_{wb}}\right]\left[\left(\frac{0.62509\,p_{vs}}{p_{atm}-1.005\,p_{vs}}\right)\right] \\ &\quad -\left[\frac{1.00416\left(T_a-T_{wb}\right)}{2501.6+1.8577T_a-4.184T_{wb}}\right] \\ &= 0.011013 \text{ kg / kg dry air} \end{aligned}$$

From equation (A.3.1) the density of the air is:

$$\begin{aligned} \rho_{av} &= (1+w)\left[1-\frac{w}{w+0.62198}\right]\left[\frac{p_{atm}}{287.08T_a}\right] \\ &= (1+0.011013)\left[1-\frac{0.011013}{0.011013+0.62198}\right]\left[\frac{100670}{287.08\times 293.15}\right] \\ &= 1.1883 \text{ kg / m}^3 \end{aligned}$$

The mean velocity of the air through the heat exchanger based on the frontal area is:

$$v_{av} = \frac{m_{av}}{\rho_{av}A_{fr}} = \frac{1.6902}{1.1883\times 0.2827} = 5.0313 \text{ m / s}$$

The pressure loss coefficient is therefore:

$$K_{he} = \frac{\Delta p_{he}}{\frac{1}{2}\rho_{av}v_{av}^2} = \frac{336}{\frac{1}{2}\times 1.1883\times 5.0313^2} = 22.34$$

D.2.2 Sample calculation for rectangular tower

Determination of air leakage correlation

As for the cylindrical tower the computer program "Massflow" was used to obtain the mass flow rates from the measured data. For the rectangular tower set-up, the obtained air leakage mass flow rates are shown in figure D.10.

A linear curve fit on the last four air leakage data points shown in figure D.10 gives the following correlation:

$$m_{avl} = 0.036872+0.00010516\left(p_{atm}-p_{in}\right) \tag{D.2.2}$$

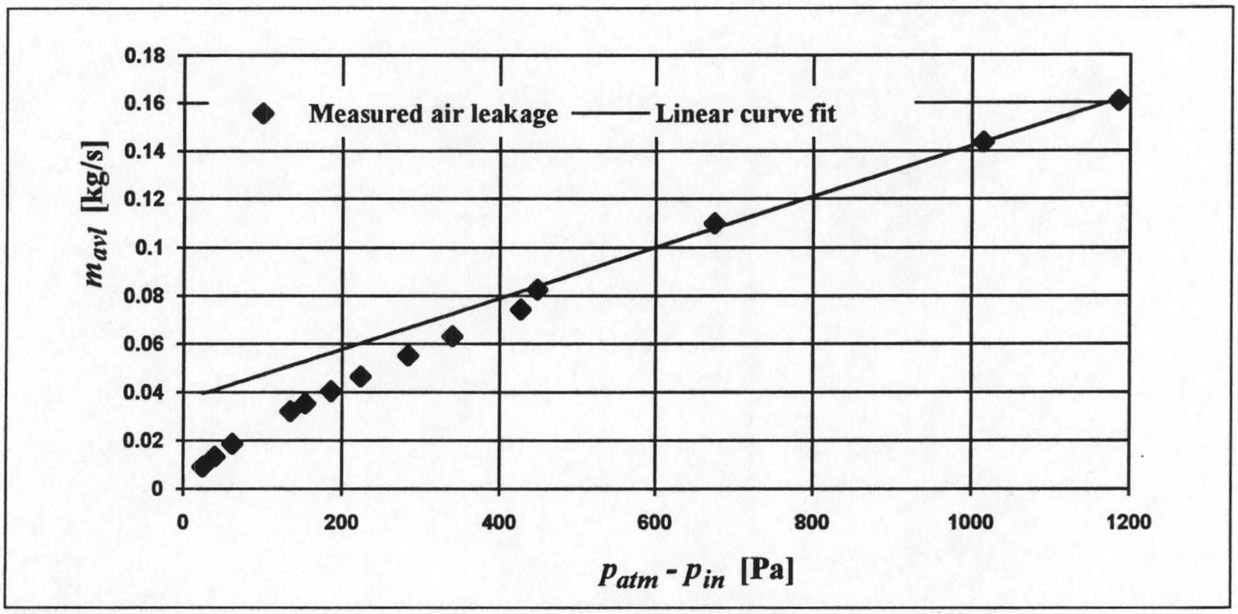

Figure D.10: *Correlation for the air leakage mass flow rate of the rectangular tower set-up.*

Determination of the pressure loss coefficient for one of the heat exchanger configurations

The atmospheric conditions are:

Atmospheric pressure	p_{atm}	= 101800 Pa
Dry bulb temperature	T_a	= 17.5 °C
Wet bulb temperature	T_{wb}	= 16 °C

The data obtained for perpendicular inflow conditions are:

Pressure drop over nozzle	$p_{ain} - p_{aon}$	= 307 Pa
Pressure drop up to nozzle	$p_{atm} - p_{ain}$	= 595 Pa
Pressure drop over heat exchanger bundle	$p_{ai} - p_{ao}$	= 143 Pa

The air mass flow rate through the nozzle is determined with the "Massflow" computer program. An air mass flow rate of m_{avt} = 1.3841 kg/s is obtained.

From equation (D.2.2), the air leakage mass flow rate is:

$$m_{avl} = 0.036872 + 0.00010516(595) = \dot{0}.099442 \text{ kg / s}$$

The corrected mass flow rate, which is the flow rate through the heat exchanger bundle is then:

$$m_{av} = m_{avt} - m_{avl} = 1.3841 - 0.099442 = 1.2847 \text{ kg / s}$$

The inlet area of the bundle can be determined as follows:

$$A_{fr} = \frac{W_i H_{he}}{2} = 1.774 \times 0.147 = 0.26078 \text{ m}^2$$

where W_i is the inlet width of the represented model tower, and is two times the width of the heat exchanger bundle tested.

From equation (A.2.1) the saturated vapour pressure at T_{wb} = 16 °C is:

$$x = \frac{273.16}{16+273.15} = 0.9447$$

$$\begin{aligned} z &= 10.79586(1-x) + 5.02808\log_{10}(x) + 1.50474 \times 10^{-4}\left[1-10^{-8.29692(1/x-1)}\right] \\ &\quad + 4.2873 \times 10^{-4}\left[10^{4.76955(1-x)} - 1\right] + 2.786118312 \\ &= 3.2594 \end{aligned}$$

$$p_{vs} = 10^z = 1817.042 \text{ Pa}$$

From equation (A.3.5) the humidity ratio of the air is:

$$\begin{aligned} w &= \left[\frac{2501.6 - 2.3263T_{wb}}{2501.6 + 1.8577T_a - 4.184T_{wb}}\right]\left[\left(\frac{0.62509\, p_{vs}}{p_{atm} - 1.005\, p_{vs}}\right)\right] \\ &\quad - \left[\frac{1.00416(T_a - T_{wb})}{2501.6 + 1.8577T_a - 4.184T_{wb}}\right] \\ &= 0.010738 \text{ kg / kg dry air} \end{aligned}$$

From equation (A.3.1) the density of the air is:

$$\begin{aligned} \rho_{av} &= (1+w)\left[1 - \frac{w}{w+0.62198}\right]\left[\frac{p_{atm}}{287.08T_a}\right] \\ &= (1+0.010738)\left[1 - \frac{0.010738}{0.010738+0.62198}\right]\left[\frac{101800}{287.08 \times 290.65}\right] \\ &= 1.2122 \text{ kg / m}^3 \end{aligned}$$

The mean velocity of the air through the heat exchanger based on the frontal area is:

$$v_{av} = \frac{m_{av}}{\rho_{av} A_{fr}} = \frac{1.2847}{1.2122 \times 0.26078} = 4.064 \text{ m / s}$$

The pressure loss coefficient is therefore:

$$K_{he} = \frac{\Delta p_{he}}{\frac{1}{2}\rho_{av}v_{av}^2} = \frac{143}{\frac{1}{2}\times 1.2122 \times 4.064^2} = 14.2852$$